Technische Universität Braunschweig

Doctoral Thesis

Effect of porosity and submergence of detached homogeneous rubble mound breakwaters on wave transmission and short term coastal erosion - A numerical study

S. M. Mojabi

November 2018

Leichtweiß-Institut für Wasserbau

exceed EXCELLENCE CENTERS

DAAD German Academic Exchange Service

Federal Ministry for Economic Cooperation and Development

This Page is Intentionally Left Blank

Technische Universität Braunschweig

Effect of porosity and submergence of detached homogeneous rubble mound breakwaters on wave transmission and short term coastal erosion - A numerical study

Von der
Fakultät Architektur, Bauingenieurwesen und Umweltwissenschaften
der Technischen Universität Carolo-Wilhelmina
zu Braunschweig

zur Erlangung des Grades eines
Doktor-Ingenieurs (Dr.-Ing.)
genehmigte

Dissertation

von
Seyed Moin Mojabi, M.Sc.

geboren am 14. Mai 1986
aus Tehran, Iran

Eingereicht am: 26. Juni.2018

Disputation am: 30. Nov.2018

..

Berichterstatter Prof. Dr. -Ing. Hocine Oumeraci

Prof. Lorenzo Cappietti

2019

This Page is Intentionally Left Blank

This Page is Intentionally Left Blank

Acknowledgements

First and foremost, I would like to express my deep gratitude to my supervisor Prof. Dr.-Ing. Hocine Oumeraci. I appreciate all his supports, and ideas which make my PhD experience constructive. His patience, deep knowledge and systematic way of thinking taught me a lot and set a good framework for the rest of my life.

I gratefully acknowledge the funding sources that made my PhD work possible. My PhD was funded by the German Academic Exchange Service (DAAD) and the German Federal Ministry for Economic Cooperation and Development (BMZ) in the frame of the Exceed-Swindon Project at Technische Universität Braunschweig. This support is gratefully acknowledged.

My wonderful colleagues at the Leichtweiß-Institute in Braunschweig have contributed greatly to my personal and professional time. The group has been a source of a good advice and collaboration. I would especially like to acknowledge Mrs Gabriele Fournier, Prof. Dr. Andreas Haarstrick, Mrs Doris Hellmann, Dr Saber M. Elsayed, Mr Rainer Kvapil, Dr Agnieszka Strusińska-Correia and Mrs Sanaz Hadadpour for their kind advice and supports

Finally, I would like to thank my family for all their kind supports and encouragement, especially my parents and my wife Mans.

Seyed Moin Mojabi
Braunschweig, 2018

Abstract

Coastal beaches are permanently threatened by erosion, so that efficient solutions for their protections with less environmental impacts are increasingly required. Among the diverse protective structures against coastal erosion, submerged porous breakwaters (SPBs) have long been recognized as one of the most environmentally friendly types of coastal structures. However, the failures experienced in diverse SPB projects worldwide have well-revealed the current knowledge gaps and the high uncertainty in the assessment of the protective efficacy of SPBs. As such breakwaters are usually highly porous, one of the most crucial knowledge gaps is the effect of structure porosity on their protective efficacy, along with the effect of structure submergence. It is worth to mention that the former effect has not yet been considered in any of the current models and predictive formulae for SPBs.

Therefore, the overall objective of this PhD study is to improve the current knowledge and modelling of the processes underlying the effect of porosity, combined with the effect of submergence, on both wave transmission and subsequent short-term coastal erosion. To achieve this overall goal and further specific goals, the following methodology with three main work phases is adopted:

(i) Using a well-validated CFD model in OpenFOAM, a systematic parameter study is performed for different breakwater submergence depths with a focus on the effect of structure porosity on wave transmission in order to better understand the underlying processes and to develop a wave transmission coefficient (WTC) formula which, for the first time, explicitly accounts for both breakwater porosity and submergence;

(ii) Based on the improved understanding and the new WTC formula from work phase i, a novel two steps approach for SPBs is implemented to improve and extend the current DELFT3D-WAVE model: (a) model improvement in order to adequately account for the effect of submergence on wave transmission, even for SPBs with steep slopes, and (b) model extension in order to account for the effect of breakwater porosity on wave transmission. This work phase also includes a systematic validation of the improved/extended model for wave transmission.

(iii) With the improvement and extension from work phase ii, the hydro-morphodynamic model DELFT3D is validated and then used to perform an extensive parameter study for different submergence depths by focusing on the effect of structure porosity on short-term coastal erosion in order to better understand the underlying processes and to develop predictive formulae, which explicitly account for the effect of both breakwater porosity and submergence on coastal erosion. For the sake of completeness, the crest width and location depth of SPB are also included in the formulae.

From the key results, which have been achieved using these approaches, the following might be worth to mention. For the first time, a WTC formula is developed which explicitly includes the effect of breakwater porosity in addition to the effect of submergence. Using this formula, the DELFT3D-WAVE module is extended and improved. As a result, for the first time, a model is obtained to account for the effect of breakwater porosity on wave transmission, including a substantial improvement of the effect of breakwater submergence, even for steep slopes of SPBs. This model improvement and extension proved to be also highly valuable for the hydro-morphodynamic model DELFT2D as demonstrated by the results of the validation and of the extensive parameter study in work phase iii. From the analysis of the results of this parameter study, for the first time, predictive formulae were derived for the protective efficacy of SPBs, which explicitly account for the effect of porosity on coastal erosion, including the effect of SPB submergence, crest width and location depth.

Among the limitations of the approaches and results of this study, which also indicate future research directions and topics, the following might be mentioned: Lack of field data for model validation as well as limited applicability of the new WTC formula for multi-layered SPBs and for SPBs with porosity n=

0- 0.3. Besides overcoming these limitations, future research should also be primarily directed towards 3D modelling to account for longshore shore transport, which is crucial for the effect of SPBs on long-term morphological changes, but also to account explicitly for the effect of the flow in and through SPBs.

Keywords: Submerged porous breakwaters; Wave transmission; Coastal erosion; Predictive formulae; Short-term; Structure porosity; Structure submergence; CFD modelling; Hydro-morphodynamic modelling.

Kurzfassung

Küstenstrände unterliegen einer ständigen Erosion, so dass effiziente Maßnahmen zu deren Schutz zunehmend benötigt werden, bei denen weniger Auswirkungen auf die Umwelt zu erwarten sind. Aus den diversen Schutzwerken gegen Küstenerosion, durchlässige Unterwasser-Wellenbrecher (DUW) gehören längst zu den umweltfreundlichsten Bauwerkstypen für den Küstenschutz. Jedoch haben die Versagensfälle in diversen DUW-Projekten weltweit große Wissenslücken und Unsicherheiten bei der Bewertung der Schutzwirkung und Wirksamkeit der DUW aufgezeigt. Da solche Wellenbrecher im Allgemeinen eine hohe Porosität haben, bezieht sich eine der kritischsten Wissenslücken insbesondere auf den Einfluss der Porosität auf die Schutzwirksamkeit der DUW, einschließlich des Einflusses der Tauchtiefe. Dabei ist zu unterstreichen, dass der erstgenannte Einfluss in keiner der bisherigen Modelle und Berechnungsansätze für DUW berücksichtigt wird.

Daher besteht das Hauptziel dieser Dissertation in der Verbesserung des Verständnisses und der Modellierung der Prozesse, die dem Einfluss der Porosität und der Tauchtiefe der DUW auf die Wellentransmission sowie auf die anschließenden kurzfristigen Veränderungen der Küstenerosion unterliegen. Um dieses Ziel sowie weitere spezifische Ziele zu erreichen, wird in drei Arbeitsphasen wie folgt methodisch vorgegangen:

(i) Mit einem gut validierten CFD-Modells in OpenFOAM wird eine systematische Parameterstudie für verschiedene DUW Tauchtiefen durchgeführt, wobei der Fokus auf den Einfluss der Porosität auf die Wellentransmission gelegt wird, um eine bessere Einsicht in die unterliegenden Prozesse zu erzielen und einen Berechnungsansatz für die Wellentransmission von DUW zu entwickeln, der erstmalig die Porosität und die Tauchtiefe des Bauwerkes explizit enthält.

(ii) Auf der Grundlage der verbesserten Einsicht und des neuen Berechnungsansatzes aus Arbeitsphase i, wird ein neues methodisches Vorgehen für DUW bestehend aus zwei Schritten implementiert, um das das derzeitige Modell DELFT3D-WAVE zu verbessern und zu erweitern: (a) Modellverbesserung um den Einfluss der Tauchtiefe auf die Wellentransmission -auch für DUW mit steilen Böschungen- angemessen zu berücksichtigen, (b) Modellerweiterung um erstmalig den Einfluss der Porosität auf die Wellentransmission zu berücksichtigen. Diese Arbeitsphase beinhaltet auch eine systematische Validierung des verbesserten und erweiterten Modells für die Wellentransmission;

(iii) Mit der Modellverbesserung und -erweiterung aus Arbeitsphase ii wird das hydro-morphodynamische Modell DELFT3D validiert und zur Durchführung einer umfangreichen Parameterstudie eingesetzt. Dabei wird der Fokus auf den Einfluss der Porosität auf die kurzfristige Küstenerosion für verschiedene Tauchtiefen gelegt, um die unterliegenden Prozesse besser zu verstehen und Berechnungsansätze zu entwickeln, die erstmalig den Einfluss der Porosität der DUW auf die Küstenerosion explizit berücksichtigen - in Kombination mit dem Einfluss der Tauchtiefe. Vollständigkeitshalber werden auch die Kronenbreite und die Wassertiefe der DUW ebenfalls in den Berechnungsansätzen berücksichtigt.

Aus den wichtigsten Ergebnissen, die auf der Basis des o.g. Vorgehens erzielt wurden, sind folgende Schlüsselergebnisse besonders herauszustreichen. Erstmalig wird ein Berechnungsansatz für die Wellentransmission von DUW entwickelt, der die Bauwerksporosität explizit enthält - einschließlich der Tauchtiefe. Mit der Verbesserung und Erweiterung des Wellenmoduls von DELFT3D steht zum ersten Mal ein Modell zur Verfügung, das in der Lage ist, den Einfluss der Porosität auf die Wellentransmission explizit zu berücksichtigen. Darüber hinaus wird eine wesentliche Verbesserung

der prädiktiven Modellfähigkeit hinsichtlich des Einflusses der Tauchtiefe auf die Wellentransmission, auch bei steilen Böschungen der DUW, erzielt. Wie die Ergebnisse der Validierung und der umfangreichen Parameterstudie in der Arbeitsphase iii deutlich verdeutlichten, erwiesen sich die o.g. Modellerweiterung und -erweiterung ebenfalls als sehr wertvoll für das hydro-morphodynamische Modell DELFT2D. Auf der Basis der gewonnenen Einsicht in die sich abspielenden Prozesse und der Analyse der Daten aus dieser Parameterstudie, wurden Berechnungsansätze für die Schutzwirksamkeit von DUW entwickelt, die den Einfluss der Porosität auf die kurzfristige Küstenerosion erstmalig explizit berücksichtigen, einschließlich des Einflusses der Tauchtiefe sowie der Kronenbreite und Wassertiefe der DUW.

Aus den diversen Einschränkungen der Verfahren und Ergebnisse dieser Studie sind folgende hervorzuheben, die auch auf die Aufgaben künftiger DUW Forschung hinweisen: Fehlen geeigneter Felddaten zur abschließenden Modellvalidierung sowie eingeschränkte Anwendbarkeit des neuen Wellentransmission-Ansatzes für DUW mit mehreren Lagen und für DUW mit geringerer Porosität (n= 0- 0.3). Zusätzlich zur Überwindung dieser Einschränkungen, sollte die künftige DUW Forschung vor allem auf die 3D Modellierung fokussieren, um also den Küstenlängstransport zu berücksichtigen, der für den langfristigen Einfluss der DUW auf die morphologischen Veränderungen vorwiegend verantwortlich ist. Dies schließt auch die explizite Berücksichtigung des Einflusses der Strömungsverhältnisse im und durch den DUW ein.

Keywords Durchlässige Unterwasser-Wellenbrecher: Wellentransmission; Berechnungsansätze; Küstenmorphologische Veränderungen; Kurzfristig; Bauwerksporosität; Tauchtiefe, CFD-Modellierung; Hydro-morphodynamische Modellierung

Abstract(Farsi)

نواحی ساحلی در نقاط مختلف جهان به طور مستمر تحت تاثیر فرسایش قرار دارند. در میان روش های متعددی که برای محافظت از سواحل در برابر فرسایش وجود دارد، استفاده از موج شکن های مستغرق که معمولا از درصد تخلخل قابل توجهی نیز برخوردارند به عنوان رویکردی با حد اقل تاثیرات منفی بر روی نواحی ساحلی شناخته می شود. با این حال، موارد زیادی از عدم موفقیت این نوع از سازه ها در محافظت از ساحل در برابر فرسایش نشان دهنده عدم قطعیت قابل توجهی در طراحی و استفاده از این نوع سازه در سیستم های حفاظت از سواحل می باشد. با توجه به اینکه موج شکن های مستغرق عموما متخلخل هستند، یکی از جدی ترین مشکلات ارزیابی و به کار گیری این سازه ها، محدودیت دانش ارزیابی تاثیر تخلخل به همراه مستغرق بودن برروی قابلیت موج شکن در حفاظت از ساحل در برابر فرسایش می باشد. لازم به ذکر است که در هیچیک از روابط یا مدل های موجود برای ارزیابی قابلیت حفاظتی موج شکن های مستغرق تاثیر تخلخل این سازه ها لحاظ نشده است. بنا بر آنچه بیان شد، هدف کلی این مطالعه عبارت است از بهبود درک کلی از تاثیر تخلخل به همراه مستغرق بودن بر عملکرد موج شکن ها در محافظت از سواحل در برابر فرسایش، و در نتیجه ارتقا دانش طراحی و ارزیابی موج شکن های مستغرق برای سیستم های محافظت از ساحل در برابر فرسایش می باشد. درراستای رسیدن به این هدف کلی، مراحل مشخصی برای این مطالعه تعریف شده اند که به شرح زیر می باشند:

الف- انجام یک مطالعه پارامتری گسترده بر روی موج شکن های با میزان مستغرق بودن متفاوت و با تمرکز بر روی پارامتر تخلخل. این مطالعه پارامتری، با استفاده ار یک مدل عددی به خوبی صحت سنجی شده در OpenFOAM انجام پذیرفته و با استفاده از نتایج آن یک فرمول جدید گذر موج از روی موج شکن توسعه پیدا میکند. لازم به ذکر است، فرمول گذر موج که در این مطالعه توسعه پیدا میکند اولین رابطه از این نوع است که به طور صریح شامل تخلخل سازه می باشد.

ب- با استفاده از فرمول توسعه داده شده در مرحله قبلی یک روش جدید گام به گام برای لحاظ کردن تاثیر تخلخل موج شکن مستغرق بر روی محاسبه میدان موج در مدل DELFT3D توسعه داده می شود. این روش شامل دو گام میباشد. گام اول شامل ارتقای قابلیت DELFT3D برای اعمال موثر و صحیح اثر مستغرق بودن موج شکن است و گام دوم شامل توسعه قابلیت مدل برای اعمال اثر تخلخل موج شکن مستغرق می باشد. در این مرحله از مطالعه، مدل DELFT3D که با روش جدید توسعه داده شده در این مطالعه ارتقا پیدا کرده به طور سیستماتیک صحت سنجی می شود.

ج- با استفاده از مدل عددی DELFT3D که در مرحله قبل ارتقا یافته، یک مطالعه پارامتری گسترده برروی تاثیر موج شکن مستغرق بر میران فرسایش ساحل در رویداد هایی با مقیاس زمانی کوتاه (مثلا طوفان) انجام می شود. برای این مطالعه پارامتری، مدل DELFT3D ارتقا یافته در برابر داده های ازمایشکاهی مرتبط صحت سنجی می شود. نتایج مطالعه پارامتری که در این مرحله انجام می شود دانش فعلی ارزیابی قابلیت موج شکن های مستغرق برای محافظت از سواحل را به طرز قابل توجهی ارتقا می دهد. همچنین، بر مبنای نتایج این مطالعه پارامتری، یک فرمول جدید برای ارزیابی کمی میزان تاثیر پارامتر های طراحی موج شکن مستغرق بر روی قابلیت این سازه ها در حفاظت از سواحل ماسه ای در رویداد های کوتاه مدت (مثلا طوفان) توسعه داده می شود. لازم به ذکر است این رابطه اولین فرمول در نوع خود است که به طور صریح تاثیر تخلخل موج شکن را لحاظ کرده است.

بر مبنای مراحلی که در بالا بیان شد، این مطالعه اولین مطالعه در نوع خود است که به طور مشخص به تاثیر تخلخل موج- شکن پرداخته است. بنا بر این، با توجه به اینکه موج شکن های مستغرق معمولا متخلخل هستند، نتایج این مطالعه به طور قابل توجه دانش کنونی ارزیابی موج شکن های مستغرق را در سیستم های حفاظت از سواحل بهبود می بخشد. از نتایج مشخص این مطالعه یک فرمول جدید محاسبه ضریب گذر موج از روی موج شکن مستغرق و هم چنین رابطه ای تحلیلی برای ارزیابی کمی

قابلیت حفاظت این سازه ها از سواحل ماسه ای در رویدادهایی با مقیاس زمانی کوتاه می باشد. لازم به ذکر است، فرمول های ذکر شده اولین روابط در نوع خود هستند که تاثیر تخلخل سازه را به صورت صریح لحاظ کردند. هم چنین روش ارایه شده برا ی لحاظ کردن موثر تاثیر مستغرق بودن موج شکن در محاسبه میدان موج قابلیت DELFT3D را در محاسبه میدان موج در ناحیه محافظت شده با موج شکن مستغرق را (حتی برای موج شکن هایی با شیب جانبی زیاد) به شکل قابل توجهی ارتقا می دهد.

در رابطه با محدودیت های کاربرد نتایج این مطالعه لازم به ذکر است که نبود داده های میدانی و آزمایشگاهی کافی برای صحت سنجی گسترده تر نتایج این مطالعه یکی از کمبودهایی است که توصیه می شود تا در مطالعات آینده برای رفع آن تلاش شود. هم چنین، لازم به ذکر است، فرمول گذر موج به دست امده در این مطالعه به طور مستقیم برای موج شکن های چند لایه که تخلخل لایه های مختلف آن به طور محسوسی با یکدیگر متفاوت است قابلیت کاربرد ندارد. علاوه بر این، برای مطالعات آینده توصیه می شود، روش به کار رفته در این مطالعه، برای بررسی قابلیت حفاظتی موج شکن در برابر فرسایش درمقایس زمانی بلند نیز مورد استفاده قرار بگیرد.

کلید واژه ها: موج شکن، تخلخل، مدلسازی عددی، فرسایش ساحل، حفاظت از ساحل ,Open FOAM ,DELFT3D

Table of contents

List of figures

List of tables

Nomenclature

Notations	Unit	Description
a	[m]	Sediment transport reference level
A	[-]	Dean shape parameter governed by D_{50}
B	[m]	Breakwater crest width
B_e	[m]	Breakwater effective crest width
c	$[m^3.m^{-3}]$	Suspended sediment concentration
c_a	$[m^3.m^{-3}]$	Suspended sediment concentration at reference level a
C	$[m^{0.5}.s^{-1}]$	Chezy parameter
c_{eq}	$[m^3.m^{-3}]$	Depth averaged equilibrium sediment concentration
C_{gx}	$[m.s^{-1}]$	Wave propagation velocity in x direction
C_{gy}	$[m.s^{-1}]$	Wave propagation velocity in y direction
C_m	[-]	Added mass coefficient
C_θ	$[rad.s^{-1}]$	Wave propagation velocity in directional space
C_σ	$[s^{-2}]$	Wave propagation velocity in frequency space
D_h	$[m^2.s^{-1}]$	Background horizontal eddy diffusivity
D_{n50}	[m]	Mean diameter of rock materials
D_v	$[m^2.s^{-1}]$	Background vertical eddy diffusivity
D_H	$[m^2.s^{-1}]$	Horizontal sediment diffusion coefficient
D_{tot}	$[kg.s^{-3}]$	Rate of total energy dissipation per unit horizontal area
D_V	$[m^2.s^{-1}]$	Vertical sediment diffusion coefficient
D_{50}	[m]	Mean diameter of bed materials
E	$[kg.s^{-2}]$	Wave energy density per unit horizontal area
E_d	$[kg.m^2s^{-2}]$	Dissipated wave energy
E_i	$[kg.m^2s^{-2}]$	Incident wave energy
E_r	$[kg.m^2s^{-2}]$	Reflected wave energy
E_t	$[kg.m^2s^{-2}]$	Transmitted wave energy
EF	[-]	Enhancement parameter
e_p	[-]	Erosion parameter
f_{bed}	[-]	Bed load transport scaling factor
$f_{morphac}$	[-]	Morphological acceleration factor
f_{sus}	[-]	Suspended sediment transport scaling factor
g	$[m.s^{-2}]$	Gravitational acceleration
h	[m]	Water depth
h_b	[m]	Breaking depth
h_p	[m]	Water depth at breakwater location (at offshore toe of the breakwater)
h_{str}	[m]	Breakwater height
H	[m]	Wave height

H_b	[m]	Breaking wave height
H_{bi}	[m]	Threshold incident breaking wave height
H_i	[m]	Incident wave height
H_o	[m]	Deep water wave height
H_{rms}	[m]	Root mean square wave height
H_S & H_{m0}	[m]	Significant wave height & Zero-moment *wave height*.
H_t	[m]	Transmitted wave height
K_d	[-]	Wave dissipation coefficient
K_r	[-]	Wave reflection coefficient
K_t	[-]	Wave transmission coefficient
$K_{tVDM2003}$	[-]	Wave transmission coefficient from VDM2003 formula
KC	[-]	Keulegan-Carpenter number
k	[-]	Wave number
k_p	[-]	Wave number related to the peak period
k_s	[m]	Bed roughness
L	[m]	Wave length
L_B	[m]	Breakwater length
L_g	[m]	Length of the gap in segmented breakwaters
L_o	[m]	Deep water wave length
L_p	[m]	Wave length related to the peak period
L_{op}	[m]	Deep water wave length related to the peak period
M_x	$m.s^{-2}$	Wave-induced force per unit mass in x direction
M_y	$m.s^{-2}$	Wave-induced force per unit mass in y direction
m= tanα	[m]	Seaward slope of the breakwater
N	$[kg.s^{-1}]$	Wave action density $N=E/\sigma_w$
$\vec{n}$	[-]	Normal vector to flow direction
n	[-]	Porosity
P	[-]	Notational permeability
p_i	[-]	Breakwater protection index
Q_b	[-]	Fraction of breaking waves
R_c	[m]	Breakwater submergence depth
R_{ce}	[m]	Effective breakwater submergence depth
$\vec{S}$	$[m.s^{-1}]$	Rate of discharge or withdrawal of water per unit area
S	$[m^3.m^{-3}.s^{-1}]$	Exchange of sediment between water column and sea bed
S_{bx}	$[m^3.m^{-1}.s^{-1}]$	Bed load transport in x direction
S_{by}	$[m^3.m^{-1}.s^{-1}]$	Bed load transport in y direction
S_{sx}	$[m^3.m^{-1}.s^{-1}]$	Suspended load transport in x direction
S_{sy}	$[m^3.m^{-1}.s^{-1}]$	Suspended load transport in y direction
S_θ	[-]	Wave spreading parameter
$\vec{s}$	[-]	Unit vector for flow direction
s	[-]	Relative density of sediment (ρ_s/ρ)

s_{op}	[-]	Wave steepness (H_s/L_{op})
t	[s]	Time
T	[s]	Wave period
T_p	[s]	Peak wave period
$\bar{U}$	[m/s]	Depth averaged flow velocity in x direction
U	[m/s]	GLM velocity in x direction
u	[m/s]	Eulerian velocity in x direction
u_r	[m.s-1]	Compression velocity normal to the surface
u_s	[m.s-1]	Stokes drift in in x direction
$\bar{V}$	[m/s]	Depth averaged flow velocity in y direction
V	[m/s]	GLM velocity in y direction
V_e	[m3.m-1]	Beach erosion volume
v	[m.s-1]	Eulerian velocity in y direction
v_s	[m.s-1]	Stokes drift in in y direction
W	[m.s-1]	Velocity field in z direction
w_s	[m.s-1]	Sediment fall velocity
x	[-]	Cross-shore axis coordinate
X_s	[m]	Distance between breakwater and shoreline
y	[-]	Longshore axis coordinate
z	[-]	Vertical coordinate in physical space
z_0	[-]	Roughness length
z_b	[m]	Bed level elevation
z_{b0}	[m]	Initial bed level
z_{bm}	[m]	Measured bed level
z_{bc}	[m]	Calculated bed level
α	[-]	Linear resistance coefficient
β	[-]	Non-linear resistance coefficient
α	[°]	Seaward slope angle of breakwater
α_{bn}	[-]	Transverse bed slope effect factor
α_{bs}	[-]	Stream-wise bed slope effect factor
α_s	[-]	Bed slope correction coefficient
β	[°]	Shoreward slope angle of breakwater
γ	[-]	Breaking index
δ	[m]	Wave set-up
δ_e	[m]	Wave set-up in the exposed area in the vicinity of
δ_p	[m]	Wave set-up in the protected area behind breakwater
Δt	[s]	Time step
Δx	[m]	Grid size in cross-shore direction
Δy	[m]	Grid size in long shore direction
Δz	[m]	Grid size in vertical (gravitational) direction

Δz_b	[m]	Distance between bed and the first computational grid point
Δz_{bm}	[m]	Bed level measurement error
η	[m]	Water surface elevation
θ	[-]	Shields parameter
θ	[deg]	Wave direction measured clockwise
θ_c	[-]	Critical Shields parameter for the initiation of motion
θ_m	[deg]	Mean wave direction
θ_{sf}	[-]	Value of Shields parameter when sheet flow occurs
$\kappa=0.41$	[-]	von Kármán constant
λ	[-]	Dimensionless breakwater design parameter
μ	$[kg.m^{-1}.s^{-1}]$	Dynamic eddy viscosity
ν	$[m^2.s^{-1}]$	Kinematic viscosity of water
ξ_{op}	[-]	Surf similarity parameter
ρ	$[kg.m^{-3}]$	Mass density of water
ρ_s	$[kg.m^{-3}]$	Mass density of sand
σ	[-]	Vertical coordinate in σ-coordinate system
σ_θ	[°]	Directional wave spreading
σ_w	$[m^2s^{-1}]$	Relative wave frequency
τ_b	$[kg.m^{-1}.s^{-2}]$	Bed shear stress
τ_{bcr}	$[kg.m^{-1}.s^{-2}]$	Critical bed shear stress
ν	$[m^2s^{-1}]$	Kinematic viscosity
ϕ_b	[-]	Porosity of the sand bed
χ	[-]	Dimensionless breakwater configuration parameter
<>	[-]	Ensemble average operator

Abbreviations

1D	One Dimensional
2D	Two Dimensional
2DH	Two-dimensional horizontal
BSS	Brier Skill Score
EF	Enhancement Factor
GLM	Generalised Lagrangian Mean
SPB	Submerged Porous Breakwaters
PEF	Porosity Effect Factor
RMSE	Root Mean Square Error
BSS	Brier Skill Score
WTC	Wave Transmission Coefficient

1 Introduction

1.1 Motivation and Problem Statement

Coastal zones support the world's most diverse and productive ecosystems which provide various vital services to humankind. Services such as, climate regulation, food supply and amenity are among the most important benefits provided by marine ecosystems. However, long stretches of coastal zones, not or insufficiently protected by ecosystems, face the permanent threat of erosion all around the world.

Coastal erosion, a gradual destruction of the coast by the impact of the sea, threatens economy, infrastructures, human activities and ecosystems in coastal zones worldwide. Fig. 1.1 shows an example of possible destructive effects of erosion in coastal areas. Coastal erosion may result in adverse effects on the coastal ecosystem (e.g. degrading water quality and vegetation; stressing corals and other habitats due to increasing sedimentation), as well as on tourism and fishery industry which are considered to be among the most important economic resources provided by coastal ecosystems. Therefore, it is of fundamental importance to preserve coastal ecosystems against the adverse effects of coastal erosion. Considering the residential value of coastal areas, it should be noted that, the coastal zones occupy less than 10% of the Earth's land surface while accommodating more than 60% of the world's population. Besides, recent estimates suggest that probably up to 75% of world's population will reside in coastal areas by 2025 (UNCED, 1992). Thus, protecting the coastal areas against erosion is also vital for residential purposes.

Fig 1.1: Destruction of the coastal road due to beach erosion, south of Bridlington, UK. (From Dailymail).

Based on the above discussion and because of economic, environmental and residential issues, coastal areas are of significant importance for societies living in these areas. Besides, the dramatic increase of erosion rate in coastal areas due to increasing sea level rise and storm severity, both caused by global climate changes, clearly imply the need of more efficient solutions for coastal protection against erosion, while preserving coastal ecosystems and beach amenity. The above discussion clearly suggests that, protecting coastal areas against erosion is a critical challenge which needs to be dealt with urgently.

Conventional coastal protection structures such as detached emerged breakwaters, although very efficient in terms of wave attenuation, result in some undesirable effects such as obstructing the view

of the sea and degrading water quality, both extremely harmful to coastal environment and tourism activities. Fig. 1.2 shows an example, where a detached emerged breakwater successfully builds up the beach in the lee of the breakwater but obstructs people's view on the sea.

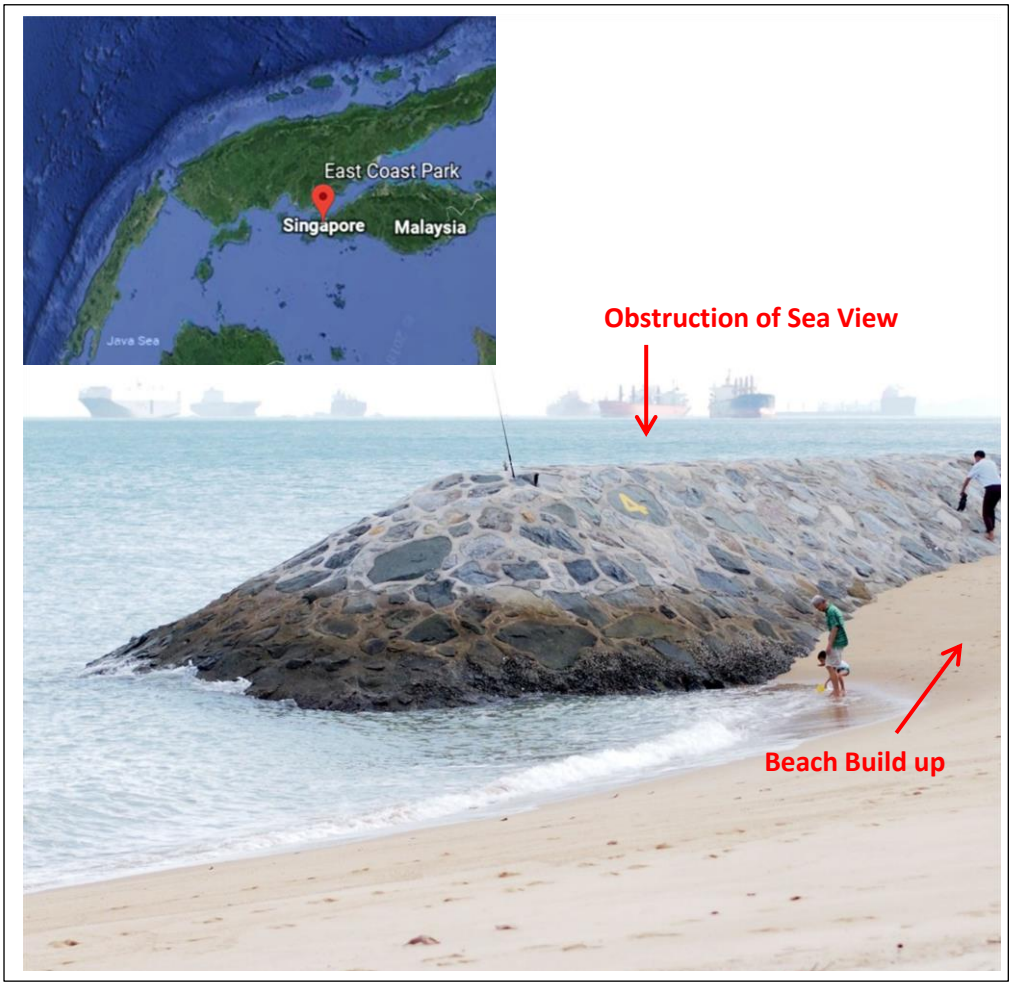

Fig 1.2: Detached emerged breakwater in the East Coast Park, Singapore. *Original photo is taken by By Filbert Koung, on 11 December, 2015 in Singapore (From National University of Singapore).*

Submerged breakwaters, even less efficient than their emerged counterparts in attenuating waves, may still represent an efficient solution with much less adverse impacts. Fig. 1.3 represents an example of a successful experiences with submerged breakwaters in the Beach Stabilization Project for Grand Cayman Marriot Hotel (Harris, 2003), Cayman Islands. However, all submerged breakwater projects are not as successful as in the Grand Cayman Marriot case. In fact, 70% of the submerged breakwaters reported by Ranasinghe and Turner (2006) resulted in unintended erosion of shoreline in the protected area, thus possibly implying serious knowledge gaps and high uncertainties associated with the effect of breakwater submergence in combination with breakwater porosity in performance of detached breakwaters.

Fig 1.3: Beach, before and after artificial reef submerged breakwater installation, Grand Cayman Mariot – south view (From Harris, 2003).

Unlike for emerged breakwaters, where a wide range of predictive formulae and design criteria are now available to evaluate their protective efficacy in coastal protection systems (e.g. Pérez Boloix 2011), for submerged breakwaters, there is a large gap of knowledge. This critical knowledge gap, along with the limited experiences on adopting this type of structures, leads to a high uncertainty in the assessment of the protective efficacy of submerged breakwaters.

In addition to the crucial knowledge gaps about the effect of submergence on the protective efficacy of breakwaters, there is also a very limited knowledge on the effect of structure porosity on the protective efficacy of submerged breakwaters. The latter is particularly important because submerged breakwaters in practice are commonly porous, and the combined effect of structure porosity and submergence makes the problem much more complex.

Based on the above discussion, there is an urgent need for further studies to improve the current understanding of design and performance of submerged breakwaters in coastal protection systems. Accordingly, this PhD aims to address the existing gaps of knowledge with respect to the effect of breakwater submergence and porosity on coastal morphology.

1.2 Objectives

Based on the problem statement described above, the primary and overall objective of this PhD study is to improve the current understanding and modelling of the protective performance of detached breakwater by addressing the current knowledge gaps associated with the effect of breakwater submergence and porosity on coastal morphology. This and further specific objectives are elaborated in section 2.4.

1.3 Methodology and organisation of the thesis

In order to achieve the objectives of this study, both numerical and experimental study approaches can be adopted. In this research, numerical modelling is the preferred approach because a systematic parameter study with a wide range of testing conditions (see WP 4 in Fig. 1.4) would be required, which is hardly feasible in the laboratory within the time frame and with the resources allocated to this study. Although the methodology of this PhD is described in details in section 2.4.2, a general overview of this methodology, which consists of five consecutive work packages, is given by Fig. 1.4

WP1	***Review and analysis of current knowledge and models***
▪ **Identifying more specifically the current knowledge gaps** ▪ **Selecting the most suitable model (s) to be considered for this research.** ▪ **Specifying the research objectives and methodology**	
WP2	***Improving/extending the selected model(s)***
WP3	***Validating and calibrating the improved/extended model***
WP4	***Performing a systematic parameter study on the effect of breakwater submergence and porosity***
WP5	***Developing predictive formulae for the protective efficacy and design criteria of submerged breakwaters***

Fig 1.4: General overview of methodology of this PhD study with five work packages (WP1-WP5)

The first work package, WP1, is addressed in chapter 2 which involves: i) Review and analysis of the current knowledge on the performance of submerged breakwaters in coastal protection systems. ii) Identifying the existing knowledge gaps with respect to effect of breakwater submergence and porosity. iii) Selecting the most suitable numerical model to be improved/extended and applied in this PhD study, and iv) Specifying in more detail the objectives and methodology of this study.

The second work package, WP2, is addressed in chapters 3 and 4. In chapter 3 a novel wave transmission coefficient formula for submerged porous breakwaters, which is necessary for improving /extending the numerical model selected in WP1, is developed and discussed. Then, in a part of chapter 4, a novel approach for implementing the new developed formula in the selected numerical model is proposed and validated. The rest of chapter 4, where the improved/extended model obtained from WP2 is calibrated and validated, is devoted to the WP3.

Chapter 5 is dedicated to WP4 and WP5, where based on a systematic parameter study, new predictive formulae and design criteria are developed to assess the protective efficacy of porous submerged breakwaters.

Finally, chapter 6 summarises the key results from WP1-WP5, including indications on their limitations as well as recommendations for future research on the performance of submerged breakwaters for coastal protection against erosion.

2 Review and analysis of current knowledge

Coastal regions are among the most dynamic landforms which are constantly changing in response to varying near-shore hydrodynamic forces and other actions. On the other hand, coastal regions are crucial for population residence, economy, amenity and ecosystems. Thus, it is often necessary to protect coastal zones against adverse effects of erosion, particularly in exposed and vulnerable areas. Detached breakwaters are typical coastal structures that are applied worldwide to protect such areas against coastal erosion. Although conventional detached emerged breakwaters are efficient for this purpose (Ranasinghe and Turner, 2006; Pérez Boloix, 2011), they are associated with undesirable effects such as obstruction of the view to the sea and degradation of water quality in the protected areas (e.g. Ranasinghe and Turner, 2006). Submerged breakwaters are also able to protect the beach against erosion with significantly less adverse effects on the water quality and the marine scenery. Though this protection is less efficient than that provided by their emerged counterparts, it has the advantage to be smoother, also in the sense that the effects on the neighbouring unprotected coastline are much less pronounced. Therefore, submerged breakwaters have been perceived to be an environmentally friendly structural measure against coastal erosion. In spite of the latter, emerged breakwaters have yet been generally favoured for beach protection (Cappietti et al 2011). Submerged breakwaters have so far deployed in Italy, Spain, Egypt, Israel, Japan, Australia and the USA (Kubowicz-Grajewska, 2015). For example, in Italy, the use of submerged breakwaters for coastal protection was started in 1980 (Lorenzoni et al., 2016) and resulted in more than 50 submerged breakwater systems by 1996 (Lamberti and Mancinelli, 1997) In addition to constructing submerged breakwaters, in Italy, many old detached emerged breakwaters have or are being converted into submerged breakwaters (Cappietti et al 2011, Mori et al 2009 and Pranzini et al 2018). Yet, a large fraction (ca.70%) of the built submerged breakwaters worldwide has failed to protect the beach, rather causing unintended erosion (e.g. Ranasinghe and Turner, 2006). This clearly implies that applying submerged breakwaters involves a high degree of uncertainty, mainly due to the higher complexity and diversity of the processes underlying the efficacy of submerged breakwaters in terms of reducing coastal erosion; but also due to the associated lack of knowledge hampering an improved design.Thus, a more systematic assessment of the current knowledge on the design and efficacy of submerged breakwaters is urgently required in order to identify more specifically the knowledge gaps and the research tasks to improve and expand the current knowledge. This chapter is therefore devoted to the review and analysis of the current knowledge related to:

(i) the effect of submerged breakwaters on nearshore sediment transport and morphological changes in coastal areas;
(ii) the design and efficacy of submerged breakwaters;
(iii) the numerical models which can be applied in this study.

Based on the results of this review and analysis, the objectives and methodology of this PhD study will be specified more precisely. Consequently, this chapter is organized as follows. Section 2.1 is devoted to examining the effect of submerged breakwaters on nearshore sediment transport and morphodynamic processes. Section 2.2 reviews the most relevant studies carried out on the design and performance of submerged breakwaters, with a focus on their main contributions and limitations. A detailed review on the available numerical models which could potentially be utilized for this study is presented in section 2.3, where the most relevant advantages and disadvantage of each model are outlined. Finally, based on the conclusions drawn from the aforementioned sections, the objectives and methodology of this thesis are more specifically defined in section 2.4. The structure of this chapter and the objectives of each section are depicted in Fig. 2.1:

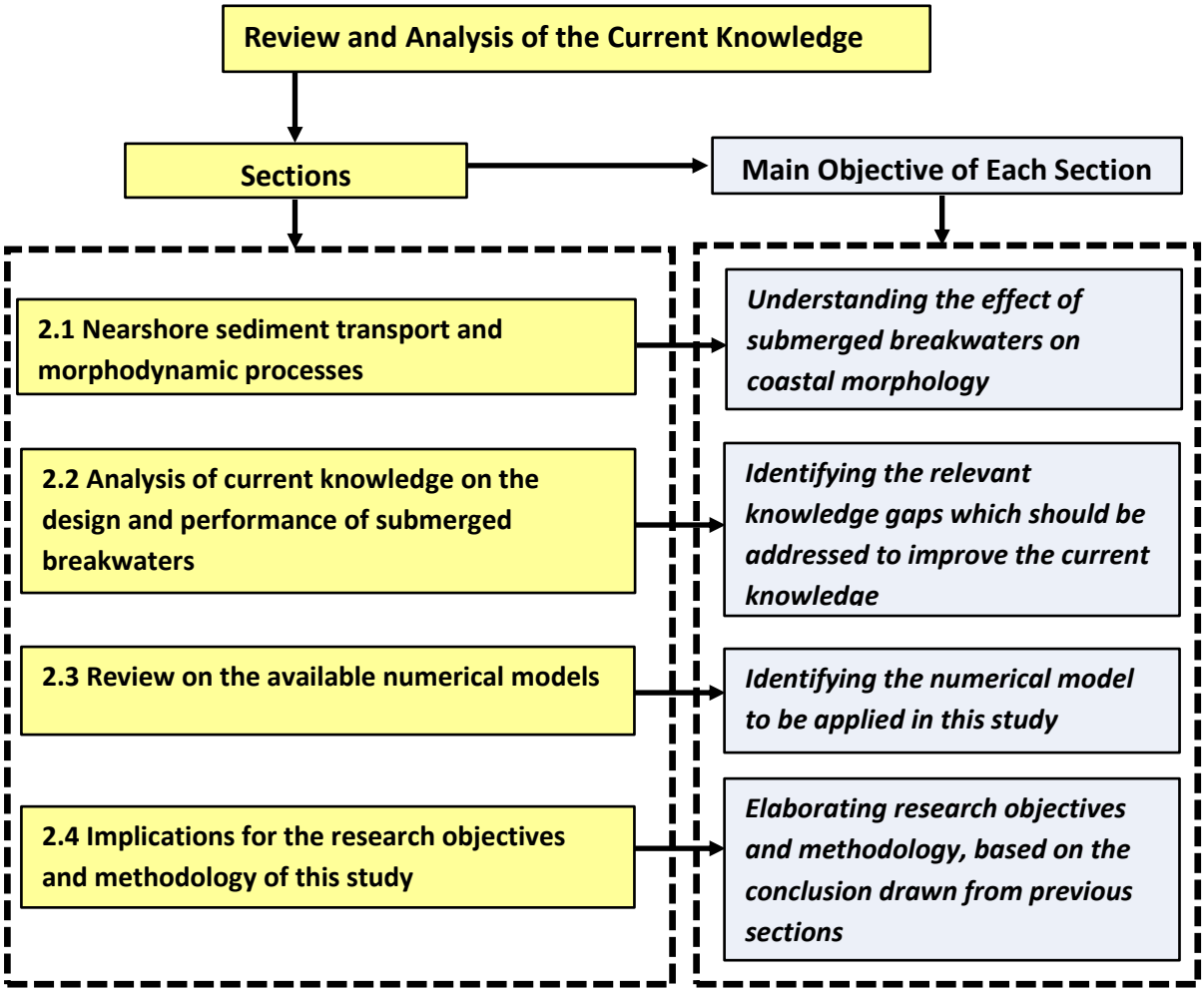

Fig 2.1: Structure of chapter 2 and main objective of each section of the chapter

2.1 Nearshore hydrodynamic and sediment transport processes

Understanding the effect of coastal structures on the beach morphology needs a basic knowledge of the nearshore sediment transport processes. Depending on the direction of sediment transport, the nearshore sediment transport processes are generally categorized into two types: cross-shore and longshore processes. Fig. 2.2 shows a schematic description of the longshore and cross-shore sediment transport processes in the nearshore. In this section, both types of sediment transport processes are briefly described and the effects of submerged breakwaters on these processes are elaborated.

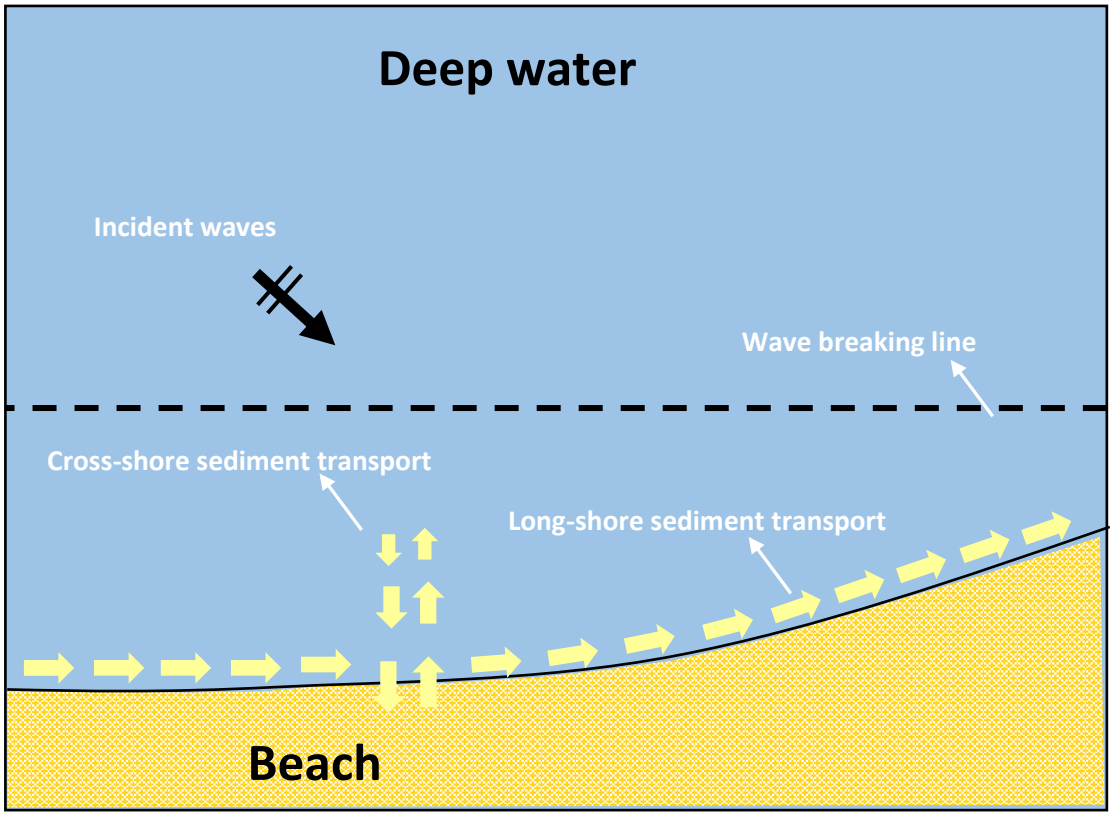

Fig 2.2: Schematic description of wave-induced nearshore sediment transport processes

2.1.1 Cross-shore hydrodynamic and sediment transport processes

As an important part of the coastal sediment transport regime, the cross-shore sediment transport plays an important role in coastal morphological changes, particularly at shorter time scales (e.g. time scale of storm event). Cross-shore sediment transport includes both offshore and onshore directed transport normal (perpendicular) to the shoreline (CEM, 2006a). The presence of submerged breakwater affects the cross-shore sediment transport pattern. Therefore, in this section, the cross-shore sediment transport in the open coast without any breakwater and in the protected coast leeward of the submerged breakwater are separately described in the following paragraphs:

(a) Cross-shore processes without breakwaters

The effect of cross-shore sediment transport on coastal morphology has yet been intensively investigated under both field and laboratory conditions, providing a good understanding of cross-shore sediment transport process in coastal regions (Li and Griffiths, 1970). Combining data analysis and cross-shore profile modelling, Ruggiero et al. (2003) showed that at short time scales cross-shore sediment transport processes play a dominant role in coastal morphological changes, as compared to longshore sediment transport. Generally, the cross-shore sediment transport rate depends on the spatial distribution (e.g. Li and Griffiths, 1970) and magnitude (Bakhtiyar et al., 2012) of the wave energy, the latter is directly proportional to the squared wave height. Detailed analyses show that the magnitude of the net cross-shore transport rate is closely related to energy dissipation, which determines the spatial distribution of wave energy (Li and Griffiths, 1970). Through a number of numerical tests, Bakhtiyar et al. (2012) showed that the increase of wave height, which results in the increase of wave energy, leads to an overall stronger sediment transport and thus more prominent morphological changes.

Outside the surf zone, the sediment transport is mainly limited to the near bed sediment transport, where the transport is weak (CEM, 2006a, Li and Griffiths, 1970) and can be directed either onshore or offshore (Van der Zandedn, 2016).

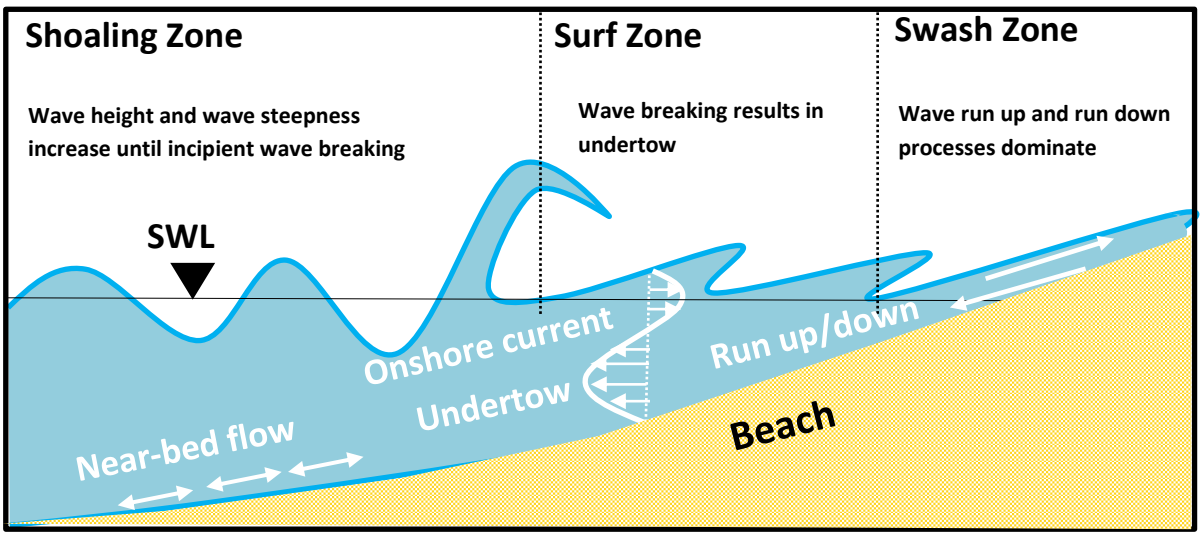

Fig 2.3: Wave-induced cross-shore flow processes driving sediment transport (Definition sketch)

Inside the surf zone, the major driving forces for morphological changes are generated by wave breaking (Li and Griffiths, 1970). The cross-shore flow, which is induced by wave breaking, is generally directed offshore in the lower part of the water column (above the wave bottom boundary) and onshore near the surface, resulting in a strongly non-uniform cross-shore flow profile over the water depth (e.g. Svendsen, 1984; Van der Zandedn, 2016). The offshore directed part of the cross-shore wave-induced flow is called *undertow* and compensates for the wave set-up and the onshore directed mass flux which are generated by the wave-breaking induced imbalance of radiation stress. This vertically non-uniform flow pattern leads to a circulation with the net offshore-directed undertow close to the bed and an onshore directed current near the surface. The former is considered of major importance for cross-shore sediment transport (e.g. Stive, 1987; Fredsoe and Deigaard, 1992; CEM, 2006a) and could transport a huge amounts of sediments in seaward direction. The wave boundary layer hydrodynamics in the surf zone has not yet been investigated in detail (Van der Zanden, 2016); however, as discussed by Svendsen (2006), inside the surf zone, cross-shore flow intensities in wave boundary layer might be ignored compared to return flow intensity. It should be noted that, rip currents, which also compensate for the shoreward mass flux are not considered in this section as they pertain to hydrodynamic processes in the plan view. Indeed, rip currents are considered in section 2.1.2 (see Fig. 2.10).

Inside the swash zone, the sediment transport is characterized by high instantaneous sediment fluxes in onshore and offshore direction, occurring respectively during the wave run-up and wave run-down. The net cross-shore sediment transport in the swash zone could be either onshore or offshore directed (Zhu and Dodd, 2015, Van der Zanden, 2016). Because of the limited predictive capability of transport models in the swash zone, some morphodynamic models do not explicitly calculate sediment transport rates at grid points covering the swash zone. Instead, sediment transport rates are calculated up to the 'wet' grid points nearest to the shoreline (e.g. DELFT3D). This approach distributes calculated erosion or accretion rates over the 'dry' and 'wet' cells adjacent to the shoreline (e.g. Deltares, 2014b). Some models calculate sediment transport rates over the complete swash zone, i.e. up to the maximum run-up distance (e.g. Walstra and Steetzel, 2003). However, these schematizations of sediment transport in the swash zone include many simplifications of swash zone dynamics and do not always yield reliable results (Van Rijn et al., 2011)

b) Cross-shore processes in the lee of submerged breakwaters

Submerged breakwaters are fully immersed structures which are mostly built porous using rock materials (Harris, 1996). The incident waves that reach the submerged breakwaters are partly reflected from the breakwater, partly dissipated over and through the breakwater, and partly transmitted leeward of the breakwater. There is very limited knowledge about wave reflection from

submerged breakwaters. Van der Meer et al. (2005) analyzed the existing laboratory data about wave reflection from submerged breakwaters and stated that, because of a huge scatter in the existing data, further research is required to obtain conclusive results about wave reflection from submerged breakwaters. Indeed, the dominant process by which submerged breakwaters protect the beach against erosion is energy dissipation through the premature breaking of the incident waves. Several cases have been reported, in which the wave energy dissipation at the structure was too small, making submerged breakwaters inefficient (e.g. Burcharth et al., 2007). The premature wave breaking induced dissipation is caused by the breakwater submergence and results in a significant reduction of wave transmission behind the structure (Kubowicz-Grajewska, 2015). However, as will be discussed in section 2.2.1, the porosity of the breakwater might also result in wave energy dissipation. In this study, the porosity n is considered as a measure of the void spaces in the material, and is expressed as the ratio of the pore volume to the total volume (i.e. $0 \leq n \leq 1$).

As mentioned before, wave energy dissipation is the main process affecting cross-shore wave-induced flow. Therefore, in addition to reducing the incident wave energy, and thus mitigating the overall sediment transport and morphological changes in the protected beach leeward of the breakwater, premature wave breaking at the submerged breakwater drives the cross-shore wave-induced flow in the vicinity of the structure (Zanuttigh et al., 2008). The premature wave breaking at submerged breakwaters results in a shoreward flow over the structure and wave set-up leeward of the structure. This shoreward mass flux and subsequent wave set-up may cause seaward return currents over and through the breakwater (e.g. Cappietti et al., 2006). The latter is called filtration flow (Zanuttigh et al., 2008) and occurs only if the breakwater is made of porous materials (Garcia et al., 2004, Zanuttigh et al., 2008, Lorenzoni et al., 2013). The offshore directed filtration flow might transport suspended sediments out of protected beach through the breakwater. Fig. 2.4 shows the main cross shore hydrodynamic processes in the vicinity of submerged breakwaters.

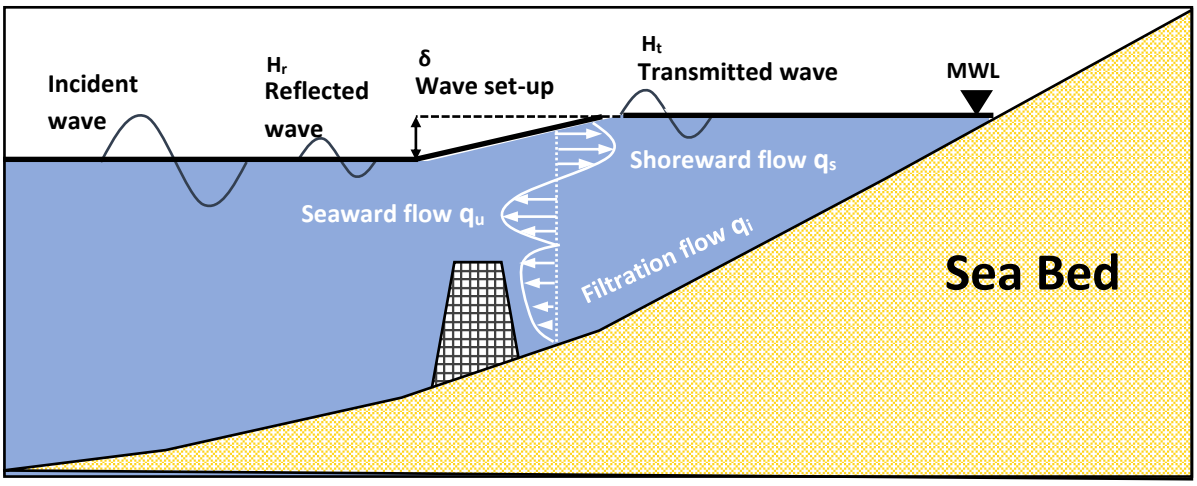

Fig 2.4: Cross-shore hydrodynamic processes in the vicinity of submerged breakwaters (Schematic)

Since the presence of submerged breakwaters mitigates the wave energy, the hydrodynamic forces in the surf and swash zones of the protected beach (see Fig. 2.3) becomes weaker, thus the overall sediment transport and morphological changes in the protected beach are also mitigated. Moreover, in case of porous submerged breakwaters, the offshore directed flow through the porous breakwater might reduce the wave set-up leeward of the submerged breakwater (Zanuttigh et al., 2008). This might weaken the undertow and the associated offshore directed sediment transport in the protected beach. A summary of the submergence and porosity induced cross-shore (2D) hydrodynamic and sediment transport processes are represented by Fig. 2.5, where the structure characteristics, hydrodynamic and sediment transport processes are presented in specific text boxes in the relevant sections, which are highlighted in blue and separated by dashed lines. The logical relation between text boxes is also represented by arrows:

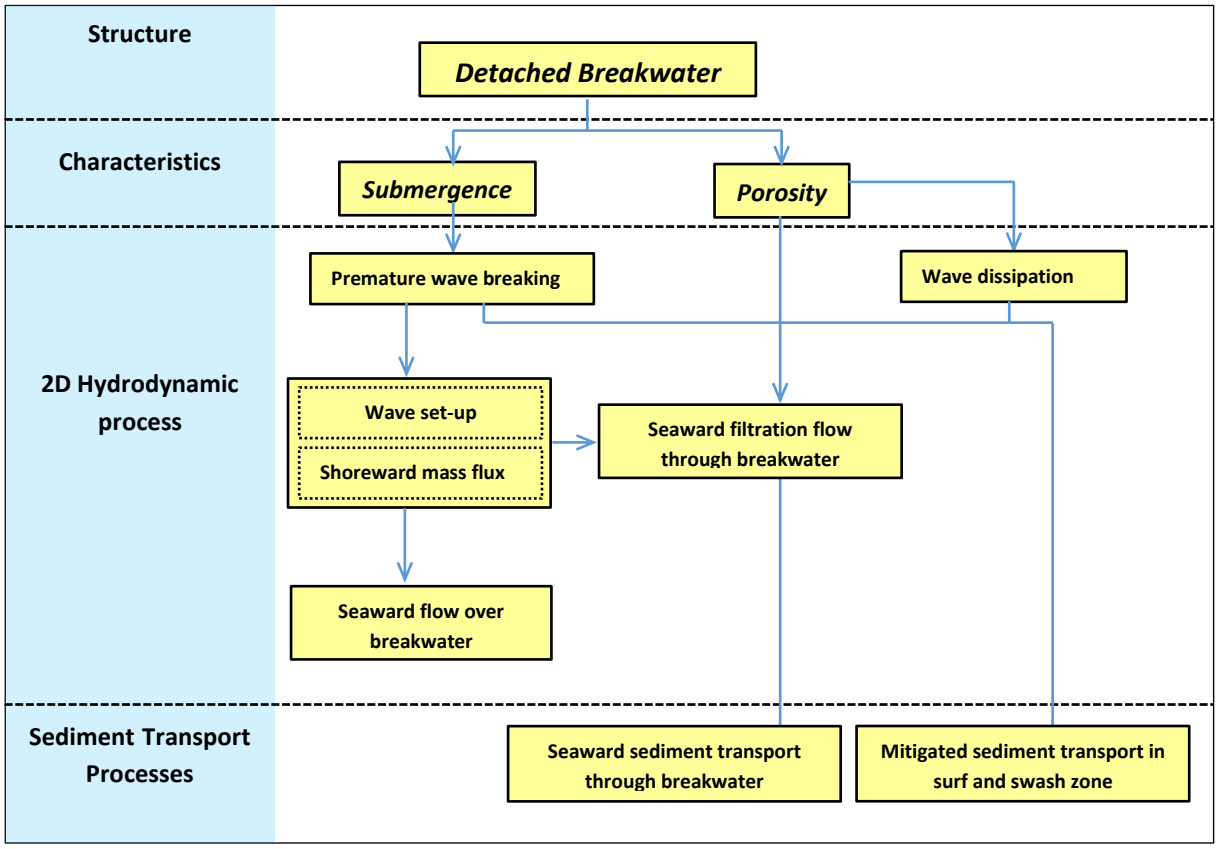

Fig 2.5: Cross-shore (2D) hydrodynamic and sediment transport processes resulting from breakwater submergence and porosity

2.1.2 Longshore hydrodynamic and sediment transport processes

The understanding of longshore sediment transport is also necessary for a reliable design of coastal structures. As mentioned in section 2.1.1, short-term morphological changes are primarily associated with cross-shore sediment transport process. In contrast, longshore transport is mainly linked to long term morphological changes (e.g. Fredsoe and Deigaard, 1992; Postachini et al., 2016). Submerged detached breakwaters affect the nearshore circulation pattern, and thus longshore currents and longshore sediment transport. Therefore, in this section the longshore sediment transport in the open coast without breakwater and in the protected coast leeward of the submerged breakwater are separately described in the following paragraphs:

(a) Longshore processes without breakwaters

Longshore sediment transport is driven by longshore currents which are generated by obliquely breaking waves (CEM, 2006b; Fredsoe and Deigaard, 1992). The longshore currents are fairly well known. When incident waves approach the coast at an oblique angle, due to the longshore component of the wave forces caused by breaking induced radiation stress gradient (e.g. Fredsoe and Deigaard ,1992; Kristensen, 2013), longshore currents flow along the beach. The resulting sediment movement is parallel to the coast and is referred to as littoral transport or longshore sediment transport.

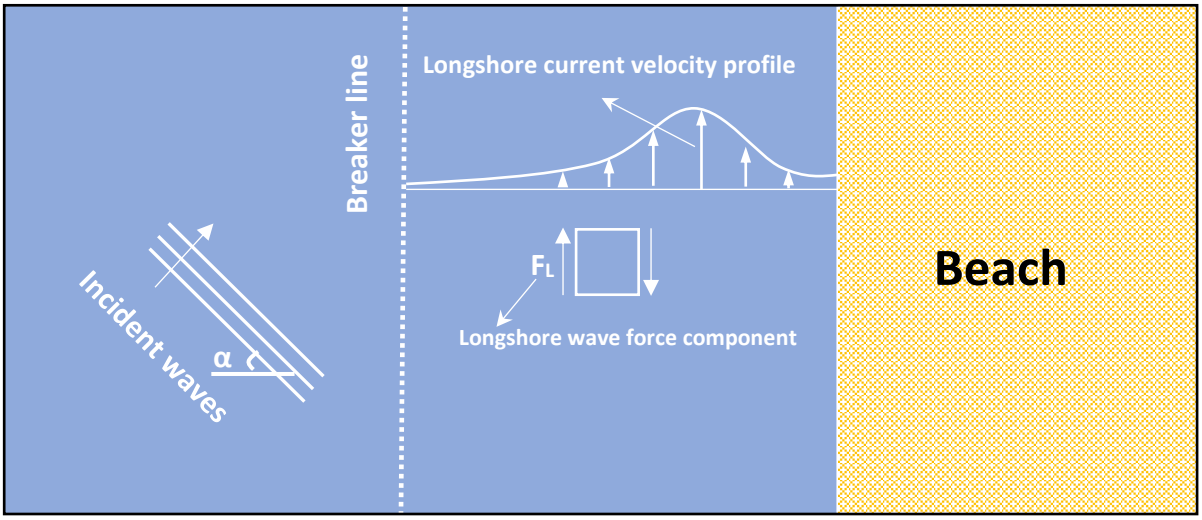

Fig 2.6: Wave-induced longshore flow processes (Schematic).

The magnitude of the longshore transport depends therefore on the height and direction of the breaking waves, as well as on the sediment characteristics. In order to simply calculate the bulk longshore sediment transport, many formulae for the integrated longshore transport rate have been developed. Among these formulae, the most widely applied is the CERC-formula (SPM, 1984). In process-based models, the empirical formulae for sediment transport rates are coupled with advection models to calculate longshore transport. A review on the most widely applied formulae to estimate longshore sediment transport in process-based models is provided by (Bayram et al., 2001).

The longshore sediment transport occurs primarily within the surf zone (CEM, 2006b). However, within the swash zone, the breaking waves are being evolved into the *surf bore* (surface roller) and start to *run up at an oblique angle*. The oblique breaking surf bores push the water up at an oblique angle in the swash zone and gravity forces causes backwash in cross-shore direction, perpendicular to the shoreline. This process forms a zig-zag sediment transport pattern which is called "*beach drift*"(Kamphuis, 1991).

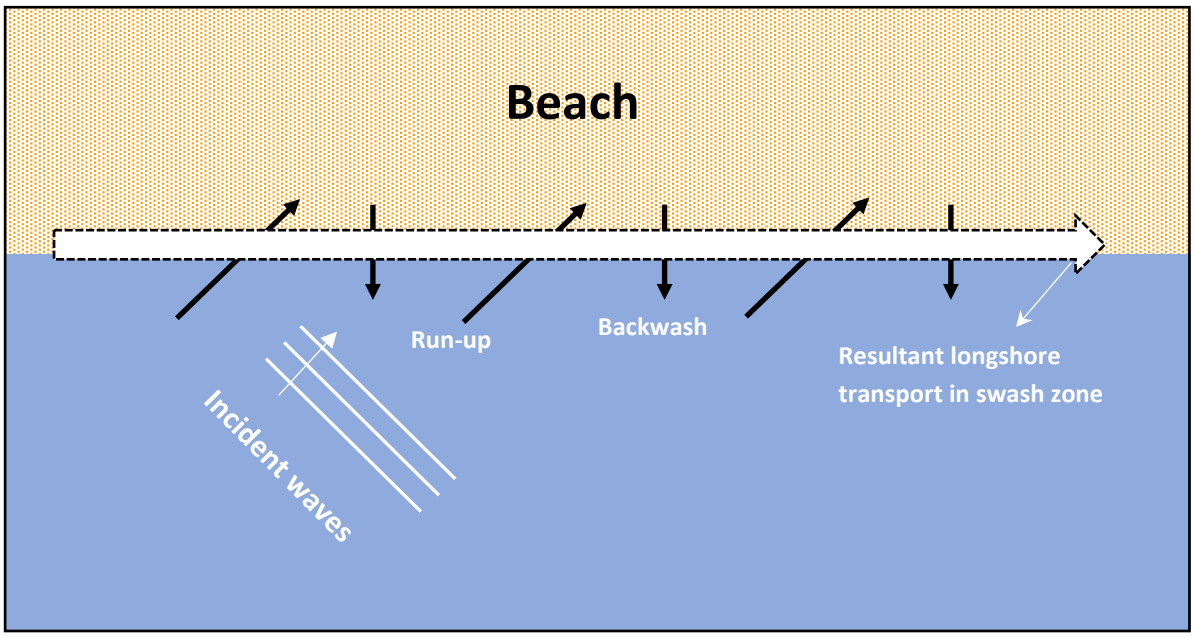

Fig 2.7: Zig-zag sediment transport pattern (beach drift) and resultant longshore transport in swash zone

Fig. 2.7 shows a schematic description of the oblique wave run-up and run-down (perpendicular to the shoreline), causing a zig-zag sediment transport pattern with a resultant longshore transport in the

swash zone. Currently, the longshore sediment transport in the swash zone is beyond the capabilities of most of the commonly applied sediment transport models such as GENESIS, DELFT3D and MIKE21. This might represent a significant limitation in sediment transport simulations where the longshore sediment transport in the swash zone becomes important, such as in estuarine beaches (Jackson et al., 2017). Although in some recently developed numerical models swash zone transport is introduced using semi-empirical models (e.g. Jiang et al, 2011), still more field and laboratory data are required to validate the applicability of these models to longshore sediment transport in the swash zone.

(b) Longshore processes in the lee of submerged breakwaters

Compared to the emerged detached breakwaters, where the longshore sediment transport pattern in the protected area leeward of the breakwater rarely results in beach erosion, (Ranasinghe and Turner, 2006; Pérez Boloix, 2011), the longshore sediment transport pattern in the lee of submerged detached breakwaters is more complicated and may cause either erosion or accretion.(Ranasinghe and Turner, 2006).

The longshore flow and sediment transport pattern in the vicinity of submerged breakwaters is mainly driven by wave breaking over the breakwater. As mentioned in section 2.1.1, premature wave breaking over the breakwater causes a shoreward flux over the structure and wave set-up behind it. The shoreward flux over the structure leads to diverging long-shore currents in the protected area (Fig. 2.8a). It should be noted that, in case of segmented submerged breakwaters, in order to maintain mass conservation, the shoreward mass flux partly leaves the protected area as a strong, localized offshore directed flow through the breakwater gaps. This offshore directed flow is called *rip current* and can transport a huge amount of sediments out of protected area (see Fig. 2.10). Besides, the wave setup in the protected area behind the breakwater causes an alongshore difference between wave set-up in exposed and protected areas, which are respectively denoted by δ_e and δ_p. This alongshore wave set-up difference causes an alongshore mean water level gradient. If $\delta_p > \delta_e$, this alongshore mean water level gradient enhances the divergent currents caused by the shoreward mass flux over the structure, while mean water level gradients caused by $\delta_p < \delta_e$, as shown in Fig. 2.8b may dominate and reverse the divergent currents near the shoreline and results in the convergent longshore currents (Ranasinghe et al., 2010, Villani et al., 2012). The latter, i.e. $\delta_p < \delta_e$, is the case, for example when the submerged breakwater is located sufficiently far from the shoreline. Under this condition, the adequately large distance between the submerged breakwater and the shoreline allows the transmitted waves to reform in the protected area. Therefore, the transmitted waves start to break in the nearshore within the protected area, thus causing a wave setup near the shoreline behind the structure. However, the reformed waves in the protected area are lower than those in the exposed area. Consequently, the wave setup in the protected area becomes lower than the wave set-up in the exposed area. Under such conditions, the longshore gradient of mean water level near the shore line dominates the divergent currents caused near the shoreline by the shoreward mass flux over the breakwater, and consequently drives convergent alongshore currents toward the protected area, as shown in Fig. 2.8b.

Wave diffraction caused by the wave height gradient between the protected and exposed area leeward of the breakwater may also result in the convergent longshore current leeward of detached breakwaters (Van Rijn, 2013). However, to the author's knowledge, the effect of wave diffraction on wave-induced longshore flows leeward of submerged breakwaters has not been investigated, probably due to the dominant effect of the longshore mean water level gradient (Vlijm, 2011; Villani et al., 2012). Wave refraction might also occur over submerged breakwaters. To the author's knowledge, this process has also never been investigated independently, and thus it is still unknown how the refraction over submerged breakwaters may influence longshore sediment transport and morphological changes in the protected area.

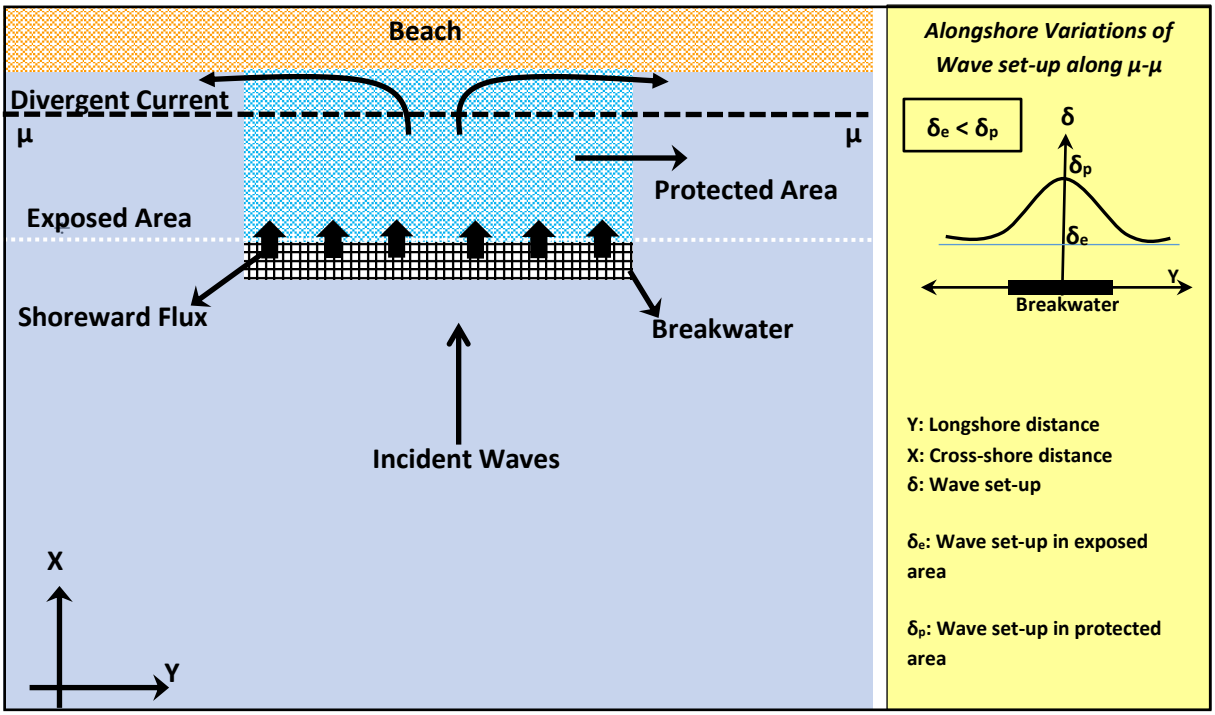

a. Divergent longshore currents.

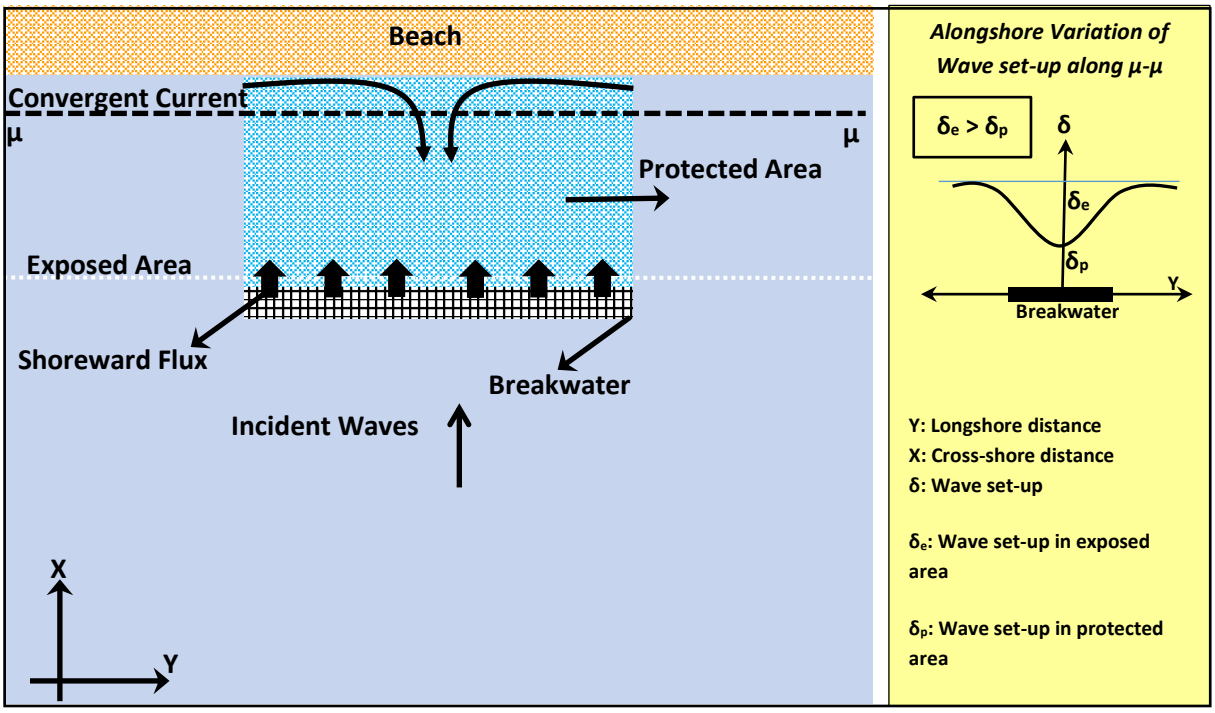

b. Convergent longshore currents.

Fig 2.8: Hydrodynamic processes resulting in diverging (a) or converging (b) longshore currents near the shoreline in the protected area behind a submerged breakwater

The presence of longshore divergent currents results in horizontal circulation pattern composed of two opposing circulation cells. This circulation pattern is called *2-cell pattern* and is perceived to cause erosive longshore sediment transport in the lee of submerged breakwaters (Ranasinghe et al., 2006; Ranasinghe et al., 2010; Ranasinghe and Turner, 2006; Dean et al., 1997; Loveless and MacLeod, 1999). Fig 2.9 shows a schematic representation of the two-cell erosive pattern formed by divergent longshore currents:

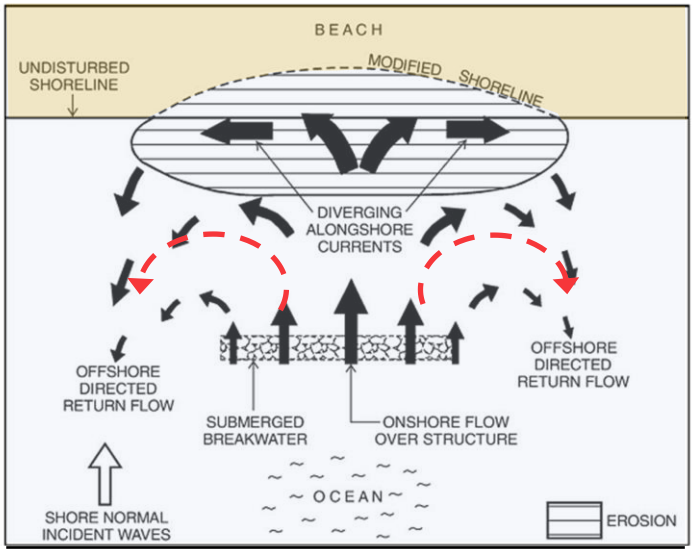

Fig 2.9: Schematic representation of an erosive 2-cell flow patterns in the lee of a submerged breakwater (Modified from Ranasinghe et al., 2006)

The convergent longshore currents also create a horizontal circulation pattern composed of four cells. This circulation pattern is termed *4-cell flow pattern* and is perceived to cause accretive longshore sediment transport pattern leeward of the breakwater (Ranasinghe and Turner, 2006 and Vlijm, 2011). Fig 2.10 shows a schematic representation of the 4-cell accretive pattern leeward of segmented breakwaters:

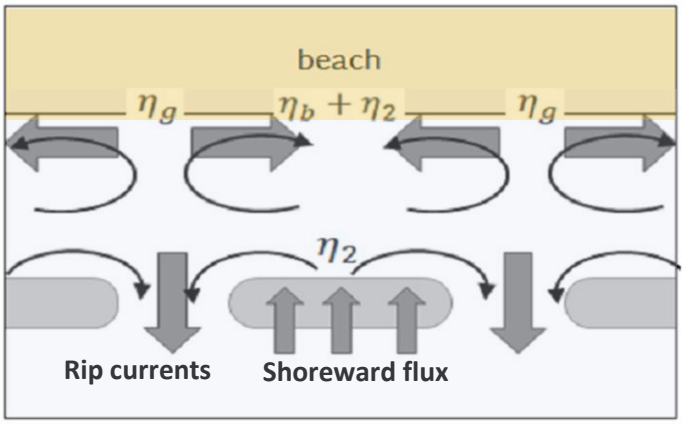

Fig 2.10: Schematic representation of an accretive 4-cell flow pattern in the lee of a submerged breakwater (Modified from Villani et al., 2012)

In the case of oblique incident waves, which generate long-shore currents in the exposed areas, this ambient longshore current interacts with the structure induced longshore currents. The resultant effect may be a weakened longshore current at the up—drift side of the shoreline behind the submerged breakwater, and an enhanced longshore current at the down-drift side (Turner et al., 2006).
This longshore current pattern can cause the formation of a skewed salient in the lee of the structure (Turner et al., 2006; Ranasinghe and Turner, 2006). Fig. 2.11 shows a schematic representation of the longshore flow pattern that may cause the formation of skewed salient in the lee of submerged breakwaters:

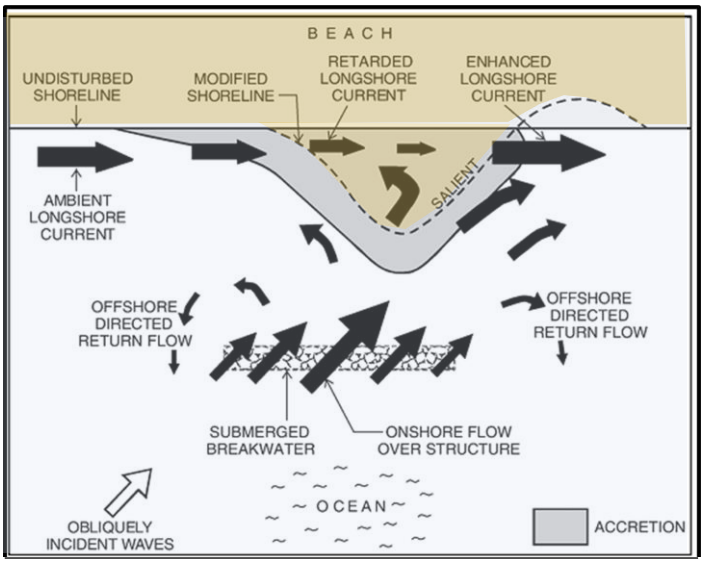

Fig 2.11: Schematic representation of the formation of skewed salient in the protected area (Modified from Ranasinghe et al., 2006)

A summary of nearshore hydrodynamic and sediment transport processes in plan view, which are caused by the breakwater submergence and porosity are represented by Fig. 2.12, where the structure characteristics, hydrodynamic and sediment transport processes are presented in specific text boxes in the relevant sections, which are marked in blue and separated by dashed lines. The logical relation between text boxes is also represented by arrows.

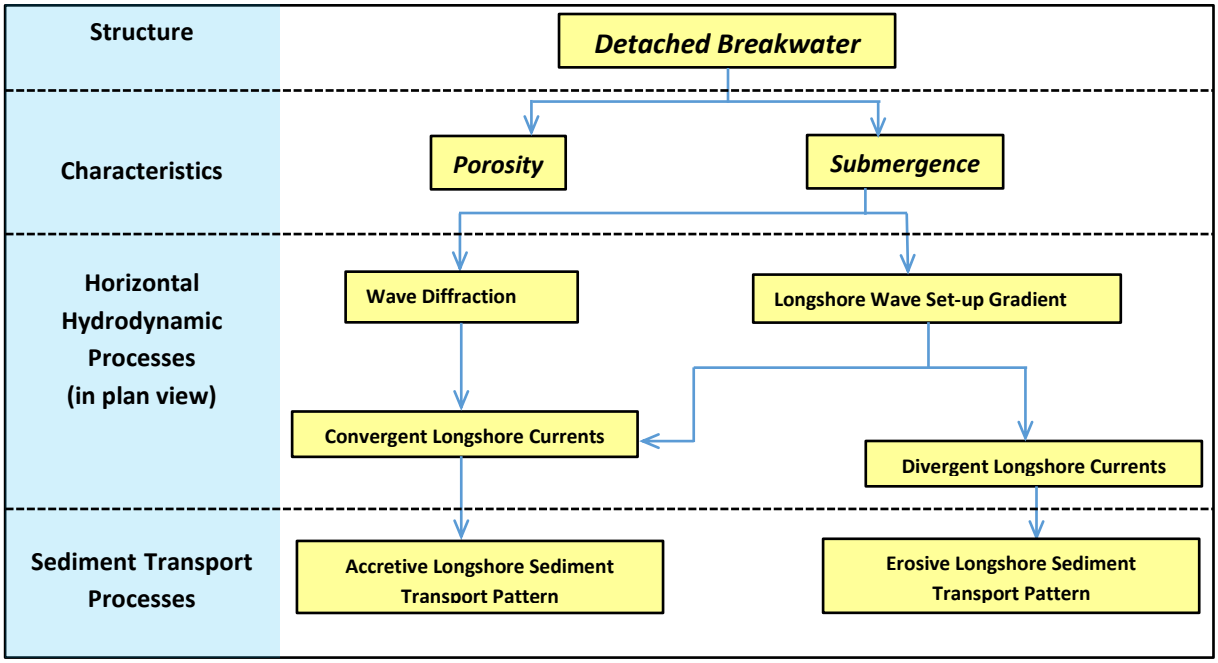

Fig 2.12: Nearshore hydrodynamic and sediment transport processes in plan view resulting from breakwater submergence and porosity

2.2 Available studies on the performance of submerged breakwaters

As mentioned above, offshore breakwaters are mainly constructed for mitigating the wave impact on beaches and protecting them against erosion. Ranasinghe and Turner (2006) reported the results of

a literature review on the monitored performance of submerged breakwater projects. They indicated that nearly 70% of the reported projects resulted in an unintended erosion. This clearly implies a serious lack of adequate knowledge on the effect of submerged breakwaters on coastal morphology.

In order to improve this knowledge, a large number of studies have been recently devoted to characterize the efficacy of submerged breakwaters. Some studies mainly focus on the ability of the breakwater to mitigate the wave action on the beach (hydraulic performance). While some studies mainly analyse the long-term (time scale of several storm events or/and months) effects of submerged breakwaters on coastal morphology, other studies rather focus on the short-term effects (time scale of a single storm event). The following sections provide a summary of the most relevant studies related to each of the aforementioned categories.

2.2.1 Hydraulic performance of submerged breakwaters

A review on hydrodynamic processes caused by wave-structure interactions are provided in section .2.1. The wave mitigation over the submerged structures arises from wave reflection and wave dissipation at the structure (see section 2.1.1). The difference between incident and transmitted wave heights triggers a set of hydraulic processes such as wave set-up and shoreward mass flux over the breakwaters, and consequently the horizontal and vertical flow recirculation leeward of the structure (see sections 2.1.1 and 2.1.1). All aforementioned processes contribute to the morphodynamic effect of the breakwaters in both short and long time scales.

Based on the discussion above, although the damping of incident waves by submerged breakwaters represents only one among all hydraulic mechanisms that arises from wave–structure interactions. As wave damping triggers other main hydraulic processes (e.g. horizontal and vertical flow circulation), in this chapter, it is considered as the key mechanism affecting the hydraulic performance of submerged breakwaters.

The morphological changes in the beach protected by submerged breakwaters are also particularly influenced by the structure capability to mitigate the wave impact on the beach (Pilarczyk, 2003a. Ahmadian and Simons, 2014, Buccinoi and Calabresse, 2007). The wave mitigation ability of submerged breakwaters is primarily described by wave transmission. Therefore, a reliable assessment of wave transmission at submerged breakwaters is an essential part of the functional design of breakwaters. Wave transmission is usually quantified by the **W**ave **T**ransmission **C**oefficient (hereafter **WTC**), K_t, which expresses the ratio between transmitted wave height just shoreward of the structure, H_t and incident wave height just seaward of it, H_i. (Fig 2.3)

$$K_t = \sqrt{\frac{E_t}{E_i}} = \frac{H_t}{H_i} \qquad 2.1$$

Here E_i, and E_t respectively stand for incident and transmitted wave energy, which are related through the energy conservation equation:

$$E_t + \underbrace{E_r + E_d}_{Mitigation} = E_i \qquad 2.2$$

Where E_r and E_d respectively stand for reflected and dissipated wave energy. As implied from the energy conservation law in Eq 2.2, submerged breakwaters mitigate the incident wave energy through the reflection and dissipation of incident waves. Thus, Eq 2.2 can be rewritten as:

$$\underbrace{\frac{E_t}{E_i}}_{K_t^2} = 1 - \underbrace{\frac{E_r}{E_i}}_{K_r^2} - \underbrace{\frac{E_d}{E_i}}_{K_d^2} \qquad 2.3$$

Here, K_r and K_d respectively stand for wave reflection coefficient and wave dissipation coefficient. Eq 2.3, clearly suggest that wave transmission coefficient parameter implicitly includes the *sum* of the of wave reflection and wave dissipation coefficient effects. Therefore, considering the wave transmission implicitly means that the *sum* of the effects of wave reflection and dissipation is considered. A common method to investigate the wave transmission is to perform physical model experiments. In such experiments, a scaled model of the entire breakwater profile is constructed and exposed to incident waves in a wave flume. Finally, based on the analysis of the measured wave conditions seaward and shoreward of the breakwater, the wave transmission characteristics are evaluated. In this regard, a large number of experimental studies have been performed to investigate the wave transmission characteristics of submerged breakwaters (Van der Meer and Daemen, 1994; d' Angremond et al., 1996; Seabroke and Hall, 1998; Van Der Meer et al., 2003; Van der Meer et al., 2005), many of them are dedicated to providing data and analyses required for developing simple practical predictive formulae for WTC. The WTC formulae serve as a practical engineering tool, especially in preliminary stages of the breakwater design for coastal protection systems. The following paragraphs are devoted to a brief review and discussion of empirically obtained WTC formulae which are most relevant for the present PhD research.

Van der Meer and Daemen (1994) reanalyzed the experimental data from earlier laboratory studies on wave transmission at low-crested structures. Based on the results, they used the mean diameter of rock materials (D_{n50}) to introduce dimensionless parameters affecting wave transmission, namely relative freeboard (R_c/D_{n50}), relative wave height (H_{si}/D_{n50}), and relative crest width (B/D_{n50}). As a result, the following simple linear relationship (hereafter **VD94**) between transmission coefficient K_t and nominal relative freeboard R_c/D_{n50} was determined:

$$K_t = a\frac{R_c}{D_{n50}} + b \qquad 2.4a$$

$$a = 0.031\frac{H_{si}}{D_{n50}} - 0.24 \qquad 2.4b$$

$$b = -5.24 s_{op} + 0.0323\frac{H_{si}}{D_{n50}} - 0.017\left[\frac{B}{D_{n50}}\right]^{1.84} + 0.51 \qquad 2.4c$$

$$s_{op} = \frac{H_{si}}{L_{op}} \qquad 2.4d$$

With: $0.075 < K_t < 0.8$

For: $-2.0 < R_c/D_{n50} < 2.0$, $1 < H_{si}/D_{n50} < 6.48$, $0.01 < s_{op} < 0.05$

Here, H_{si} is the incident significant wave height, L_p characteristics wave length ($L_p = gT_p^2/2\pi$), and T_p is the peak period. Van der Meer and Daemen (1994) pointed out that the applicability of VD94 is limited to relative incident wave height H_{si}/D_{n50}=1-6 and wave steepness S_{op} = 0.01-0.05. They argued that, although the VD94 suggests promising results despite the scatter of the data, its apparent disadvantage is the non- applicability to structures (e.g. impermeable structures) for which a mean diameter of rock materials D_{n50} is difficult to define. The effect of breakwater slope is not included in

VD94 formula expressed by Eq. 2.4. However, as shown by d' Angremond et al (1996) and Hur et al. (2011), the wave transmission decreases with decreasing submerged breakwater slope.

As a response to the need for a predictive WTC formula applicable to both impermeable and porous structures, one of the currently most applied formulae was proposed by d' Angremond et al. (1996). In their study, the same approach as that adopted by Van der Meer and Daemen (1994) was applied, but the proposed WTC formula is mainly based on the outer dimensions of the structures (e.g. freeboard R_c, crest width B):

$$K_t = a\frac{H_{si}}{R_c} + b\left[\frac{B}{H_{si}}\right]^c \left(1 - e^{-0.5\xi_{op}}\right) \qquad 2.5a$$

$$\xi_{op} = \frac{\tan\alpha}{\sqrt{s_{op}}} \qquad 2.5b$$

$a = -0.4 \quad b = 0.8 \quad c = 0.31$ Impermeable Breakwater

$a = -0.4 \quad b = 0.64 \quad c = -0.31$ Porous Breakwaters

For: $-2.5 < R_c/H_{si} < 2.5$

With: $0.075 < K_t < 0.75$

Here, tanα is the offshore slope of the breakwater. The WTC formula expressed by Eq. 2.5, hereafter **DA96**, includes parameters ***a***, ***b and c*** where the latter two (in 2nd term of Eq. 2.5) differ for impermeable and porous structures. Although DA96 is also applicable to porous structures, the formula does not include explicitly the effect of varying porosity on WTC.

Seabroke and Hall (1998) performed a series of laboratory tests to assess the hydrodynamic performance of submerged rubble-mound breakwaters under a wide range of design and wave conditions. In this study, a wide range of wave conditions and structure parameters (e.g. slope steepness, submergence depth, crest width) were considered. Based on the analysis of the results, the most important parameter governing the wave transmission was found to be dependent on the submergence conditions: (i) for lower submergence conditions ($R_c/H_{si} < 1$), it is the relative submergence R_c/H_{si} and (ii) for higher submergence conditions ($R_c/H_{si} > 1$), the crest width B becomes more important. The WTC formula proposed by Seabroke and Hall (1998) is as follows:

$$K_t = 1 - \exp\left[-0.65\left(\frac{R_c}{H_{si}}\right) - 1.09\left(\frac{H_{si}}{B}\right)\right] - 0.047\left[\frac{R_c}{D_{n50}}\frac{B}{L_p}\right] + 0.067\left[\frac{R_c}{D_{n50}}\frac{H_{si}}{B}\right] \qquad 2.6$$

For $0 < B \times R_c/(L_p \times D_{n50}) < 7.08$ and $0 < H_{si} \times R_c/(B \times D_{n50}) < 2.14$

The above WTC formula, hereafter **SH98**, is well bounded over the range of experimental data measured in the study. However, for very small or very large crest width *B*, SH98 yields physically incorrect results. Furthermore, SH98 does not account for the effect of varying structure porosity, though the tested breakwaters were permeable.

Van Der Meer et al. (2003) argued that DA96 is based on a limited data set and its applicability could be improved through refitting DA96 to a wider dataset. They reanalysed the DA96 using a larger dataset obtained by combining the datasets provided by d' Angremond et al. (1996) and those from the

DELOS project (Van Der Meer et al., 2003), and came up with an improved WTC formula for impermeable structures with.

$$K_t = -0.3\frac{R_c}{H_{si}} + 0.75\left(1 - e^{-0.5\xi_{op}}\right) \qquad \xi_{op} < 3 \tag{2.7a}$$

$$K_t = -0.3\frac{R_c}{H_{si}} + 0.75\left[\frac{B}{H_{si}}\right]^{-0.31}\left(1 - e^{-0.5\xi_{op}}\right) \qquad \xi_{op} \geq 3 \tag{2.7b}$$

With: $0.075 < K_t < 0.80$

For: $-2.5 < R_c/H_{si} < 2.5$, $0.37 < B/H_{si} < 43.48$, $0.02 < s_{op} < 0.06$

The larger data set used by Van Der Meer et al. (2003) is limited to impermeable structures. Accordingly, the WTC formula expressed by Eq. 2.7, hereafter **VDM2003**, applies only to impermeable structures.

Van der Meer et al. (2005) combined and refined smaller available datasets at the time to obtain larger dataset. The obtained larger dataset includes wave transmission coefficient data pertaining to both impermeable and porous structures. Van der Meer et al. (2005) applied DA96 to the refined dataset and found that DA96 only fits well the data for relative crest width $B/H_{si}<8$. Therefore, Van der Meer et al. (2005) proposed an improved formula, which is applicable to larger B/H_{si} values. For the improved formula, the maximum transmission coefficient K_{tu} is expressed as a function of relative crest width B/H_{si} as expressed by Eq. 2.8c

$$K_t = -0.4\frac{H_{si}}{R_c} + 0.64\left[\frac{B}{H_{si}}\right]^{-0.31}\left(1 - e^{-0.5\xi_{op}}\right) \qquad For \quad \frac{B}{H_{si}} < 10 \tag{2.8a}$$

$$K_t = -0.35\frac{H_i}{R_c} + 0.51\left[\frac{B}{H_{si}}\right]^{-0.65}\left(1 - e^{-0.41\xi_{op}}\right) \qquad For \quad \frac{B}{H_{si}} \geq 12 \tag{2.8b}$$

with:

$$K_{tu} = -0.006\frac{B}{H_{si}} + 0.93 \qquad K_{tl} = 0.005 \tag{2.8c}$$

For: $-5.0 < R_c/H_{si} < 5.0$, $0.37 < B/H_{si} < 102.12$, $0.002 < s_{op} < 0.07$

Here K_{tl} denotes the lower limits of wave transmission formula expressed by Eqs. 2.8a and 2.8b. Van der Meer et al. (2005) argued that the presence of porosity in the structure results in a weaker wave transmission.

Lorenzoni et al. (2016) performed an experimental study with a focus on the analysis of the effect of sea-storm characteristics and structure design on the wave transmission in submerged breakwaters. This analysis is based on the results of a series of laboratory tests carried out by Lorenzoni et al. (2013) to investigate the response of the cross-shore beach profile to traditional rubble-mound breakwaters. The experimental configuration was designed to reproduce the coastal defence system of the sandy beach of Gabicce Mare along the Italian Adriatic coast (see Lorenzoni et al., 2013). In this study, three configurations for emerged (A, D, E) and three configurations for submerged (B, C, F) breakwaters are examined.

The schematic representation of the design parameters varied in these configurations are shown by Fig. 2.13

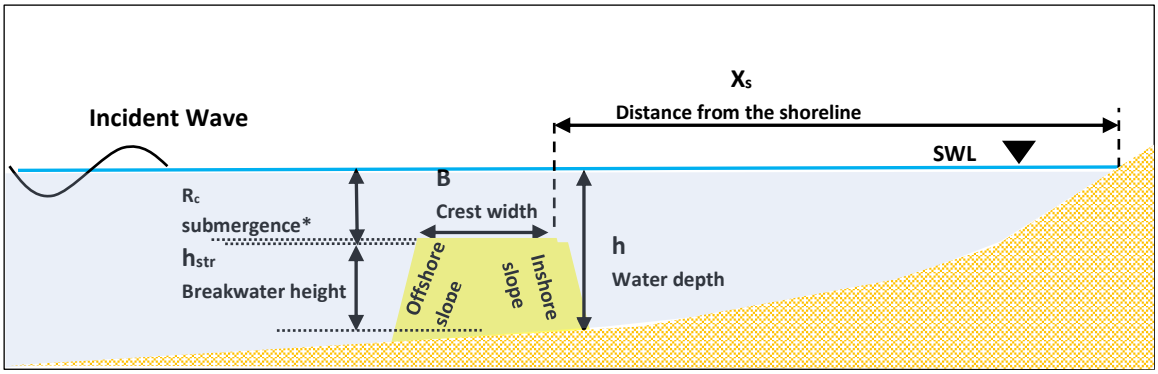

Fig 2.13: Definition of the breakwater parameters used by Lorenzoni et al. (2013) for the configurations in Table 2.1

The values of the design parameters depicted in Fig. 2.13 are given by Table 2.1

Table 2.1: Parameters of the various examined breakwater configurations (see parameter definitions in Fig 2.13)

Configuration	Rc (mm)	B (mm)	h (mm)	Inshore slope	Offshore slope	Distance from the shoreline (m)
A	+75	60	286	2:3	1:1	480
B	-25	65	700	2:3	1:1	480
C	-25	110	500	1:4	1:3	660
D	+75	95	150	2:3	1:1	620
E	+115	95	200	2:3	1:1	620
F	-25	100	700	2:3	1:1	620

The dimensions of the physical models of breakwaters were selected so that they represent typical offshore breakwaters commonly used in coastal defence systems of Adriatic beaches (Lorenzoni et al., 2016). The wave conditions reproduced in the wave flume represented intense sea storms observed in the Adriatic Sea, during 1999, 2002 and 2004. Results of the study revealed that, as expected, the mitigation of incident waves is better for emerged configurations than for submerged ones. In order to analyse the relation between the wave transmission, breakwater design parameters (see Fig. 2.12), and wave conditions, Lorenzoni et al. (2016) introduced the dimensionless parameter Φ that accounts for the breakwater configuration and wave conditions:

$$\Phi = \left(\frac{H_{si}}{L_p}\right)^{3}\left(\frac{B}{L_p}\right)^{0.5}\left(\frac{h_{str}}{h}\right)^{1.5} \qquad 2.9$$

Fig. 2.14 shows the relationship between the dimensionless parameter Φ and transmission coefficient K_t for various breakwater configurations

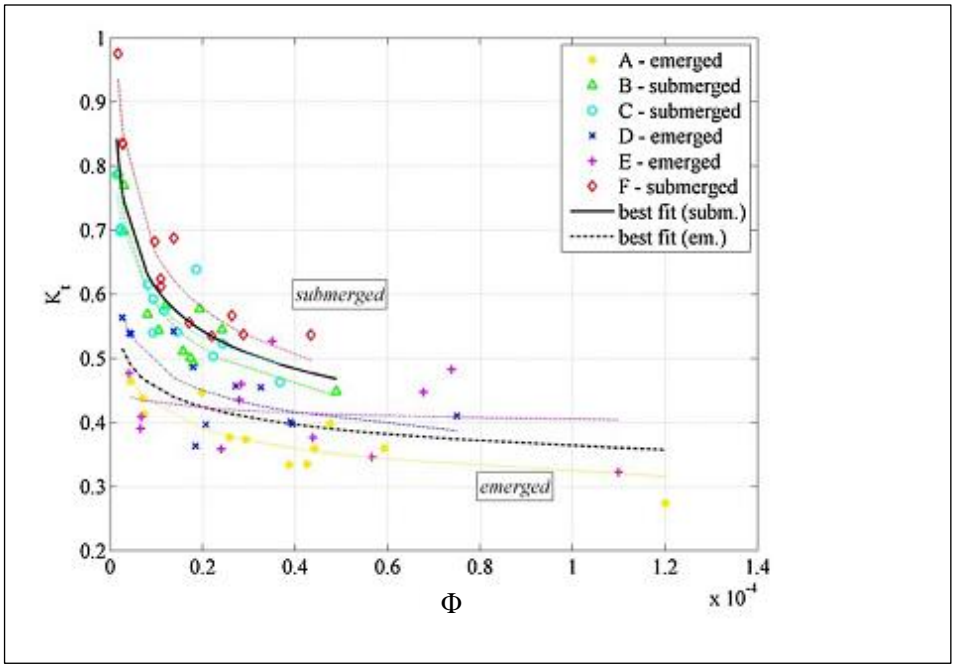

Fig 2.14: Relation between wave transmission coefficient K_t and parameter Φ as defined in Eq. 2.9 (Lorenzoni et al., 2016

The results plotted in Fig. 2.14 suggest that breakwater configurations located closer to shore result in smaller K_t compared to those located farther from the shore. As two major limitations, it should be noted that neither the effect of submergence, nor the effect of porosity on wave transmission has been considered in this study. Although, Lorenzoni et al. (2016) analysed a relatively large number of laboratory tests to study the relation between breakwater design, wave condition, and WTC, this study does not yield any predictive relationship for K_t, Table 2.2 provides a summary of the predictive formulae for WTC discussed above:

Table 2.2: Summary of currently most relevant WTC formulae for submerged breakwaters

Reference	Formula	Applicability	Limitations
Van der Meer and Daemen (1994) **VD94**	$K_t = a\frac{R_c}{D_{n50}} + b$ $a = 0.031\frac{H_{si}}{D_{n50}} - 0.24$ $b = -5.24 s_{op} + 0.0323\frac{H_{si}}{D_{n50}} - 0.017\left[\frac{B}{D_{n50}}\right]^{1.84} + 0.51$ $s_{op} = \frac{H_{si}}{L_p}$	$-2<R_c/D_{n50}<2$ $1< H_{si}/D_{n50}<6$ $0.01< s_{op}<0.05$	• Not applicable for impermeable structures • Not applicable for structure without specific size of materials
D' Angremond et al. (1996) **DA96**	$K_t = a\frac{H_{si}}{R_c} + b\left[\frac{B}{H_{si}}\right]^c\left(1-e^{-0.5\xi_{op}}\right)$ $a=-0.4 \quad b=0.64 \quad c=-0.31$ For Permeable Breakwaters $a=-0.4 \quad b=0.8 \quad c=0.31$ For Impermeable Breakwaters $\xi_{op} = \frac{\tan\alpha}{\sqrt{s_{op}}}$	$2.5<R_c/H_{si}<2.5$	• Based on limited dataset • No account for structure • Porosity
Seabroke and Hall (1998) **SH98**	$K_t = 1-\exp\left[-0.65\left(\frac{R_c}{H_{si}}\right)-1.09\left(\frac{H_{si}}{B}\right)\right]$ $-0.047\left[\frac{R_c}{D_{n50}}\frac{B}{L_p}\right]+0.067\left[\frac{R_c}{D_{n50}}\frac{H_{si}}{B}\right]$	$0<B\times R_c/(L_p\times D_{n50})<7.08$ $0<H_{si}\times R_c/(B\times D_{n50})<2.14$	• Not bounded for very large or very small crest width B • No account for structure porosity
Van Der Meer et al(2003) **VDM2003**	$K_t = -0.3\frac{R_c}{H_{si}} + 0.75\left(1-e^{-0.5\xi_{op}}\right) \quad \xi_{op}<3$ $K_t = -0.3\frac{R_c}{H_{si}} + 0.75\left[\frac{B}{H_{si}}\right]^{-0.31}\left(1-e^{-0.5\xi_{op}}\right) \quad \xi_{op}\geq 3$	$-2.5<R_c/H_{si}<2.5$ $0.37< B/H_{si}<43.48$ $0.02< s_{op}<0.06$	• Not applicable for porous structures
Van der Meer et al. (2005) **VDM2005**	$K_t = -0.40\frac{H_{si}}{R_c} + 0.64\left[\frac{B}{H_{si}}\right]^{-0.31}\left(1-e^{-0.5\xi_{op}}\right) \quad \frac{B}{H_{si}}<10$ $K_t = -0.35\frac{H_{si}}{R_c} + 0.51\left[\frac{B}{H_{si}}\right]^{-0.65}\left(1-e^{-0.41\xi_{op}}\right) \quad \frac{B}{H_{si}}\geq 12$	$-5.0<R_c/H_{si}<5.0$ $0.37< B/H_{si}<102.12$ $0.002< s_{op}<0.07$	• No account for structure porosity

Although VD94 and SH94 implicitly account for the effect of porosity through including D_{n50} which represents the size of porous materials, none of the existing WTC formulae explicitly accounts for the breakwater porosity. However, few studies have been carried out recently to investigate the effect of porosity on wave transmission

Ting et al. (2004) carried out an experimental study to investigate effect porosity on the transformation of non-breaking waves over submerged structures. The porosity values examined in this research varied from 0.421 to 0.912. Various porosities with different breakwater geometries were considered to obtain more information about porosity effects on wave fields. In this study, eight model geometries, each with six different porosities (in total 48 cases) were examined in the laboratory

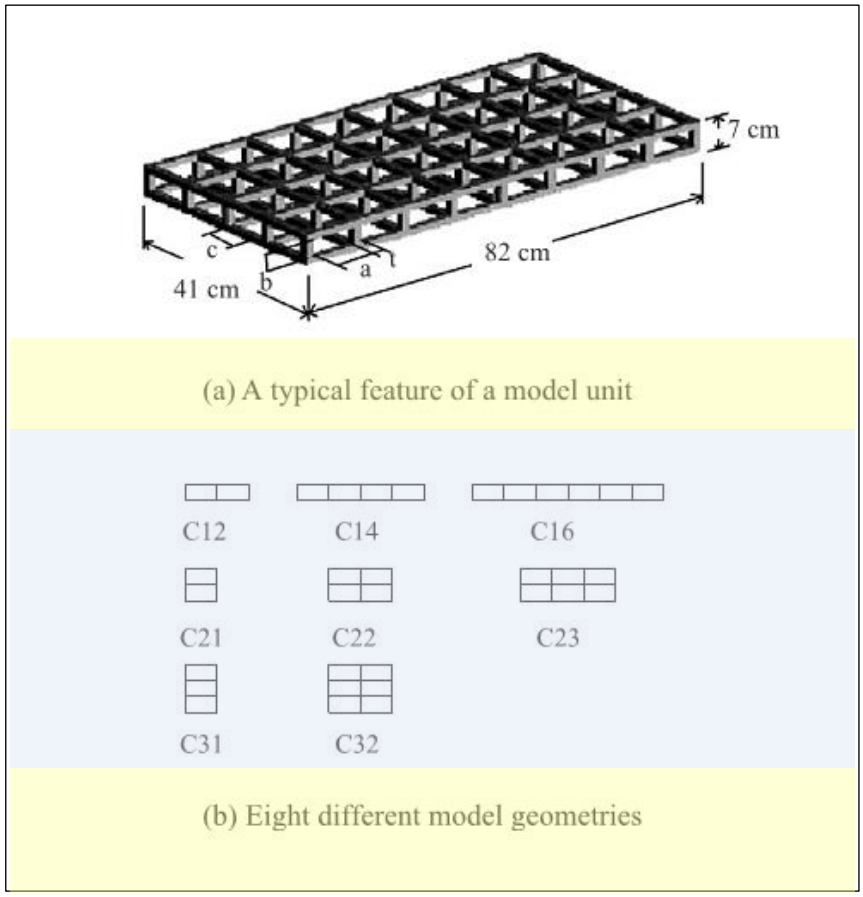

Fig 2.15: Different examined model geometries (Ting et al., 2004)

Based on the experimental measurements Ting et al. (2004) showed that, when porosity is 0.912, the effect of breakwater geometry on transmission of non-breaking waves is not clear and K_t values lie between 0.85 and 1.0

Although results of this study are presented as a series of scatter plots for various examined geometries, from which no predictive formula was derived, results of this study imply that:

(i) The effect of porosity on wave transmission becomes significant as the breakwater submergence decreases;
(ii) Lower values of porosity result in lower wave transmission;
(iii) For a given porosity, lower submergence and higher crest width result in lower wave transmission.
(iv) With decreasing porosity, the effect of breakwater submergence and crest width on wave transmission becomes more noticeable;

Rahman and Akter (2014) performed a laboratory study on porous vertical submerged and emerged breakwaters. The results suggest that the porosity and submergence might have a noticeable effect on wave transmission. It was also observed that the WTC decreases with increasing relative breakwater crest width (*B*/*L*). The results also show that for B/L=0.25 to 0.355, the increase of porosity from 0.45 to 0.75 leads to the increase of the WTC.

Losada et al., (1997) carried out a limited set of laboratory tests related to the analysis the effects of permeability of submerged breakwaters on wave transmission under non-breaking wave conditions. As a part of this study, both wave transmission and reflection coefficients (K_t & K_r) were measured in each experimental tests. The values of transmission and reflection coefficients obtained by Losada et al. (1997) are plotted in Fig. 2.16 as a function of relative water depth kh, where k is the wave number and h the water depth

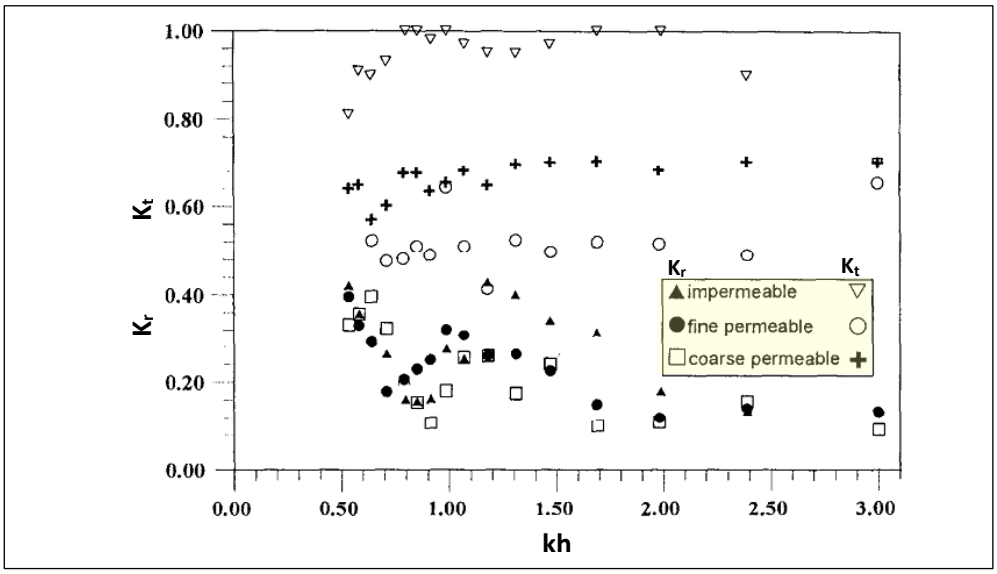

Fig 2.16: Effect of permeability of submerged breakwaters on transmission and reflection coefficients K_t & K_r as a function of relative water depth kh. (Modified from Losada et al., 1997)

As can be seen in Fig. 2.16, maximum WTC is observed for the impermeable case. As discussed by Losada et al. (1997), under non-breaking wave conditions, the dissipation induced in the porous structure plays the key role in wave transmission. The results show that, for a given geometry, WTC increases significantly with increasing porosity from 0.52 to 0.62. Although the results of this study provide a good insight into the effect of breakwater porosity on wave transmission, they are still not adequate to develop a WTC formula which explicitly includes the breakwater porosity, and thus to overcome the limitations of the existing WTC formulae with respect to breakwater porosityBreaching development and related geomorphological processes

2.2.2 Long-term morphodynamic effects of submerged breakwaters

A reliable estimate of the long-term effects of submerged breakwaters on coastal morphology is necessary for the application of this type of structures in coastal protection. Unlike emerged breakwaters, for which the effect of structure design on the long-term beach response to the breakwater has been widely studied (Rosati, 1990 and Pérez Boloix, 2011), the design of submerged breakwaters has not yet been adequately investigated. Therefore, more recently, some studies have been carried out to improve the design criteria and guidance for a better prediction of the long-term effect of submerged breakwaters on the coastal morphology.

Based on numerical simulations using the GENESIS model described in section 2.3, Hanson and Krause (1990) proposed the following criteria for the shoreline response to a detached breakwater with a given transmission coefficient K_t:

$$X_s / L_B < 48(1 - K_t)\left(\frac{H_o}{h}\right) \quad \text{Salient formation} \qquad 2.10a$$

$$X_s / L_B < 11(1 - K_t)\left(\frac{H_o}{h}\right) \quad \text{Tombolo formation} \qquad 2.10b$$

Here L_B is the length of breakwater and X_s the distance between the breakwater and the initial shoreline. These criteria were also verified for submerged breakwaters against some limited prototype data (Hanson and Krause, 1990), but they are not able to predict beach erosion as observed for many cases in the field.

Browder et al. (1996) reported a 3-year monitoring study on the efficacy of a submerged breakwater system made by Prefabricated Erosion Prevention (**P.E.P)** reefs for shore protection in Palm Beach (Florida, USA). The observed erosion throughout the project area, primarily in the lee of the breakwater implied the presence of divergent longshore currents in the lee of the breakwater. They argued that, although these currents were never directly measured in the field, they could be observed in the 1:16 fixed bed laboratory study carried out in the three-dimensional wave basin to evaluate the hydrodynamic response of the beach to Palm Beach P.E.P reefs. Fig. 2.17 illustrates an example of the trajectories of neutrally buoyant tracers observed in the laboratory, showing that, for normal incident wave conditions, the submerged breakwater induces divergent currents that originate from the center line of the structure in the leeside and flow toward the ends of the breakwater system, where the currents return offshore. More details of the laboratory tests are given by Dean et al. (1994).

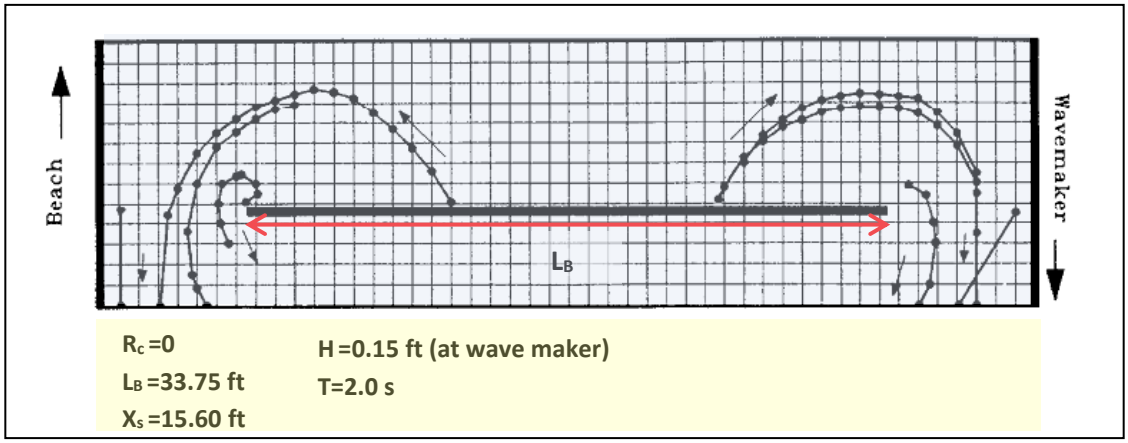

Fig 2.17: Example for the circulation pattern observed in the physical model study by means of neutrally buoyant tracers, implying to the divergent longshore currents. (Modified from Browder et al., 1996)

The magnitude of these alongshore currents were found to be affected by the breakwater submergence, the length of the structure, the distance between the structure and the beach, and the incident wave height (Dean et al., 1997). Although this study provides an insight into the design parameters affecting the flow pattern leeward of the submerged breakwaters, the flow measurements were not further analyzed to develop practical criteria for evaluating the effect of submerged breakwater design on horizontal circulation pattern and possibly associated morphological changes in the protected beach.

It should be noted that, in the laboratory test represented by Fig. 2.17, the ratio between the breakwater distance from the shoreline and length of breakwater is X_s/L_B=0.44 which agrees with erosive condition found by Cáceres et al (2005) (see Fig. 2.22)

Black and Andrews (2001) used the aerial photographs of the coastlines of south eastern Australia and New Zealand to quantify the shape and dimension of the salient observed in the lee of natural reefs and Islands. Based on the results, they developed a predictive relationship between the salient geometric characteristics and the reef dimensions. Ranasinghe and Turner (2006) plotted this relationship and compared it with a similar predictive relationship proposed by Silvester and Hsu (1997) for emerged breakwaters (Fig. 2.18).

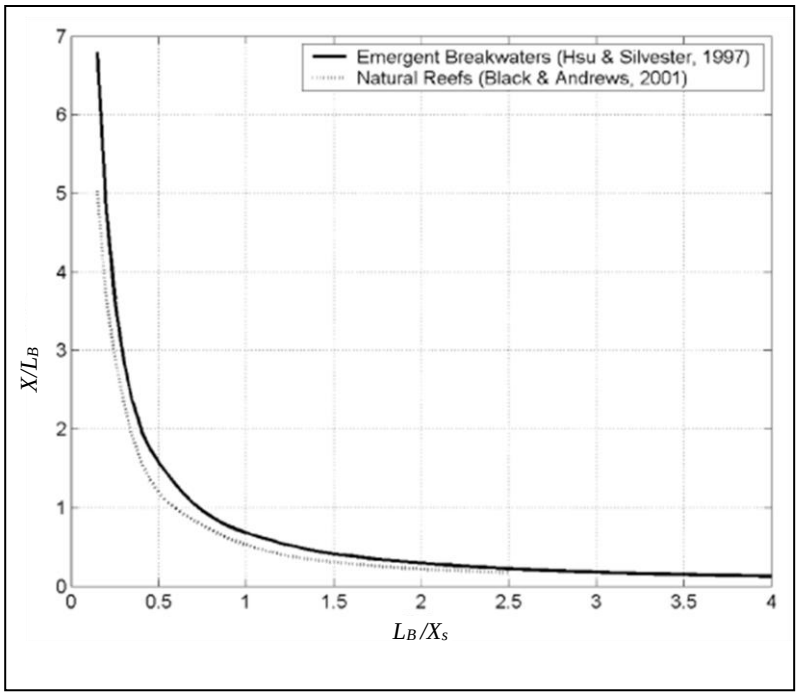

Fig 2.18: Relationships between the relative alongshore length of the structure L_B/X_s and relative distance between salient apex and structure X/L_B (with X denoting the distance between the structure and salient apex) for natural submerged reefs (Black and Andrews, 2001) and emergent breakwaters (Silvester and Hsu, 1997). (Ranasinghe and Turner, 2006)

As shown by Fig. 2.18, for a given distance between structure and shoreline, a longer structure leads to more accretion. The predictive formula proposed by Black and Andrews (2001) suggests that, similar to emerged breakwaters, for any combination of submerged breakwater length and distance from the shore, salient is formed in the beach protected by the breakwater. This is clearly in contrast to the fact that a significant portion of submerged structures cases has been reported to cause unintended erosion (Ranasinghe and Turner, 2006). Thus, the application of this predictive relationship for practical submerged breakwater design problems seems highly questionable.

Turner et al. (2001) performed a 1:50 scaled laboratory experiment to investigate the hydrodynamic and morphological impacts of the yet well-known Gold Coast artificial reef structure. Because of the large size of the reef model, it was not feasible to use movable bed material and thus lightweight materials were employed to reproduce the structure-induced shoreline changes. The experimental facilities and observed shore-line erosion/accretion pattern are shown in Figs. 2.19a and 2.19b. All tested waves were oblique with respect to the initial shoreline. The formation of a salient behind the structure and the down-drift erosion are shown in Fig 2.19b. These morphological changes are attributed to the interaction between the structure-induced divergent currents and the ambient

longshore current, resulting in the weakening of the ambient longshore current along the up-drift section of the shoreline behind the reef and its enhancement along the down-drift section.

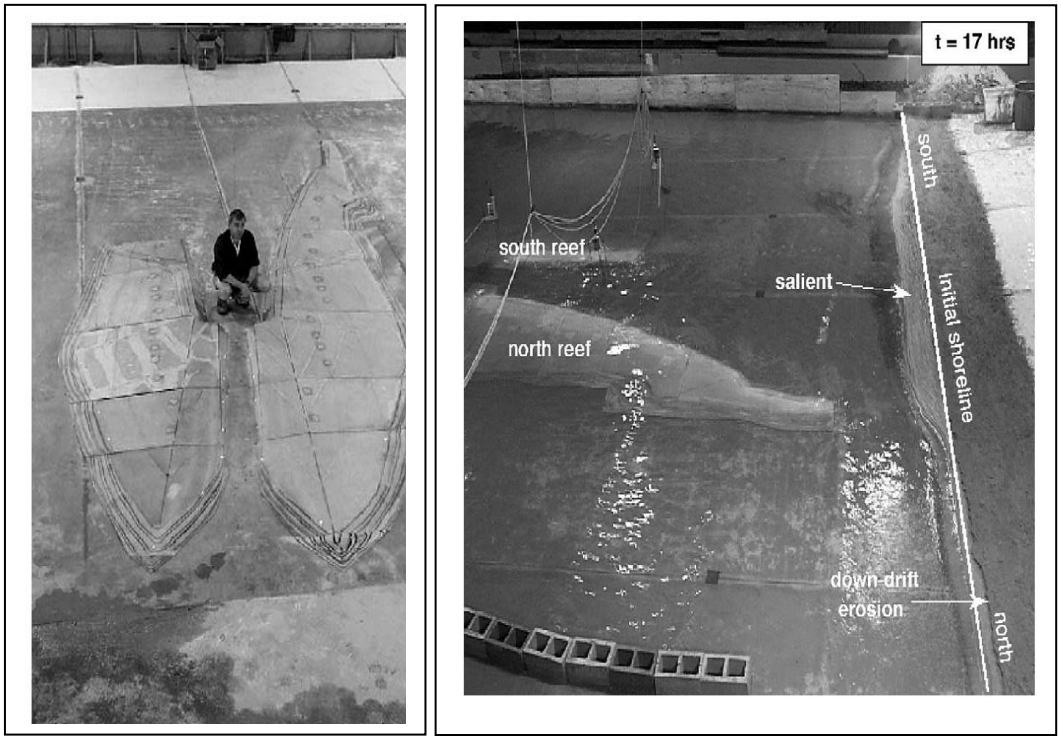

***(a)** Overview of the physical model* ***(b)** Salient growth and down-drift erosion in the lee of the structure*

Fig 2.19: Physical model of the Artificial Surf Break at the Gold Coast, Australia (Turner et al., 2001).

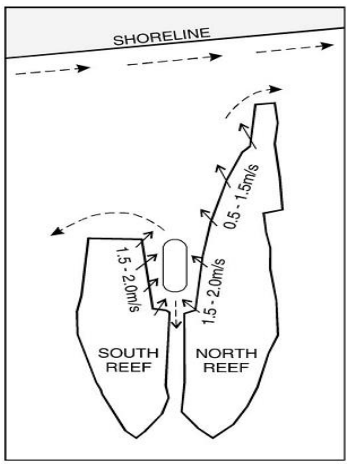

Fig 2.20: Nearshore circulation pattern observed in the laboratory study on the Artificial Surf Break of the Gold Coast, Australia. (Turner et al., 2001)

Cáceres et al. (2005) performed a numerical study to investigate the effect submerged breakwater parameters on coastal morphology. In addition to the commonly considered breakwater parameters such as length and distance from the shoreline (e.g. Hanson and Krause, 1991; Black and Andrews, 2001) the effect of breakwater submergence and incident wave height are also examined by Cáceres et

al. (2005). For this purpose, they applied the morphological changes obtained after 200 hours of simulations in the protected zone behind the structure, which is delimited by the structure heads as lateral boundaries, the structure itself as the up-wave alongshore boundary, and the undisturbed shoreline at a distance X_s as the down-wave boundary (Fig. 2.21)

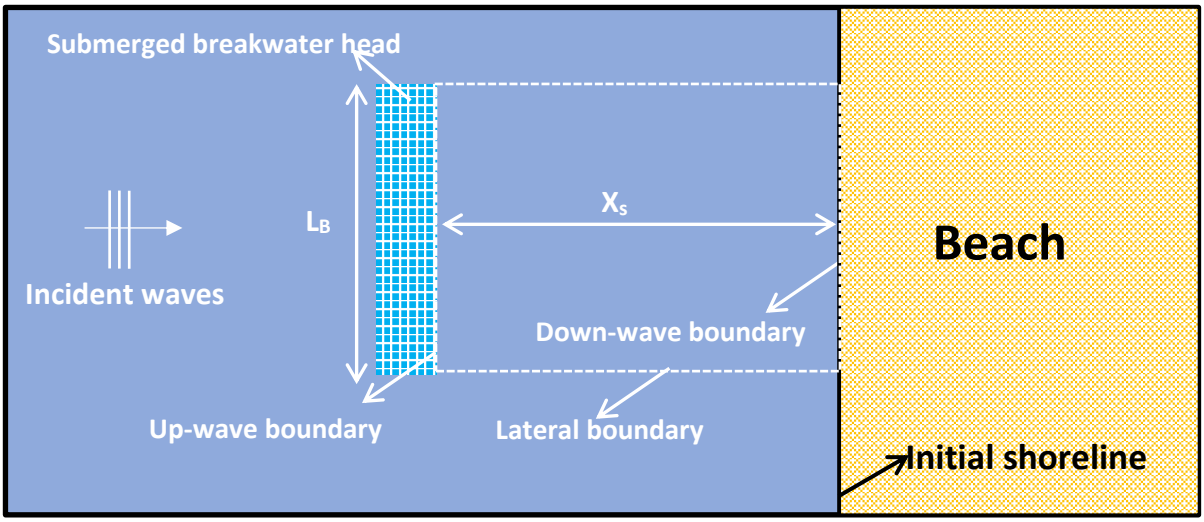

Fig 2.21: Protected zone in computational domain as defined by Cáceres et al. (2005). Dashed lines represent the boundaries of the defined protected area

Different configurations for a submerged structure have been examined in the numerical simulations, with R_c= -0.5m and -1.0m, X_s= 95, 150, 185, 275, 350, 480, 600, 700 and 800 m, and with the significant incident wave height of H_s=1m, 2m and period of T=4s. In order to illustrate that the morphodynamic effect of submerged breakwaters is mainly controlled by the breakwater location with respect to the shoreline, the averaged seabed evolution $\overline{z_b}$ is plotted in Fig. 2.22 against the relative breakwater distance from the shoreline X_s/L_B:

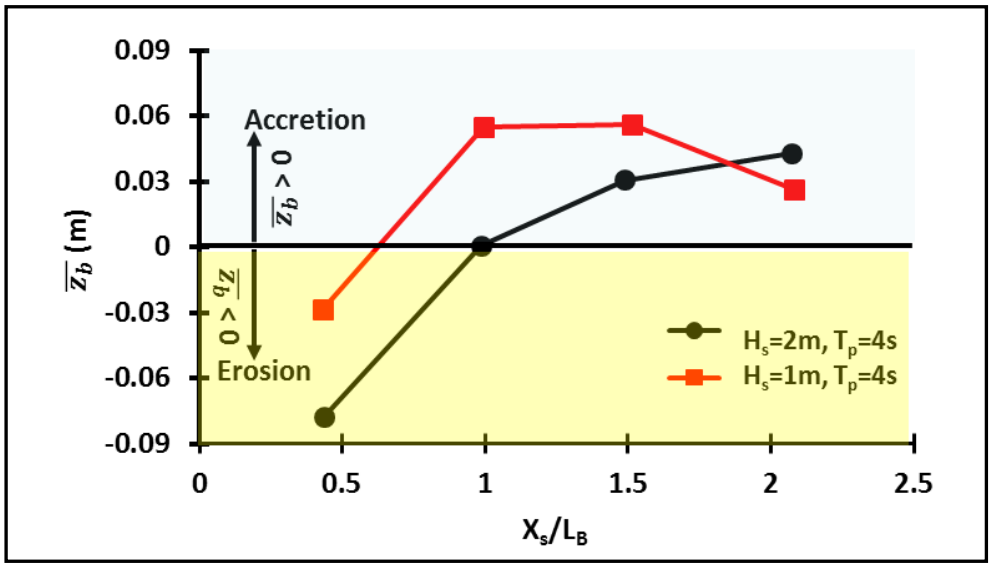

Fig 2.22: Averaged seabed level changes $\overline{z_b}$ (- for erosion and + for accretion) in the defined protected area as a function of X_s/L_B under shore-normal waves (Modified from Cáceres et al., 2005)

As shown by Fig. 2.22, a structure located close to the shoreline (X_s/L_B< 1) results in erosion, while a structure farther from the shoreline results in accretion. Furthermore, Fig. 2.22 also shows the effect of high (H_s=2.0 m) as compared to low (H_s=1.0 m) wave energetic condition on the minimum critical value of the relative distance X_s/L_B to avoid the occurrence of shoreline erosion: X_s/L_B > 1 for H_s=2.0 m

and X_s/L_B >0.55 for H_s=1.0 m; this suggests that the determination of the X_s- threshold (e.g. Fig. 2.26) should also account for the incident wave height.

For the above mentioned range of conditions tested, Cáceres et al (2005) concluded that the breakwater submergence does not have noticeable effects on the overall sediment transport and morphological changes. However, the tested range of conditions is rather limited to draw any final conclusions on the applicability of the results to predict the effect of submerged breakwater design on coastal morphology. Moreover, the effect of structure porosity on the morphological changes in protected area has not been considered.

Ranasinghe et al. (2006) applied MIKE 21 (see section 2.3) to study the shoreline response to an idealized impermeable V-shaped multi-functional submerged structure (artificial surfing reef). In total, 15 numerical simulations were carried out, in which varying distance between initial shoreline and apex of structure crest (X_s), submergence depth (R_c), and wave incidence direction (θ) clockwise from the shore normal direction were examined for movable bed conditions. For the modelling of the bed material, sand with D_{50} = 0.25 mm was selected, and the non-erodible condition was applied to the submerged breakwater footprint area. All numerical simulations were run until morphodynamic equilibrium, defined as the state for which seabed change rates are below 1 cm/day. As reported by Ranasinghe et al. (2006), the maximum simulation period to reach morphodynamic equilibrium was 2 months. In this study, the effect of submerged breakwater on coastal morphology is quantified by the maximum calculated displacement of the 1 m depth contour (Y), for which negative values indicate landward displacement (i.e. erosion) and positive values indicate seaward displacement (i.e. accretion). The predicted mode (erosion/. accretion) and magnitude of shoreline response (Y) for all fifteen numerical simulations performed by Ranasinghe et al. (2006) are summarized in Table 2.3.

Table 2.3: Mode and magnitude of shoreline response obtained from MIKE 21 simulations by Ranasinghe et al. (2006)

Xs (m)	SNCL1		OBCL1		SNCL2	
	Shore-normal waves R_c= -0.5 m		Oblique waves R_c= -0.5 m , θ=7°		Shore-normal waves R_c= -1.0 m	
	Test	Y(m)	Test	Y(m)	Test	Y(m)
100	SNCL1-100	-30	OBCL1-100	-25	SNCL2-100	-20
150	SNCL1-150	-10	OBCL1-150	20	SNCL2-150	-10
250	SNCL1-250	65	OBCL1-250	50	SNCL2-250	50
350	SNCL1-350	55	OBCL1-350	40	SNCL2-350	50
450	SNCL1-450	30	OBCL1-450	30	SNCL2-450	25

Y=maximum displacement of the 1 m depth contour. Y<0: landward displacement (i.e. erosion), and Y>0: seaward displacement (i.e. accretion). X_s=distance from initial (undisturbed) shoreline to apex of structure crest. SNCL=shore normal wave condition and OBLC = oblique wave incidence

A can be initially concluded from the result presented in Table 2.3, beyond a certain offshore distance (Here X_s =250 m), the effect of the structure on shoreline evolutions starts to disappear.

Moreover, based on the results, Ranasinghe et al. (2006) argued that the structure submergence only slightly affects the magnitude of erosion/accretion in the lee of the structure, which could be understood from the absolute value of Y (i.e. lower absolute value of Y means lower magnitude of shoreline response). As discussed by Ranasinghe et al. (2006), the lower crest level (i.e. higher submergence) results in a slightly decreased accretion/erosion, while the mode of shoreline response. (i.e. erosion/accretion) was observed not to be affected by submergence. However, later Ranasinghe et al. (2010) showed that the decrease of breakwater submergence may change the mode of shoreline response.

Overall, the simulation results confirm that, in shore-normal wave condition (Labelled by SNCL in Table 2.3), the 2-cell and 4- cell circulation pattern, which are shown by Fig. 2.23b and 2.24b, respectively correspond to beach erosion and accretion. Numerical simulation results also show that, under oblique wave condition (Labelled by OBCL in Table 2.3), the longshore flow pattern may result in skewed morphological changes (see Fig. 2.25). Numerical simulation results also show that, with the increase of distance between breakwater and undisturbed shoreline, the erosive shoreline response changes into accretive response. Based on the above discussion, depending on the design parameters, submerged breakwaters may result in shoreline erosion or accretion in the protected area. This is basically different from the beach response to emergent breakwaters, where generally shoreline accretion occurs under all conditions. Figs. 2.23-2.25 show some examples of numerical simulation results, highlighting the key results summarized above:

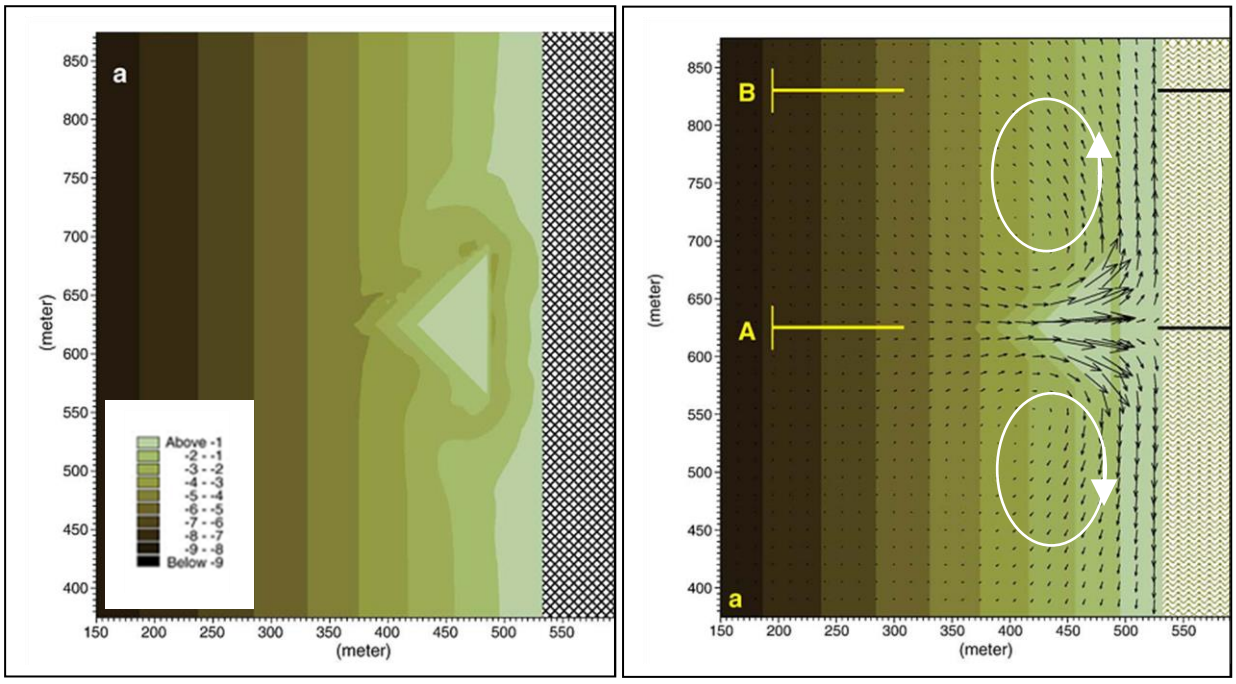

***a**: Final bathymetry* ***b**: Flow Pattern*

Fig 2.23: Example results from the numerical simulations for test SNCL1-100 (Modified from Ranasinghe et al., 2006)

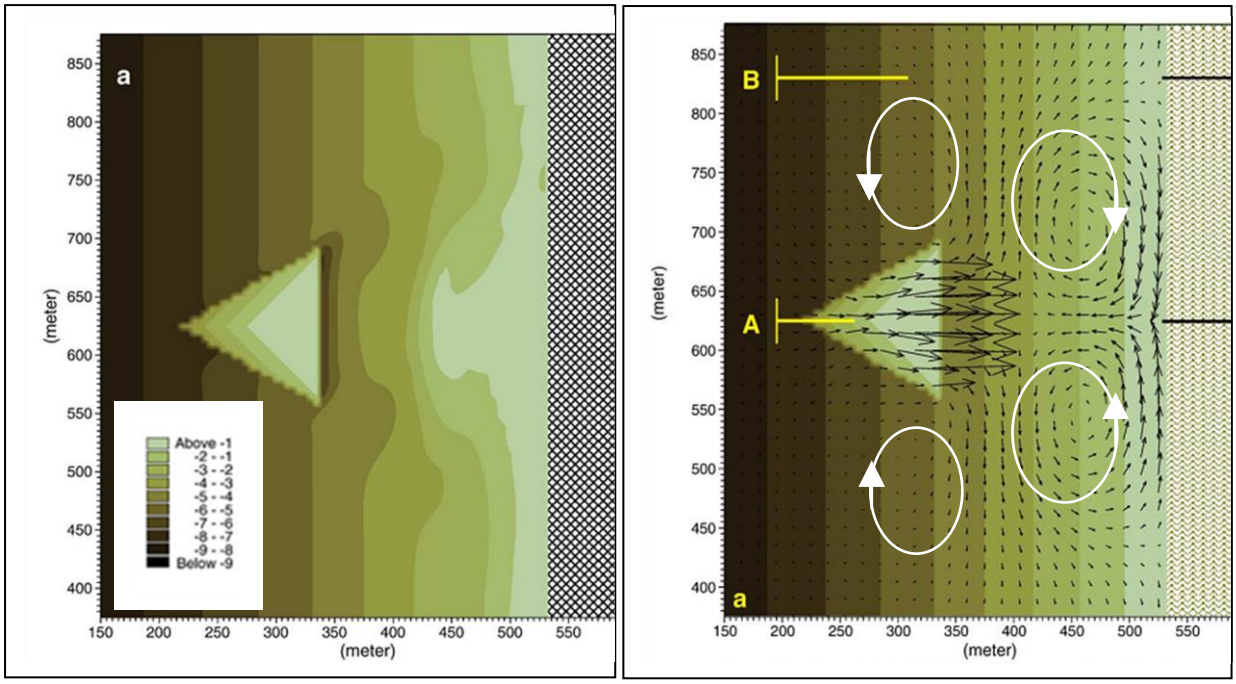

***a**: Final bathymetry* ***b**: Flow Pattern*

Fig 2.24: Example results from the numerical simulations for test SNCL1-250 (Modified from Ranasinghe et al., 2006)

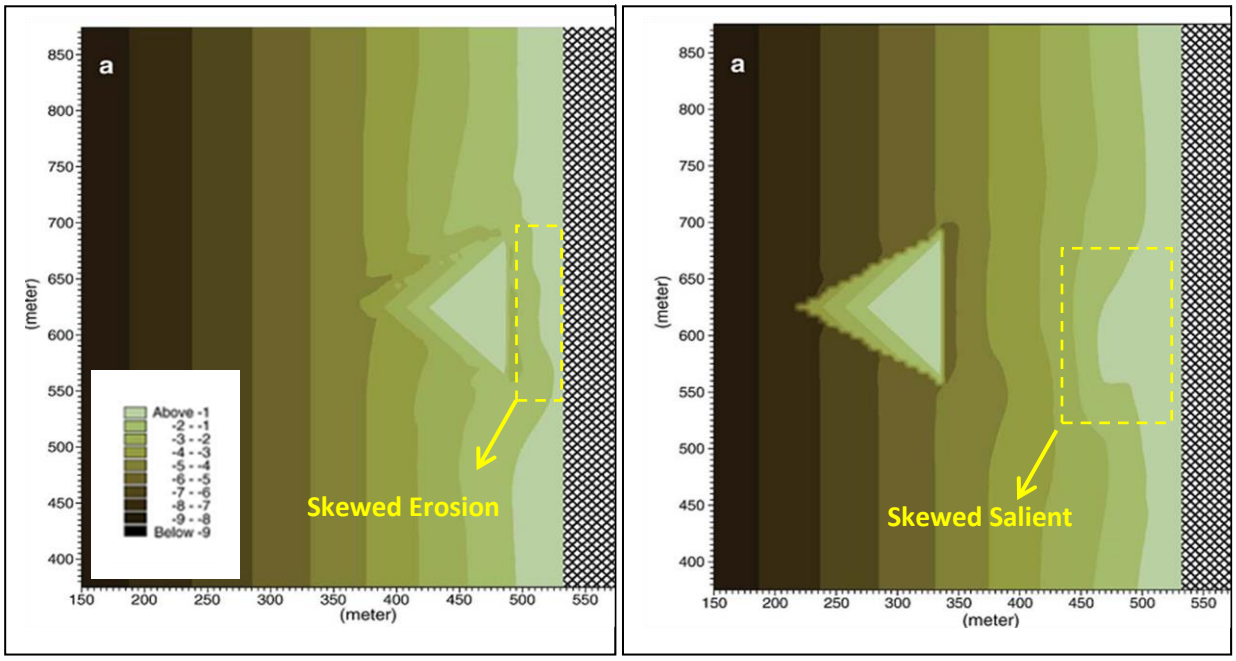

***a**: OBCL1-100* ***b**: OBCL1-250*

Fig 2.25: Example results from the numerical simulations for the oblique wave condition (Modified Ranasinghe et al., 2006)

Ranasinghe et al. (2006) concluded that in addition to the distance between breakwater and initial shoreline, the wave incidence angle may also have a noticeable effect on morphological changes in the beach protected by submerged breakwaters. Accordingly, for both oblique and normal incident wave conditions, Ranasinghe et al. (2006) used numerical simulation results to propose a very preliminary design curve relating the predicted magnitude of shoreline response (Y) to distance between the undisturbed shoreline and structure (X_s), the alongshore length of the structure (L_B), and the natural surf zone width (SZW). The obtained design curves presented in Fig. 2.26a suggest that, regardless of wave incidence direction, accretion can be expected for X_s/SZW >1.5 while X_s/SZW <1 will result in shoreline erosion.

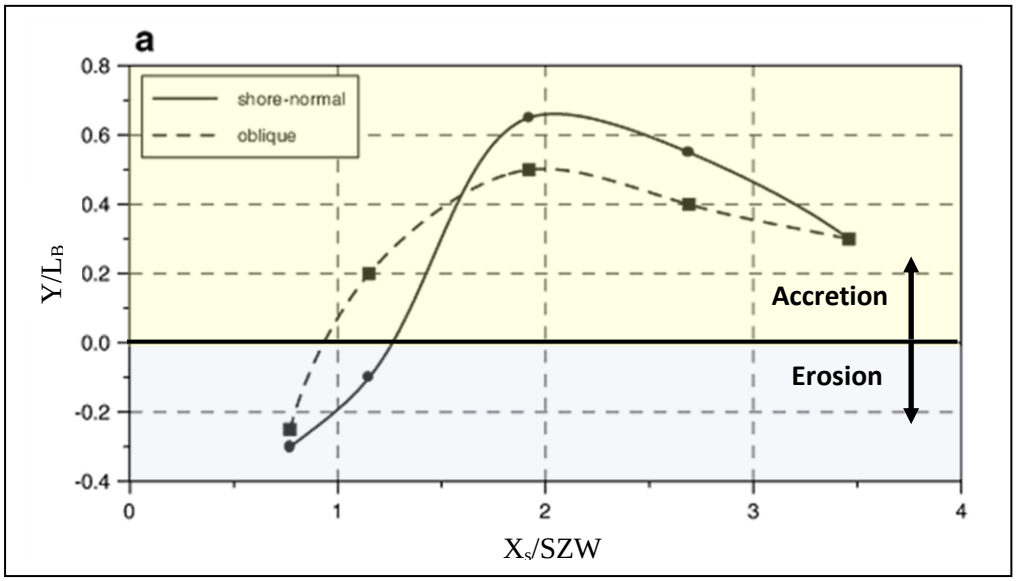

(a) *For shore normal and oblique wave incidence and crest level (-0.5m).*

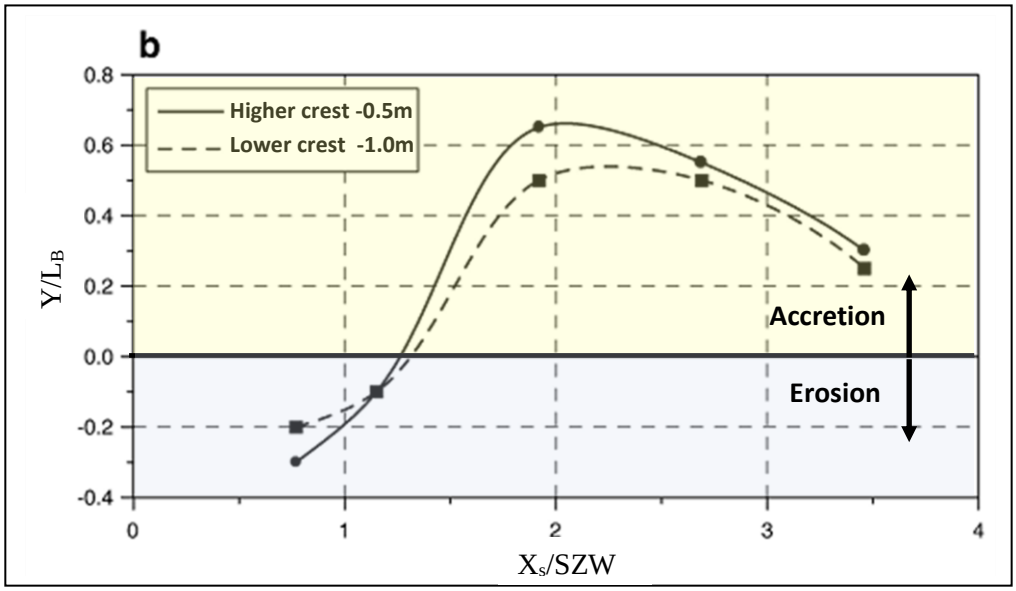

(b) *For higher and lower structure crest levels in shore normal wave condition.*

Fig 2.26: Relative shoreline accretion (+) and erosion (-) Y/L_B vs relative structure distance from undisturbed shoreline .X_s/SZW with L_B = alongshore length of the structure and SZW= natural surf zone width (Modified from Ranasinghe et al., 2006)

Ranasinghe et al. (2006) rightly suggested that the 2DH circulation pattern in the vicinity of submerged breakwaters might serve as an efficient proxy to identify the mode of shoreline response

(i.e. erosion/accretion) to submerged breakwaters. In fact, this simplified approach is much less computationally demanding than morphodynamic modelling and makes numerical studies on the mode of shoreline response to a large number of design alternatives more affordable. Though the results of this study are specifically related to the shoreline response to the V-shaped submerged breakwater and thus cannot be readily applied for common "linear" breakwaters, the results indicate that one of the highest research priorities is to determine the threshold of the parameters affecting the mode of shoreline response (e.g. critical distance X_s). Moreover, the breakwater porosity, which might have a noticeable effect on the nearshore wave and flow field has not been considered in this study.

Ranasinghe et al. (2010) performed a numerical study to investigate the effect of key structural and environmental parameters on the mode of shoreline response (i.e. erosion/accretion) to a single submerged breakwater. Since most of submerged breakwaters are constructed parallel to the shoreline, this study focused on the shoreline response to a single shore-parallel submerged breakwater. In this study, on the basis of results presented by Ranasinghe et al (2006), the wave induced flow pattern was considered as a proxy to identify the mode of shoreline response. Thus, 2-cell and 4-cell wave-induced flow pattern were respectively assumed equivalent to erosive and accretive shoreline response. In this study, MIKE21 was utilized for the 42 numerical simulations with shore-normal incident wave conditions. The range of tested structural parameters was selected so that all the examined values cover the range of common prototype values, thus highlighting the engineering relevance of the numerical simulations. Based on the simulation results, the following relationship, which expresses the threshold between the modes of shoreline response (erosion vs accretion) as a function of wave conditions and structural parameters, is proposed:

$$\frac{h}{H_{so}} = 2 \times Log\left[\left(\frac{R_c}{h}\right)^{1.5}\left(\frac{L_B}{h}\right)^{0.5}\left(\frac{A^3}{h}\right)^2\right] + 0.65 \qquad 2.11$$

Here A is the shape parameter (governed by D_{50}) in the equilibrium profile equation (Dean, 1991) and H_{so} is the deep water significant wave height.

As shown in Fig. 2.27, the suggested response function defines a clear separation between erosive and accretive shoreline responses. Fig. 2.27 also shows that, with the increase of distance between the shoreline and breakwater X_s, which is equivalent to the increase of water depth at breakwater location h, the parameter h/H_o increases and $(R_c/h)^{1.5}(L_B/h)^{0.5}(A^3/h)^2$ decreases, thus the shoreline response to the structure tends to switch from erosive to accretive mode. This implication supports the findings of previous studies (e.g. Ranasinghe et al., 2006). The predictive formula expressed by Eq. 2.16 is based on the assumption that the wave period may have a weak effect on the mode of shoreline response. However, the wave period affects the breaking depth (Ranasinghe et al., 2010) and consequently the surf zone width. As shown by Ranasinghe et al. (2006), the latter may affect the mode of shoreline response under certain conditions (see Fig. 2.26). Thus, the applicability of Eq. 2.11 for different wave periods needs to be further investigated in future studies.

The 42 simulations with shore-normal waves were re-run with oblique incident wave conditions, in which the mean wave direction was set to 10° from the shore-normal direction that could be reasonably assumed as the upper bound of obliqueness in most nearshore areas (Ranasinghe et al., 2010). The mode of shoreline response obtained from the oblique wave simulations were similar to those obtained for shore-normal waves. Thus, the straight line expressed by Eq. 2.11, might be considered to determine shoreline response mode for both shore-normal and oblique wave incidence. The simulation results show that, reducing the breakwater submergence may have a noticeable effect and change the mode of shoreline response. Moreover, it was observed that, the mode of shoreline response is not affected by the crest width for high submergence (i.e. R_c = -1.0 m in this study). In

contrast, for low submergence (i.e. R_c = -0.5m in this study), the increase of crest width may change the mode of shore-line response.

Although this study represents a noticeable advancement toward a deeper insight into the effect of the key structure and environmental parameters on the mode of shoreline response to a single shore-parallel submerged breakwater, the impermeable structure assumption limits the applicability of the results of this study. Moreover, the proposed criterion expressed by Eq. 2.11 is only able to predict the mode of shore-line response and does not provide any means for evaluating the relative protective performance of various design alternatives with the same mode of response.

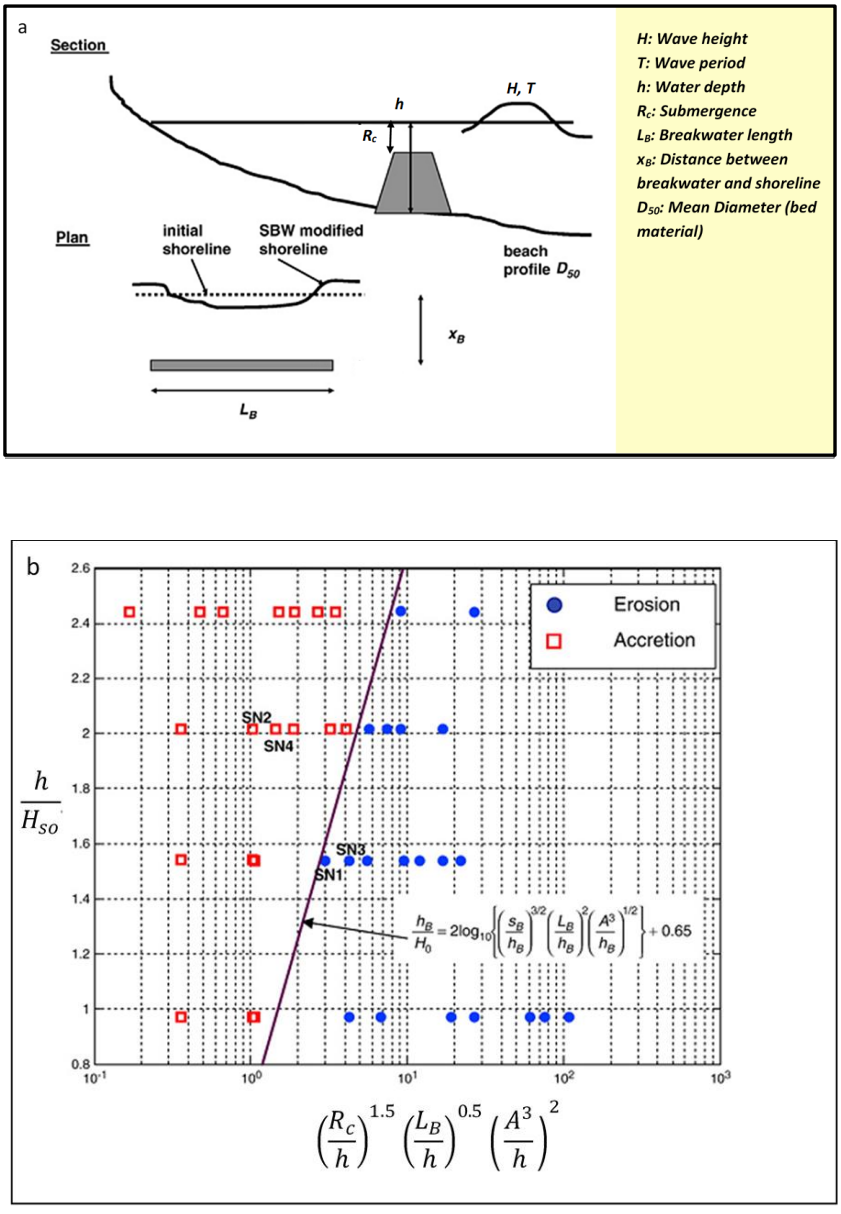

Fig 2.27: a) Definition sketch of wave and structure parameters in Eq. 2.11 (Ranasinghe et al., 2010). b) Threshold between accretive and erosive shoreline response to a single submerged breakwater described by dimensionless wave and structure parameters in Eq. 2.11 (Ranasinghe et al., 2010).

Vlijm (2011) applied the DELFT3D model described in section 2.3 to study the effect of a single submerged breakwater on the wave-induced hydrodynamic and morphological changes in the protected sand beach. Besides, the relation between the initial wave-induced flow pattern in the vicinity of the submerged breakwater and the equilibrium shoreline response is also investigated. Following the approach suggested by Ranasinghe et al. (2006), the -0.5m depth contour is used to evaluate the shore-line response, and each numerical simulation was run until the equilibrium condition is reached. Results of this study show that the 2-cell and 4-cell flow patterns respectively resulted in erosion and accretion along the shoreline in the beach protected by a single submerged breakwater. An example of the simulated initial wave induced flow pattern and corresponding equilibrium morphological changes is shown by Fig. 2.28, where L_B and X_s respectively stand for length of the breakwater and the breakwater distance from the initial shoreline.

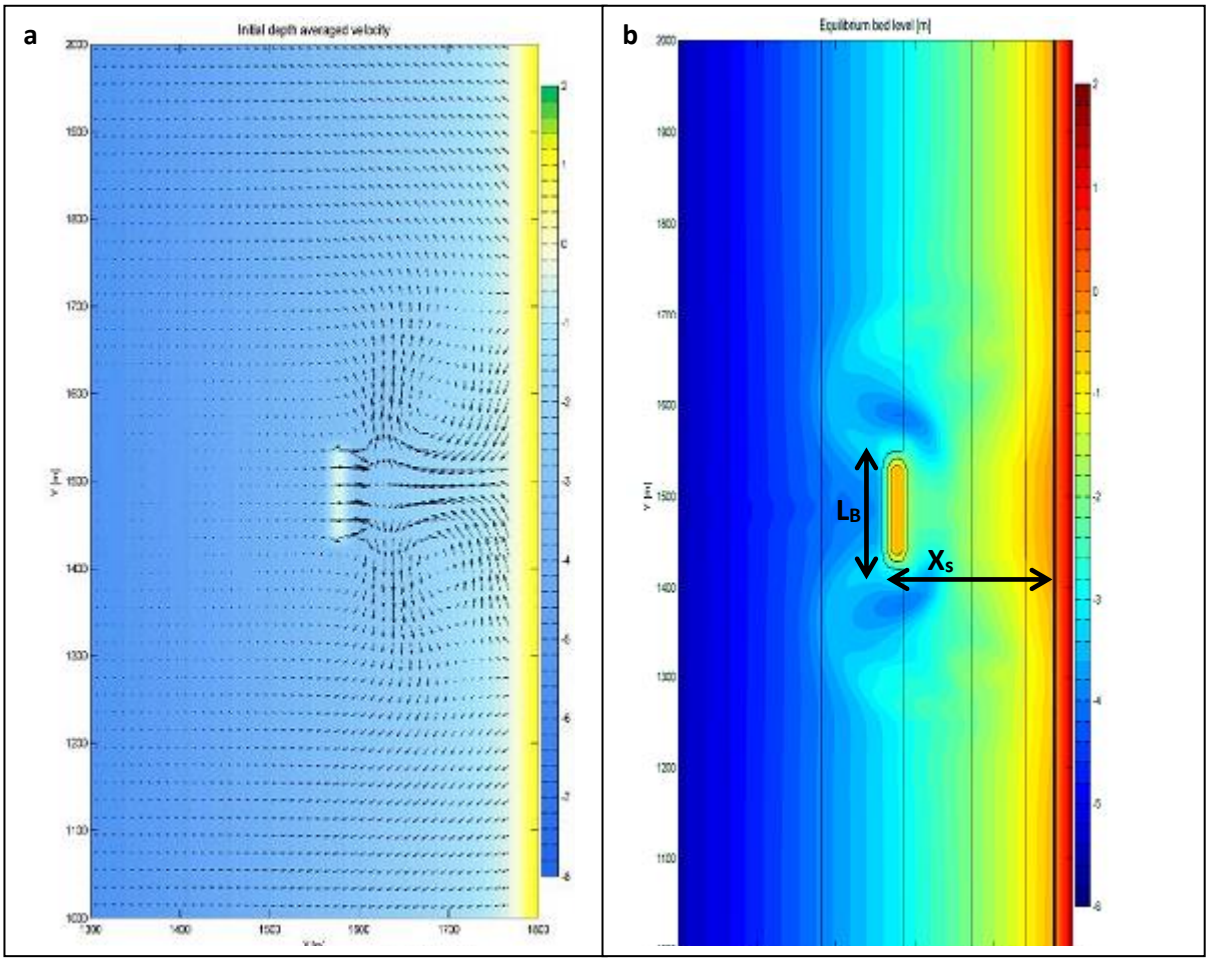

Fig 2.28: a) Initial depth averaged horizontal flow pattern and. b) Equilibrium bed level for L_B=100m and X_s=200m (From Vlijm, 2011)

The results show that, increasing the distance between the breakwater and the beach may change the mode of beach response from the erosive to accretive response. In other word, for a given breakwater length L_B, the breakwater location close to the shoreline (Xs<150 m) results in erosion, while accretion occurs when moving the breakwater further offshore. An example of numerical simulation results which has a clear implication for the effect of breakwater distance X_s on the shoreline response is shown by Fig. 2.29.

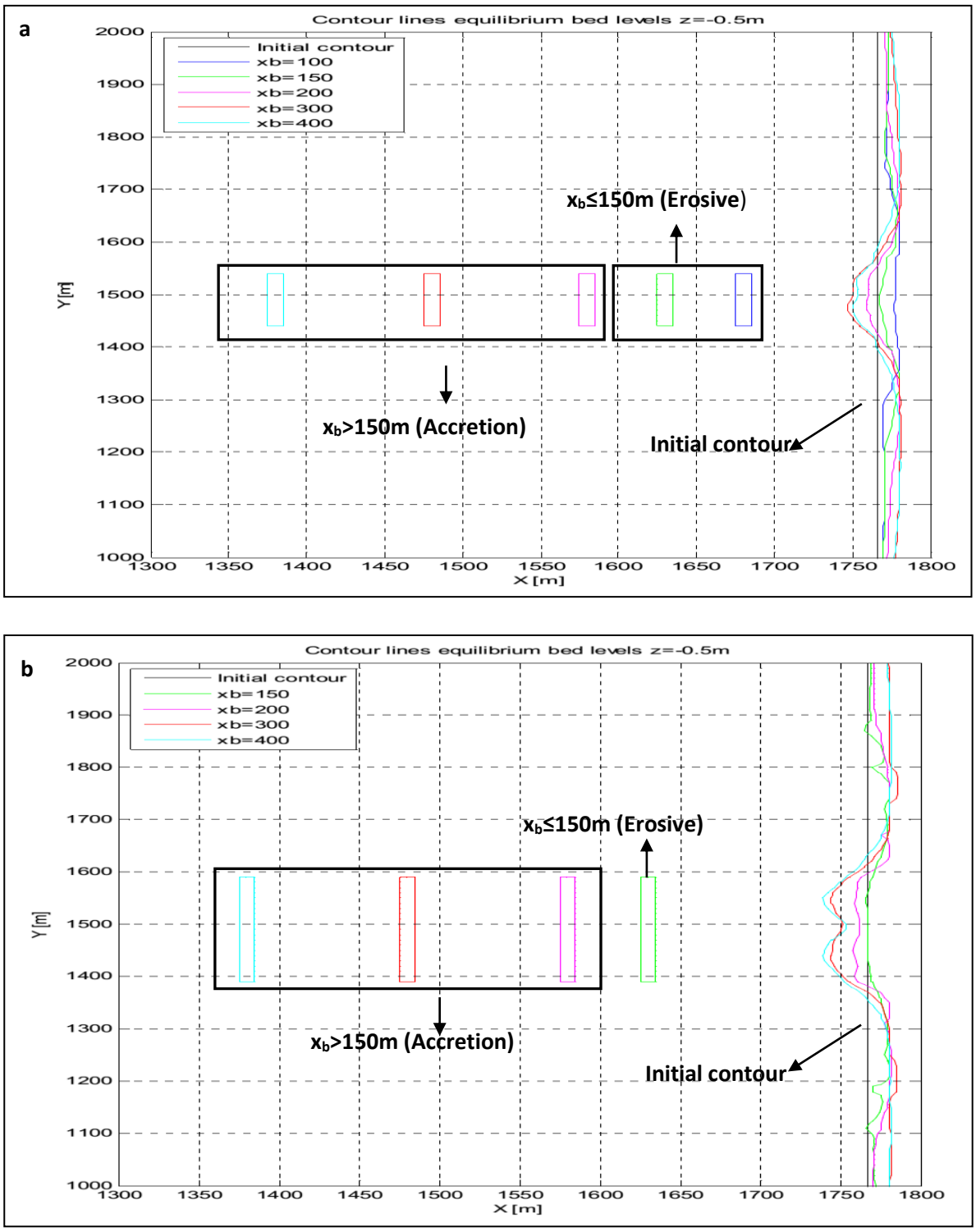

Fig 2.29: Equilibrium shape of -0.5m depth contour for a) L_B=100 and b) L_B=200m (Modified from Vlijm, 2011)

In this study, the effect of breakwater submergence and crest width on coastal morphology is not directly considered. However, based on hydrodynamic results, Vlijm (2011) suggested that the decrease of breakwater submergence and the increase of the crest width enhance the accretive flow pattern in the lee of the breakwater (see Figs. 2.8b and 2.10). However, as stated by Vlijm (2011), the effect of

submergence is more important compared to the effect of crest width. Although the findings of this study agree with the results of previous study carried out by Ranasinghe et al. (2006), the number of numerical simulations is not sufficient to provide the adequate data required for developing functional relationships between submerged breakwater design parameters and shoreline response. Furthermore, the effect of breakwater porosity is omitted in this study.

Using the DELFT3D model, Van der Baan (2013) performed a series of numerical simulations to investigate the effects of design parameters of segmented submerged breakwaters on the mode of shoreline response (i.e. erosion/accretion) in order to extend Eq. 2.11 and make it applicable for shoreline response to segmented submerged breakwaters. The results suggest that the lateral confinement, which represents the ratio between the length of the gap L_g and the length of the structure L_B, is a key parameter to account for the difference between the shoreline response to a single SBW and the response to a segmented SBW. Based on the numerical simulation results, Van der Baan (2013) suggested a predictive function which can be used to distinguish between erosive and accretive shoreline responses to segmented submerged breakwaters, representing an extension of Eq. 2.11:

$$\frac{h}{H_{so}} = 2 \times Log\left[\left(\frac{R_c}{h}\right)^{1.5}\left(\frac{L_B}{h}\right)^{0.5}\left(\frac{A^3}{h}\right)^{2}\right] + 0.65 \times G\left(\frac{L_g}{L_B} \quad \frac{h}{H_{so}}\right) \qquad 2.12a$$

$$G\left(\frac{L_g}{L_B} \quad \frac{h}{H_{so}}\right) = \left[1.22\left(\frac{L_g}{L_B}\right)^{2} - 3.67\left(\frac{L_g}{L_B}\right) + 3.22\right] \times \left[0.4\left(\frac{h}{H_{so}}\right)^{2}\right] \qquad 2.12b$$

For: $0.25 < L_g/L_b < 2.5$, $0.06 \leq Rc/H_o \leq 0.60$, $h/H_{so} > 1.25$,

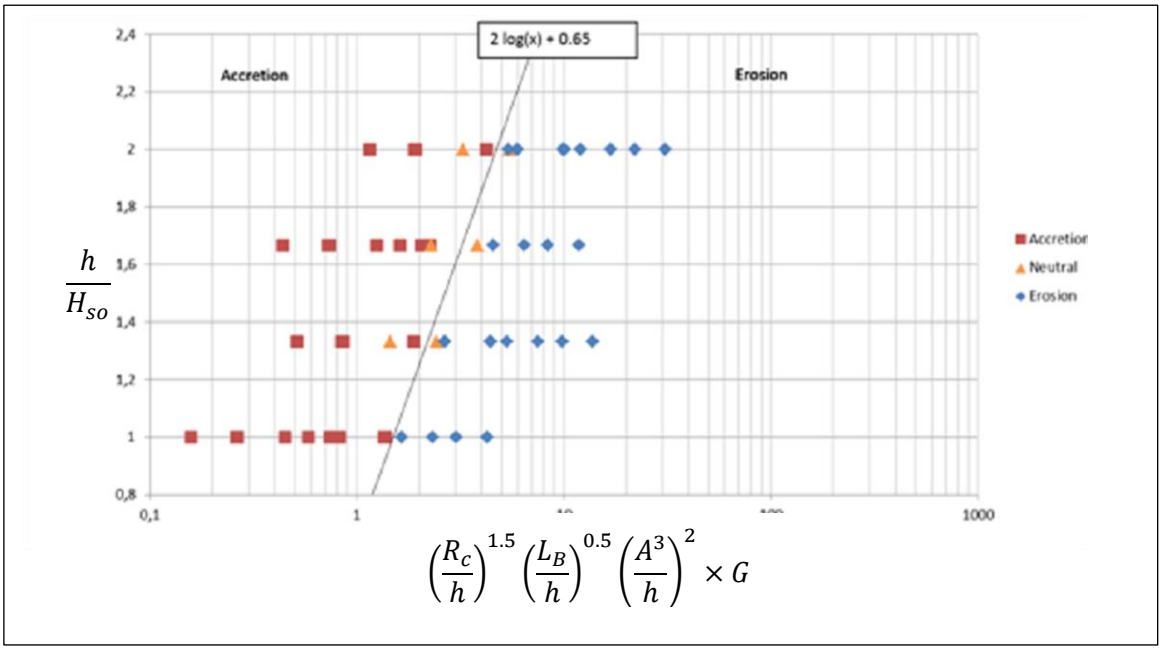

Fig 2.30: Threshold between accretive and erosive shoreline response to a segmented submerged breakwater described by Eq. 2.12 in terms of dimensionless wave and structure parameters (Van der Baan, 2013). The blue circles and red squares respectively denote accretive and erosive conditions.

Here R_c is the breakwater submergence, L_B is the length of breakwater, h is the water depth at breakwater location, L_g is the gap width and A is the shape parameter (governed by D_{50}) in the equilibrium profile equation (Dean, 1991). As can be seen in Fig. 2.30, Eq. 2.12 distinguishes between the erosive and accretive response of the beach to segmented submerged breakwaters. This is the first and only criterion suggested to evaluate the mode of shoreline response to segmented submerged breakwaters and further research, especially field and experimental studies on this topic would be required. Moreover, this criterion is only applicable to impermeable breakwaters, which is rarely the case in coastal engineering practice. It should be noted that, similar to Eq. 2.11, the effect of different wave periods on the applicability of Eqs. 2.12a and 2.12b needs to be further investigated.

Martinelli et al. (2006) performed a series of laboratory tests in a flume and a wave basin. The results show that a salient forms leeward of the submerged breakwater when the distance from the shoreline exceeds approximately half the structure length, and also tombolo never forms in the lee of submerged breakwater. Additional numerical simulations with MIKE 21 were also performed to get a deeper insight of the flow and sediment transport pattern in the prototype scale. The overall erosion/deposition pattern predicted by numerical simulations was found to be in a good agreement with the experimental observations. The results suggest that the overall erosion increases with the increase of the gap between breakwaters. Although this study is among the rare laboratory studies performed on the effect of submerged breakwater on coastal morphology, the number of tests is too limited to develop quantitative design criteria for submerged breakwaters

2.2.3 Short- term morphodynamic effects of submerged breakwaters

Accurate evaluations of the protective efficacy of submerged breakwaters need also to take into account the morphological changes in response to a short-term event (e.g. time scale of one storm event). However, in spite of the serious lack of knowledge about the short-term shoreline response to submerged breakwaters, very few studies have been carried out on this topic. In this section, the most relevant studies performed on the short-term morphological changes leeward of submerged breakwaters are summarized and their contributions and limitations with respect to the current knowledge are outlined.

Lorenzoni et al. (2013) carried out and reported a 2D laboratory moveable bed study, which was focused on the protective performance of various detached breakwater configurations. This study was a part of a more general project for the coastal defence of the beach of Gabicce Mare (Italy). The main objective was to investigate the relation between the detached breakwater configuration and protected beach profile evolution. They attempted to analyse the advantages and disadvantages of the emerged and submerged breakwaters to obtain some suggestions for optimized breakwater designs in terms of the highest protective performance under a storm event. The analysis of the results was mainly focused of the effect of the freeboard and the distance of the breakwaters from the shore.

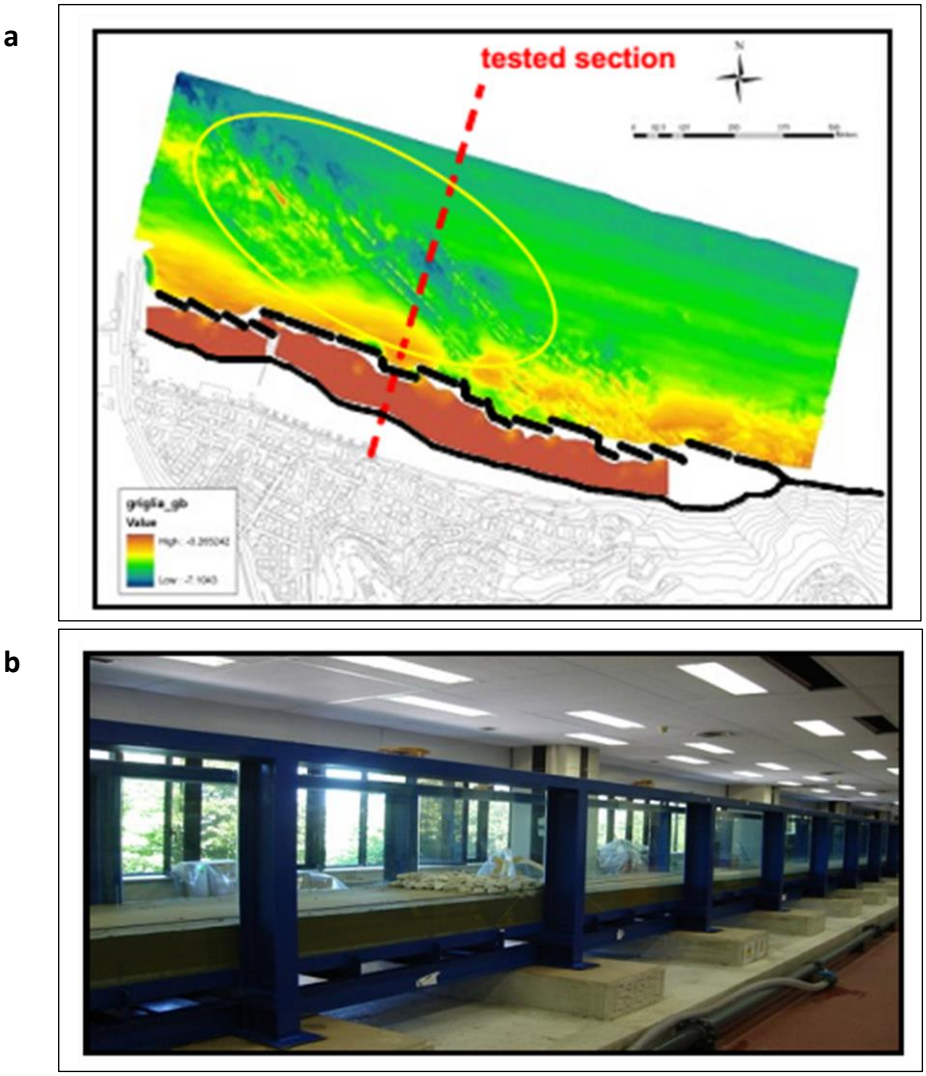

Fig 2.31: a) Survey map of the area under study, and b) physical movable model in the 2D flume. (Lorenzoni et al., 2013).

The results revealed that, for both emerged and submerged configurations under the same wave conditions, the breakwater configurations located closer to the beach have a higher protective efficacy compared to those located further from the beach. Besides, it was found that, as obviously expected, submerged breakwaters ($R_c < 0$) have less protective efficiency than their emerged counterparts ($R_c > 0$) under the same wave conditions. Although this study was an initial step to investigate the relation between design of submerged breakwaters and the protective efficacy of the structure against short-time events (e.g. sea-storms), the results of this study are too scattered to develop a reliable functional relationship for the design of submerged breakwaters in coastal protection systems. Besides, in addition to the non-consideration of the effect of variation of submergence $R_c<0$, the effect of breakwater porosity is also totally neglected.

In response to the lack of adequate data to evaluate the protective efficacy of submerged breakwaters under short-term events, Postacchini et al. (2016) performed a detailed numerical study on the influence of different breakwater configurations on the beach response. This study was the first study that includes a large number of tests to analyse the effect of incident wave conditions and structure parameters on short-term coastal morphological changes. The main focus of this study was put on the effect of the distance between the shoreline and a pair of submerged breakwaters. Some additional simulations were also performed to evaluate the effect of the structure crest width (Fig. 2.32).

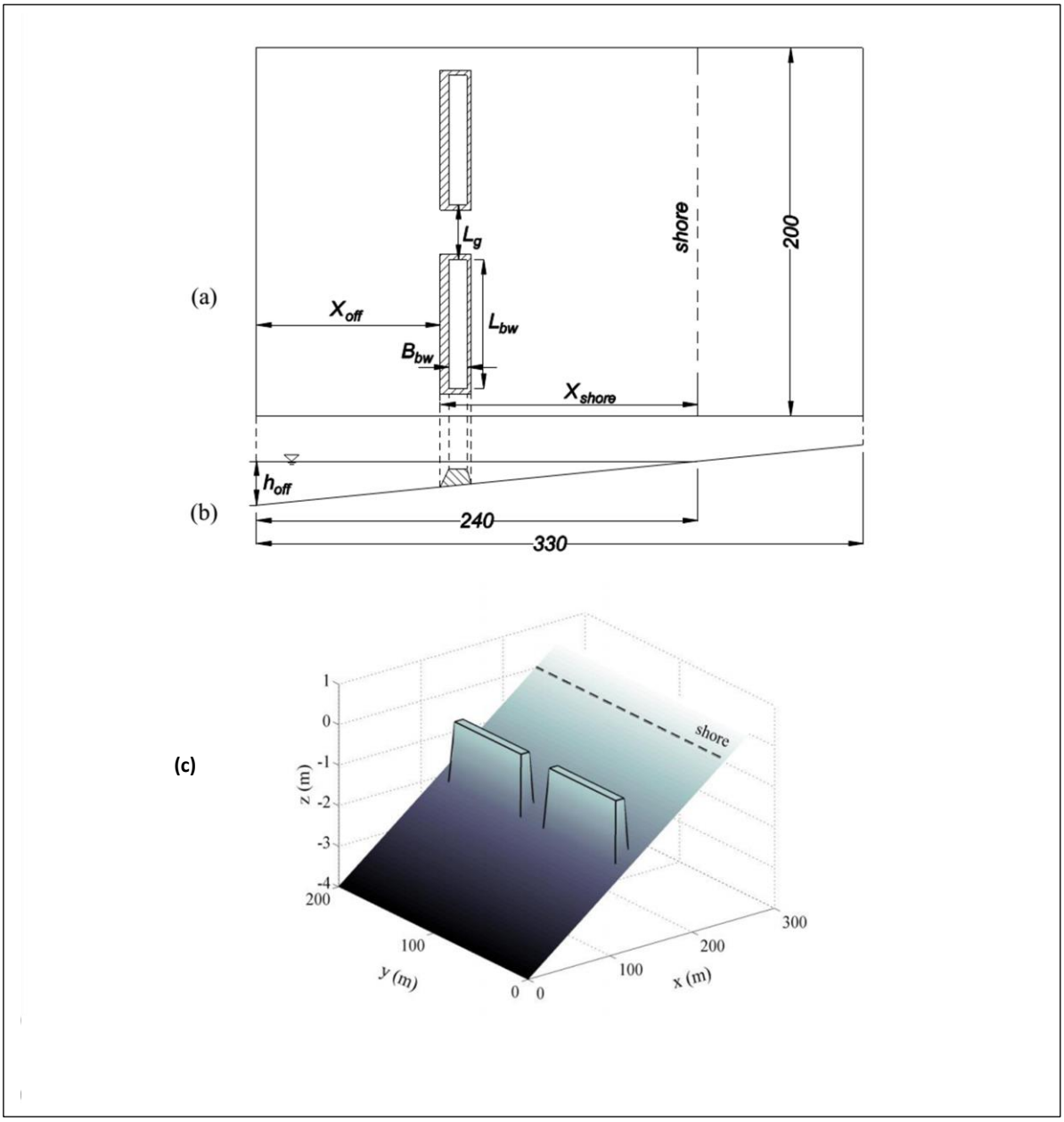

Fig 2.32: Plan view(a) and cross-section (b) of submerged breakwaters with a 3D view of the initial configuration (c) used for numerical tests (Postacchini et al., 2016).

In order to run realistic simulations, the input wave conditions were generated based on the data collected by an Italian wave measurement network buoy located offshore of Falconara Marittima (Ancona, Italy). The morphological changes were characterized by the maximum variations of the cross shore bed profile, as calculated during the numerical tests. Although, a relatively large number of numerical tests were carried out, predictive formulae that relate the wave conditions and breakwater design to characteristic morphological changes were not developed. Fig. 2.33 shows the maximum calculated relative seabed variation (made dimensionless by incident significant wave height $H_{si)}$ as a function of the non-dimensional parameter χ_0 (defined in the figure):

$$\chi_0 = \left[\frac{H_{si}}{h}\right]^2 \left[\frac{B}{L_p}\right]^{0.5}$$

H_s: Significant incident wave heighat breakwater position
L_p:Peak period wave length at breakwater position
h: Water depth at breakwater location
B: Breakwater crest width

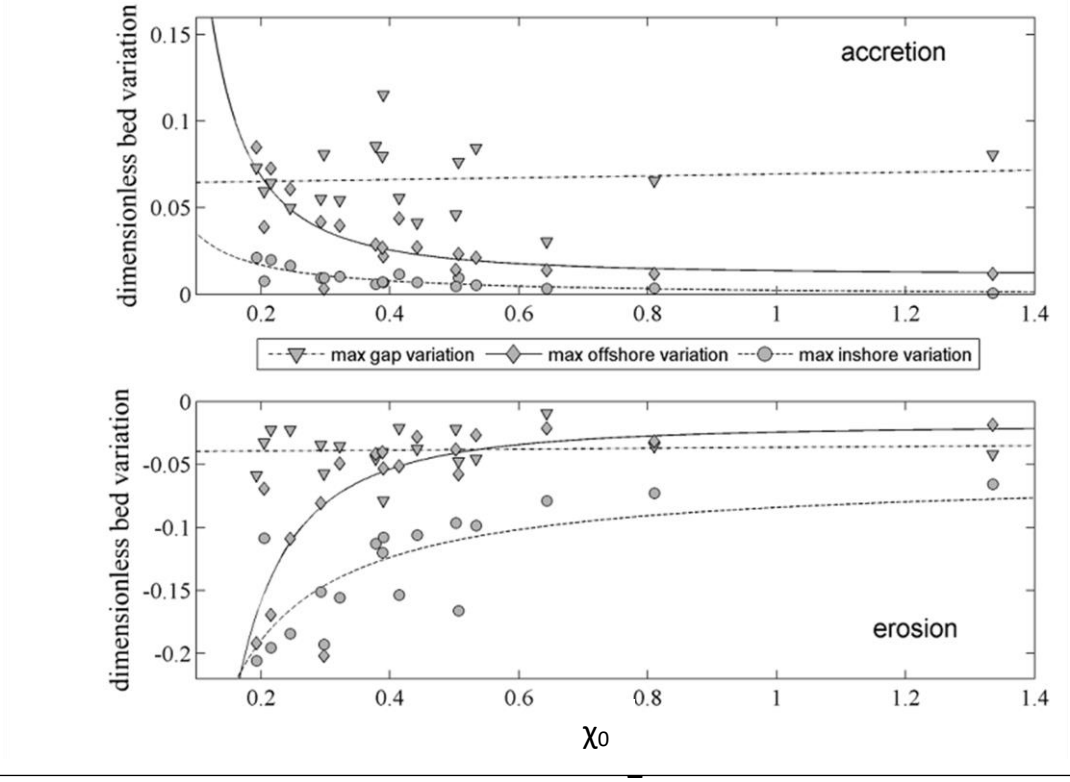

Fig 2.33: Variation of maximum dimensionless seabed variation against $\chi 0$: in the gap (▼, dash-dotted line), offshore (♦, solid line) and inshore (●, dashed line). (Modified form Postacchini et al., 2016).

Though the results provide only a very preliminary insight into the effects of various influencing parameters on the protective efficacy of a pair of submerged impermeable breakwaters, the most important implication to be drawn for design is that, the more the breakwater is located away from the shore, the higher is the erosion in the protected area. Besides, results suggest that a larger crest width results in weaker overall morphological changes in the protected beach. This work can be considered as a preliminary study on the effect of breakwater design on the short-term morphological changes in the beaches protected by a pair of submerged breakwaters; moreover, the effect of varying structure submergence and porosity have not been considered.

2.2.4 Key results and implications of the reviewed/analysed studies

As discussed in sections 2.1.1 and 2.1.2, submerged breakwaters are intended to protect the coast against erosion by mitigating the incident wave energy, thus altering the nearshore flow and sediment transport pattern. Ranasinghe and Turner (2006) showed that a noticeable fraction (70%) of submerged breakwater projects, whose performance had been documented up to 2006, adversely resulted in unintended erosion of the protected beach. This clearly implies a lack of adequate knowledge on the functioning and protective efficacy of submerged breakwaters. Due to the lack of adequate field data,

it is hardly possible to draw any final conclusions about the relation between submerged breakwater design and the performance of the structure under field conditions. Accordingly, the current knowledge about the performance of submerged breakwaters is mainly based on numerical and laboratory studies. The available studies on the functioning and protective efficacy of submerged breakwaters are mainly categorized in studies focusing on (i) their efficacy in terms of wave damping (hydraulic performance), (ii) their long-term morphodynamic effects (time scale of several storm events or/and months), and (iii) their short term morphodynamic effects (time scale of a single storm event).

Studies on wave mitigation abilities mainly consider the hydraulic performance of the submerged breakwaters which is expressed in terms of wave transmission (see section 2.2.1). In order to study wave transmission in submerged breakwaters, a wide range of empirical wave transmission coefficient (WTC) formulae has been proposed (see review in Table 2.2). The main limitation of these formulae is that, they do not explicitly consider the effect of porosity on wave transmission, though submerged breakwaters are commonly porous (e.g. rock material). Only few studies have addressed the effect of breakwater porosity on wave transmission (e.g. Losada et al., 1997; Ting et al., 2004; Rahman and Akter, 2014). The most important implications from the results of these studies are outlined below:

- For a given breakwater geometry (e.g. cross-shore profile of the breakwater) the use of porous structures instead of impermeable structures reduces wave transmission (Losada et al., 1997). This reduction of wave transmission can be attributed to the wave energy dissipation inside the porous structure.

- Within the range of porosity values considered in the reviewed studies (i.e. from 0.42 to 0.912), the increase of breakwater porosity results in an increase of the wave transmission (e.g. Losada et al., 1997; Ting et al., 2004; Rahman and Akter, 2014)

However, the aforementioned results only qualitatively describe the effect of porosity and they cannot be efficiently applied to the design of submerged breakwaters. Therefore, the lack of a novel wave transmission formula which explicitly includes the breakwater porosity is an important research gap that must be addressed.

Studies on the long-term morphodynamic effects of submerged breakwaters are relatively numerous (e.g. Martinelli et al., 2006; Ranasinghe et al., 2006; Ranasinghe et al., 2010; Turner et al., 2001; Vlijm, 2011) and mostly based on numerical modelling. These studies usually provide relatively small datasets, mainly due to high computational costs (e.g. Ranasinghe et al., 2006) needed for long-term morphological simulations. However, as outlined below, the results of these studies have important implications for evaluating the performance of submerged breakwaters in coastal protection systems:

- Increasing the distance between the breakwater and beach can change the mode of long-term beach morphological response from erosive to accretive response (Martinelli et al., 2006; Ranasinghe et al., 2010; Vlijm, 2011).

- In some cases, the breakwater submergence is observed to slightly affect the morphological changes behind the structures (Cáceres et al., 2005; Ranasinghe et al., 2006). In contrast, Ranasinghe et al. (2010) showed that, changing breakwater submergence, might reverse the mode of shoreline response (i.e. changing from erosive to accretive response with the decrease of submergence, or vice versa). Therefore, more studies are needed to specify the exact conditions under which the effect of breakwater submergence on [long-term] morphological changes become important

- The increase of crest width, which has been proved to decrease wave transmission (see section 2.2.1), might have a favorable effect on beach accretion (e.g. Ranasinghe et al., 2010; Vlijm, 2011).

- 2-cell and 4-cell flow pattern in the vicinity of submerged breakwaters respectively correspond to erosive and accretive [long-term] shoreline response. The strong relationship between the type of wave-induced flow pattern in the vicinity of submerged breakwater and the mode of shoreline response is revealed by Ranasinghe et al. (2006) and confirmed by Vlijm (2011)

Moreover, based on the limited datasets provided by the available studies, some predictive relationships (Ranasinghe et al., 2006; Ranasinghe et al., 2010; Cáceres et al., 2005; Black and Andrews, 2001; Hanson and Krause, 1990) have been developed to assess the long-term morphological changes in the beaches protected by submerged breakwaters (e.g. Eqs 2.10). However, these formulae have major limitations as outlined below:

- Some of the existing formulae do not predict the beach erosion (e.g. Black and Andrews, 2001; Pilarczyk, 2003; Hanson and Krause, 1990) in the lee of the submerged breakwaters. This is not consistent with the observed performance of submerged breakwaters, either in the field (Ranasinghe and Turner, 2006) or in numerical studies (e.g. Ranasinghe et al., 2006; Vlijm, 2011).
- The existing predictive relationships obtained from numerical simulations are mostly based on limited data (e.g. Cáceres et al., 2005; Ranasinghe et al., 2006), thus making their robustness questionable.

Although breakwater porosity might have a significant effect on wave transmission and thus on the protected beach morphology, none of the available studies performed on the long-term morphological changes consider the effect of breakwater porosity

Studies on the short-term morphodynamic effects of submerged breakwaters are relatively rare. As mentioned in section 2.2.3, in addition to the long-term morphodynamic effects of submerged breakwaters, the study of the beach response to short-term events (e.g. storm surge) is also needed for functional designs. However, this aspect has rarely been investigated for submerged breakwaters and the available studies (e.g. Postacchini et al., 2016; Lorenzoni et al., 2013) only give a very preliminary insight into the relation between submerged breakwater parameters and short-term morphological response of the protected beach. The most important implications of these studies for evaluating the [Short-term] effect of breakwater parameters on coastal morphology are outlined below:

- Wider crest width and lower submergence result in a decrease of beach erosion

- A decrease of the distance between beach and breakwaters also results in less beach erosion

No predictive formula is yet available to evaluate the morphological response of the protected beach to short-term events (e.g. time scale of one storm event). Moreover, none of the available studies consider the effect of structure porosity on the short-term response of beaches protected by submerged breakwaters.

The studies reviewed in this chapter show that significant advances have been made using both numerical models (e.g. Cáceres et al., 2005; Ranasinghe et al., 2006; Vlijm, 2011; Van der Baan 2013) and physical models (e.g. Browder et al., 1996; Turner et al., 2001; Martinelli et al., 2006; Lorenzoni et al., 2013). Commonly numerical modelling is preferred, due to huge prohibitive costs and efforts associated with the experimental tests, especially in detailed parameter studies. Thus, a review of the most widely used models in coastal engineering is required in order to identify the most appropriate numerical model to be considered in this PhD study

2.3 Available numerical models

Assessing This section presents a brief review on the numerical models which could be utilized to study the effect of detached submerged breakwaters on coastal morphology, and thus to evaluate the protective efficacy of this type of structures for coastal protection. In this section, DELFT3D, MIKE, TELEMAC, XBEACH and GENESIS, which are the most widely applied coastal engineering models, are briefly described, including their capabilities and limitations to study the effect of breakwater porosity and submergence on coastal morphology. For each reviewed model, a very brief introduction of the model, a short description of the hydrodynamic and sediment transport modules of the model, some illustrative example applications (if reported in the available literature) are presented, together with a summary of the main capabilities and limitations of the model for this study. For the sake of clarity, the underlying governing equations and associated numerical schemes are not described below; the interested reader may refer to the related references provided for each model.

2.3.1 DELFT3D

The DELFT3D (Lesser et al., 2004; Lesser, 2009) is an open source modelling system developed by Deltares in close cooperation with Delft University of Technology. DELFT3D is able to reproduce short wave generation and propagation, flow, transport of constituents carried by water (e.g. sediment, heat, and salinity), morphological changes, ecological processes and water quality in coastal areas, estuaries and rivers. DELFT3D can perform numerical simulations using both structured rectangular and curvilinear computational grids. DELFT3D consists of several integrated modules and components; among them the modules relevant to this study are briefly described in the following sections.

2.3.1.1 Wave Module

In order to simulate water wave generation and propagation, two options are available in DELFT3D, namely *DELFT3D-WAVE* and *Surface Roller* model. Both options are briefly described below:

DELFT3D-Wave:

The wave module in Delft3D, Delft3D-WAVE (SWAN) is an interface for SWAN [**S**imulating **WA**ves **N**earshore] (Booij et al., 1999),a well-known third generation wave spectrum model. The DELFT3D WAVE module (SWAN) calculates the wave spectral parameters through solving the conservation of action density equation over the computational grid. The DELFT3D-WAVE (SWAN) is able to account for wave shoaling, wave generation by wind, wave breaking, whitecapping, bottom friction, non-linear wave-wave interactions, bottom and current induced refraction, diffraction, and wave transmission through, blockage by or reflection against obstacles (Deltares , 2014a). Therefore, DELFT3D-WAVE is able to include the major wave propagation processes due to breakwater submergence.

Surface Roller Model:

Surface roller model is an extension of the DELFT3D-FLOW module (Deltares, 2014b) and is able to particularly account for the effect of short wave groupiness on water motions and of the generation of long waves (infragravity waves). This effect is caused by time and spatial variations of wave and roller energy, which result in the generation of long-bounded waves that travel along with groups of short waves. Including this process enables the model to represent both hydrodynamics and sediment transport in the swash zone. The surface roller model has never been applied to simulate wave propagation over submerged breakwaters. This is most probably due to the inadequacy of breaking parameterization applied in the model for steep slopes (*The author observed numerical instability when he applied surface roller mode to submerged breakwaters*)

2.3.1.2 Flow Module

At the heart of the DELFT3D modelling system is the flow module, DELFT3D-FLOW, which is a multidimensional (2D or 3D) hydrodynamic and transport (e.g. sediment, heat, salinity) simulation tool. If the horizontal flow variation over the water column is negligible, then the 2DH depth-averaged approach can be used (e.g. 2/4-cell flow pattern in the lee of submerged breakwaters), while 3D modelling can be applied when the horizontal flow and transport field varies noticeably across the water depth. The ability to choose 3D simulations enables DELFT3D to fully represent the undertow (see Fig. 2.2) and the resulting seaward sediment transport. In Delft3D-FLOW, the shallow water equations, are written and solved in the GLM (*Generalized Lagrangian Mean*) reference frame (Groeneweg and Klopman, 1998), enhancing the wave induced flow representation in the numerical model (Walstra et al., 2001). DELFT3D-FLOW is able to account for wind forces, Coriolis forces, density variations, tidal propagations, atmospheric pressure and wind shear stress. Besides, important wave-induced effects such as streaming in the wave boundary layer and turbulence are taken into account by the Delft3D-FLOW module (Walstra et al., 2001).

2.3.1.3 Sediment Transport Module

The sediment transport component, which is an integrated part of the DELFT3D -FLOW, enables the model to calculate both non-cohesive and cohesive sediment transport rates as well as morphological changes caused by sediment transport gradients and exchange of sediments between the bed and water column (Deltares, 2014b). Using the results of DELFT3D-FLOW, the sediment transport module is able to calculate bed load and suspended load rates separately. In DELFT3D, the bed load is calculated by classical sediment transport (empirical) formulae available in the literature (Deltares, 2014b) and the suspended load is determined by solving the advection-diffusion equation for suspended sediment concentration. The bed level changes are also calculated using sediment mass conservation equation (Exner equation).

2.3.1.4 Example Applications

According to the literature and in comparison with other available numerical models, DELFT3D has been more widely applied to study the effect of submerged breakwaters on the nearshore hydrodynamic processes and the resulting coastal morphological changes (e.g. van der Hout, 2008; van der Baan, 2013; Vlijm, 2011; van der Biezen et al., 1999).

Fig 2.28 and 2.29 provide some example applications using DELFT3D to study flow and morphological changes in the vicinity of submerged breakwaters (see section 2.2.2).

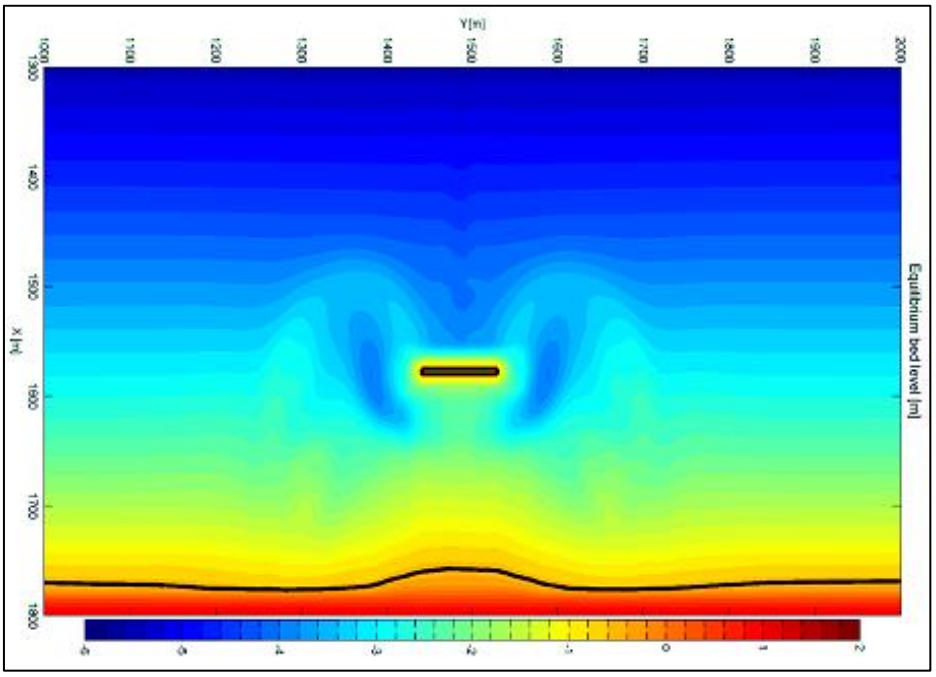

Fig 2.34: Example application for shoreline evolution caused by accretive flow pattern in the lee of submerged breakwater using DELFT3D. (From Vlijm, 2011).

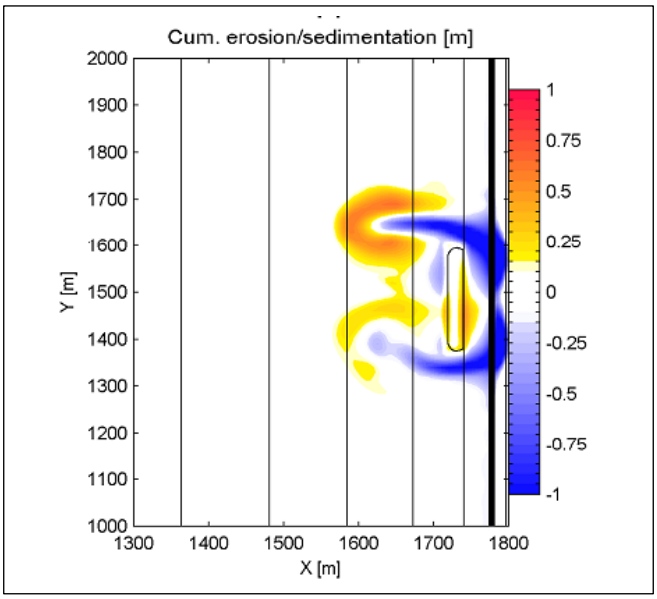

Fig 2.35: Example application for cumulative erosion/sedimentation modelling leeward shore-parallel single submerged breakwaters using DELFT3D. (From Vlijm, 2011).

The black line in Fig. 2.34 represents the -0.5 m depth contour line selected close to evaluate the shoreline evolution (see section 2.2.2). Overall, the example applications of DELFT3D in Fig. 2.34 and 2.35 show that the model is able to predict beach erosion and accretion leeward of the submerged breakwaters

2.3.1.5 Summary

Summarising, DELFT3D is potentially able to reproduce the key wave propagation and hydrodynamic processes in the vicinity of submerged breakwaters. DELFT3D-WAVE is able to account

for wave breaking, wave diffraction and wave refraction, due to the submergence of the breakwater (see section 2.1.2). DELFT3D -FLOW is able to reproduce 2-cell and 4-cell circulation patterns, which are due to the effect of breakwater submergence on nearshore horizontal flow pattern. Besides, DELFT3D uses more advanced schemes to represent wave-induced flow.

However, in spite of the aforementioned advantages, like most of coastal engineering modelling systems that use phase-averaged wave modules, if DELFT3D-WAVE is used for wave generation and propagation, DELFT3D is not able to adequately reproduce sediment transport in the swash zone. Moreover, DELFT3D is not able to represent the effect of breakwater porosity on wave transmission (see section 2.2.1) and on seaward filtration flow through the porous breakwater (see section2.1.1b)

2.3.2 MIKE

MIKE is a commercial modelling system developed by ***D**anish **H**ydraulic **I**nstitute* (DHI). A wide range of add-on modules which are available in MIKE make it an ideal coastal engineering modelling package for simulating wave generation and propagation, flow, sediment transport and bed level changes, pollutant transport and water quality in coastal areas, estuaries and rives. MIKE is able to perform numerical computations on the unstructured (flexible) mesh, providing the model with a high flexibility for representing complex geometries and smooth representation of boundaries in the areas under study. The modules of the MIKE modelling system which are relevant to this study are described below.

2.3.2.1 Wave Module

MIKE consists of some wave modules; among them MIKE SW, MIKE PMS and MIKE BW are most widely applied in coastal engineering. These modules are briefly described below:

MIKE 21 SW (DHI, 2017a) is a spectral wind wave model which is able to simulate growth, decay and transformation of wind-generated waves and swells. The spectral wave module is based on the action density balance equation and includes all wave generation and propagation processes outlined for DELFT3D-WAVE (see section 2.3.1.1) with the exception of wave diffraction (DHI, 2017a).

MIKE 21 PMS (DHI, 2017b) is a wave model which is based on the parabolic approximation of mild-slope equation. This module is able to account for wave breaking, wave shoaling, refraction and diffraction. MIKE 21 PMS could be forced by specifying both regular (monochromatic) and irregular wave conditions along the offshore boundary.

MIKE 21 BW (DHI, 2017c) is a state-of-the-art numerical tool for modelling short and long period waves in ports, harbours and coastal areas. MIKE 21 BW is based on the numerical solution of time domain expression of the Boussinesq wave equation and is able to reproduce important water wave processes such as wave reflection, refraction, diffraction, breaking, bottom friction and nonlinear wave-wave interaction. However, MIKE21 BW is not able to account for wave generation by wind.

MIKE SW and PMS can be coupled with the hydrodynamic and sediment transport modules of the MIKE modelling system. However, it is not possible to couple MIKE BW with the hydrodynamic and sediment transport modules, and thus MIKE BW **can't** be utilized to study sediment transport and morphological changes in coastal areas (DHI, 2015a)

2.3.2.2 Hydrodynamic Module

The hydrodynamic module of MIKE, MIKE HD (DHI, 2017d), is a 2D/3D hydrodynamic model developed to calculate 2D/3D free surface flows. MIKE HD is based on the numerical solution of 2D/3D system of shallow water equations and accounts for wave-induced flow, wind forces, Coriolis forces, density variations, ice coverage, tidal propagation and precipitation/evaporation. MIKE HD is coupled

with the sediment transport modules of MIKE, and is able to account for bed level changes obtained from the sediment transport modules.

2.3.2.3 Sediment Transport Module

Two sediment transport modules are available in MIKE modelling package, enabling the model to simulate cohesive (mud) and non-cohesive (sand) sediment transport and the related bed level changes:

- **MIKE ST** (DHI, 2017e): The non-cohesive 2D/3D sediment transport module, MIKE ST, calculates the sediment transport rate and its related bed level changes for non-cohesive sediments (sand) under the effect of wave and current actions

- **MIKE MT** (DHI, 2017f): The 2D/3D cohesive sediment transport module, MIKE MT, calculates the erosion, transport, and deposition of cohesive sediments (mud). MIKE MT also accounts for mechanisms such as flocculation and resuspension.

MIKE ST also includes the shoreline-morphology scheme which enhances the stability of shoreline calculations in long-term simulations. Other aspects of sediment transport module are similar to what described for to DELFT3D (see section 2.3.1.3). In other word: i)The flow field calculated by hydrodynamic module is used to calculate sediment transport rates. ii) The bed load and suspended load are determined separately. iii) The suspended load is calculated by solving advection-diffusion equation for suspended sediment concentration. iv)The bed level changes are calculated using Exner equation.

It should be noted that, for 2D and 3D simulations, MIKE is referred to as MIKE 21 and MIKE 3 respectively. For example, for a 2D simulation, the sediment transport modules of MIKE are referred to as MIKE 21 ST and MIKE 21 MT.

2.3.2.4 Example Applications

Previous studies in which MIKE modelling system has been applied to investigate the effect of submerged breakwater design on coastal hydrodynamics and morphological changes have been described in section 2.1.2 (e.g. Ranasinghe and Turner, 2006; Ranasinghe et al.,2010).

The examples applications in Figs. 2.23- 2.25 illustrate the capability of MIKE 21 to predict beach accretion and erosion, which respectively caused by 4-cell and 2-cell flow patterns in the lee of submerged breakwaters. Fig. 2.36 also provides an example application using MIKE21 as an engineering tool to study the effect of submerged breakwater on wave-induced flow pattern in the vicinity of the structure. It illustrates the capability of MIKE21 to predict the 2-cell and 4-cell flow patterns in the vicinity of single shore-parallel submerged breakwater. It also suggests that, when the submerged breakwater is located close to the beach, the 2-cell erosive flow pattern may appear while moving submerged breakwaters further seaward might generate the 4-cell accretive flow pattern, agreeing with the results of the earlier studies (e.g. Ranasinghe and Turner, 2006; Cáceres et al., 2005)

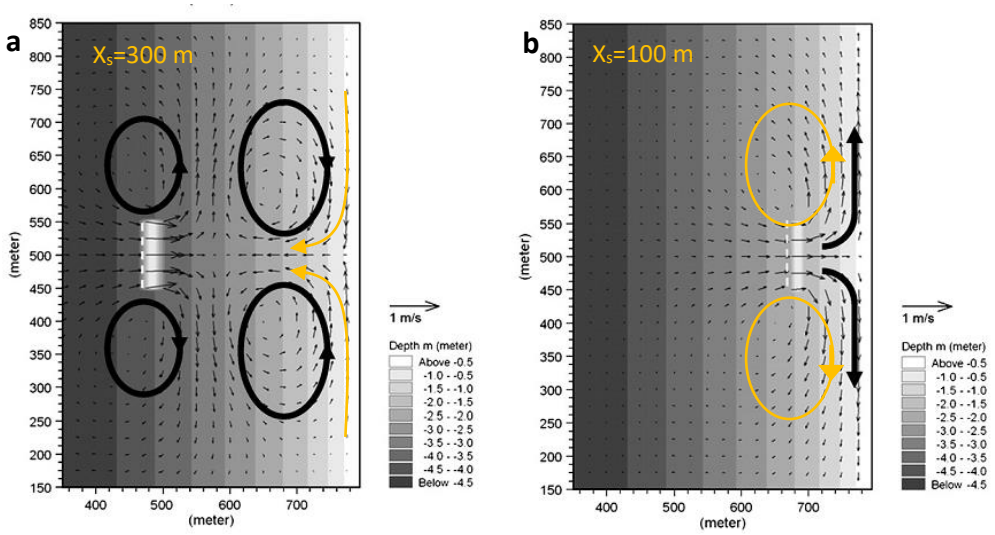

Fig 2.36: Example of using MIKE 21 to study the effect of submerged breakwater layout on nearshore circulation pattern (Modified from Ranasinghe et al., 2010). The significant wave height is 2 m and peak period is 10 s for both cases. The breakwaters are located at a) 300 m from the shore at the depth of 4 m and b) 100 m from the shore at the depth of 2 m. (The orange elements are added to the original figure by the author for further illustration)

2.3.2.5 *Summary*

MIKE is able to consider the effect of breakwater submergence on the near-shore wave field (e.g. breaking induced dissipation, wave refraction, wave diffraction), similar to DELFT3D. Besides, MIKE uses an unstructured mesh, which makes the mesh generation much easier in coastal areas with complex geometries

However, like DELFT3D when applied in the phase averaged mode (see section 2.3.1.1), MIKE also suffers from limitations in representing swash zone sediment transport. On the other hand, DELFT3D utilizes more advanced schemes to represent wave induced-flow (see section 4.2.2). Moreover, like DELFT3D, MIKE is also not able to represent the effect of breakwater porosity on wave transmission (see section 2.2.1) and on the flow through the porous submerged breakwater (see section 2.1.1b). It is also important to stress that, unlike DELFT3D, MIKE is still not an open source model and therefore its application for research purposes is difficult.

2.3.3 TELEMAC

The open source TELEMAC modelling system is developed by the Laboratoire National d'Hydraulique et Environnement (L.N.H.E.), a research department of the French Electricity Board (EDF-DRD), and is distributed by SOGREAH. TELEMAC uses unstructured grids which enhances the model ability to represent complex geometries in coastal areas. The TELEMAC modelling system includes different modules for modelling of waves, free surface hydrodynamics, sediment transport and bed level changes, water quality, and groundwater flows. The modules of TELEMAC, which are relevant to this study, are described below:

2.3.3.1 *Wave Module*

The wave module of TELEMAC, TOMAWAC (EDF R&D, 2017; Benoit et al., 1997), is a third generation phase averaged model that describes the evolution of the wave energy spectrum in arbitrary conditions of wind, currents and bathymetry .TOMAWAC accounts for wind-driven wave generation,

shoaling, wave breaking, white-capping, wave-wave interaction, wave refraction, diffraction, and bottom friction.

2.3.3.2 Hydrodynamic Module

For calculating free surface and flow velocities, two hydrodynamic modules are available in TELEMAC:

- TELEMAC 2D (Lang, 2010) solves two dimensional shallow water equations to calculate the free surface and depth-averaged horizontal velocities. It can also represent float tracking and the movement of a dissolved substance which possibly affect the vertically averaged fluid density.

- TELEMAC 3D (France, 2007) solves the three dimensional RANS equations (with or without the hydrostatic pressure assumption) to calculate free surface and three-dimensional flow field.

Hydrodynamic modules of TELEMAC accounts for bed level changes, wave forcing, tidal forcing, Coriolis forces, density variations, meteorological phenomena such as atmospheric pressure, wind, turbulence, and bottom friction.

2.3.3.3 Sediment Transport Module

The sediment transport module of the TELEMAC modelling system is called SISYPHE (Tassi and Villaret ,2014) which is applicable to non-cohesive (sand) sediments, cohesive sediments (mud) and sand-mud mixtures. SISYPHE sediment transport module uses the results of the flow computation from both TELEMAC 2D and TELEMAC 3D to calculate sediment transport rates and bed level changes. Similar to the sediment transport module in DLEFT3D and MIKE, SISYPHE is able to calculate bed load and suspended load transport rates separately, the latter is determined by solving depth-integrated advection-diffusion equations for suspended sediment concentration. The bed level changes are also calculated using the Exner equation.

2.3.3.4 Example Applications

To the author's knowledge, no application of TELEMAC for modelling the effect of submerged breakwaters on coastal hydrodynamic and morphology is reported in the available literature.

2.3.3.5 Summary

Although TELEMAC is potentially able to represent the major wave propagation and wave-induced flow processes associated with breakwater submergence, to the author's knowledge, no application of TELEMAC for this purpose has yet been reported in the literature. Moreover, like DELFT3D and MIKE, TELEMAC is not able to consider the effects of breakwater porosity.

2.3.4 XBeach

XBeach (Roelvink et al., 2009) is a 2DH (depth averaged) open source modelling system which is developed by a consortium of UNESCO-IHE, Delft University of Technology and the University of Miami. XBEACH is specifically developed to simulate the storm impacts on barrier coasts. In addition

to conventional hydro-morphodynamic processes that can also be normally reproduced by other 2DH models, XBeach is able to successfully represent long wave (infra-gravity waves) transformation, overwash, inundation and the storm impacts such as breaching and dune erosion (Elsayed, 2017). The model has been validated with a series of analytical, laboratory and field test cases using a standard set of parameter setting. The integrated modules of XBeach are briefly described below:

2.3.4.1 Wave Module

The wave module in XBeach is available in three different modes as outlined below:

- *Stationary mode (Phase-averaged)*: The model solves the stationary wave action balance equation on the scale of wave groups, but neglecting infra-gravity waves. In this mode, the processes that are resolved by the model are, wave shoaling, wave breaking, wave refraction and bed friction.

- *Surfbeat mode (instationary)*: The model solves time-dependent wave action balance equation. In this mode, in addition to short wave variations on the wave group scale, the long waves associated with them are also resolved.

- *Non-hydrostatic mode (phase-resolving):* The model solves the non-linear shallow water equations including a non-hydrostatic pressure scheme, enabling the model to reproduce the propagation and decay of individual waves. For the non-hydrostatic mode, the model needs much higher spatial resolution and smaller time steps, making this mode much more computationally expensive.

2.3.4.2 Flow Module

The flow module in XBeach calculates flow velocities and surface elevation variations through solving the non-linear mass balance equation and shallow water momentum equations. The XBeach Flow module includes a hydrostatic mode and a non-hydrostatic mode, the latter enables the model to account for all wave motions (including short waves).In XBeach, shallow water equations are also written and solved in the GLM (*Generalized Lagrangian Mean*) reference frame.

2.3.4.3 Sediment Transport Module

The sediment transport module in XBeach calculates the suspended sediment transport rate and bed level changes. The sediment transport module solves the depth-averaged advection-diffusion equation to calculate suspended sediment transport using the results of hydrodynamic calculations performed by the flow module. The bed updating algorithm in the sediment transport module can accounts for important storm impacts such as breaching and avalanching (Elsayed, 2017).

2.3.4.4 Example Applications

The application of XBEACH for modelling the effect of submerged breakwaters on coastal hydrodynamic and morphology is not reported in the available literature. Thus, no example is provided here.

2.3.4.5 Summary

Based on the above discussion, the only advantage of XBeach over MIKE and DELFT3D is that the model is able to represent more comprehensively swash zone hydrodynamics and important storm impacts such as dune erosion and breaching. However, Harley et al. (2011) evaluated the XBEACH capabilities to predict the storm effects on the Emilia-Romagna coastline in Northern Italy, where a system of segmented submerged breakwaters protects the beach. Results of the study showed that XBeach is inappropriate to study cross-shore profile evolution behind the submerged breakwaters. As discussed by Harley et al. (2011), this limitation is due to unrealistic over estimation of the set-up of the mean water level caused by the effect of breakwater submergence. Besides, the model does not include the effect of breakwater porosity on wave transmission.

2.3.5 GENESIS

The need to calculate long-term shoreline change and compare performance of numerous engineering alternatives over long spatial and time scales has led to a wide application of the one-line (shoreline response) models. Among the available one-line models, the generalized shoreline change model GENESIS (Hanson and Kraus, 1989) is one of the most commonly used models in practice (Hanson and Kraus, 2011).

One-line models such as GENESIS are 2D alongshore sediment transport models which reproduces the time evolution of the shoreline positions. The key assumption of one-line models is that, the calculated erosion and accretion at each point shifts the cross-shore profile in landward and seaward directions respectively, while the shape of the profile remains constant. The erosion/accretion at each point is calculated based on the conservation of alongshore sediment transport in a given model segment. In GENSEIS, like other one-line models, the longshore sediment transport across the active beach profile is calculated using bulk alongshore transport equations such as the CERC formula (SPM, 1984). GENESIS has been further developed to accommodate the shoreline response to beach nourishment, seawalls, sand transport around and through the shore normal structures (e.g. groins) and wave transmission in detached breakwaters. However, GENESIS cannot explicitly model cross-shore transport which represents the dominant mode of sediment transport under short-term events such as storm. Further details on the predictive capabilities and some other limitations of GENESIS can be found in the literature (Hanson and Kraus 1989, 2011). The GENESIS modelling system is composed of two major modules, which are described below.

2.3.5.1 Wave Module

The wave calculation module of the GENESIS is called the internal wave transformation model, as opposed to the other, completely independent, external wave transformation model which can be optionally utilized to supply nearshore wave information to GENESIS. As an external wave module, the linear wave transformation model RCPWAVE (Ebersole et al., 1986) is one of the most appropriate options to be used with GENESIS (Hanson and Kraus, 1989). The wave module in GENESIS calculates, under simplified conditions, breaking wave height and angle (with respect to the shoreline) using the input wave data. The internal wave module is able to account for wave diffraction, shoaling and refraction, and transmission for detached breakwaters.

2.3.5.2 Sediment Transport Module

The sediment transport module solves the one-line sand conservation equation to calculate shoreline change. To calculate the bulk longshore sand transport rate, a wide range of expressions such as CERC (SPM, 1984) longshore transport formula is available in the model. These expressions are mainly based on empirical results.

2.3.5.3 Example Applications

One-line models such as GENESIS have mostly been applied for simulating shoreline response to zero or low transmission structures such as fully emergent detached breakwaters. However, for submerged breakwaters, GENESIS could be applied to investigate, among other detached breakwater characteristics, the effect of wave transmission on the shoreline response (e.g. Hanson et al., 1989; Wamsley and Hanson, 2003). Some applications of GENSESIS to study the effect of submerged breakwaters on coastal morphology have been mentioned in section 2.2.2 (see Eqs 2.8 and 2.9). Fig. 2.37 provides an additional example of the application of GENESIS to study the effect of wave transmission on the shoreline evolution leeward of submerged breakwaters:

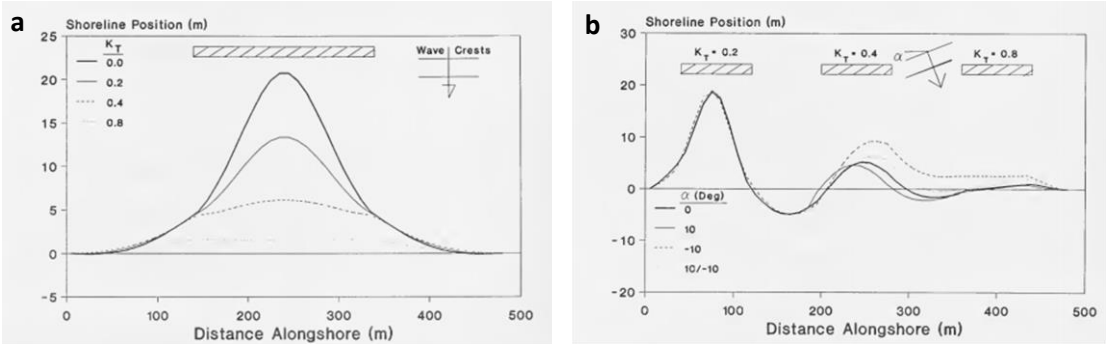

Fig 2.37: Example application for shoreline change modelling: a) Leeward of a single submerged breakwater. b) Leeward of segmented submerged breakwater using the GENESIS (From, Hanson et al., 1989).

2.3.5.4 Summary

Though GENESIS, certainly the most popular and most advanced among the available one-line models, has been widely used worldwide as a tool for the preliminary design of breakwaters in coastal protection systems, it is not able to adequately consider the effect of submergence, as it cannot reproduce the two-dimensional nearshore wave-induced flow pattern in the vicinity of submerged breakwaters (see Figs.2.9 and 2.10). Reproducing such flow pattern, typical for submerged breakwaters, are crucial as they may explain the erosion and accretion processes observed in many case studies behind the structure (e.g. Ranasinghe et al., 2006; Ranasinghe and Turner, 2006). Moreover, although GENESIS is able to consider the transmissivity of breakwater caused by the structure submergence, it is, like all other models, not able to account for the effect of breakwater porosity (see Table. 2.2)

2.3.6 Key results and implications of the analysis of the reviewed numerical models

Among the models reviewed in this section, GENESIS is not able to account for the effect of breakwater submergence, XBeach is found to overestimate the wave set-up leeward of submerged breakwaters, and TELEMAC has not yet been applied to study the effect of submerged breakwaters on

nearshore hydrodynamics and morphological changes. Therefore, the selection should be made between MIKE and DELFT3D, which have been applied in a number of relevant studies. As mentioned before, MIKE uses unstructured mesh, which provides high flexibility for mesh generation in complex coastal areas. This is the main advantage of MIKE over DELFT3D. However, as discussed before, DELFT3D can better reproduce the effect of waves on nearshore hydrodynamic (e.g. wave induced flow and wave induced turbulence). Besides, unlike MIKE, DELFT3D has an open source access and thus the application of the model for research and development purposes is more convenient. Therefore, DELFT3D is selected for this study. This decision will be further justified through a detailed model validation presented in chapter 4. A comparative summary of the available numerical models is given in Table. 2.4:

Table 2.4: Summary of advantages and disadvantages of reviewed numerical models in this study

Model	Advantages	Disadvantages
DELFT3D	• **Major Included Relevant Processes:** ▪ Wave breaking ▪ Refraction/Diffraction ▪ Wave-induced flows ▪ Full undertow currents ▪ Breakwater transmissivity ▪ Reflection from breakwater • **Wide Relevant Applications** • **GLM Flow formulation** • **Open source availability**	• **Major Relevant Limitations:** ▪ Porosity dissipation ▪ Filtration flow thorough porous breakwater ▪ Swash zone dynamics
MIKE	• **Major Included Relevant Processes:** ▪ Wave breaking ▪ Refraction/Diffraction ▪ Wave-induced flows ▪ Full undertow currents ▪ Breakwater transmissivity • **Wide Relevant Applications** • **Unstructured Mesh**	• **Major Relevant Limitations:** ▪ Wave reflection ▪ Porosity dissipation ▪ Filtration flow thorough porous breakwater ▪ Swash zone dynamics • **Commercial**

Table. 2.4, continue from the previous page

XBEACH	• **Major Included Relevant Processes:** ▪ Wave breaking ▪ refraction ▪ Wave-induced flows ▪ Swash zone dynamics • **GLM Flow Formulation** • **Open source availability**	• **Major Relevant Limitations:** ▪ Wave Reflection ▪ Porosity dissipation ▪ Filtration flow thorough porous breakwater ▪ Full undertow currents • **No Reported Relevant Application**
TELEMAC	• **Major Included Relevant Processes:** ▪ Wave breaking ▪ Refraction-diffraction ▪ Wave-induced flows ▪ Full undertow currents • **Unstructured mesh** • **Open source availability**	• **Major Relevant Limitations:** ▪ Wave reflection ▪ Porosity dissipation ▪ Filtration flow thorough porous breakwater ▪ Swash zone dynamics • **No Reported Relevant Application**
GENESIS	• **Major Included Relevant Processes:** ▪ Breakwater Transmissivity • **Computationally cheap** • **Open source availability**	• **Major Relevant Limitations:** ▪ Wave reflection ▪ Wave breaking ▪ Wave-induced flow ▪ Porosity dissipation ▪ Swash zone dynamics

It should be noted that, like the other models discussed in this section, DELFT3D is not able to include the porosity effects on the wave transmission and on the filtration flow through the porous body of the breakwater. As mentioned later (see section 2.4.2), in this study, only the limitation of DELFT3D with respect to the effect of porosity on wave transmission is addressed. Thus the effect of porosity on filtration flow through the breakwater (see Fig. 2.4) is not considered. As can be concluded from section 2.1.1, omitting the filtration flow may lead to a higher wave set-up, and consequently to more erosion of the protected beach. Therefore, the results obtained without considering the filtration flow may result in an overestimation of the erosion of the protected beach.

2.4 Implications for the research objectives and methodology of this study

The available studies on the protective efficacy of submerged breakwater are subdivided into three major categories: (i) effect on the incident waves (hydraulic performance), (ii) long-term morphodynamic effects and (iii) short-term morphodynamic effects. The results of the review and analysis of the current knowledge as presented in section 2.2.4, show major gaps as outlined below:

- The hydraulic performance, which is formulated in terms of wave transmission, has been extensively studied and a wide range of relevant wave transmission formulae have been developed for engineering practice (see section 2.2.1). These WTC formulae adequately consider the effect of breakwater submergence. However, none of the existing WTC formulae (see Table 2.2) explicitly include the combined effect of breakwater submergence and breakwater porosity, though submerged breakwaters are generally porous and porosity might have a noticeable effect on the performance of the structure.

- The available studies on the morphodynamic effects of submerged breakwaters (both in long-term and short-term) do not explicitly consider the effect of breakwater porosity, thus omitting the combined effect of porosity and submergence. However, the results of these studies, at least provide a qualitative description of the effect of breakwater submergence on coastal morphology.

- The available studies on morphodynamic effects of submerged breakwaters mostly provide limited datasets, which are not adequate to develop robust predictive formulae and design criteria for engineering practice.

- Recently, a limited number of studies have attempted to develop predictive formulae for evaluating long-term morphodynamic effects of submerged breakwater. However, compared to long-term moprhodynamic effects, the short-term morphodynamic effect of submerged breakwaters have been studied very rarely and no predictive formula is available to evaluate the short-term morphodynamic effect of submerged breakwaters.

In order to expand the current knowledge about the design and protective efficacy of submerged breakwaters, this PhD is aimed to address the gaps of knowledge indicated above.

Moreover, it was also shown that none of the reviewed numerical models is yet able to account for the effect of the porosity on the hydraulic performance of submerged breakwaters and the associated coastal morphological changes, so that the hydro-morphodynamic model to be adopted in this study necessarily needs to be improved/extended for this purpose. Among the reviewed models, the open source model DELFT3D has been identified as the most appropriate candidate (see Section 2.3.6), which will be extended/improved accordingly.

2.4.1 Specification of the objectives

In this research study, numerical modelling is the preferred approach, because it is more appropriate for a large and detailed parameter study, which is hardly feasible in the laboratory within the time frame and with the resources allocated for this PhD. Accordingly, the following objectives are set:

(i) Getting a deep understanding of the hydrodynamic and sediment transport processes in the vicinity of porous submerged breakwaters.

(ii) Selecting the most appropriate numerical model among the available coastal engineering models to be considered in this study.

(iii) Improving/extending the selected numerical model to enable it to account for the combined effect of breakwater porosity and submergence on short-term coastal erosion.

(iv) Calibrating and validating the improved/extended model, in order to establish the calibrated/validated numerical set-up for a systematic parameter study on the effect of breakwater porosity and submergence on short-term coastal erosion.

(v) Applying the calibrated/validated numerical set-up for aforementioned parameter study, in order to generate a large dataset that also considers the effect of breakwater porosity, so that the new dataset can be utilized to substantially improve the current knowledge.

(vi) Analyzing the dataset generated by the parameter study, in order to develop novel predictive formulae and design criteria to evaluate the effect of breakwater porosity and submergence on short-term coastal erosion, and thus the protective efficacy of the structure.

The methodology adopted in this study to achieve the aforementioned objectives will be described in the next section

2.4.2 Specification of the methodology

A full In order to achieve the aforementioned objectives, this PhD research is divided into 5 consecutive work packages (WP1-WP5) as outlined below and illustrated in Fig 2.39:

WP1- Review/analysis of current knowledge and models

The objective of this work package is to get a deep understanding of hydrodynamic and sediment transport processes in the vicinity of porous submerged breakwaters and adopting an appropriate approach to study the effect of breakwater porosity and submergence on coastal morphology, in order to expand the current knowledge on the design and protective efficacy of this sort of structures. This WP is devoted to: (i) Understanding the effect of breakwater porosity and submergence on nearshore hydrodynamic and sediment transport processes; (ii) The state of the art review on the design and protective efficacy of submerged breakwaters; (iii) Specification of the current gaps of knowledge about the design and protective efficacy of submerged breakwaters, especially with respect to the effect of porosity and submergence; (iv) Reviewing the main capabilities and limitations of the most widely applied coastal engineering models; (v) Selecting the best applicable model which could be potentially improved/extended to be employed for this study; (vi) Specifying the objectives and methodology of this study. WP1 has already been addressed in this chapter.

WP2-Improving/Extending the selected numerical model

The objective of this work package is to provide an improved/extended modelling system which is able to account for the combined effect of structure porosity and submergence on near-shore hydrodynamic and the associated morphodynamic processes. Accordingly, this WP is dedicated to (i) Applying OpenFOAM for performing a detailed numerical parameter study on the effect of breakwater porosity and submergence on wave transmission; (ii) Analyzing the results of the parameter study in order to develop a novel wave transmission formula which explicitly includes the breakwater porosity, as well as breakwater submergence; (iii) Applying this formula in DELFT3D-WAVE to extend the applicability of the model to account for the effect of breakwater porosity on the near-shore wave field in the protected area leeward of submerged breakwaters. The details of the numerical parameter study on wave transmission in porous submerged breakwaters and developing the novel wave transmission formula are presented in chapter 3 of this thesis. The introduction of the novel developed WTC formulae in DELFT3D-WAVE will also be elaborated and systematically validated in chapter 4.

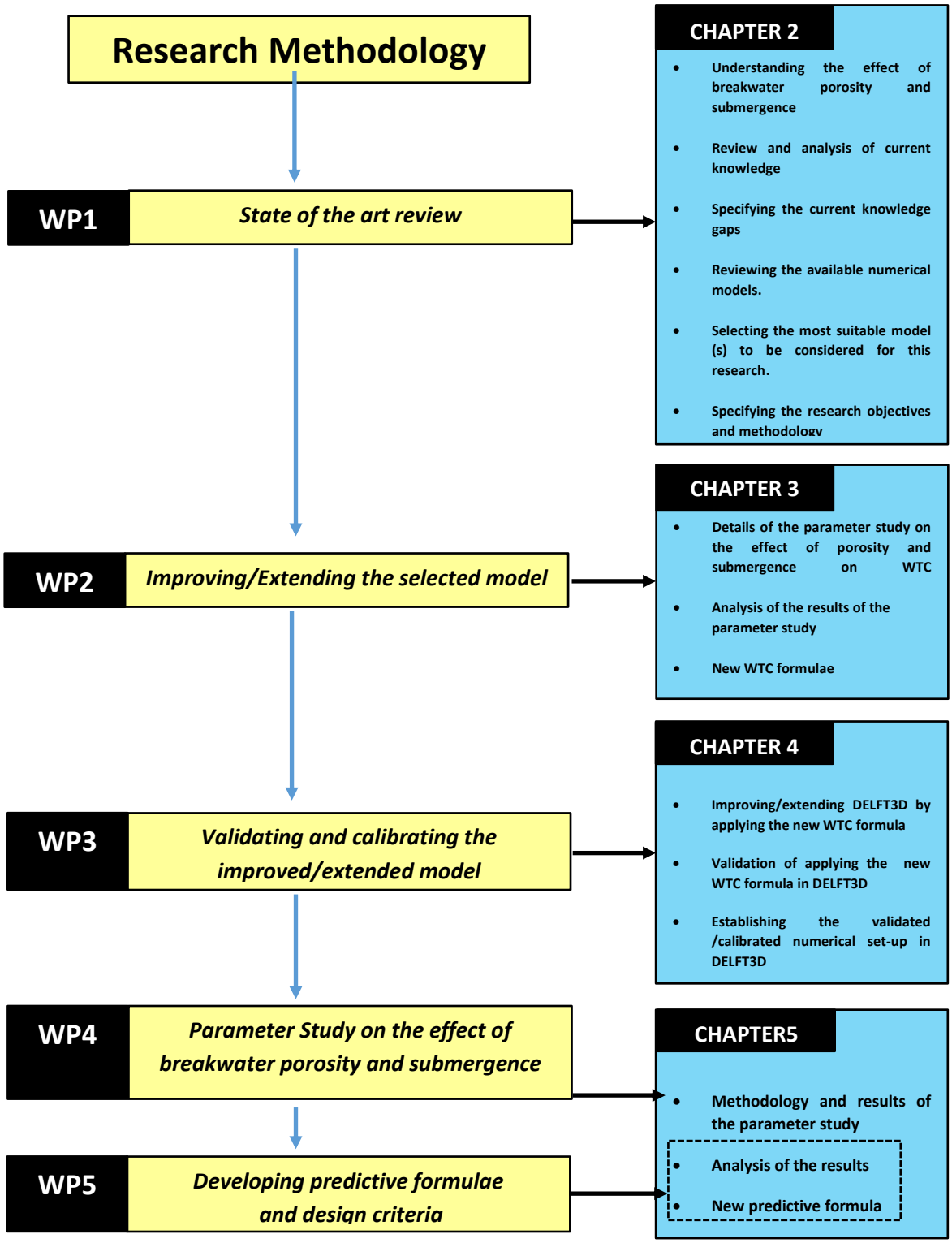

Fig 2.38: Structure of the PhD study, work packages (WP) and expected results of each chapter

WP3-Validating and calibrating the improved/extended hydro-morphodynamic model

The objective of this work package is to provide a well calibrated and validated numerical set-up in DELFT3D to be applied for the parameter study described in WP4. Accordingly, WP3 is dedicated to calibrating and validating the extended/improved DELFT3D against a well-documented benchmark

experimental study. Details of the benchmark experimental study, model calibration and model validation are elaborated in chapter 4

WP4- Parameter Study on the effect of breakwater porosity and submergence

This work package is fully devoted to apply the validated and calibrated numerical set-up in DELFT3D, as established in WP3, to perform a detailed study on the effect of different parameters of submerged breakwaters on short-term coastal erosion. The main focus of the parameter study is on the effect of breakwater porosity and submergence; however, other design parameters will also be considered for the sake of completeness. Details of the methodology and results of the parameter study are presented in chapter 5.

WP5- Developing predictive formulae and design criteria

This work package is fully dedicated to the analysis of the results of the parameter study in order to develop novel predictive formulae and criteria to be used in preliminary design of submerged breakwaters for evaluating the effect of breakwater design parameters, especially porosity and submergence, on short-term coastal erosion in the protected coast. Details of the development of the predictive formulae and criteria are presented in chapter 5.

It should be noted that, unlike long-term morphodynamic effects, the short-term morphodynamic effects of submerged breakwaters have been very rarely studied.

As mentioned in section 2.4, although few formulae have been developed to evaluate the long-term effects of submerged breakwaters on coastal morphology, no predictive formula is still available to evaluate the short-term morphodynamic effects of submerged breakwaters. Thus, the focus of WP4 and WP5 described above would be on short-term coastal erosion in the beaches protected by SPBs. Therefore, in this study, only the cross-shore processes (see Fig. 2.6) associated with short-term (e.g. time scale of a single storm) morphological changes would be considered. On the other hand, because of the critical importance of beach erosion, WP4 and WP5 focuses on the effect of SPBs on the erosion of the protected beach by short-term events such as storms (see also Chapter 5). It should be noted that, as stated in section 2.3.6 and implicitly mentioned in the description of WP2 in this section, the filtration flow (flow thorough the porous body of the breakwater) is beyond the scope of the model extensions/improvements carried out in WP2 and WP3. Accordingly, among the results of the parameter study in WP4, the erosion of the protected beach might be overestimated. Therefore, the results and conclusions which will be drawn from WP4 and WP5 might be considered as rather conservative.

3 Wave transmission formulae to account for structure porosity

Wave transmission is one of the most important processes governing the morphological changes in the areas protected by offshore breakwaters. In fact, the efficiency of the offshore breakwaters in coastal protection systems is closely related to their capability to mitigate the wave impact on the beach (see section 2.1). Therefore, a reliable assessment of the **W**ave **T**ransmission **C**oefficient (Hereafter, WTC) represents an essential part of the functional design of breakwaters.

However, although the breakwater porosity may significantly affect WTC (Losada et al., 1997; Ting et al., 2004; Rahman and Akter, 2014), only very few studies considered the porosity effect on the wave transmission at submerged breakwaters. As mentioned in section 2.2.1, no WTC prediction formula including the effect of the structure porosity has yet been proposed. Since the use of submerged porous breakwaters as control structures for natural and nourished beaches are increasingly becoming more attractive, the effect of porosity needs to be better understood and explicitly introduced in the WTC formulae for submerged porous breakwaters.

In this chapter, as a response to the aforementioned gaps of knowledge, a novel WTC formula which explicitly takes the effect of breakwater porosity into account, is developed for submerged breakwaters. For this purpose, a numerical model set-up is established in the OpenFOAM CFD modeling suite, which is potentially able to reproduce all processes influencing wave transmission in submerged breakwaters (i.e. wave reflection and wave dissipation, as expressed by Eq. 2.2). The numerical model set-up is then validated and utilized to perform a systematic parameter study on wave transmission at submerged breakwaters. The main focus of the parameter study presented in this chapter is on the breakwater submergence and porosity. Yet, for the sake of completeness, the effect of crest width is also investigated. Finally, the results of the parameter study are analyzed to develop a novel WTC formula which explicitly accounts for the porosity of the structure.

Based on the methodology described above, this chapter is organized as follows. Section 3.1 is devoted to the description of the approach adopted for the numerical study presented in this chapter. Section 3.2 provides a brief description of the CFD model in OpenFOAM, including the underlying governing equations and representation of porous flow. Section 3.3 is devoted to the description of the numerical parameter study, including the numerical model set-up and validation, testing performance, and analysis of the results with the main focus on the combined effects of porosity and submergence on wave transmission. Section 3.4 is devoted to the development of the novel WTC formula which explicitly accounts for the effect of porosity. Finally, section 3.5 summarizes the key implications of the results for this PhD research.

3.1 Numerical study

The common method to study wave transmission in breakwaters is to build a scaled physical model of the structure and to expose the model to a wide range of wave conditions in a wave flume and/or in a wave basin. Although laboratory studies may provide a deep insight into the processes underlying wave transmission, they have several limitations (e.g. scale and laboratory effects; extensive costs, manpower and time). Considering the fact that a parameter study with a sufficiently wide range of wave conditions and structure parameters is required to better understand and explicitly consider the effect of structure porosity on wave transmission, laboratory studies are hardly feasible, considering the associated tremendous amount of work and prohibitive costs, and also the constraints due to the time frame of the PhD study. Therefore, an alternative method using numerical simulations or analytical solutions can be adopted (e.g. Sollitt and Cross, 1972; Do and Suh, 2011; Sulisz, 1985; Rambabu and Mani, 2005, Liu and Le, 2013). However, in most of practical coastal engineering problems, where it is necessary to include wave breaking, the existing analytical approaches are not applicable.

Unlike the existing analytical solutions, numerical simulations using Computational Fluid Dynamic (CFD) models have the advantage of resolving wave breaking. Thus, CFD modelling can be used to study all processes associated with wave transmission at submerged porous breakwaters. Fortunately, the rapid advances in computational resources and capabilities allow us now to apply numerical models as practical and reliable tools for real coastal engineering problems. Among the available numerical models, the best options are two-phase Navier-Stokes (Hereafter NS) models because:

i) NS-based CFD models yield a very detailed description of the entire three-dimensional flow field.
ii) NS-based CFD models can also account for non-linear processes and turbulent flow within the porous zones
iii) Two-phase models do not require the estimation of pressure and velocity at the water surface (boundary between air and water). This estimation might introduce a noticeable source of errors in the numerical solution.

In this study, the open source CFD library OpenFOAM is applied for the parameter study. An introduction of OpenFOAM is given in section 3.2. Following the approach suggested in previous studies (e.g. Karim et al., 2008; Hieu and Vinh, 2012), in order to set-up the numerical model and to study wave structure interactions, it is necessary to validate the numerical model against reliable experimental data. Accordingly, OpenFOAM is validated against the results of an experimental study on wave transmission at a submerged porous breakwater carried out by Hieu and Tanimoto (2006).

The detailed description of the numerical model set-up and the model validation is given in sub-section 3.3.1. The validated numerical set-up is then applied to investigate the effect of porosity of submerged breakwaters on WTC. The numerical parameter study is described in sub-section 3.3.2. In order to quantify the effect of porosity on the wave transmission coefficient, a new **P**orosity **E**ffect **F**actor (PEF) is introduced in this study:

$$PEF = \frac{K_t(n)}{K_t(n=0)} \qquad 3.1$$

$$\Rightarrow K_t(n) = PEF \times K_t(n=0)$$

Where $K_t(n)$ is the WTC of the porous breakwater, n is the porosity of the structure and $K_t(n=0)$ is the reference WTC which corresponds to the WTC of an impermeable breakwater with the same design as that of the porous breakwater under study (see Section 3.4). A detailed description of the analysis of the numerical simulation results and the development of practical formulae for $K_t(n)$ and PEF are provided in section 3.4.

3.2 Introduction to OpenFOAM®

The open source CFD library OpenFOAM has increasingly become popular in the last years within both academic and engineering communities. OpenFOAM involves the numerical schemes to solve Raynolds Averaged Navier Stokes (Hereafter RANS) equation using the volume of fluids (Hereafter VOF) technique (Berberović et al., 2009). Examples of the use of OpenFOAM to study coastal structures were recently seen (e.g. Higuera et al., 2013). However, OpenFOAM suffered from the inability of adequately generating and absorbing surface waves. Jacobsen et al (2012) addressed this problem and developed a wave generation toolbox which enables OpenFOAM to accurately simulate surface wave generation and absorption. This development brings a new toolbox to OpenFOAM which is called Waves2Foam. In this study, *"Wave2Foam"* solver is utilized from within OpenFOAM to reliably simulate wave generation and propagation.

3.2.1 Governing Equations

"Wave2Foam" solves the VARANS (del Jesus et al., 2012) equations for the incompressible two phase flow and tracks the free surface movements using the VOF technique within the framework of OpenFOAM modeling system. Governing equations in Waves2Foam are given below:

$$\nabla.\vec{u} = 0 \tag{3.2}$$

$$\frac{\partial \rho.\vec{u}}{\partial t} + \nabla.\left[\rho\vec{u}\vec{u}^{T}\right] = -\nabla.p^{*} - \vec{g}.\vec{x}\nabla\rho + \nabla.\left[\mu.\nabla.\vec{u} + \rho\vec{\tau}\right] + \sigma_{T}\kappa_{\gamma}\nabla\gamma \tag{3.3}$$

$$\vec{\tau} = \frac{2}{\rho}\mu_{t}\vec{S} - \frac{2}{3}kI \tag{3.4}$$

$$S = \frac{1}{2}\left(\nabla.\vec{u} + (\nabla.\vec{u})^{T}\right) \tag{3.5}$$

where μ is the dynamic molecular eddy viscosity; p^{*} is the pressure, S is the strain rate tensor and μ_t is the dynamic eddy viscosity. Continuity and momentum equations (Eq. 3.2 and Eq. 3.3) are simultaneously solved to calculate the pressure and velocity field. For more details on the solution of the governing equations in OpenFOAM see Higuera et al. (2014).The last term in momentum equation, Eq. 3.3, in which σ is the surface tension coefficient and κ is the curvature of the interface, accounts for surface tension effects.

The volume of fluid approach (VOF) is used in the model to track the free surface. The VOF equation which is solved in the OpenFOAM to track the free surface movement is given below (Berberović et al., 2009):

$$\frac{\partial \gamma}{\partial t} + \nabla.\left[\vec{u}\gamma\right] + \nabla.\left[\vec{u}_{r}\gamma(1-\gamma)\right] = 0 \tag{3.6}$$

Here $\gamma=0$ and $\gamma=1$ represent air and fluid phases, respectively. The last term on the left-hand side, where u_r is a velocity vector normal to the surface, represents the compression term and applies an artificial compression to the interface (Afshar, 2010). For further details, see Jacobsen et al (2012) and Afshar (2010).

3.2.2 Porous Flow Representation in OpenFOAM®

In order to take the effect of structure porosity on the flow field into account, Jensen et al (2014) transformed the set of VARANS equations given in section 3.2.1 (i.e. Eq. 3.2, 3.3 and 3.6) to VARANS equations which are applicable to porous medium. The mathematical formulation of continuity, momentum, and free surface tracking equations modified by Jensen et al (2014) are given below:

$$\frac{\partial}{\partial x_i}\langle \bar{u}_i \rangle = 0 \tag{3.7}$$

$$(1+C_m)\frac{\partial}{\partial t}\frac{\langle \rho \bar{u}_i \rangle}{n} + \frac{1}{n}\frac{\partial}{\partial x_i}\frac{\langle \rho \bar{u}_i \rangle \langle \bar{u}_j \rangle}{n} = \frac{\partial \langle \bar{p} \rangle^f}{\partial x_i} + g_j x_j \frac{\partial \rho}{x_i} + \frac{1}{n}\frac{\partial}{\partial x_j}\mu_e\left(\frac{\partial \langle \bar{u}_i \rangle}{\partial x_j} + \frac{\partial \langle \bar{u}_j \rangle}{\partial x_i}\right) + F_i \tag{3.8}$$

where $<\bar{u}_{ii}>$is the volume averaged ensemble averaged velocity over the total control volume including the solids of the porous media and $\mu_e = \mu_t + \mu$ is the efficient dynamic eddy viscosity, which is the sum of molecular dynamic and turbulent dynamic eddy viscosity denoted by μ and μ_t respectively.

The turbulent dynamic eddy viscosity μ_t can be calculated by the turbulence models available in the OpenFOAM modelling system. OpenFOAM has a wide variety of turbulence models, including k-ω SST turbulence model (Menter, 1994) which was successfully applied by del Jesus et al (2012) for numerical simulation of interaction between waves and coastal structures. The distinctive feature of k-ω SST is that, this turbulence model is a combination of k-ε and k-ω models. This results in a good performance of k-ω for the boundary layer flow regions, and a good performance of k-ε for the free surface flow region. As described in details by Jacobsen et al., (2012), with VARANS equations, OpenFOAM accounts for the surface roughness in calculating the turbulent quantities (e.g. k and ω) at the bottom, and thus the wave energy dissipation due to the bottom roughness. Therefore, the bottom roughness is taken into account in the total energy dissipation over the breakwater. It should be noted that, for turbulent flow calculations in OpenFOAM, the bottom roughness is taken into account through applying the wall function (Zhou, 2017).

When the momentum equation is volume averaged in a porous medium, two terms appear that represent frictional forces from the porous medium and inertia forces from the individual grains (Jensen et al., 2014). The resistance and inertia forces in Eq 3.8 are respectively represented by F_i and C_m. Jensen et al. (2014) proposed to apply the extended Darcy–Forchheimer equation to account for the contribution of the friction forces:

$$Fi = a\rho\langle \bar{u}_i \rangle + b\rho\sqrt{\langle \bar{u}_j \rangle \langle \bar{u}_j \rangle}\langle \bar{u}_i \rangle \tag{3.9}$$

Parameters ***a*** and ***b*** are linear and non-linear resistance parameters which are given by van Gent (1995):

$$a = \alpha \frac{(1-n)^2}{n^3}\frac{\mu}{\rho D_{50}} \tag{3.10}$$

$$b = \beta\left(1 + \frac{7.5}{KC}\right)\frac{1-n}{n^3}\frac{1}{D_{50}} \tag{3.11}$$

Here D_{50} is the grain diameter, $KC = u_m T / (nD_{50})$ the Keulegan-Carpenter number, u_m is the maximum oscillating velocity and T is the period of the oscillations.

The inertia forces in Eq 3.8 are also represented by the added mass coefficient C_m, for which the following expression is provided by van Gent (1995):

$$C_m = \gamma_p \frac{1-n}{n} \qquad 3.12$$

where γ_P is an empirical coefficient. Jensen et al. (2014) also modified the original surface tracking equation in OpenFOAM (Eq. 3.6) to enable the model to track the free surface interface inside the porous media:

$$\frac{\partial \gamma}{\partial t} + \frac{1}{n}\frac{\partial}{\partial x_i}.\left[\langle \bar{u}_i \rangle \gamma\right] + \frac{1}{n}\frac{\partial}{\partial x_i}.\left[\langle \bar{u}_i^r \rangle \gamma(1-\gamma)\right] = 0 \qquad 3.13$$

3.3 Numerical Parameter Study

As discussed before, a reliable prediction of WTC is a crucial part of functional design of detached breakwaters in coastal protection systems. Although several laboratory studies have been performed to determine empirical formulae for WTC (e.g. Van der Meer and Daemen, 1994; d' Angremond et al., 1996; Seabroke and Hall, 1998; Van der Meer et al., 2005), none of the existing WTC formulae takes the effect of structure porosity into account. Since the effect of structure porosity on wave transmission might be noticeable (e.g. Losada et al., 1997; Rahman and Akter, 2014) and in order to extend the potential applications of submerged porous breakwaters as an environmentally friendly component of coastal protection systems, an attempt is made in this study to develop a new WTC formula for submerged breakwaters, which accounts for the effect of porosity. Therefore, a detailed investigation of the porosity effects on wave transmission is necessarily required. For this purpose, a numerical parameter study is performed in this study. As suggested in previous studies (e.g. Karim et al., 2009; Hieu and Vinh, 2012, Losada et al., 2008), a numerical model set-up is established in OpenFOAM, validated and applied to perform the numerical parameter study. It should be noted that, since the linear and non-linear resistance parameters (see Eq 3.9) used in CFD model is given by the formulae proposed by Van Gent (1995), which are developed for homogeneous rubble-mound materials, the scope of this numerical study would be homogeneous rubble-mound breakwaters.

The numerical model set-up is established and validated in sub-section 3.3.1 to reproduce the experimental study carried out by Hieu and Tanimoto (2006) (Hereafter HT2006). The parameter study consists of 84 numerical tests including all possible combinations of four different submergence R_c, three different crest widths B and seven different structure porosities n which range from 0 (impermeable structure) to 0.6. The numerical tests cover almost the full range of possible structure porosities with small porosity intervals of 0.1. The parameter study procedure will be described in details in section 3.3.2. Finally, on the basis of numerical results, the effect of porosity and submergence on wave transmission will be analyzed as described respectively in sub-sections 3.3.3 and 3.3.4. Based on the analysis of the results, a new WTC formula is finally developed and discussed. The development of the new WTC formula will be described in detail in section 3.4.

3.3.1 Numerical model set-up and validation

The numerical model configuration is set up on the basis of the experimental study performed by Hieu and Tanimoto (2006). This laboratory study was carried out at the Hydraulic Laboratory of Saitama University, Japan. The wave flume is 18 m long, 0.7 m high and 0.4 m wide. The seaward toe of the submerged breakwater is located 10.5 m from the wave maker. The model breakwater is 0.33 m high, 1.16 m wide at the base, and 0.3 wide at the crest. The breakwater is made of rock material with mean diameter D_{n50} = 2.5cm and porosity n=0.45 (see Fig. 3.1). The incident wave height and period are respectively H=0.092 m and T=1.6 s. Water surface variations are measured at 38 wave gauge locations distributed along the flume

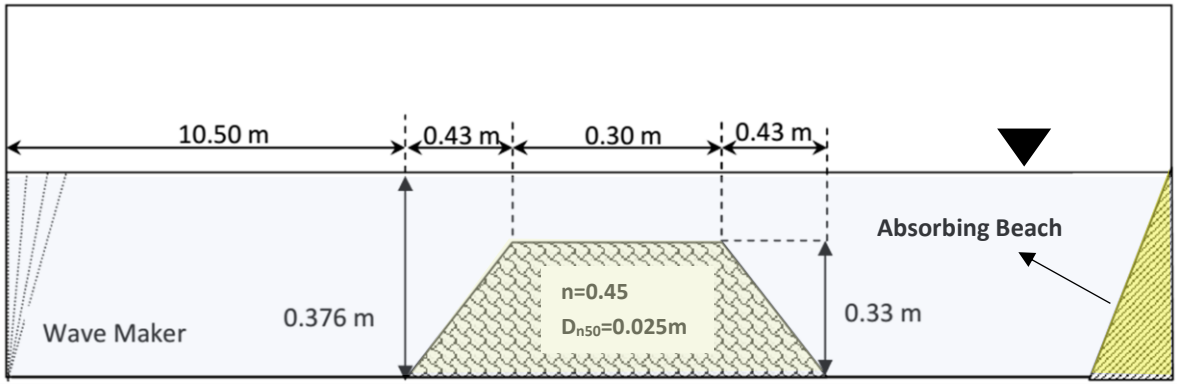

Fig 3.1: Submerged porous breakwater tested in the Hydraulic Laboratory of Saitama University, Japan, by Hieu and Tanimoto (2006) (not scaled)

In the numerical model set-up, relaxation zones are considered to avoid reflection of waves from the end of the flume and further to avoid waves reflected internally in the computational domain (Jacobsen et al., 2012). Two relaxation zones at the beginning and end of the wave channel were implemented with the length of 3m. Further numerical examinations revealed that, the length of the relaxation zone has a negligible effect on the numerical simulation results. It should be noted that, the length of the relaxation zone must not be so long that wave measurement locations fall inside the relaxation zone (see also, Jacobsen et al., 2012). The numerical model set-up is shown by Fig. 3.2, where R_c stands for submergence depth, B for crest width, h for water depth and WG for wave gauge. From the 38 wave gauges used in the laboratory test, only WG6, WG8, WG13, WG27, WG 29 and WG 32, which are used for analysis of the results, as shown in Fig. 3.2

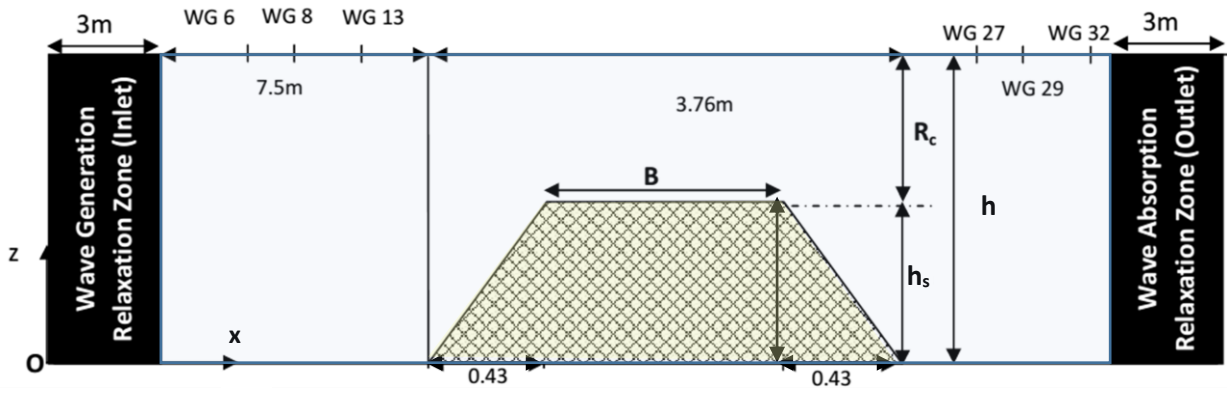

Fig 3.2: Numerical model set-up (not scaled)

In order to examine the convergence of the solution on different computational grids, preliminary tests were performed to find an optimal mesh size that yields accurate and efficient solutions. A preliminary coarse grid was generated and refined continuously until reaching the optimum grid, where more refinement no longer affects the numerical simulation results. The optimal computational grid was achieved with the smallest grid sizes of approximately 0.005 m in vertical direction (Z-axis) and 0.01 m in in the horizontal direction (X-axis). The quiescent condition was applied to the water surface over the entire computational domain at t = 0. For each test, the total simulation time was 20

wave periods, which was found to be long enough to provide stable results in all tests. However, in the analysis of the numerical results, the data from the first 5 wave periods were discarded to avoid initial instabilities. Sampling for each test was performed at 100 Hz (i.e. with time step of 0.01 s) over the period of numerical simulation. An array of three gauges denoted by WG6, WG8 and WG 13 is implemented in front of the structure to record the data, which are necessary for wave reflection analysis carried out to decompose incident and reflected waves. The incident wave height is calculated using the least square method of Mansard and Funke (1980) [Hereafter, MF80]. Transmitted waves are sampled using WGs 27, 29 and 32 located leeward of the breakwater. The exact locations of the wave gauges are given in Table 3.1, where the positions are measured with respect to the origin located at the wave maker (see Fig. 3.2).

Table 3.1: Locations of wave gauges implemented in the numerical model set-up shown in Fig. 3.2

Wave Reflection Analysis		**Wave Transmission analysis**	
Wave gauge	**Location**	**Wave gauge**	**Location**
WG6	X=9.52m	WG27	X=11.51m
WG8	X=9.84m	WG29	X=11.66m
WG13	X=10.5m	WG32	X=11.96m

The locations of these three wave gauges are selected, so that the MF80 geometrical requirements are satisfied. The laboratory measurements reported by Hieu and Tanimoto (2006) are used for the validation of the numerical model described above. The constant coefficients α, β and C_m in the numerical model (see Eqs. 3.10, 3.11 and 3.12), need to be determined prior to the numerical simulation. The variation of C_m has been found to be of negligible importance in most of the cases (e.g. del Jesus, 2012 and Higuera et al., 2014). Therefore, it is recommended to keep the value of C_m= 0.34 in the numerical simulations (e.g. Van Gent, 1995; Losada, 2008; del Jesus, 2012 and Higuera et al., 2014). Thus, parameters α and β, which are called resistance coefficients in Eqs.3.10 and 3.11, are the only two free parameters which need to be determined. However, a precise description of α and β coefficients is still beyond the existing knowledge. In order to determine α and β prior to the numerical simulation, these parameters might be obtained through experimental tests, predictive formulae or model calibration. Each of these approaches is discussed further below.

Laboratory tests

Burcharth and Andersen (1995) reported empirically determined resistance coefficients obtained from various experimental data. However, none of the reported experimental data were obtained under oscillatory flow induced by wave action. Van Gent (1995) performed the laboratory tests in the U-tube to determine α and β in both unidirectional and oscillatory flow conditions. Based on the results, Van Gent (1995) suggested the values α = 1000 and β= 1.1 for resistance coefficients, although α and β may depend on the structure porosity, and on the orientation and shape of the rock material. However, further numerical simulations revealed that resistance coefficients proposed by Van Gent et al. (1995) (Hereafter VG95) might not be valid for breaking wave conditions (Liu et al., 1999; Garcia et al., 2004; Losada et al., 2008), because the experimental tests in which VG95 are obtained did not consider wave breaking.

Predictive Formulae

Lara et al. (2011) suggested the following relationships between resistance coefficients and the material properties (median grain size D_{50} and porosity n):

$$\alpha = 4409.22 D_{50}^{0.43} \quad 3.14$$

$$\beta = 12.27 \times \frac{n^3}{(1-n)^{1.5}} D_{50}^{-01075} \quad 3.15$$

Equations 3.14 and 3.15, hereafter LA2011, provide a straightforward way to estimate the resistance coefficients α and β. However, to the author's knowledge, the applicability range of LA2011 have never been discussed in the literature. Therefore, applying LA2011 to practical coastal engineering problems might introduce a high uncertainty.

Model Calibration

The resistance coefficients α and β have been determined through model calibration in several studies (e.g. Losada et al., 2008; Karim et al., 2009; Wellens et al., 2010; Higuera et al., 2014; Jensen et al., 2014). This is mainly due to the lack of reliable method to predict the proper values of α and β. The model calibration often evaluates the resistance coefficients for one specific application and provides a set of applicable coefficients for the given case. However, the applicability of the coefficients obtained through model calibration to another case with different hydrodynamic conditions is questionable. This is the major limitation of applying the model calibration approach to determine resistance coefficients, especially for the parameter studies in which a very wide range of hydrodynamic conditions is considered. In order to provide a set of resistance coefficient with the broadest possible applicability, Jensen et al. (2014) applied OpenFOAM to perform a detailed calibration study covering a wide range of flow regimes in porous media, ranging from Forchheimer flow regime (*Rep* = 62) to fully turbulent flow regime (*Rep* = 2750) as defined by the Reynolds number *Rep* related to mean grain size D_{50} and porosity n (see Jensen et al. 2014). In that study, the resistance coefficients for the linear and non-linear resistance terms were investigated in detail over the parameter space, for a wide range of flow conditions ranging from Forchheimer to turbulent flow regimes. Based on the results, Jensen et al. (2014) suggested that α = 500 and β = 2.0 (hereafter, JE2014) is the unique set of resistance parameters that could adequately represent the flow in porous media for all aforementioned flow regimes. Jensen et al (2014) showed that, using JE2014, OpenFOAM is able to accurately reproduce the wave- structure interaction in both two and three dimensional simulations. Jensen et al (2014) draw this conclusion based on a number of model validations, among which the most relevant validation cases supporting this conclusion are briefly presented in Fig. 3.3, where the successful applications of JE2014 in OpenFOAM are shown for predicting: i) The velocity of wave induced flow inside porous breakwaters (Figs 3.3c and 3.3d), and ii) Wave reflection coefficient (Fig 3.3e).

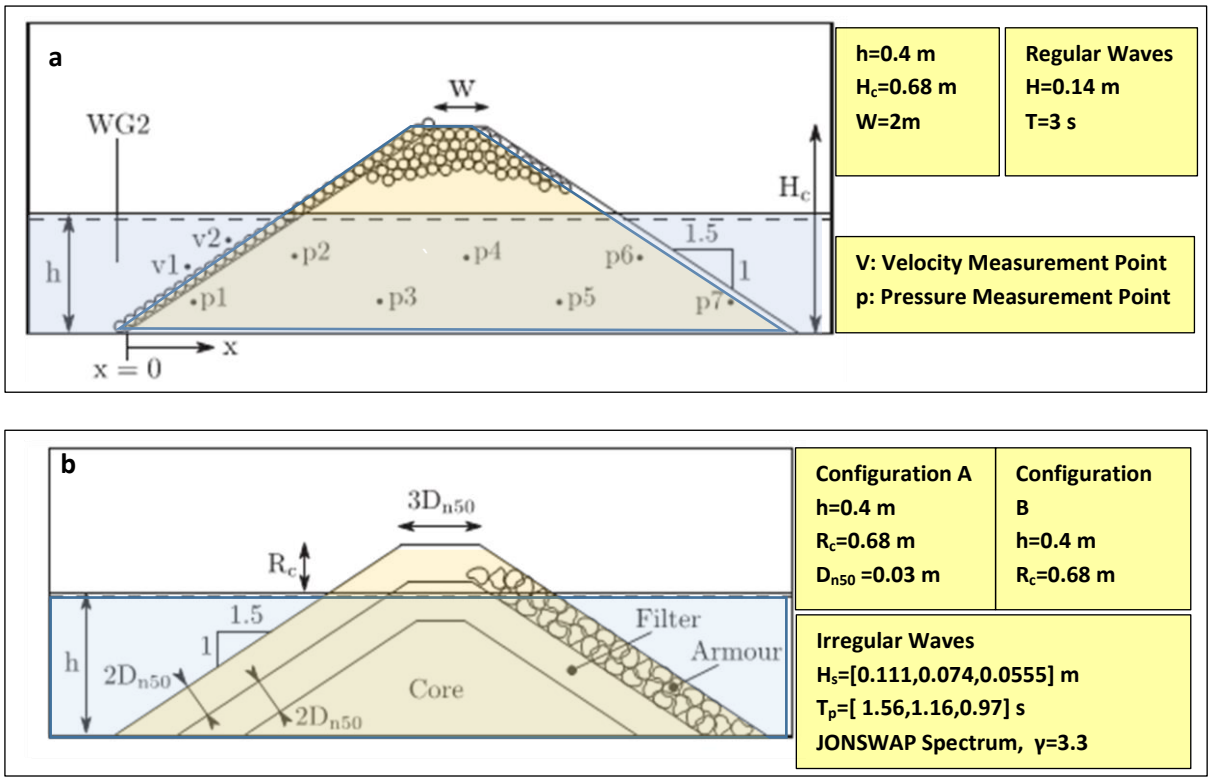

Fig 3.3: Two-dimensional validation cases reported by Jensen et al., (2014): a) Sketch of the laboratory tests by Vistisen (2012). b) Sketch of the laboratory tests by Bruce et al. (2009). c) Ensemble average velocities at point v1. d) Ensemble average velocities at point v2. e) Reflection coefficients as compared to the empirical relation presented in Zanuttigh and van der Meer (2006). (Modified form Jensen et al., 2014)

In spite of the promising results obtained by Jensen et al. (2014) using JE2014, the applicability of JE2014 to flow conditions defined by *Rep* > 2750 or *Rep* < 62 might be questionable. Indeed, although Jensen et al. (2014) did not suggest any applicability conditions in terms of Reynolds number *Rep*, this point needs further investigation in the future. In the parameter study performed in this chapter, the porosity of the structure and consequently the flow regime widely varies. Thus, JE2014 seems to be the most appropriate choice for the numerical parameter study. Accordingly, JE2014 is used for the numerical model validation. The comparison between measurements and numerical results obtained using JE2014 is shown by Figs. 3.3

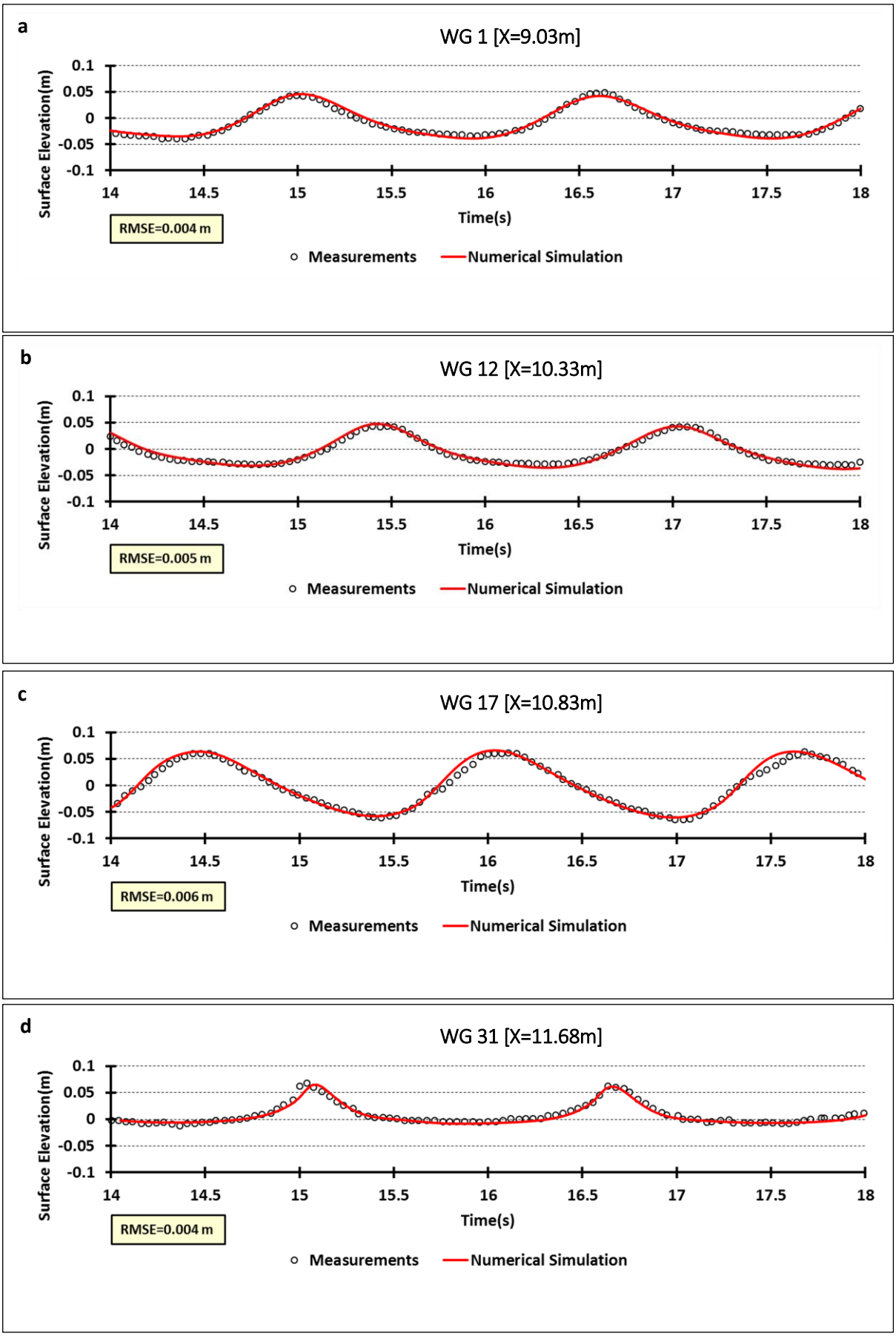
a
WG 1 [X=9.03m]
Surface Elevation(m)
0.1
0.05
0
-0.05
-0.1
14
14.5
15
15.5
16
16.5
17
17.5
18
Time(s)
RMSE=0.004 m
Measurements
Numerical Simulation
b
WG 12 [X=10.33m]
Surface Elevation(m)
RMSE=0.005 m
Measurements
Numerical Simulation
c
WG 17 [X=10.83m]
Surface Elevation(m)
RMSE=0.006 m
Measurements
Numerical Simulation
d
WG 31 [X=11.68m]
Surface Elevation(m)
RMSE=0.004 m
Measurements
Numerical Simulation

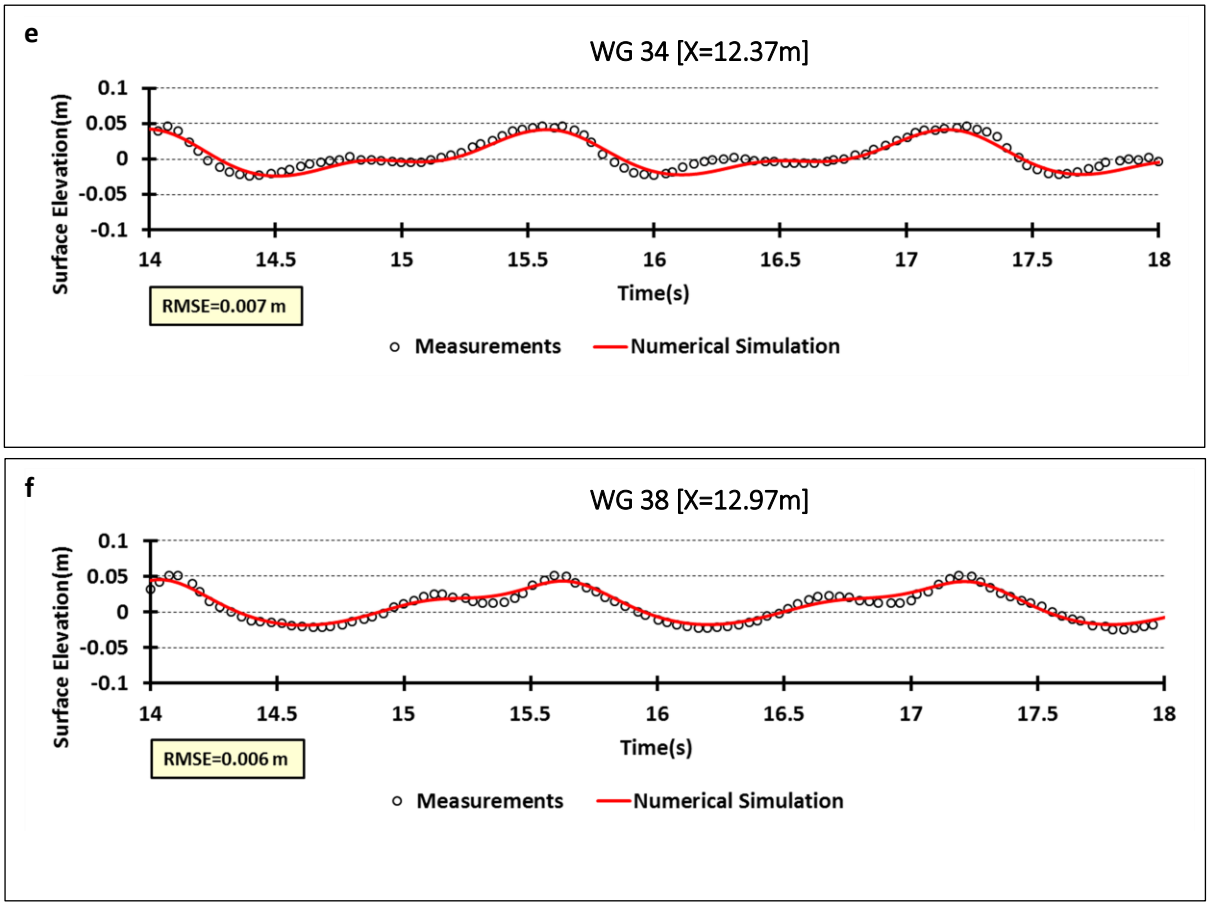

Fig 3.4: Numerical vs. measured wave profiles in HT2006 obtained using JE2014 resistance coefficients (α = 500 and β = 2.0) at different locations. (WG locations are given with respect to the origin shown in Fig, 3.2).

As can be seen in Fig. 3.4 the use of JE2014 resistance coefficients α = 500 and β = 2.0 as suggested by Jensen et al. (2014) results in a very good agreement between numerical simulation results and measurements in front (i.e. WG1, WG 12 and WG17) and leeward (i.e. WG31, WG34, WG38) of the SPB. In addition, as shown in Fig. 3.3, the successful application of JE2014 resistance coefficients in OpenFOAM to simulate the interactions between wave and porous breakwaters have already been proved by Jensen et al. (2014).

However, in order to further confirm and quantify the accuracy of numerical results, root mean squared error (RMSE) is applied as the statistical indicator. As shown in Fig. 3.4, for all WGs, the low values of root mean square error RMSE as compared to range of surface elevation values plotted in the figure, imply to a good agreement between measurements and numerical results. Such a result, along with validation results presented by Jensen et al. (2014) (see Fig. 3.3) justify that JE2014 (i.e. α = 500 and β = 2.0) is the most appropriate yet available set of resistance parameters which could be applied in the present study.

Although, JE2014 is selected for this study, for the sake of completeness, the other sets of resistance coefficient suggested in the literature for similar applications (e.g. Van Gent, 1995; Wellens et al., 2010; Lara et al., 2011, Jensen et al., 2014) are examined and the sensitivity of the results to these values are analyzed (Fig. 3.5).

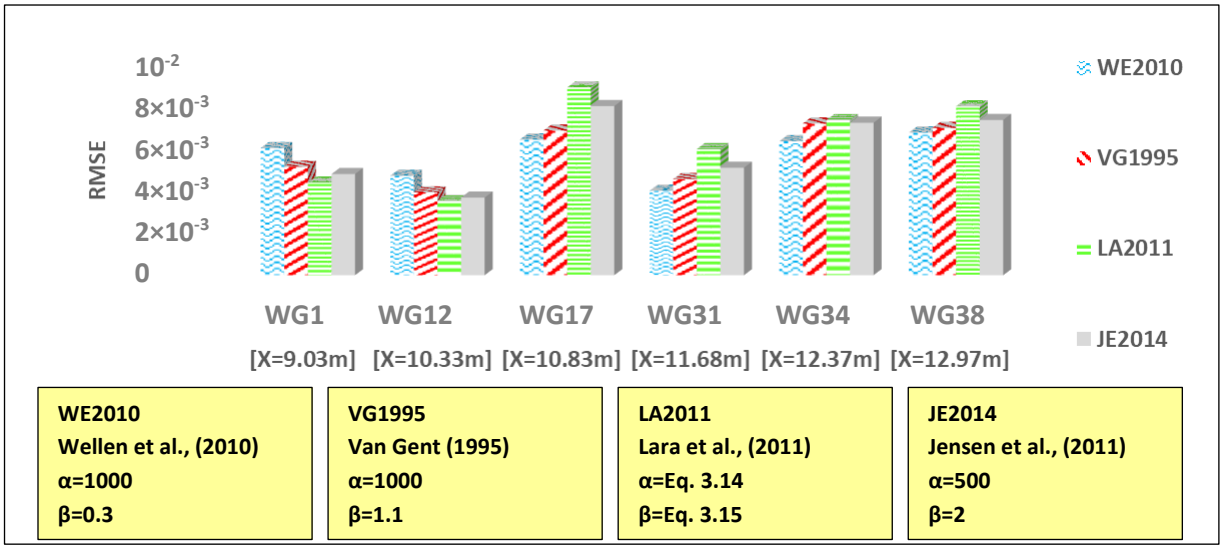

Fig 3.5: Root Mean Square Error (RMSE) at five wave gauges WG using resistance coefficients suggested in different studies (Locations are given with respect to the origin shown in Fig. 3.2).

As shown in Fig. 3.5, for all examined sets of resistance coefficient (i.e. α and β), the RMSE value at each wave gauge is low compared to the range of recorded surface elevation, suggesting a good model accuracy for the examined resistance coefficients. However, as mentioned before, because of its wider range of applicability, JE2014 is selected for this parameter study in which the porosity widely varies.

3.3.2 Testing Performance and Procedure

In order to investigate the effect of porosity and submergence of breakwaters on wave transmission under a wide range of design conditions, the parameter study is performed in the two-dimensional numerical wave flume described and validated in sub-section 3.3.1.

In the parameter study performed in this PhD research, twelve different structure geometries which are composed of four different submergence depths R_c and three different crest widths B have been selected for a closer examination in the numerical model.

For a homogeneous submerged rubble-mound breakwater, which is the scope of this study, various ranges of practical porosity values have been proposed in different studies. Among the latter, typically, Van Gent (1995) considered n=0.388-454 as the practical range of porosity in porous coastal structures. Similarly, Karim et al., (2009) proposed the porosity range of n=0.3-0.6.

This study, with aims at providing a more extensive range of applicability, looks further beyond the practical range of porosity suggested in previous studies and examines the porosity range of n=0-0.6. It should be noted that, for porosity values which are beyond the practical range of porosity (e.g. for $0<n<0.3$ as discussed in section 3.3.3), the validity of the results is to be further verified against experimental or field measurements which are currently not available. Accordingly, for each specific breakwater geometry, seven porosities ranging from n=0 (impermeable structure) to n=0.6 are tested. It should be noted that, based on the experimental data reported by Seabroke and Hall (1998), for submerged rubble-mound breakwaters, varying the mean diameter of porous materials has a negligible effect on the wave transmission coefficient. Accordingly, in this study, the size of porous material is not considered as an influential parameter and is thus kept unchanged (i.e. D_{n50}=0.025m) in all tests.

The possible combinations of structure porosities, submergence depths and crest widths, result totally in 84 numerical tests. Each numerical test is labeled by a test ID representing parameters examined in that test. Table 3.2 provides an explanation on the meaning and interpretation of the notations used in the test IDs.

Table 3.2: Interpretation of symbols used in test IDs

Symbol	Description	Examined Values	
R	Depth of submergence	**R0:**	**Rc=0.000m**
		R2:	**Rc=0.02m**
		R4.6:	**Rc=0.046m**
		R10:	**Rc=0.100m**
B	Crest width	**B15:**	**B=0.15m**
		B30:	**B=0.30m**
		B60:	**B=0.60m**
n	Structure Porosity	**n0:**	**n=0.0**
		n10:	**n=0.1**
		. .	. .
		n60:	**n=0.6**
R4.6B30-n45	Serial number labelling the test with **n=0.45, Rc= 0.046m and B=0.3m**		

Various structure submergence, which are denoted by R0, R1, R2 and R3, are made by changing the still water depth (h=0.33 m for R_c=0, h=0.35 m for R_c=0.02 m, h=0.376 for R_c=0.046 m and h=0.43 for R_c=0.10 m). Regular waves with H=0.092 m and T=1.6 s are generated at the inlet boundary according to the Stokes Second Order wave theory. The application of the latter is verified on the basis of the modified wave theory selection diagram given by Sorensen (2005) shown in Fig. 3.6, where the red lines represents exemplary the determination of the applicable wave theory for h=0.33m (R_c=0, see Table 3.2).

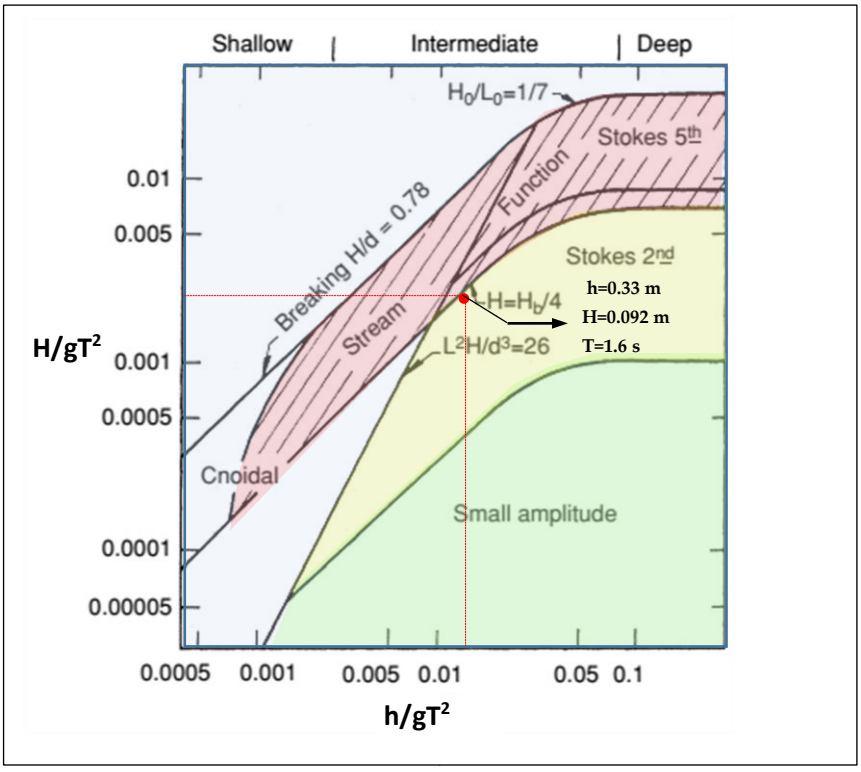

Fig 3.6: Wave selection diagram. Red lines represent the exemplary selection of wave theory for Rc=0 (Modified from Sorensen, 2005)

The L-Davis package for wave analysis, developed at LWI, is used to analyze the numerical results in both time and frequency domains. The wave reflection analysis, which is performed to separate the incident and reflected waves, is verified through a comparison between the measured (sampled) waves and the superposition of the calculated reflected and incident wave components. An example of this verification in test R4.6B30-n45 at WG13 (see Fig. 3.2) is shown by Fig.3.7

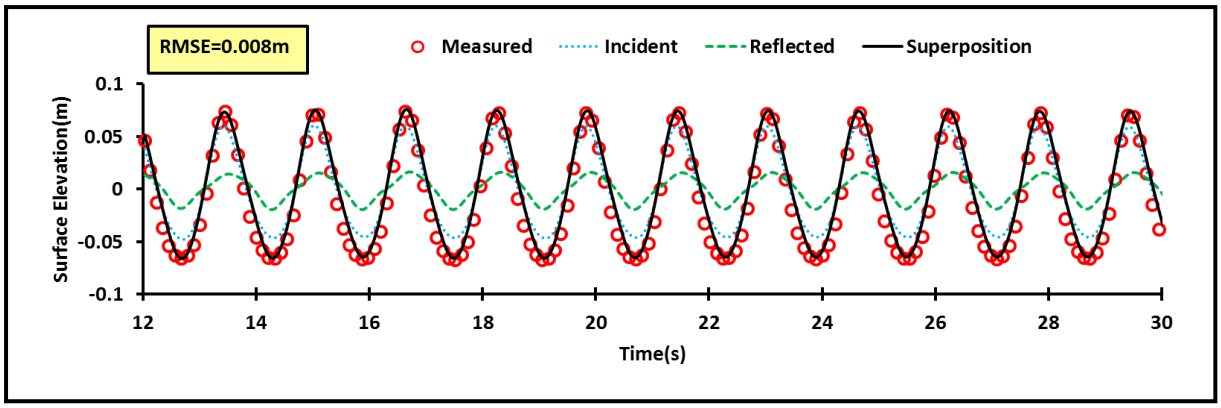

Fig 3.7: Verification of the wave reflection analysis exemplarily for WG13, R4.6B30-n45

As shown by Fig. 3.7, the very good agreement between the measured wave (numerical simulation results at WG13) and the superposition of the incident and reflected wave components, which are obtained from the reflection analysis at WG13, is also confirmed by the low Root Mean Square Error of RMSE=0.008. The transmitted wave spectrum at WG27 in the test R4.6B30-n45 is also shown is Fig. 3.8. As it is expected on the basis of previous studies on wave transmission over submerged breakwaters (e.g. Losada et al., 1997; Van der Meer, 2001; Garcia et al., 2004) the incident wave energy is transferred to higher harmonics behind the structure. In fact, the energy of the first harmonic is dissipated during wave transmission while the energy of the second and third harmonics starts to grow. It should be noted that, the measured wave spectrum is not derived from the measured surface elevation and Fig. 3.8 only shows that the model is able to reproduce the transfer of wave energy to higher harmonics due to wave transmission at submerged breakwaters

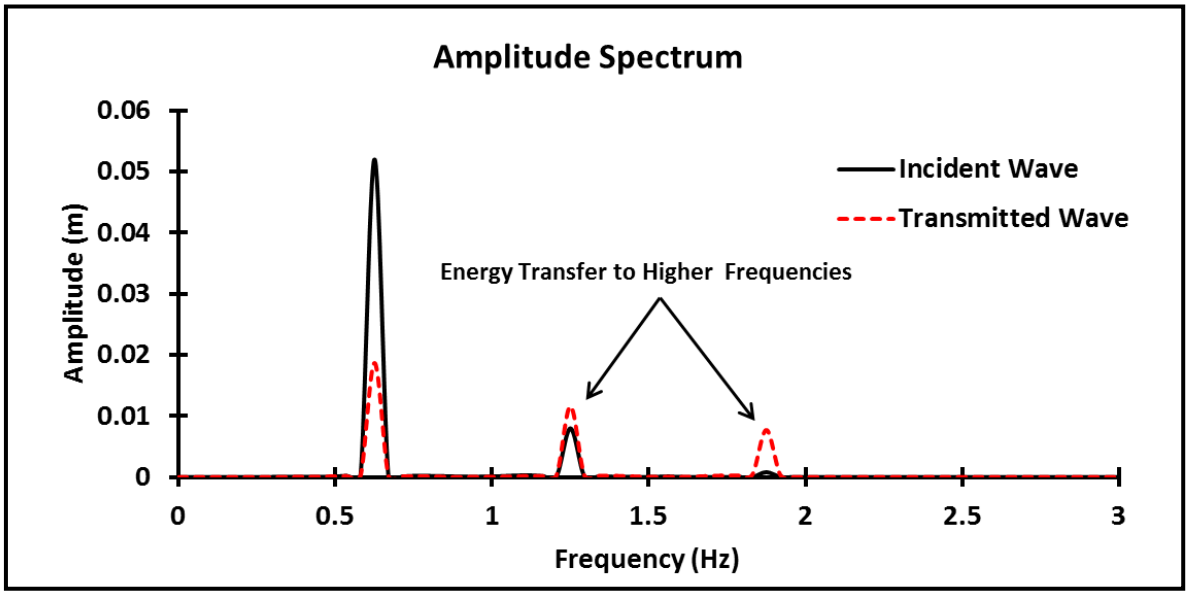

Fig 3.8: Amplitude spectrum of incident and transmitted waves at WG27 R4.6B30-n45 , for which the comparison between measured and calculated water surface elevation is given in Fig. 3.4d

The comparison between wave profiles obtained in the wave gauges located shoreward of the breakwater (i.e. WG27, WG29 and WG32) clearly shows that wave profile continuously evolve from

one location to the other (see Fig. 3.4d-f). Therefore, in order to calculate the **W**ave **T**ransmission **C**oefficient **WTC**, the conventional definitions of WTC using the ratio of wave heights become inappropriate (Hieu and Tanimoto, 2006) due to continuously evolving wave profiles along the flume. Accordingly, WTC is calculated on the basis of wave energy (see also Eq. 2.1, section 2.2.1):

$$K_t = \sqrt{\frac{E_t}{E_i}} = \frac{H_{tm0}}{H_{im0}} \qquad 3.16$$

Here, K_t stands for wave transmission coefficient, E_i for incident wave energy, E_t for transmitted wave energy, H_{m0i} and H_{m0t} respectively for zero momentum incident and transmitted wave height obtained from wave analysis performed by L-Davis wave analysis package, For each tests, the threshold incident breaking wave height H_{bi}, which is the lowest incident wave height resulting in wave breaking over the submerged breakwater, is calculated using the empirical formula proposed by Calabrese et al. (2008):

$$\frac{H_{bi}}{R_c} = A\frac{L_o}{R_c}\left[1-\exp(-1.5\frac{\pi R_c}{L_0})\right] \qquad 3.17a$$

$$A = 0.17\exp\left(0.56P - 0.28m\right) \qquad 3.17b$$

With P=0 for impermeable breakwaters
P=0.6 for homogeneous porous breakwaters

Where m=tanα is the seaward slope of the structure, L_o the deep water wave length and P is notational permeability introduced by van der Meer (1988). Eq. 3.17 is the only predictive formula which could be used to explicitly predict breaking condition (i.e. $H_i/H_{bi} \geq 1$) as a function of incident wave conditions and breakwater design parameters. Calabrese et al. (2008) showed that, in general, Eq. 3.17 can efficiently predict the wave-breaking over submerged breakwaters.

A summary of 84 numerical tests including all possible combinations of seven porosities n={0, 0.1, 0.2, 0.3, 0.4, 0.5, 0.6}, four submergence R_c={0, 0.03 m, 0.06 m, 0.10 m} and three crest width B= {0.15 m, 0.3 m 0.6 m} are provided in Table 3.3, where k is the wave number, h water depth and H_{bi} threshold incident breaking wave height according to the breaking criterion over SPBs in Eq 3.17.

Table 3.3: Summary of numerical tests performed in the parameter study

Test ID	n	T (s)	H_i (m)	H_{bi} (m)	H_{bi}/H_i	h (m)	k	Kh	H/L	Rc (m)	B (m)	R_c/H_i	kB	K_t
R0B15-n0	0.00	1.60	0.09	-	-	0.35	2.35	0.82	0.03	0.00	0.15	0.00	0.35	0.48
R0B15-n10	0.10	1.60	0.09	-	-	0.35	2.35	0.82	0.03	0.00	0.15	0.00	0.35	0.20
R0B15-n20	0.20	1.60	0.09	-	-	0.35	2.35	0.82	0.03	0.00	0.15	0.00	0.35	0.19
R0B15-n30	0.30	1.60	0.09	-	-	0.35	2.35	0.82	0.03	0.00	0.15	0.00	0.35	0.22
R0B15-n40	0.40	1.60	0.09	-	-	0.35	2.35	0.82	0.03	0.00	0.15	0.00	0.35	0.26
R0B15-n50	0.50	1.60	0.09	-	-	0.35	2.35	0.82	0.03	0.00	0.15	0.00	0.35	0.32
R0B15-n60	0.60	1.60	0.09	-	-	0.35	2.35	0.82	0.03	0.00	0.15	0.00	0.35	0.39
R0B30-n0	0.00	1.60	0.09	-	-	0.35	2.35	0.82	0.03	0.00	0.30	0.00	0.71	0.42
R0B30-n10	0.10	1.60	0.09	-	-	0.35	2.35	0.82	0.03	0.00	0.30	0.00	0.71	0.12
R0B30-n20	0.20	1.60	0.09	-	-	0.35	2.35	0.82	0.03	0.00	0.30	0.00	0.71	0.11
R0B30-n30	0.30	1.60	0.09	-	-	0.35	2.35	0.82	0.03	0.00	0.30	0.00	0.71	0.11
R0B30-n40	0.40	1.60	0.09	-	-	0.35	2.35	0.82	0.03	0.00	0.30	0.00	0.71	0.15
R0B30-n50	0.50	1.60	0.09	-	-	0.35	2.35	0.82	0.03	0.00	0.30	0.00	0.71	0.22
R0B30-n60	0.60	1.60	0.09	-	-	0.35	2.35	0.82	0.03	0.00	0.30	0.00	0.71	0.31
R0B60-n0	0.00	1.60	0.09	-	-	0.35	2.35	0.82	0.03	0.00	0.60	0.00	1.41	0.33
R0B60-n10	0.10	1.60	0.09	-	-	0.35	2.35	0.82	0.03	0.00	0.60	0.00	1.41	0.09
R0B60-n20	0.20	1.60	0.09	-	-	0.35	2.35	0.82	0.03	0.00	0.60	0.00	1.41	0.07
R0B60-n30	0.30	1.60	0.09	-	-	0.35	2.35	0.82	0.03	0.00	0.60	0.00	1.41	0.09
R0B60-n40	0.40	1.60	0.09	-	-	0.35	2.35	0.82	0.03	0.00	0.60	0.00	1.41	0.12
R0B60-n50	0.50	1.60	0.09	-	-	0.35	2.35	0.82	0.03	0.00	0.60	0.00	1.41	0.16
R0B60-n60	0.60	1.60	0.09	-	-	0.35	2.35	0.82	0.03	0.00	0.60	0.00	1.41	0.24
R0B15-n0	0.00	1.60	0.09	0.01	7.08	0.35	2.30	0.81	0.03	0.02	0.15	0.22	0.35	0.59
R2B15-n10	0.10	1.60	0.09	0.02	5.11	0.35	2.30	0.81	0.03	0.02	0.15	0.22	0.35	0.33
R2B15-n20	0.20	1.60	0.09	0.02	5.11	0.35	2.30	0.81	0.03	0.02	0.15	0.22	0.35	0.35
R2B15-n30	0.30	1.60	0.09	0.02	5.11	0.35	2.30	0.81	0.03	0.02	0.15	0.22	0.35	0.37
R2B15-n40	0.40	1.60	0.09	0.02	5.11	0.35	2.30	0.81	0.03	0.02	0.15	0.22	0.35	0.40
R2B15-n50	0.50	1.60	0.09	0.02	5.11	0.35	2.30	0.81	0.03	0.02	0.15	0.22	0.35	0.43
R2B15-n60	0.60	1.60	0.09	0.02	5.11	0.35	2.30	0.81	0.03	0.02	0.15	0.22	0.35	0.46
R2B30-n0	0.00	1.60	0.09	0.01	7.08	0.35	2.30	0.81	0.03	0.02	0.30	0.22	0.69	0.47
R2B30-n10	0.10	1.60	0.09	0.02	5.11	0.35	2.30	0.81	0.03	0.02	0.30	0.22	0.69	0.25
R2B30-n20	0.20	1.60	0.09	0.02	5.11	0.35	2.30	0.81	0.03	0.02	0.30	0.22	0.69	0.25
R2B30-n30	0.30	1.60	0.09	0.02	5.11	0.35	2.30	0.81	0.03	0.02	0.30	0.22	0.69	0.27
R2B30-n40	0.40	1.60	0.09	0.02	5.11	0.35	2.30	0.81	0.03	0.02	0.30	0.22	0.69	0.31
R2B30-n50	0.50	1.60	0.09	0.02	5.11	0.35	2.30	0.81	0.03	0.02	0.30	0.22	0.69	0.35
R2B30-n60	0.60	1.60	0.09	0.02	5.11	0.35	2.30	0.81	0.03	0.02	0.30	0.22	0.69	0.40
R2B60-n0	0.00	1.60	0.09	0.01	7.08	0.35	2.30	0.81	0.03	0.02	0.60	0.22	1.38	0.41
R2B60-n10	0.10	1.60	0.09	0.02	5.11	0.35	2.30	0.81	0.03	0.02	0.60	0.22	1.38	0.19
R2B60-n20	0.20	1.60	0.09	0.02	5.11	0.35	2.30	0.81	0.03	0.02	0.60	0.22	1.38	0.19

R2B60-n30	0.30	1.60	0.09	0.02	5.11	0.35	2.30	0.81	0.03	0.02	0.60	0.22	1.38	0.18
R2B60-n40	0.40	1.60	0.09	0.02	5.11	0.35	2.30	0.81	0.03	0.02	0.60	0.22	1.38	0.20
R2B60-n50	0.50	1.60	0.09	0.02	5.11	0.35	2.30	0.81	0.03	0.02	0.60	0.22	1.38	0.24
R2B60-n60	0.60	1.60	0.09	0.02	5.11	0.35	2.30	0.81	0.03	0.02	0.60	0.22	1.38	0.31
R4.6B15-n0	0.00	1.60	0.09	0.03	3.17	0.38	2.27	0.85	0.03	0.05	0.15	0.50	0.34	0.62
R4.6B15-n10	0.10	1.60	0.09	0.04	2.24	0.38	2.27	0.85	0.03	0.05	0.15	0.50	0.34	0.43
R4.6B15-n20	0.20	1.60	0.09	0.04	2.24	0.38	2.27	0.85	0.03	0.05	0.15	0.50	0.34	0.45
R4.6B15-n30	0.30	1.60	0.09	0.04	2.24	0.38	2.27	0.85	0.03	0.05	0.15	0.50	0.34	0.47
R4.6B15-n40	0.40	1.60	0.09	0.04	2.24	0.38	2.27	0.85	0.03	0.05	0.15	0.50	0.34	0.49
R4.6B15-n50	0.50	1.60	0.09	0.04	2.24	0.38	2.27	0.85	0.03	0.05	0.15	0.50	0.34	0.52
R4.6B15-n60	0.60	1.60	0.09	0.04	2.24	0.38	2.27	0.85	0.03	0.05	0.15	0.50	0.34	0.56
R4.6B30-n0	0.00	1.60	0.09	0.03	3.17	0.38	2.27	0.85	0.03	0.05	0.30	0.50	0.68	0.57
R4.6B30-n10	0.10	1.60	0.09	0.04	2.24	0.38	2.27	0.85	0.03	0.05	0.30	0.50	0.68	0.37
R4.6B30-n20	0.20	1.60	0.09	0.04	2.24	0.38	2.27	0.85	0.03	0.05	0.30	0.50	0.68	0.38
R4.6B30-n30	0.30	1.60	0.09	0.04	2.24	0.38	2.27	0.85	0.03	0.05	0.30	0.50	0.68	0.40
R4.6B30-n40	0.40	1.60	0.09	0.04	2.24	0.38	2.27	0.85	0.03	0.05	0.30	0.50	0.68	0.43
R4.6B30-n50	0.50	1.60	0.09	0.04	2.24	0.38	2.27	0.85	0.03	0.05	0.30	0.50	0.68	0.46
R4.6B30-n60	0.60	1.60	0.09	0.04	2.24	0.38	2.27	0.85	0.03	0.05	0.30	0.50	0.68	0.50
R4.6B60-n0	0.00	1.60	0.09	0.03	3.17	0.38	2.27	0.85	0.03	0.05	0.60	0.50	1.36	0.49
R4.6B60-n10	0.10	1.60	0.09	0.04	2.24	0.38	2.27	0.85	0.03	0.05	0.60	0.50	1.36	0.31
R4.6B60-n20	0.20	1.60	0.09	0.04	2.24	0.38	2.27	0.85	0.03	0.05	0.60	0.50	1.36	0.31
R4.6B60-n30	0.30	1.60	0.09	0.04	2.24	0.38	2.27	0.85	0.03	0.05	0.60	0.50	1.36	0.33
R4.6B60-n40	0.40	1.60	0.09	0.04	2.24	0.38	2.27	0.85	0.03	0.05	0.60	0.50	1.36	0.35
R4.6B60-n50	0.50	1.60	0.09	0.04	2.24	0.38	2.27	0.85	0.03	0.05	0.60	0.50	1.36	0.39
R4.6B60-n60	0.60	1.60	0.09	0.04	2.24	0.38	2.27	0.85	0.03	0.05	0.60	0.50	1.36	0.44
R10B15-n0	0.00	1.60	0.09	0.06	1.53	0.43	2.16	0.93	0.03	0.10	0.15	1.09	0.32	0.76
R10B15-n10	0.10	1.60	0.09	0.09	1.02	0.43	2.16	0.93	0.03	0.10	0.15	1.09	0.32	0.66
R10B15-n20	0.20	1.60	0.09	0.09	1.02	0.43	2.16	0.93	0.03	0.10	0.15	1.09	0.32	0.66
R10B15-n30	0.30	1.60	0.09	0.09	1.02	0.43	2.16	0.93	0.03	0.10	0.15	1.09	0.32	0.67
R10B15-n40	0.40	1.60	0.09	0.09	1.02	0.43	2.16	0.93	0.03	0.10	0.15	1.09	0.32	0.68
R10B15-n50	0.50	1.60	0.09	0.09	1.02	0.43	2.16	0.93	0.03	0.10	0.15	1.09	0.32	0.69
R10B15-n60	0.60	1.60	0.09	0.09	1.02	0.43	2.16	0.93	0.03	0.10	0.15	1.09	0.32	0.71
R10B30-n0	0.00	1.60	0.09	0.06	1.53	0.43	2.16	0.93	0.03	0.10	0.30	1.09	0.65	0.72
R10B30-n10	0.10	1.60	0.09	0.09	1.02	0.43	2.16	0.93	0.03	0.10	0.30	1.09	0.65	0.61
R10B30-n20	0.20	1.60	0.09	0.09	1.02	0.43	2.16	0.93	0.03	0.10	0.30	1.09	0.65	0.61
R10B30-n30	0.30	1.60	0.09	0.09	1.02	0.43	2.16	0.93	0.03	0.10	0.30	1.09	0.65	0.62
R10B30-n40	0.40	1.60	0.09	0.09	1.02	0.43	2.16	0.93	0.03	0.10	0.30	1.09	0.65	0.64
R10B30-n50	0.50	1.60	0.09	0.09	1.02	0.43	2.16	0.93	0.03	0.10	0.30	1.09	0.65	0.65
R10B30-n60	0.60	1.60	0.09	0.09	1.02	0.43	2.16	0.93	0.03	0.10	0.30	1.09	0.65	0.67
R10B60-n0	0.00	1.60	0.09	0.06	1.53	0.43	2.16	0.93	0.03	0.10	0.60	1.09	1.29	0.74
R10B60-n10	0.10	1.60	0.09	0.09	1.02	0.43	2.16	0.93	0.03	0.10	0.60	1.09	1.29	0.56

R10B60-n20	0.20	1.60	0.09	0.09	1.02	0.43	2.16	0.93	0.03	0.10	0.60	1.09	1.29	0.56
R10B60-n30	0.30	1.60	0.09	0.09	1.02	0.43	2.16	0.93	0.03	0.10	0.60	1.09	1.29	0.57
R10B60-n40	0.40	1.60	0.09	0.09	1.02	0.43	2.16	0.93	0.03	0.10	0.60	1.09	1.29	0.59
R10B60-n50	0.50	1.60	0.09	0.09	1.02	0.43	2.16	0.93	0.03	0.10	0.60	1.09	1.29	0.61
R10B60-n60	0.60	1.60	0.09	0.09	1.02	0.43	2.16	0.93	0.03	0.10	0.60	1.09	1.29	0.64

*The threshold incident breaking wave height H_{bi} is calculated by the empirical formula of Calabrese et al (2008) given by Eq.3.17, as the lowest incident wave height for which breaking occurs over the SPB.

3.3.3 Effects of Porosity on Wave Transmission

In this section, results of numerical tests summarized in Table 3.3 are analyzed to investigate the effect of porosity on the transmission coefficient K_t. Fig. 3.9 shows the variation of wave transmission coefficient K_t obtained from the parameter study versus structure porosity n. In order to analyze the results presented in Fig. 3.9, it should be noted that:

i) The accuracy and reliability of the numerical solution of the transformed VARANS equation (Eqs. 3.7, 3.8 and 3.13) in porous media might be questionable for very low values of porosity n *as* the applicability of underlying Darcy-Forchheimer Equations *for* 0<n<0.3 is questionable.

ii) The numerical simulations often have some problems with respect to the numerical stability for very low porosity values (i.e. n=0-0.1).

Based on the aforementioned reasons, the results of numerical parameter study presented in Fig. 3.9 should be applied carefully for 0<n<0.3, especially in the in the transition zone from impermeable (n=0) to porous (n=0.1) structures, where sharp reduction of K_t due to increase of porosity n is observable while it is not possible to examine the porosity values between n=0 and n=0.1.

However this limitation does not adversely affect the engineering relevance of the results of this parameter study as the porosity of costal structures normally varies between n=0.3 and n=0.6. It should be noted, although the numerical results might be questionable for 0<n<0.3, numerical tests for 0<n<0.3 are performed and presented with the aim of:

i) getting a preliminary understanding of the effect of porosity on wave transmission in 0<n<0.3.

ii) providing some data to be compared with future relevant studies.

Based on the above discussion and depending on the breakwater porosity, the results presented in Fig 3.9 are divided in two distinct parts, namely an uncertain range for 0<n<0.3 and a conventional range for 0.3≤n≤0.6:

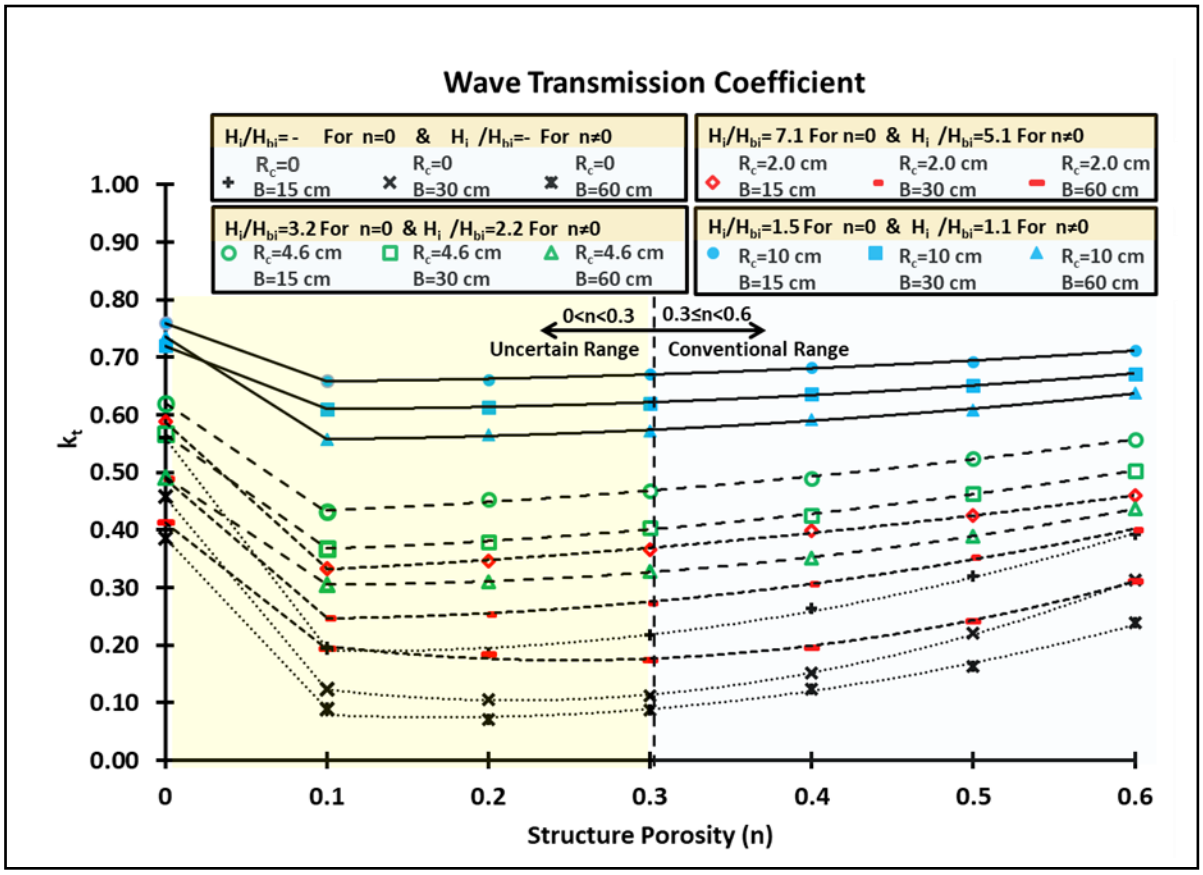

Fig 3.9: Variation of wave transmission coefficient Kt versus porosity n

The curves $K_t = K_t(n)$, which represent wave transmission coefficient K_t versus structure porosity n, are plotted in Fig. 3.9 for three crest widths (B=0.15, 0.30 and 0.6m) and four submergence depths (R_c=0; 2; 4.6 and 10 cm). Results presented in Fig. 3.9 shows that:

i) For given breakwater design parameters (i.e. submergence R_c and crest width B), in comparison with the impermeable structure, the porous structure results in a lower wave transmission coefficient K_t.

ii) In porous structures, the increase of breakwater porosity increases the K_t

The reduction of the wave transmission coefficient in submerged breakwaters due to the porosity of the structure agrees with the results of previous studies (e.g. d'Angremond et al., 1996; Losada et al., 1997; Rambabu andMani, 2005; Van der Meer et al., 2005) (see also Fig. 2.16 and Eqs. 2.5a and 2.5b), and can be attributed to the wave energy dissipation caused by friction inside the porous structure (Losada et al., 1997). In other words, from the physical point of view, since the porosity of structure reduces the wave reflection, based on the energy conservation concept $E_t + E_r + E_d = E_i$ (see also Eq 2.1), it can be concluded that, the decrease of wave transmission is due to the increase of wave energy dissipation inside the porous structure. Furthermore the increase of wave transmission coefficient due to the increase of porosity can be explained by the increased wave energy that passes through the structure.

In other words, the numerical simulation results shown in Fig. 3.9 suggest that for n=0.1-0.2, the higher wave transmission through the porous structure due to the increase of porosity, starts to compete against energy dissipation. When porosity n increases within the range n=0.3-0.6, wave transmission through the structure becomes dominant and transmission coefficient K_t steadily increases with the increase of porosity. The increase of transmission coefficient K_t in porous

breakwaters with increasing porosity n also agrees with laboratory observations reported in previous studies (Losadat et al.,1997; Ting et al., 2014; Rahman and Akter, 2014) (see also Fig. 2.16)

Numerical simulation results in Fig. 3.9 also show that the increase of crest width reduces the wave transmission coefficient. The same effect of crest width on wave transmission was also reported by Seabroke and Hall (1998). This crest width effect could also be attributed to the flow dissipation inside the porous materials. In fact, the breakwaters with larger crest widths have a larger body of porous materials. Thus, the flow dissipation inside the porous materials occurs in a larger extent, resulting in a lower wave transmission coefficient in the lee of the breakwater

The variation of wave transmission coefficient K_t versus structure porosity n is shown for each crest width B with the four submergence depths R_c in Figs. 3.10a, 3.10b and 3.10c.The ratio of the incident wave height H_i and breaking wave height H_{bi}, which also describes the intensity of wave breaking over the submerged breakwater, is also given for each submergence depth R_c. For a given breakwater submergence R_c and crest width B, the magnitude of the dissipative effect of porosity in the transition zone between impermeable condition n=0 and porous condition n=0.1, is quantified by parameter m1 which represents the slope of the line connecting the K_t(n=0) to K_t(n=0.1).

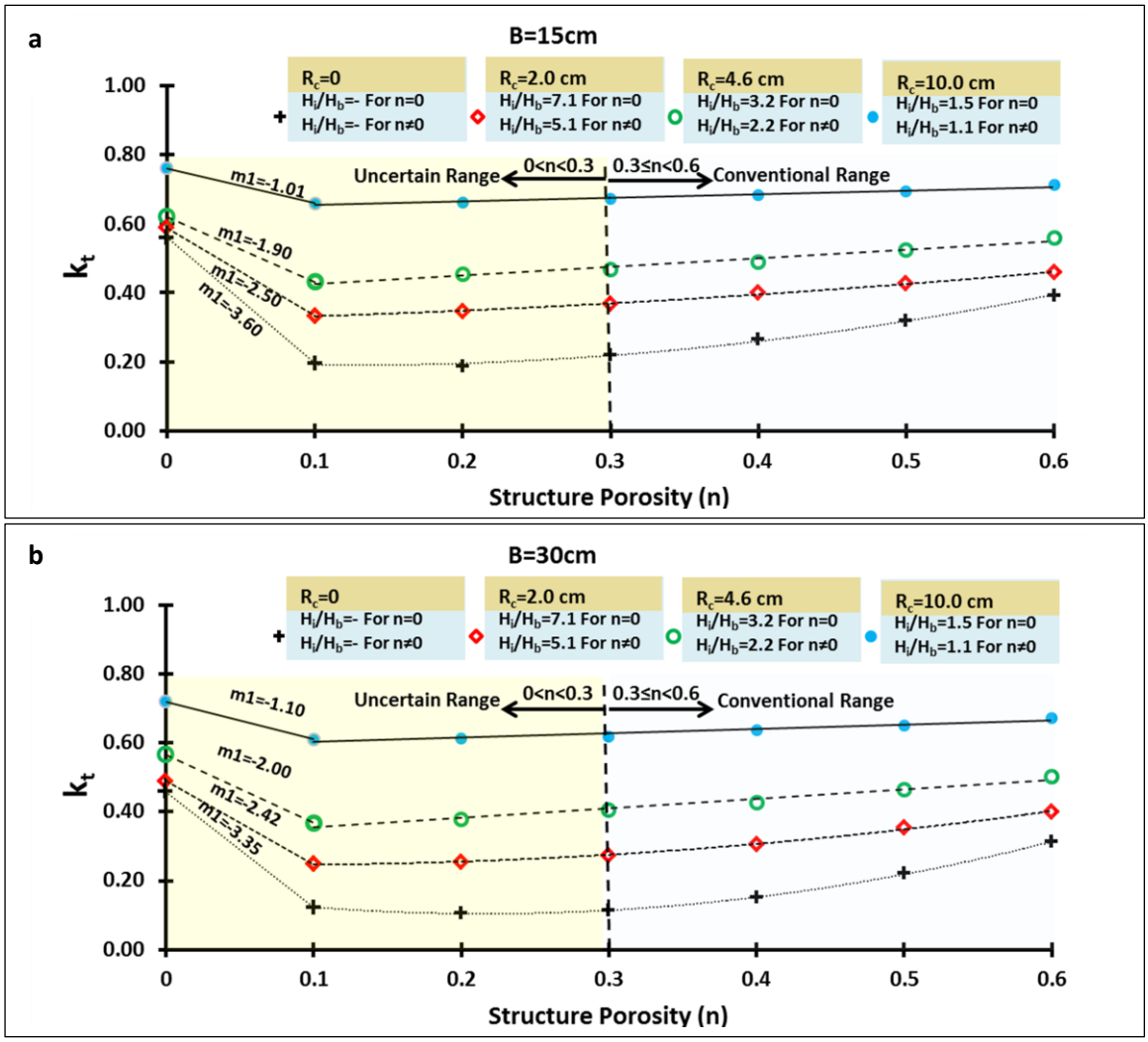

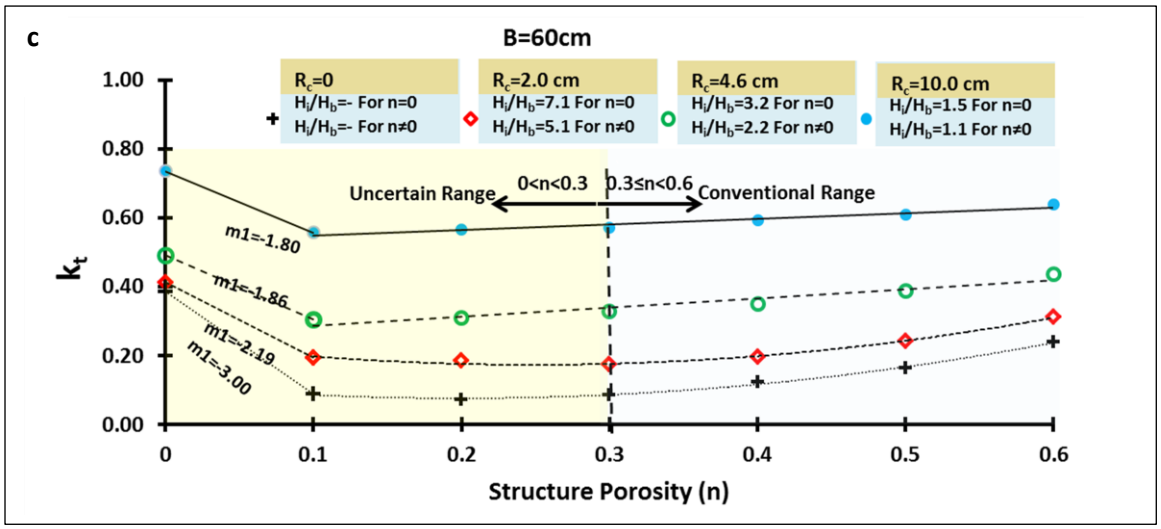

Fig 3.10: Variation of transmission coefficient Kt versus structure porosity n for each of the three considered crest widths B with different submergence depths Rc

Fig. 3.10 shows that, for all examined crest widths, higher submergence R_c results in lower absolute values of m1 which implies that wave transmission K_t decreases at a lower rate with increasing porosity from n=0 (impermeable breakwaters) to n=0.1. In other words, the dissipative effects of porosity in submerged breakwaters become weaker with increasing submergence depth R_c. As mentioned before, based on the energy conservation concept (see Eq. 2.1), the reduction of K_t in transition zone n=0-0.1 is due to wave energy dissipation inside the porous structure. Thus, the weaker dissipative effect of porosity observed for increasing the submergence might be explained by the fact that the wave energy dissipation in porous structures decreases with the decrease of the wave-induced flow velocity inside the porous medium in larger water depth (Solitt and Cross, 1972). The increase of breakwater submergence means that the porous body of the breakwater, in which wave energy dissipation occurs, is located in deeper parts of the water column where lower wave-induced flow velocities prevail as observed in the previous studies (Lara et al., 2006). Thus, the porous body of the breakwater is subjected to lower velocity flow and the effect of energy dissipation on wave transmission becomes weaker.

3.3.4 Effects of Submergence on Wave Transmission

The main effect of structure submergence is to cause premature wave breaking over the structure which represents the main reason for the incident wave energy dissipation (see also section 2.1.1). In this section, the numerical results shown in Fig 3.9 are further investigated with respect to the effect of breakwater submergence. For this purpose, wave transmission coefficient K_t versus relative submergence R_c/H_i is provided in Fig. 3.11 for three breakwater crest widths B, showing that K_t steadily increases with increasing R_c/H_i. This might be attributed to two main reasons:

- Higher relative submergence R_c/H_i causes weaker wave breaking over the breakwater and wave dissipation inside the breakwater (for porous breakwaters), resulting in less energy dissipation over and through the breakwater.

- Higher relative submergence reduces wave reflection from the breakwater and thus more wave energy passes leeward of the structure

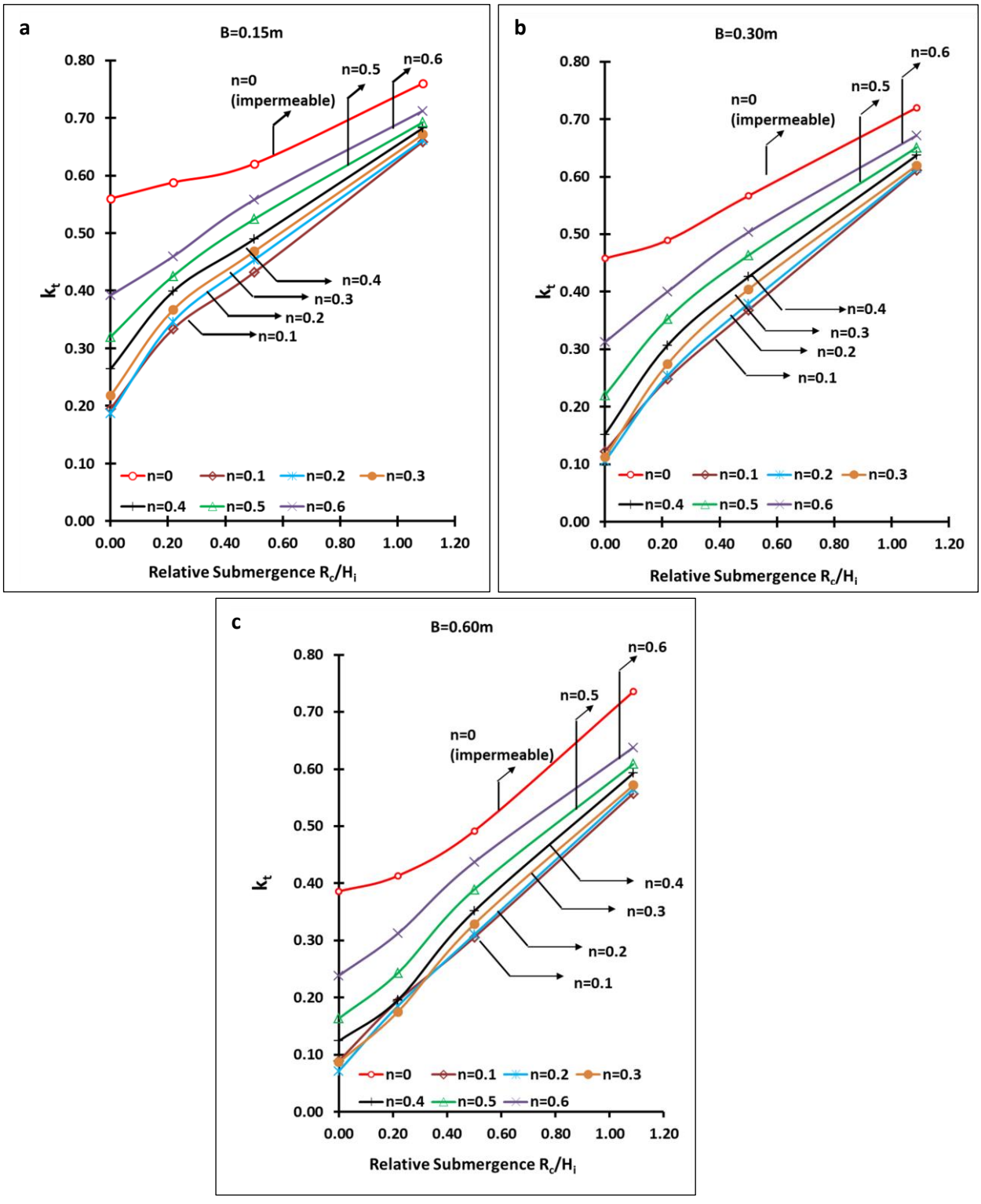

Fig 3.11: Transmission coefficient Kt versus relative submergence Rc/Hi for different crest widths B and structure porosity n=0-0.6

The K_t curves shown in Fig. 3.11 do not directly provide any new implication for the effect of submergence on wave transmission. However, since the numerical results shown in Fig. 3.11 include a wide range of structure porosities, they can be further analysed to compare the importance of porosity effects and submergence effects.

For this purpose, because for all tested porosities (n=0.1-0.6) WTC steadily increases with the increase of relative submergence R_c/H_i, implying the same variation trend of K_t versus R_c/H_i for all

tested porosities, it is possible to simplify the analysis by introducing a representative porosity curve (n_{avr} = 0.45).

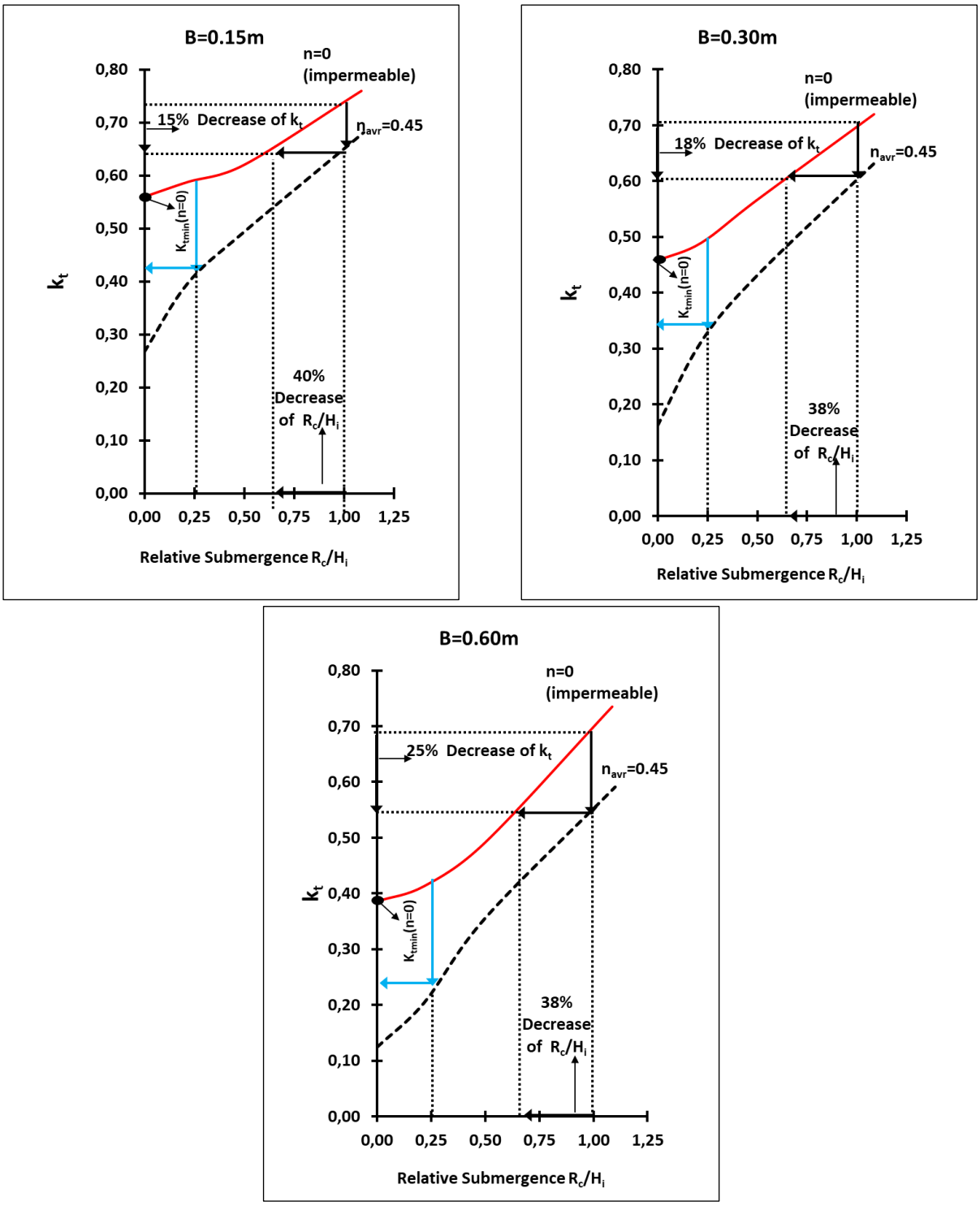

Fig 3.12: Transmission coefficient Kt vs. relative submergence depth Rc/Hi for the representative Kt curve (porosity navr=0.45) and for the Kt curve with porosity n=0 (impermeable breakwater)

Fig. 3.12 shows the variation of representative curve (K_t for n_{avr}=0.45) and impermeable curve (K_t for n=0) against relative submergence. The representative K_t curve, which is denoted in Fig. 3.11 by n_{avr}=0.45, is the average of all K_t(n) curves in Fig. 3.11, with n=0.3-0.6 which represents the range of practical porosity values.

For a given submergence and crest width, the vertical distance between impermeable breakwater curve $K_t(n=0)$ and representative porosity curve $K_t(n_{avr}=0.45)$ in Fig. 3.12, i.e. $K_t(n=0)$-$K_t(n=0.45)$, might represent the overall reduction of transmission coefficient K_t due to breakwater porosity. As shown by Fig. 3.12, for a high relative submergence value such as $R_c/H_i=1.0$, where the effect of porosity on the reduction of K_t tends to become minimum, the use of porous breakwaters yield 15-25% reduction of K_t as illustrated by downward black arrows in Fig. 3.12. On the other hand, in order to reach the same level of K_t reduction in impermeable breakwaters (see impermeable breakwater curves $K_t(n=0)$ plotted in red), the relative submergence has to be reduced by ca. 40% as illustrated by the backward black arrows. This clearly implies that, in order to reduce the wave transmission at submerged breakwaters, the effect of making breakwater porous might be equivalent to a noticeable reduction of relative submergence depth R_c/H_i (e.g. 40% for $R_c/H_i=1.00$). However, for lower values of relative submergence depths such as $R_c/H_i=0.5$, where the dissipative effect of porosity is stronger, the use of porous breakwater may reduce K_t so that the reduced K_t becomes lower than the minimum K_t on the impermeable curve which is denoted by K_{tmin} (n=0) in Fig 3.12(see red curve). This means that, in submerged breakwaters, for low values of relative submergence R_c/H_i, where the dissipative effect of porosity is strong, the use of porous breakwater may reduce the wave transmission coefficient K_t to a level which cannot be achieved by reducing the breakwater submergence of an impermeable breakwater while the structure is still kept submerged (see also blue arrows in Fig. 3.12). Therefore, for low submergence impermeable breakwaters (e.g. $R_c/H_i=0.5$), the porosity of breakwater might cause a level of K_t reduction, which cannot be achieved by a reduction of breakwater submergence. From the above discussions, two main conclusions might be drawn:

i) In order to reduce wave transmission behind submerged breakwaters, using a porous structure instead of an impermeable structure may represent a more efficient and practical alternative for reducing submergence

ii) For low relative submergence of breakwaters, using porous structures might be the only way to achieve a certain level of K_t reduction while the structure is kept submerged (i.e. without converting to an emerged structure)

3.4 Development of an improved WTC formula to account for structure porosity

The quantitative prediction of wave transmission is crucial for the design of detached breakwaters. Although wave transmission for submerged porous breakwaters has been widely investigated, and in spite of the noticeable effect that porosity may have on wave transmission, the available WTC formulae only account for the outer dimensions of the structures without explicitly considering the structure porosity (see section 2.2.1). Furthermore, none of the previous studies carried out on the porosity effect on WTC propose practical design criteria or predictive formulae for engineering applications. To close this gap, based on the numerical results reported in sub-section 3.3.3, in this section a formula is developed, which accounts for the effect of structure porosity on wave transmission at submerged porous breakwaters.

In order to analyze the effect of porosity on WTC for a given structure geometry, the transmission coefficient for an impermeable breakwater with the same geometry (i.e. same submergence R_c and crest width B is taken as a reference WTC for comparison with the WTC obtained for each examined porous breakwater.

In order to quantify the effect of porosity on WTC, the **P**orosity **E**ffect **F**actor (PEF) given by Eq. 3.1 is introduced in this study. The variation of Porosity Effect Factor (PEF) against porosity *n* is calculated on the basis of numerical results reported in sub-section 3.3.3, as shown in Fig. 3.13

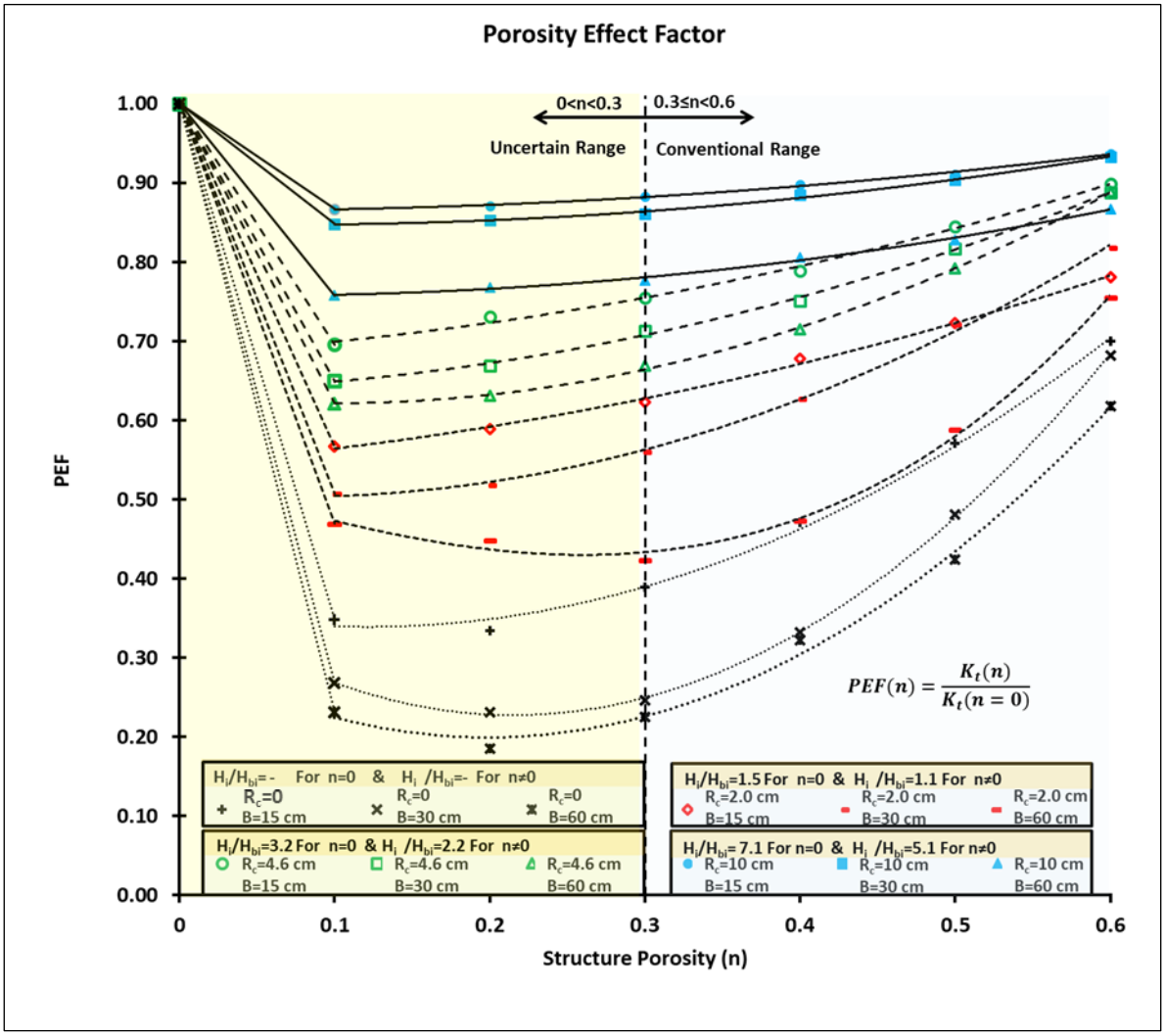

Fig 3.13: Porosity Effect Factor PEF versus breakwater porosity n, based on the numerical results from sub-section 3.3.3 (see also Fig. 3.9)

The PEF values plotted in Fig. 3.13 show that the increase of submergence weakens the effect of porosity and the increase of prosody between n=0.3 and n=0.6 weakens the effect of submergence. This clearly suggests that porosity and submergence mutually influence each other. This point will be further discussed in this chapter.

It should be noted that, similar to wave transmission coefficient values K_t presented in Fig 3.9, depending on the breakwater porosity, results are divided in two distinct parts, namely an Uncertain Range for 0<n<0.3 and a Conventional Range for 0.3≤n≤0.6. The variation of PEF versus porosity n can be considered in three different regions :

- **Region I: In the transition zone (n=0-0.1), the increase of porosity noticeably reduces PEF**

Numerical simulation results show that, changing the structure porosity *n* from n=0 to n=0.1 results in the *PEF* reduction which ranges from between 14% (for R_c=10 cm & B=15 cm) and 77% (for R_c=0 & B=60 cm)

- **Region II: For n=0.1-0.2, the increase of porosity has a relatively weak effect on PEF**

Numerical results show that the *PEF* variation due to increasing the structure porosity n from n=0.1 to n=0.2 does not follow a certain trend in all test. For example, with the increase of porosity in some series of tests, like for R_c=4.6 cm & B=15 cm, PEF increase, while it decreases for R_c=0 &B=15 cm. However, in all cases, the variation of PEF from n=0.1 to n=0.2 is negligibly small as compared to PEF variation from b=0.2 to n=0.6.

- **Region III: For n=0.2-0.6, the increase of porosity steadily increases PEF**

Numerical results show that, for n=0.2-0.6, the increase of porosity steadily increases the PEF. The only exception is the test series with R_c=4.6 cm &B=60 cm, in which increasing the porosity of the structure from n=0.2 to n=0.3 decreases the PEF. This decrease of PEF implies that, under these conditions, energy dissipation dominates over wave transmission due to increase of porosity from n=0.2 to n=0.3. This dominant effect of dissipation could be attributed to the large crest width which results in a larger extent over which dissipation occurs and thus higher porous flow dissipation.

The variation of PEF against porosity *n* is formulated for each aforementioned porosity regions. For n=0-0.1, WTC and the corresponding PEF values are not discussed in details because:

i) The accuracy of the results is questionable for 0<n≤0.1 (see section 3.3.3).

ii) Porosity values between n=0 and n=0.1 are not common in coastal engineering designs.

Therefore, in order to formulate PEF for *Region I* (n=0-0.1), linear interpolation is applied:

$$PEF(n) = \frac{PEF(n=0.1) - PEF(n=0)}{0.1-0} \times (n-0) \qquad n = 0-0.1 \qquad 3.19$$

Where PEF(n=0.1) and PEF(n=0) are respectively the porosity effect factor for n=0.1 and n=0 (impermeable structure). Thus, with a good formula for PEF(n=0.1), variations of PEF in Region I can be formulated. Based on the numerical results, variations of PEF(n=0.1) against the relative submergence R_c/H_i is plotted in Fig. 3.14, where data points clearly suggest that PEF(n=0.1) can be expressed as a function of breakwater submergence R_c and crest width B. The best fit curve to the data points shown in Fig. 3.14 is obtained as follows:

$$PEF(n=0.1) = 1 - 0.69 \times (kB)^{0.144} \times \exp\left[-1.33\frac{R_c}{H_i}\right] \qquad R^2=0.99 \qquad 3.20$$

Finally, from Eq. 3.19 and Eq. 3.20, PEF in *Region I* (n=0-0.1) can be expresses as:

$$PEF(n) = 1 - (6.9n) \times (kB)^{0.144} \times \exp\left[-1.33\frac{R_c}{H_i}\right] \qquad n = 0-0.1 \qquad 3.21$$

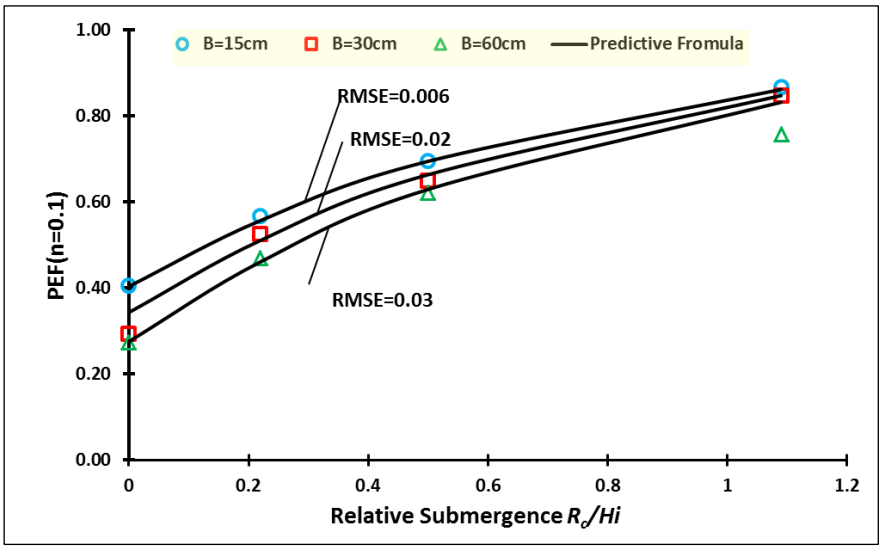

Fig 3.14: Porosity effect factor PEF (n=0.1) versus relative submergence Rc/Hi for different crest widths B

In *Region III* (n=0.2-0.6), the regression analysis is performed through following steps

1- For each crest width, a regression analysis is performed for each of the examined relative submergence depths R_c/H_i, resulting in regression lines in the form of $PEF = E \times n + F$. The regression lines are shown in Figs 3.15a,b &c for crest widths B=0.15m, 0.30m &0.60m, respectively

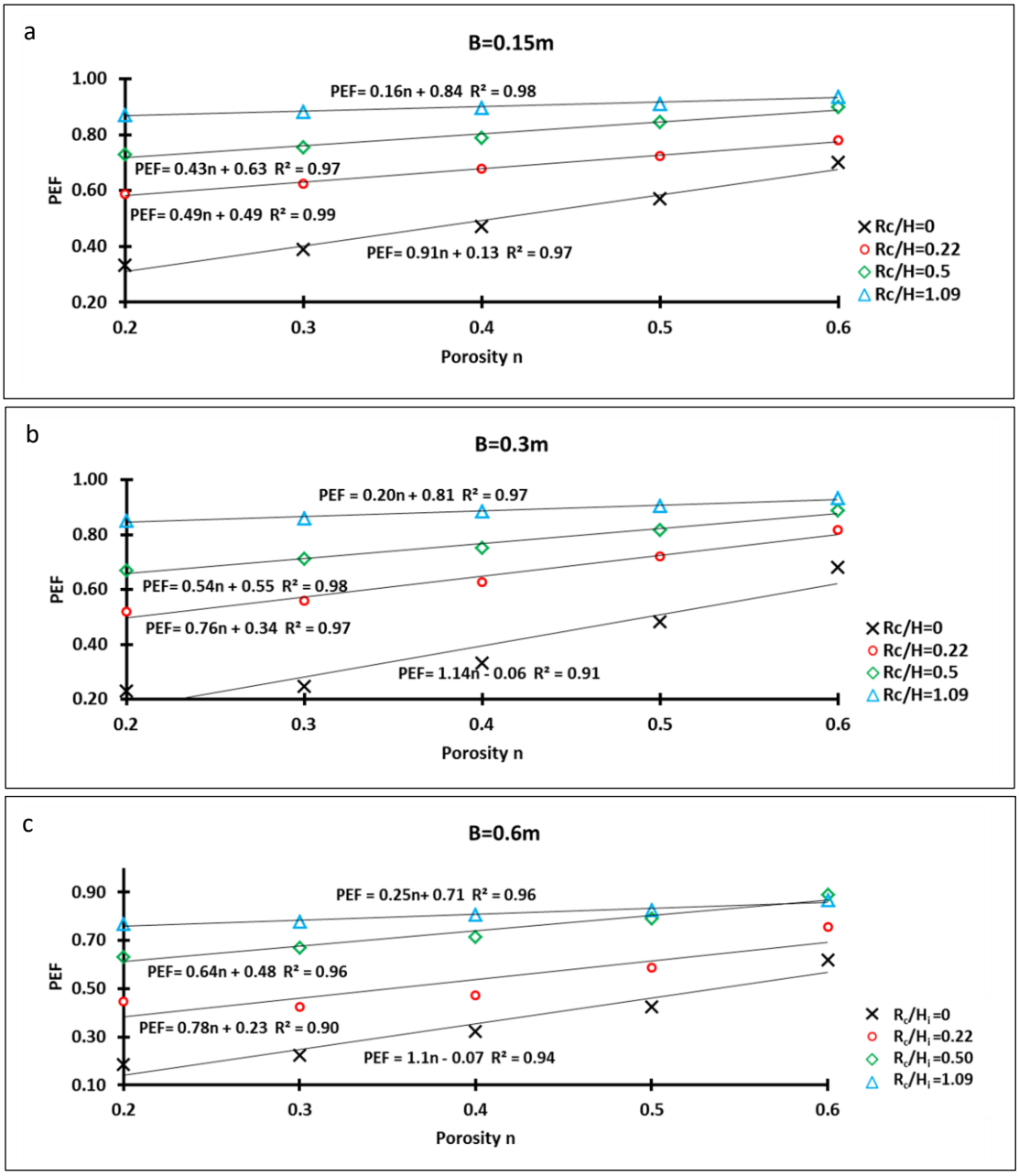

Fig 3.15: Regression lines fitted to PEF values for n=0.2-0.6, for varying relative submergence R_c/H_i and crest width B

The values of the slope steepness E and intercept F of regression lines shown in Fig. 3.15 are summarized in Table 3.4

Table 3.4: Summary of slope E, intercept F and determination coefficient R^2 of regression lines $PEF = E \times n + F$ shown in Fig. 3.15

R_c/H_i	kB	E	F	R^2
0	0.35	0.91	0.13	0.97
0	0.71	1.14	-0.06	0.91
0	1.41	1.1	-0.08	0.94
0.22	0.34	0.49	0.49	0.99
0.22	0.69	0.76	0.34	0.97
0.22	1.38	0.78	0.23	0.90
0.5	0.34	0.43	0.63	0.97
0.5	0.68	0.54	0.55	0.98
0.5	1.36	0.64	0.48	0.96
1.09	0.32	0.16	0.84	0.98
1.09	0.65	0.20	0.81	0.97
1.09	1.29	0.25	0.71	0.96

2- The following functions are defined to fit to the values of slope steepness E and intercept F of the regression lines:

$$E = E1 \times (kB)^{E2} \times (n) \times \exp\left(E3 \times \frac{R_c}{H_i}\right) \qquad 3.22a$$

$$F = \exp\left[\frac{F1 \times kB + F2}{F4 \times \frac{R_c}{H_i} + F5}\right] \qquad 3.22b$$

After a systematic trial and error, the fitting coefficients of Eqs. 3.22a and 3.22b are obtained as E1=1.22, E2=0.29, E3=-1.53, F1=0.2, F2=0.19, F4=0.1 and F5=-1.00. Accordingly, E and F can be expressed as:

$$E = 1.22 \times (kB)^{0.29} \times (n) \times \exp\left(-1.53 \frac{R_c}{H_i}\right) \quad \text{with } R^2=0.93 \qquad 3.23a$$

$$F = \exp\left[\frac{0.2kB + 0.19}{0.1 - \frac{R_c}{H_i}}\right] \quad \text{with } R^2=0.95 \qquad 3.23b$$

Based on the above discussion, for n=0.2-0.6, the PEF can be expressed as follows:

$$PEF = 1.22 \times (kB)^{0.29} \times (n) \times \exp\left(-1.53 \frac{R_c}{H_i}\right) + \exp\left[\frac{0.2kB + 0.19}{0.1 - \frac{R_c}{H_i}}\right] \qquad n = 0.2 - 0.6 \qquad 3.24$$

As mentioned before, in *Region II* (n=0.1-0.2), the variation of PEF is relatively weak compared to the variation of PEF from n=0.2 to n=0.6 and does not follow a certain trend. Thus, it is recommended to calculate *PEF* for n=0.1-0.2 using a linear interpolation between PEF (n=0.1) and PEF (n=0.2):

$$PEF = 110\times\left[PEF(n=0.2)-PEF(n=0.1)\right]\times(n-0.1) + PEF(n=0.1) \quad for \quad n=0.1-0.2 \tag{3.25}$$

From Eqs. 3.21 and 3.24, *PEF* can be expressed as follows:

$$PEF = \begin{cases} 1-6.3(n)\times\exp\left[-1.17\dfrac{R_c}{H_i}\right] & for \quad n=0-0.1 \\ 1.22\times(kB)^{0.29}\times(n)\times\exp\left(-1.53\dfrac{R_c}{H_i}\right)+\exp\left[\dfrac{0.2kB+0.19}{0.1-\dfrac{R_c}{H_i}}\right] & for \quad n=0.2-0.6 \end{cases} \tag{3.26}$$

For:

$$0\le n\le 0.6, \qquad 0<\frac{R_c}{H_i}<1.1 \quad \& \quad 0.3<kB<1.4$$

It should be noted that, for 0<n<0.3, Eq. 3.26 should be used with caution due to the limitation of the parameter study results within this range of porosity values (see Section 3.3.3).

Given the above predictive formulae for *PEF* to be used for the development of the new WTC formula which accounts for the effect of porosity, a reliable formula for reference transmission coefficient K_t (n=0) is required (see Eq. 3.1). In this study, the WTC formula of Van der Meer et al (2003) (see Eq. 2.5), which is the most recent and best calibrated WTC formula for submerged impermeable breakwaters, is adopted as the most appropriate alternative to estimate reference K_t (i.e. for n=0).

$$K_t(n=0)=K_{t[VDM2003]} \tag{3.27}$$

Fig. 3.16 depicts the scatter between K_t predicted by VDM 2003 (Eq. 2.7) and K_t obtained from the numerical results for submerged impermeable breakwaters (n=0).

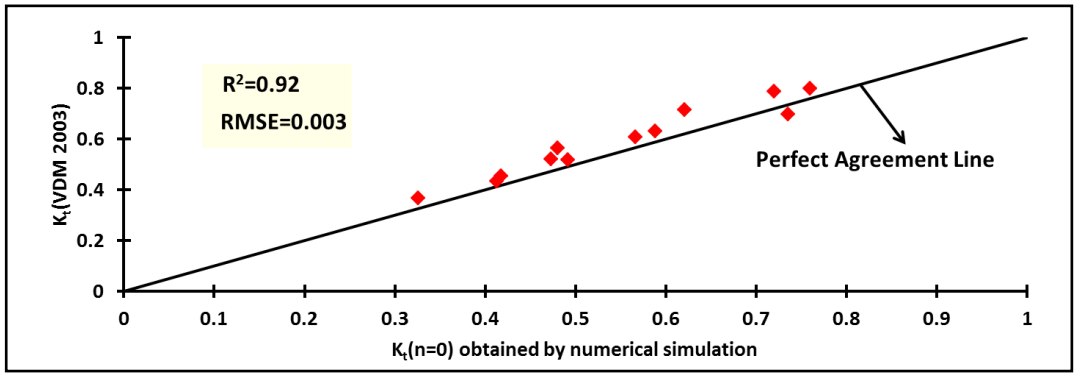

Fig 3.16: Comparison between K_t obtained from numerical results and from VDM2003 (Eq. 2.7) for submerged impermeable breakwaters (n=0)

The relatively high coefficient of determination (***R²=0.92***) and low Root Mean Square Error (***RMSE=0.003***) suggest a good agreement between values of WTC predicted by VDM2003 (Eq. 2.7) and those obtained from numerical tests performed on impermeable breakwaters (n=0). Thus, from Eq. 3.1, the new WTC formula can be expressed as follows:

Porosity Effect from Eq. 3.26 for 0≤n≤0.6, 0≤R_c/H_i≤1.1, 0.3≤kB≤1.4

$$K_t(n) = K_{t[VDM2003]} \times PEF \qquad 3.28$$

Submergence Effect from Eq. 2.5 for-2.5<R_c/H_i<2.5, 0.37< B/ H_{si} <43.48, 0.02< S_{op}<0.06

Here $K_t(n)$ is the transmission coefficient of the submerged porous breakwater, n is the porosity of the structure, $K_{t(VDM2003)}$ is the reference transmission coefficient calculated by VDM2003 (Eq. 2.7) and PEF is the porosity effect factor obtained by Eq. 3.26. Fig. 3.17 shows the scatter between K_t predicted by the new developed WTC formula expressed by Eq 3.28 and K_t obtained from the numerical results.

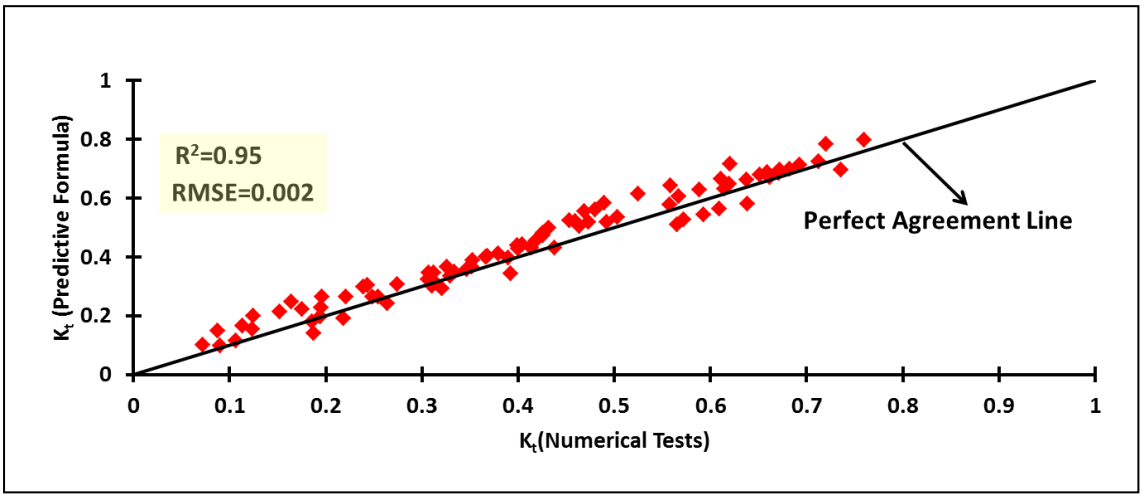

Fig 3.17: Transmission coefficient K_t predicted by Eq. 3.28 versus K_t obtained by numerical simulations for submerged breakwaters with porosity n=0-0.6.

Again, the high coefficient of determination (***R²=0.95***) and the low Root Mean Square Error (***RMSE=0.002***) suggest a good agreement between numerical results and the new developed WTC formula. Furthermore, it is physically expected that for a very large relative submergence depth, the structure porosity does not affect wave transmission. This physical boundary condition is expressed by Eq. 3.29

$$\frac{R_c}{H_i} \to \infty \Rightarrow PEF(n) \to 1 \Rightarrow Kt \to K_{t[VDM2003]} \quad \text{(see Eq. 3.26)} \qquad 3.29$$

Similarly, it is expected that an infinitely low porosity structure acts as an impermeable structure. This physical boundary condition is also expressed as follows:

$$n \to 0 \Rightarrow PEF \to 1 \Rightarrow Kt \to K_{t[VDM2003]} \quad \text{(see Eq. 3.19)} \qquad 3.30$$

According to what discussed above, the improved WTC formula (Eq 3.28) presented in this section satisfies the following conditions

i) Providing a good agreement with the numerical simulation results
ii) Yielding physically sound results when $n \to 0$ and $R_c/H_i \to \infty$

However, for infinitely large crest width B, Eq. 3.28 (where Eqs. 2.7 and 3.26 are respectively used for calculating $K_{t[VDM2003]}$ and PEF) does not show a physically sound behaviour. Indeed, it is physically expected that, if the crest width becomes infinitely large, the transmitted wave height must tend to zero due to infinite wave energy dissipation over the structure. However, for engineering practice, this limitation is practically not relevant as the validity range of Eq. 3.26 in terms of relative crest width kB ($k=2\pi/L$ is the wave number) is $0.3<kB<1.4$, which is fairly applicable to a wide range of SPBs reported in the literature.

Due to the complexity of site specific considerations, physical experiments are commonly used for design applications; yet, Eq. 3.28 might provide a good preliminary design tool for submerged porous breakwaters. Fig 3.18a-c show a comparison between numerical results and the new developed WTC formula given by Eq. 3.28:

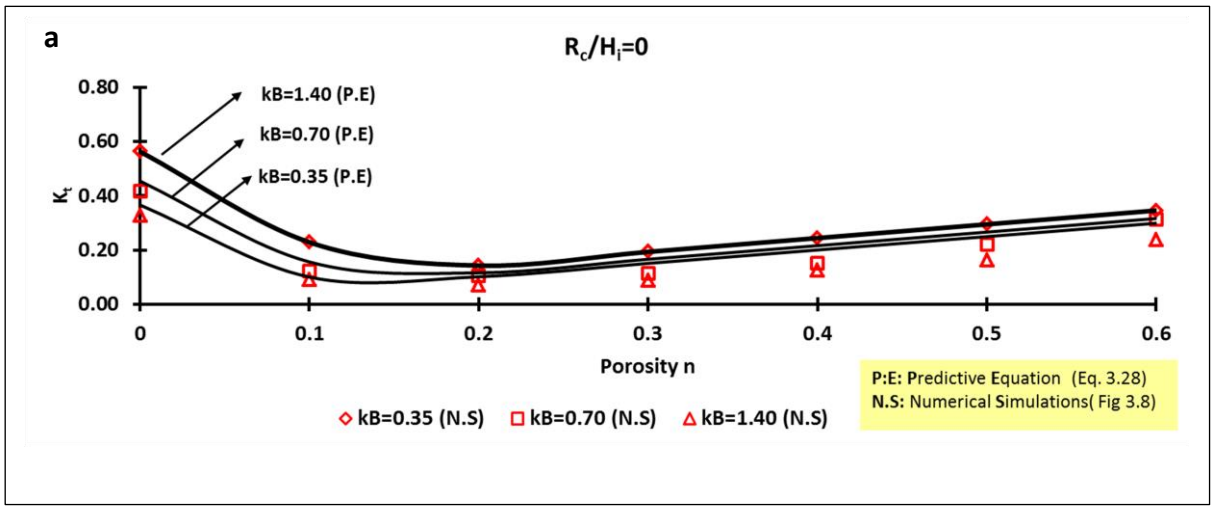

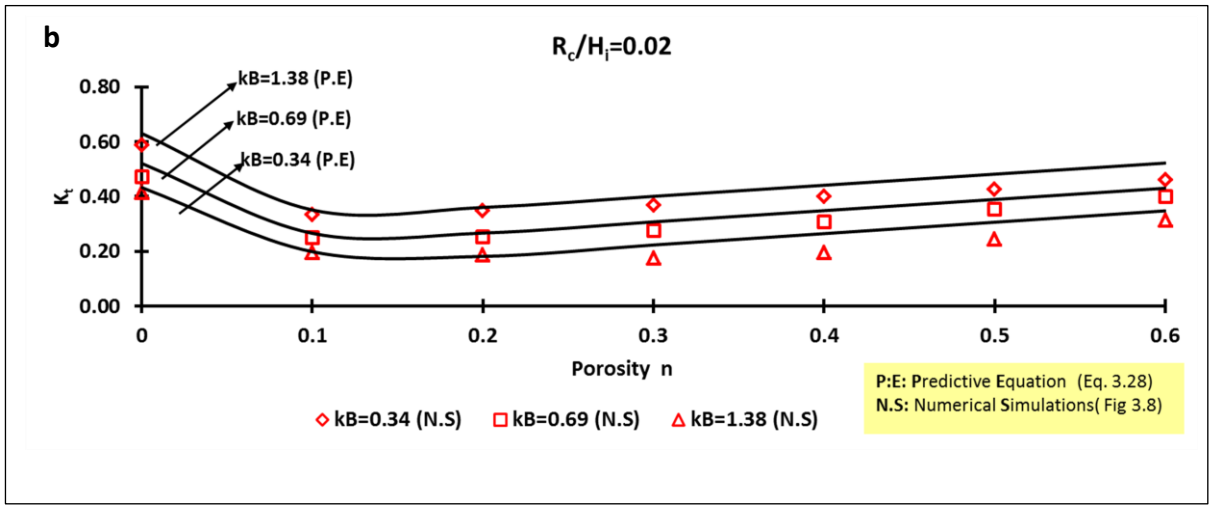

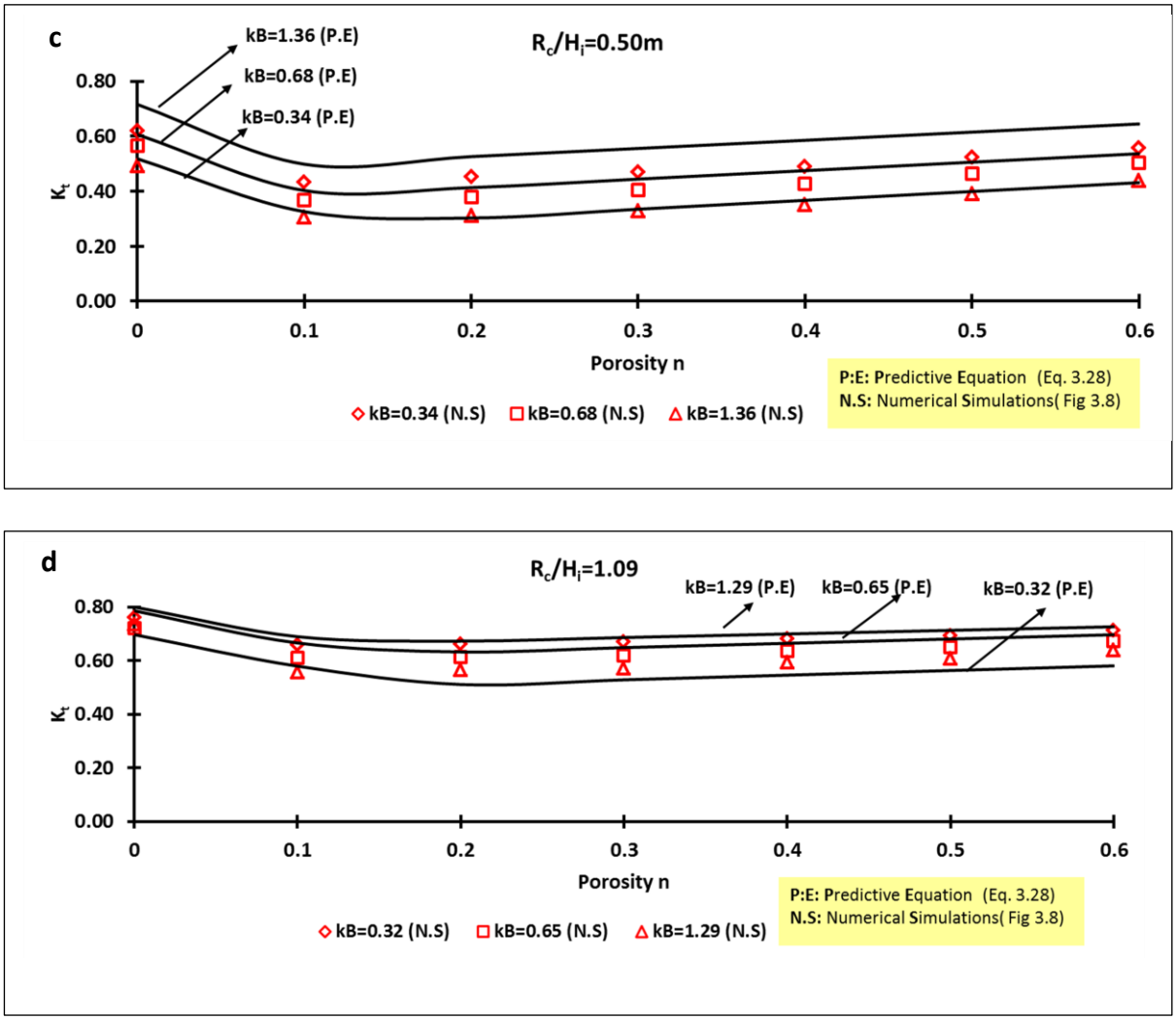

Fig 3.18: Comparison between K_t obtained from numerical results and K_t obtained from Eq. 3.28 for each of the four relative submergence depths R_c/H_i ,with different relative crest width kB (k=wave number)

In order to evaluate the applicability of the new developed WTC formula, Eq 3.28 is applied to the experimental test cases reported from previous laboratory studies on submerged porous breakwaters. Although, a large number of experimental studies have been carried out on porous submerged breakwaters, only for few test cases, the values of the structure porosity which is necessary for applying Eq. 3.28 is reported. Thus, a limited number of laboratory tests, which are summarized in Table 3.5, can be used to evaluate the proposed new WTC formula (Eq. 3.28):

Table 3.5: Summary of laboratory tests used for evaluating the proposed new WTC formula (Eq. 3.28)

	Reference	H (m)	T (s)	n (-)	Rc (m)	B (m)	K_t (Eq. 3.28)	K_t (Measured)
T1	Lara at al. (2006)	0.1	2.4	0.5	0.05	1	0.461	0.464
T2		0.1	3.2	0.5	0.05	1	0.467	0.463
T3	Rojanakamthorn et al., (1990)	0.6	1.54	0.4	0.06	3.25	0.408	0.307
T4		0.56	1.45	0.4	0.045	0.1	0.741	0.610
T5	Kramer et al (2005)	0.14	1.97	0.45	0.05	0.25	0.507	0.521
T6		0.6	1.32	0.45	0.05	0.25	0.632	0.683
T7		0.6	1.32	0.45	0.05	0.1	0.707	0.767

Fig 3.19 shows the scatter between the values of K_t calculated by Eq. 3.28 and those obtained from laboratory tests given by Table 3.5.

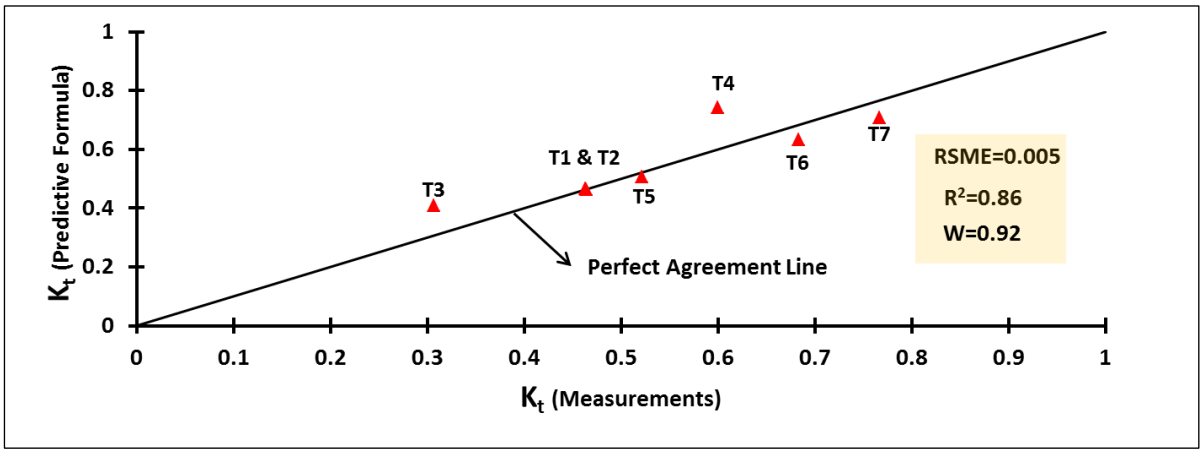

Fig 3.19: Scatter plot for Kt predicted by Eq. 3.28 and Kt obtained from laboratory tests in Table 3.5

As shown in Fig. 3.19, the calculated determination coefficient (R^2) and Root Mean Square Error (*RMSE*) are respectively 0.85 and 0.005. For further evaluation of Eq 3.28 against the laboratory tests given in Table 3.5, the Wilmott index *W*, which is proposed by Wilmott (1981) to overcome the insensitivity of determination coefficient R^2 to differences in the observed and predicted means and variances (For more details see Wilmott, 1981), is also utilized. The Wilmott index *W* is expressed as follows:

$$W = 1 - \frac{\sum_{j=1}^{n}\left[y(j)-x(j)\right]^2}{\sum_{j=1}^{n}\left[\left|y(j)-\bar{x}\right|+\left|x(j)-\bar{x}\right|\right]^2} \qquad 3.31$$

where x(j) are the observed data, y(j) are the predicted data, and $\bar{x}$ is the mean of x(j). A value of W= 1 indicates perfect agreement, and a value of W = 0 indicates total disagreement. The calculated Wilmott index W=0.92 obtained from the comparison between laboratory measurements and the new developed WTC results suggests that the new WTC formula given by Eq. 3.28 estimates K_t fairly well.

Although the predictive formula shows a fairly good agreement with laboratory measurements, the available laboratory results are too limited to definitely evaluate the robustness of the new WTC formula given by Eq 3.28; for this purpose, more experimental data are required. Therefore, this verification can be considered as tentative. In order to overcome this limitation, further studies need to be carried out to investigate WTC in SPBs with low porosity (i.e. 0<n<0.3), and also to provide wider data sets describing the effect of breakwater porosity on WTC in submerged breakwaters. Moreover, since the transmission coefficient might be influenced by scale effects, performing large-scale experimental studies which can be used to verify numerical studies, similar to that presented in this chapter, would be one of the urgent tasks in future studies.

In addition to the limitations discussed above, Eq. 3.28 is obtained for submerged breakwaters with a uniform porosity and thus it is not directly applicable to layered breakwaters, which are constructed from armour and core layers with different porosities. This limitation will be addressed in details in chapter 4

3.5 Implications for the present study

Considering the importance of porosity effects for wave transmission behind submerged breakwaters, in this chapter a numerical parameter study is carried out to investigate this effect. For this purpose, a numerical model in OpenFOAM is set up and validated against laboratory tests of submerged breakwaters (HT2006). The validated numerical model is then applied for the parameter study. Based on the results, a substantially improved understanding of the effect of porosity on wave transmission is achieved. The main results of this chapter and their implications for the present study are summarized below:

- For n=0.1-0.6, the **W**ave **T**ransmission **C**oefficient (WTC) of submerged porous breakwaters is lower than that of an impermeable breakwater with the same dimensions and wave conditions (i.e. R_c and B; T, H_i and h). This conclusion is in accordance with the previous laboratory observations (e.g. d'Angremond et al., 1996; Losada et al., 1997; Van der Meer et al., 2005)

- For n=0.3-0.6, WTC steadily increases with the increase of structure porosity. This observation is also in accordance with the previous experimental studies (Losada et al., 1997; Ting et al., 2014; Rahman and Akter, 2014).

- The effect of structure porosity on wave transmission decreases with increasing submergence R_c and increases with increasing crest width B

- In order to enhance the hydraulic performance of submerged breakwaters in terms of wave transmission, the use of porous structures instead of impermeable structures might provide a more efficient and practical solution compared to reducing submergence depth R_c

- In the design of breakwaters with low submergence (R_c/H_i=0.5), the use of a porous structure may be the only practical alternative for reducing wave transmission to a certain level, without converting the submerged breakwater to an emerged one

Based on the results of the numerical parameter study, new formulae are developed for WTC prediction (see Eq. 3.28 with Eqs 3.26 and 2.7). In particular, they show:

- a good agreement with numerical results (see Fig. 3.17, R^2=0.95 and RMSE=0.002)
- a physically sound tendency for infinitely large submergence (i.e. $R_c/H_i \rightarrow \infty$) and infinitely small porosities (i.e. $n \rightarrow 0$)
- a fairly good agreement with available laboratory measurement (R^2=0.85, RMSE=0.005 and W=0.92 see Fig 3.19)

The proposed new formulae explicitly take the porosity effects into account. This achievement is unique as compared to the previous similar studies.

In spite of the aforementioned promising results obtained from evaluation of the new developed WTC formulae, considering the applicability of the new WTC formulae two main limitations might be mentioned:

- The proposed new formulae cannot be directly applied to layered breakwaters, which typically consists of a core made of quarry run and armour layers made of coarser rock. In chapter 4, a new approach to apply the new formulae to layered breakwaters, which consist of an impermeable core and a permeable armour layer, is proposed and elaborated to meet the requirement of this PhD. A similar approach might be developed to define an equivalent porosity for another type of layered SPBs.
- More experimental data are necessary to evaluate the applicability of the new WTC formula, especially for low porosity range of n=0-0.3 where no experimental data are available for validation. Therefore, more laboratory and field measurements would be required to provide the necessary data for further verification of the new developed WTC formula, especially for low porosity range (i.e. $0<n<0.3$).

4 DEFLT3D: model description, extension, calibration and validation

As discussed in Chapter 2 (see section 2.3.4), in this study, DELFT3D model is selected to perform the hydro- morphodynamic simulations, which are required for the analysis of the effect of breakwater porosity and submergence on coastal morphology. As also discussed in section 2.3.1, DELFT3D is not able to consider the effects of breakwater porosity on wave transmission at submerged breakwaters. Based on the research methodology described in section 2.4, this chapter is devoted to further extend the DELFT3D model, in order to enable the model to account for the combined effect of breakwater porosity and submergence on the nearshore wave field leeward of the breakwater and thus on the coastal morphology in the protected area.

Therefore, this chapter mainly describes: (i) the implementation of the porous submerged breakwater in DELFT3D. (ii) the numerical set-up of a well-calibrated and validated model in DELFT3D, which can be used to study the effect of breakwater porosity and submergence on coastal morphology. Accordingly, this chapter is organized as follows. Section 4.1 is devoted to a detailed description of DELFT3D and its constituent modules which are utilized in this study. Section 4.2 is focused on the description and validation of a new approach proposed to extend the applicability of DELFT3D by implementing the combined effects of breakwater porosity and submergence on wave transmission in DELFT3D-WAVE. Section 4.3 describes the model calibration and validation, as well as the calibrated and validated model set-up which provides the numerical tool to be applied in Chapter 5 for a systematic parameter study on the effect of breakwater porosity and submergence on coastal morphology. Finally, the implications of the results are drawn in Section 4.4.

4.1 DELFT3D: description of the model and modules applied in this study

This section is devoted to a more detailed description of DELFT3D, which was briefly outlined in section 2.3.1. For this purpose, the theoretical background and underlying governing equations of the constituent modules of DELFT3D applied in this study, namely DELFT3D-WAVE and DELFT3D-FLOW are elaborated. Accordingly, section 4.1.1 provides the description of DELFT3D-WAVE, including the governing equations and parameterization utilized to represent the wave propagation processes considered by the model. Section 4.1.2 outlines the DELFT3D-FLOW including the details of free surface flow, sediment transport and morphology, and turbulence closure components of the module which are applied in this study.

4.1.1 Wave module

The DELFT3D-WAVE module, which is applied in this study, represents an interface for the well-known third generation wave spectrum model of **SWAN** [**S**imulating **WA**ves **N**earshore] (Booij et al., 1999). The DELFT3D-WAVE module (SWAN) describes the evolution of the wave action density and solves the action density balance equation over the computational grid. In the *Cartesian* coordinates, the action balance equation reads:

$$\frac{\partial N}{\partial t}+\frac{\partial\left(C_{gx}N\right)}{\partial x}+\frac{\partial\left(C_{gy}N\right)}{\partial y}+\frac{\partial\left(C_{\theta}N\right)}{\partial\theta}+\frac{\partial\left(C_{\sigma_w}N\right)}{\partial\sigma_w}=\frac{S(\sigma_w,\theta)}{\sigma_w} \qquad 4.1$$

where $N(\sigma_w,\theta)= E(\sigma_w,\theta)/ \sigma_w$ is wave energy density $E(\sigma_w,\theta)$ divided by relative frequency σ_w, C_{gx} and C_{gy} are the propagation velocity components of $N(\sigma_w,\theta)$ in x and y direction respectively, $C_{\sigma w}$ and C_{θ} are the propagation velocities in σ_w and θ space. The fourth term on the left-hand side, represents depth-induced and current-induced refraction (with propagation velocity C_{θ} in θ-space).

The term $S(\sigma_w,\theta)$ on the right hand side of Eq. 4.1 is the source term accounting for wave breaking induced dissipation, $S_{br}(\sigma_w,\theta)$, white-capping induced dissipation $S_w(\sigma_w,\theta)$, quadruplet wave-wave interaction $S_{nl4}(\sigma_w,\theta)$ and triad wave-wave interaction $S_{nl3}(\sigma_w,\theta)$:

$$S(\sigma_w,\theta)=S_{ds,br}(\sigma_w,\theta)+S_{ds,w}(\sigma_w,\theta)+S_{nl3}(\sigma_w,\theta)+S_{nl4}(\sigma_w,\theta) \quad 4.2$$

Although DELFT3D-WAVE (SWAN) can take the effect of wave generation by wind into account, it is omitted here because this is not relevant to this study. The following paragraphs provide a general description of the most relevant physical processes implemented in DELFT3D-WAVE (SWAN), which are considered in this study (For more details see Deltares, 2014a):

- **Dissipation by depth-induced wave breaking**

Depth-induced wave breaking in SWAN is represented by the bore-based model of Battjes and Janssen (1978). Extending the expression of Eldeberky and Battjes (1996) to include the spectral directions, the mean rate of energy dissipation per unit horizontal area due to depth-induced wave breaking for each directional and frequency component is expressed as:

$$S_{ds,br}(\sigma_w,\theta)=-\frac{D_{tot}}{E_{tot}}E(\sigma_w,\theta) \quad 4.3$$

Where σ represents the relative angular frequency, θ the wave direction, H_b the breaking wave height, E_{tot} the total wave energy and D_{tot} the rate of total energy dissipation per unit horizontal area due to wave breaking:

$$D_{tot}=-\frac{1}{4}\alpha_{BJ}Q_b\left(\frac{\sigma_w}{2\pi}\right)H_b^2 \quad 4.4$$

$$E_{tot}=\int_0^{2\pi}\int_0^{\infty}E(\sigma_w,\theta)d\sigma_w d\theta \quad 4.5$$

α_{BJ} is the coefficient to determine the dissipation rate. The default value for this parameter in SWAN is $\alpha_{BJ}=1$. The fraction of breaking waves Q_b is expressed as:

$$\frac{1-Q_b}{LnQ_b}=-8\frac{E_{tot}}{H_b^2} \quad 4.6$$

$$H_b=\gamma h_b \quad 4.7$$

γ is the breaker index and h_b is the breaking water depth. In DELFT3D-WAVE, the default value of the breaker index is set equal to $\gamma=0.73$, which is the mean value obtained from the data set provided by Battjes and Stive (1985).

- **Dissipation by Whitecapping**

Wave energy dissipation by whitecapping is dominated by the wave steepness. In SWAN, the whitecapping formulations are based on a pulse-based model (Hasselmann, 1974), as adapted by the WAMDI group (1988):

$$S_{ds,w}(\sigma_w,\theta)=-\Gamma\bar{\sigma}\frac{k}{\bar{k}}E(\sigma_w,\theta) \quad 4.8$$

where Γ is a steepness dependent coefficient, k is the wave number, and $\overline{\sigma_w}$ and $\bar{k}$ denote a mean relative frequency and a mean wave number, respectively (Deltares, 2014a):

$$\overline{\sigma} = \frac{\int_0^{2\pi}\int_0^{\infty} \sigma_w E(\sigma_w,\theta)\, d\sigma_w d\theta}{E_{tot}} \qquad 4.9$$

$$\bar{k} = \left[\frac{\int_0^{2\pi}\int_0^{\infty} \frac{1}{\sqrt{k}} E(\sigma_w,\theta)\, d\sigma_w d\theta}{E_{tot}} \right]^2 \qquad 4.10$$

- **Dissipation due to bottom friction**

The formulations of the bottom friction models that have been selected for DELFT3D-WAVE can all be expressed in the following form:

$$S_{ds,b}(\sigma_w,\theta) = -C_{bottom} \frac{\sigma_w^{\,2}}{g^2 \sinh^2(kd)} E(\sigma_w,\theta) \qquad 4.11$$

Here, C_{bottom} is the bottom friction coefficient. In DELFT3D-WAVE, the empirical model of JONSWAP (Hasselmann et al., 1973), the drag law model of Collins (1972) and the eddy viscosity model of Madsen et al. (1988) can be adopted to determine the parameter C_{bottom}.

- **Nonlinear wave-wave interactions**

In deep and intermediate water, four-wave interactions (so-called *quadruplets*) are important, whereas in shallow water three-wave interactions (so-called *triads*) dominate the evolution of the wave spectrum. DELFT3D-WAVE is able to account for both quadruplet and triad wave-wave interactions. For a detailed description of triad and quadruplet wave-wave interaction see Holthuijsen (2007).

In deep water, quadruplet wave-wave interactions dominate the evolution of the wave spectrum. This process redistributes the wave energy over the spectrum (the redistribution is said to be conservative). In SWAN, the simple expression of Hasselmann (1981) is applied to represent quadruplet wave-wave interactions in finite-depth for a JONSWAP-type spectrum.

In very shallow water, triad wave-wave interactions transfer energy from lower frequencies to higher frequencies. The Lumped Triad Approximation (LTA) derived by Eldeberky and Battjes (1995) is used in SWAN to represent triad wave-wave interaction.

- **Transmission Through and Over Obstacles**

SWAN is able to describe wave transmission through/over transmissive detached breakwaters in DELFT3D-WAVE. Such structures are represented as a (line of) sub-grid obstacles along which wave height is locally reduced by a factor K_t (wave transmission coefficient K_t defined as the ratio of the wave height before and the wave height behind the structure, see Section 2.2.1). The wave transmission coefficient (WTC) required in DELFT3D-WAVE can be either provided as an input parameter, or calculated using the WTC formulae provided in SWAN. Since, the existing WTC formulae do not

explicitly take the effect of porosity into account (see section 2.2), none of the aforementioned options in DELFT3D is able to account for the effect of porosity on wave transmission. In order to address this limitation and extend the applicability of DELFT3D-WAVE for representing the effect of breakwater porosity, combined with the effect of breakwater submergence on wave transmission at porous submerged breakwaters, the WTC formulae developed in chapter 3 (Eq. 3.28) can be applied to estimate transmission coefficient K_t in DELFT3D-WAVE. This issue will be elaborated further in Section 4.2.

- **Refraction and Diffraction**

The effect of refraction and diffraction implemented in DELFT3D–WAVE is expressed in terms of the directional turning rate of the individual wave components of the wave spectrum and is based on a phase-decoupled refraction-diffraction approximation (Holthuijsen et al., 1993). This approximation is based on the mild-slope equation for refraction and diffraction, without considering the phase information (For more details see Holthuijsen et al., 2003)

4.1.2 Flow module

The DELFT3D-FLOW module solves the unsteady shallow-water and transport equations in 2DH (depth-averaged) or 3D mode. If the flow variation in the vertical direction is negligible, then the depth-averaged approach can be adopted, while 3D modelling is applied when the horizontal flow field varies noticeably across the water depth.

Following the shallow water assumption, in DELFT3D-FLOW, the vertical momentum equation is reduced to the hydrostatic pressure relation as vertical accelerations are assumed to be negligibly small compared to gravitational acceleration. This assumption makes the DELFT3D model suitable for flow and transport modelling in shallow waters (e.g. lakes, rivers, coastal areas). In typical applications of shallow water equations, the wave effects are only incorporated via wave breaking- induced shear stress at the surface, the wave-induced mass flux and an increased bed shear stress. Thus, other Important wave effects such as streaming in the wave boundary layer and wave induced turbulence are not considered. Walstra et al. (2001) addressed this limitation and enhanced the DELFT3D-FLOWcapabilities to account for the wave effects more accurately, through the following improvements:

- The wave-induced mass flux is included using the second order stokes drift.
- The effect of wave breaking is introduced in the k-ε turbulence closure
- The effect of dissipation in the near-bed wave boundary layer is implemented in the k-ε turbulence model.
- The effect of streaming (wave-induced current in the wave boundary layer in the wave direction) is represented as a time averaged shear stress.

The components of DELFT3D-FLOW applied in this study are based on the system of equations that consists of the shallow water equations, equations for both suspended and bed-load transport of sand (non-cohesive), sediment mass conservation equation (Exner equation) for bed morphological updating, and turbulence closure models. These are briefly described in the following sections:

(a) Shallow water equations

In this study, the σ-gr id coordinates (Phillips, 1957) is used for numerical simulation. In the σ-grid coordinates, the vertical grid consists of layers bounded by two σ-planes, which are not strictly horizontal but follow the bottom topography (σ=-1.0) and the free surface (σ=0.0). Because the σ-grid is boundary fitted, both to the bottom and to the moving free surface, a smooth representation of the bed

level changes is obtained. The number of layers over the entire horizontal computational area is constant, irrespective of the local water depth (Fig. 4.1). The distribution of the relative layer thickness is usually non-uniform, allowing for higher resolution in areas of interest such as the near surface area (e.g. for wave simulations) or the near bed area (e.g. for sediment transport simulations).

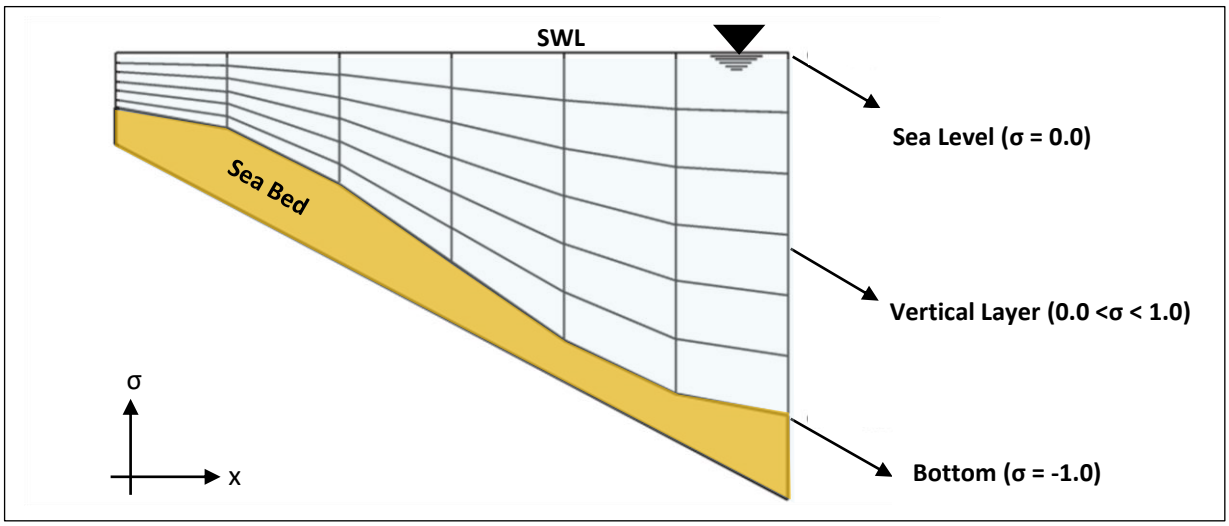

Fig 4.1: Exemplary representation of six vertical layers with equal thickness of layers in σ-coordinate system (Modified from Lesser, 2009)

As indicated in Fig. 4.1, the σ-coordinate system is represented as:

$$\sigma = \frac{z - \eta}{h} \qquad 4.12$$

Where h is the total water depth, z the vertical co-ordinate in physical space and η the free surface elevation above the reference plane (at z = 0). Under the so-called 'shallow water assumption', which implies that vertical accelerations are negligible compared to gravitational acceleration, the vertical momentum equation reduces to the hydrostatic pressure:

$$\frac{\partial P}{\partial \sigma} = -\rho g h \qquad 4.13$$

Thus, the three dimensional system of shallow water equations solved in the DELFT3D-FLOW consists of a continuity equation and two horizontal momentum equations which are respectively given by Eqs. 4.14, 4.15 and 4.16:

$$\frac{\partial \eta}{\partial t} + \frac{\partial \left(h\overline{U}\right)}{\partial x} + \frac{\partial \left(h\overline{V}\right)}{\partial y} = S \qquad 4.14$$

$$\frac{\partial U}{\partial t} + U\frac{\partial U}{\partial x} + V\frac{\partial U}{\partial y} + \frac{W}{h}\frac{\partial U}{\partial \sigma} = -\frac{1}{\rho_0}P_x + M_x + F_x + \frac{1}{h^2}\frac{\partial}{\partial \sigma}\left(\upsilon_v \frac{\partial U}{\partial \sigma}\right) \qquad 4.15$$

$$\frac{\partial V}{\partial t}+V\frac{\partial V}{\partial y}+U\frac{\partial V}{\partial x}+\frac{W}{h}\frac{\partial V}{\partial \sigma}= \qquad 4.16$$

$$-\frac{1}{\rho_0}P_y+M_y+F_y+\frac{1}{h^2}\frac{\partial}{\partial \sigma}\left(\upsilon_v\frac{\partial V}{\partial \sigma}\right)$$

where W represents the vertical velocity, $\bar{S}$ represents the contributions per unit area due to the discharge or withdrawal of water and $\bar{U}$, $\bar{V}$ represent the depth-averaged horizontal velocity in x and y direction respectively. The other parameters in Eqs. 4.14, 4.15 and 4.16 will be described later in this section. In the numerical simulations, which include the waves, the hydrodynamic equations are written and solved in the GLM (*Generalized Lagrangian Mean*) reference frame (Groeneweg 1999). In GLM formulation, the wave-induced driving forces are more accurately described (Lesser, 2009). The relationship between the GLM velocity and the Eulerian velocity is expressed by:

$$U=u+u_s \qquad 4.17 \qquad\qquad V=v+v_s \qquad 4.18$$

where U and V are GLM velocity components, u and v are Eulerian velocity components, and u_s and v_s are the Stokes' drift components. For more details on the implementation of GLM theory in DELFT3D, see Walstra et al. (2001). Although Coriolis forces are taken into account in DELFT3D-FLOW, they are omitted in momentum equations described here. In Eqs 4.15 and 4.16, M_x and M_y represent the contributions of wave forces computed by DELFT3D-WAVE. The forcing due to wave breaking is represented as shear stress at the water surface (Dingemans et al. 1987):

$$\vec{M}=\frac{D}{\omega}\vec{k} \qquad 4.19$$

Where, D = Dissipation rate due to wave breaking (W/m²), ω = wave angular frequency (rad/s), and k = wave number vector (rad/m). The horizontal pressure terms in Eqs 4.15 and 4.16, P_x and P_y, are expressed as:

$$\frac{1}{\rho_0}P_x=g\frac{\partial \zeta}{\partial x}+g\frac{h}{\rho_0}\int_\sigma^0\left(\frac{\partial \rho}{\partial x}+\frac{\partial \sigma'}{\partial x}\frac{\partial \rho}{\partial \sigma'}\right)d\sigma' \qquad 4.20$$

$$\frac{1}{\rho_0}P_y=g\frac{\partial \eta}{\partial y}+g\frac{h}{\rho_0}\int_\sigma^0\left(\frac{\partial \rho}{\partial y}+\frac{\partial \sigma'}{\partial y}\frac{\partial \rho}{\partial \sigma'}\right)d\sigma' \qquad 4.21$$

The horizontal Reynold's stresses, which are respectively denoted by F_x and F_y in Eqs. 4.15 and 4.16 are determined using the eddy viscosity concept (e.g. Rodi, 1993):

$$F_x=\upsilon_H\left(\frac{\partial^2 U}{\partial x^2}+\frac{\partial^2 U}{\partial y^2}\right) \qquad 4.22 \qquad\qquad F_y=\upsilon_H\left(\frac{\partial^2 V}{\partial x^2}+\frac{\partial^2 V}{\partial y^2}\right) \qquad 4.23$$

In order to solve the shallow water equations described above, the horizontal and vertical eddy viscosity (ν_H and ν_V) needs to be prescribed. In a 3D simulation, the selected turbulence closure model (see section 4.1.2.3) calculates the vertical eddy viscosity. Horizontal eddy viscosity may either be specified by the user as a constant or space varying parameter, or can be computed using a sub-grid model for horizontal large eddy simulation (HLES). The HLES model available in DELFT3D-FLOW is based on theoretical considerations presented by Uittenbogaard (1992) and is fully discussed by Van Vossen (2000). Besides, in order to solve the systems of equations, the bed and free surface boundary

conditions should be defined. In the σ-coordinate system, the bed and the free surface respectively correspond to σ=-1 and σ=0 planes. Therefore, the vertical velocities at these boundaries are simply:

$$W(\sigma=-1)=0 \qquad 4.24 \qquad W(\sigma=0)=0 \qquad 4.25$$

To apply the boundary condition at the bed (σ=-1) in Eqs. 4.15 and 4.16, bed friction is considered as follows:

$$\left[\frac{\nu_v}{h}\frac{\partial U}{\partial \sigma}\right]_{\sigma=-1}=\frac{\tau_{bx}}{\rho} \qquad 4.26$$

$$\left[\frac{\nu_v}{h}\frac{\partial V}{\partial \sigma}\right]_{\sigma=-1}=\frac{\tau_{by}}{\rho} \qquad 4.27$$

where τ_{bx} and τ_{by} are the components of bed shear stress τ_b in *x*and *y* direction respectively:

$$\tau_b=\frac{g\rho\vec{u}_b|\vec{u}_b|}{C_{3D}^2} \qquad 4.28$$

$$C_{3D}=\frac{\sqrt{g}}{\kappa}\ln\left(1+\frac{\Delta z_b}{2z_0}\right) \qquad 4.29$$

Here u_b is the bed shear velocity (flow velocity in the first layer just above the bed), z_0 is a user-defined roughness height and Δz_b is the distance between the bed and the first computational grid point above the bed.

(b) Sediment transport and morphology

Sediment transport and morphology is an integrated component of the DELFT3D–FLOW module. It accounts for suspended sediment transport, bed load sediment transport and subsequent bed level changes.

Van Rijn (1993) considers sediment transport below the reference level *a* as "bedload sediment transport" and sediment transport above the reference level as suspended-load. The exchange of sediment between the bed and water column is assumed to develop through the near-bottom layer that is entirely above Van Rijn's reference height. This layer is called the *reference layer* and is referred to as the kmx-layer for the sake of brevity. The suspended sediment transport is described using the advection-diffusion equation:

$$\frac{\partial c}{\partial t}+\frac{\partial(cU)}{\partial x}+\frac{\partial(cV)}{\partial y}+\frac{\partial(cW)}{\partial \sigma}= \qquad 4.30$$

$$h\left[\frac{\partial}{\partial x}\left(D_H\frac{\partial c}{\partial x}\right)+\frac{\partial}{\partial y}\left(D_H\frac{\partial c}{\partial y}\right)\right]+\frac{1}{\sigma}\left(D_V\frac{\partial c}{\partial \sigma}\right)+hS$$

where D_H and D_V are respectively horizontal and vertical diffusion coefficient. The term S in Eq 4.30 involves source and sink terms which account for the exchange of sediment between water column and sea bed through the *'reference layer'* that is located immediately above Van Rijn's reference height ***a*** as shown in Fig. 4.2.

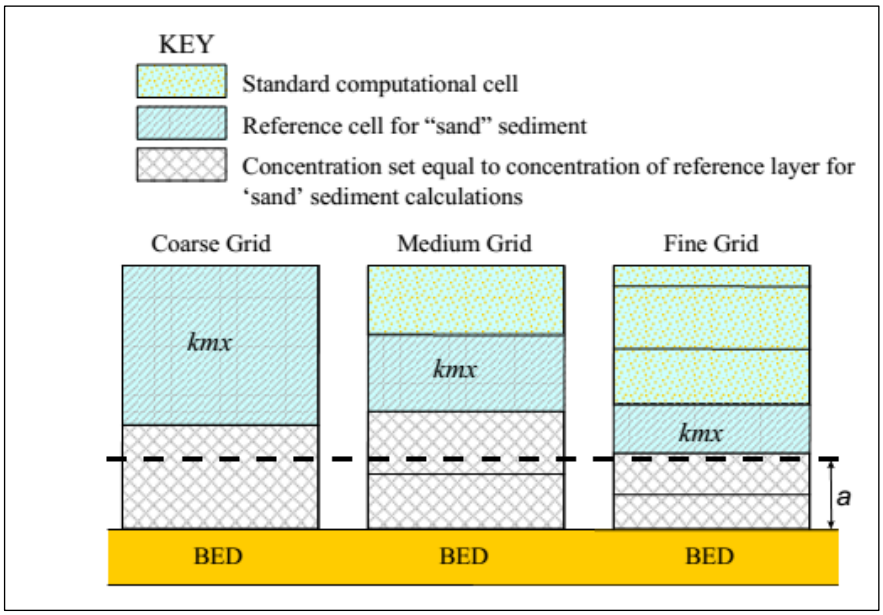

Fig 4.2: Location of kmx layer with respect to Van Rijn's reference height a (Deltares, 2014b)

Suspended sediment '***Source***' and '***Sink***' terms on Eq 4.30 are expressed as:

$$Source = f_{sus} c_a \left(\frac{D_v}{\Delta z} \right) \qquad 4.31$$

$$Sink = c_{kmx} \left(\frac{D_v}{\Delta z} + w_s \right) \qquad 4.32$$

Where w_s is the sediment fall velocity D_V is the vertical diffusion coefficient at the bottom of the reference cell, Δz is the vertical distance between the *kmx* layer and the Van Rijn's reference level ***a*** below which the sediment transport is considered as *"bed-load sediment transport"* (see Fig. 4.3)

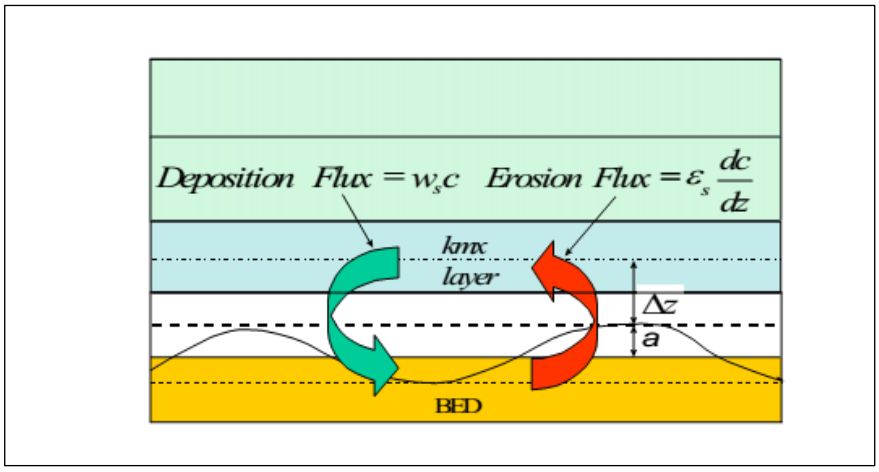

Fig 4.3: Schematic representation of flux bottom boundary condition (Deltares, 2014b)

Bed-load transport in DELFT3D is calculated according to the following approach: first, the magnitude and direction of the bed-load transport at the cell centers are calculated. Then the transport rates at the cell interfaces are determined and corrected for bed-slope effect. Some of the existing sediment transport formulae prescribe the bed-load transport direction whereas others predict just the magnitude of the sediment transport. In the latter case, the initial transport direction is assumed to be equal to the direction of the near-bed flow direction. As shown in Fig. 4.4, the control volume for bed level change calculations is centred on the water level points. The bed-load transport vector

components are actually required at the velocity points, rather than at the water level points, where the bedload transport in x and y direction (*Sb,x* and *Sb,y)* are calculated. By default, the "upwind" numerical scheme is used to determine the bed-load transport components at velocity points as this method ensures the numerical stability of the calculated bed level changes (Deltares, 2014b). For each active velocity point, the upwind direction is determined by summing the bed-load transport components at the water level points on either side of the velocity point and taking the *upwind direction* relative to the resulting net transport direction. The bedload transport component at a velocity point is then set equal to the component computed at the immediate upwind water level point (see Fig. 4.4). In the example shown in Fig. 4.4, the bed-load transport component $S_{b,uu}{}^{(m,n)}$ is set equal to $S_{b,x}{}^{(m,n)}$ and the component $S_{b,vv}{}^{(m,n)}$ is set equal to $S_{b,y}{}^{(m,n+1)}$.

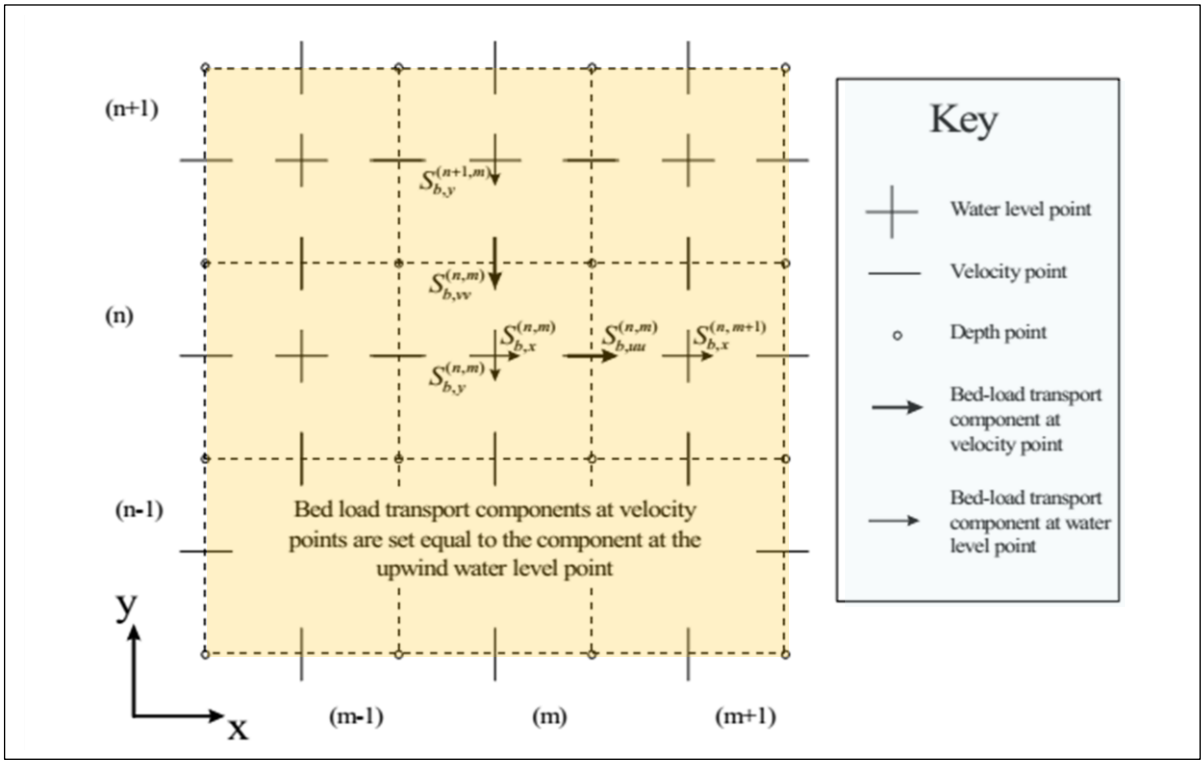

Fig 4.4: Determining the bed-load transport components at velocity points (Modified from Deltares, 2014b)

Bedload transport is affected by bed slope. Two bed slope directions could be defined with respect to the flow direction:

1) The bed slope in the direction of the near-bed flow (referred to as the longitudinal bed slope)
2) The slope in the direction perpendicular to the near-bed flow (referred to as the transverse bed slope).

The effect of longitudinal bed slope on the bed-load transport is expressed as:

$$S'_{bx} = \alpha_s S''_{bx} \qquad 4.33 \qquad S'_{by} = \alpha_s S''_{by} \qquad 4.34$$

where S_{bx}'' and S_{by}'' are the initial sediment transport rate in x and y direction respectively. The bed slope correction coefficient α_s is calculated according to Bagnold (1966):

$$\alpha_s = 1 + \alpha_{bs}\left[\frac{\tan(\phi)}{\cos\left(\tan^{-1}\left(\frac{\partial z}{\partial s}\right)\right)\times\tan\left(\phi - \frac{\partial z}{\partial s}\right)} - 1\right] \quad 4.35$$

Where α_{bs} is the user-defined calibration parameter (default = 1.0), φ is the sediment angle of repose and ∂z/∂s is the bed slope in flow direction. The additional bed load sediment transport due to the transverse bed slope is subsequently calculated perpendicular to the main bed-load transport vector. The magnitude of this vector is calculated using the formulation expressed by Van Rijn (1993), based on Ikeda (1982) as presented by:

$$S_{bn} = f_{norm}\left|S_b'\right| \quad 4.36$$

$$f_{norm} = \alpha_{bn}\sqrt{\frac{\tau_{bcr}}{\tau_b}}\frac{\partial z}{\partial n} \quad 4.37$$

Where ∂z/∂n is the bed slope normal to the flow direction, α_{bn} is a user-defined calibration parameter, τ_{bcr} the critical bed shear stress, τ_b the bed shear stress, and S_b' the magnitude of the bed-load transport vector (adjusted for longitudinal bed slope only):

$$S_b' = \sqrt{(S_{bx}')^2 + (S_{by}')^2} \quad 4.38$$

The two components of S_{bn} are then added to the two components of the bedload transport vector as follows:

$$S_{bx} = f_{bed}\times\left[S_{bx}' - f_{norm}\times S_{by}'\right] \quad 4.39$$
$$S_{by} = f_{bed}\times\left[S_{by}' + f_{norm}\times S_{bx}'\right]$$

The change in bottom level caused by the suspend load and bed-load transport is then calculated using the sediment mass conservation equation (Exner Equation):

$$(1-n)\frac{\partial z}{\partial t} + \frac{\partial(S_{bx+}S_{sx})}{\partial x} + \frac{\partial(S_{by+}S_{sy})}{\partial y} = 0 \quad 4.40$$

Where S_{sx} and S_{sy}, which respectively accounts for suspended load transport rates in x- and y-direction, are calculated based on the computed sand concentration fields:

$$S_{sx} = \int_a^h\left(Uc - \varepsilon_{sx}\frac{\partial c}{\partial x}\right)dz \quad 4.41$$

$$S_{sy} = \int_a^h\left(Vc - \varepsilon_{sy}\frac{\partial c}{\partial y}\right)dz \quad 4.42$$

Here ε_{sx} and ε_{sy} are respectively suspended sediment diffusion coefficients in x and y directions. In order to select the sediment transport formula, a wide variety of sediment transport formulae are available in DELFT3D (for detailed description of all sediment transport formulae, see Deltares 2014b). The sediment transport formulae developed by Bijker (1971) and Van Rijn (1993), which are also

available in DELFT3D, are among the most widely applied formulae to calculate sediment transport in numerical hydro-morphodynamics models for coastal areas (Van De Graaff et al., 2003). The formula by Van Rijn (1993) is not applicable to the size of sediments used in this study. Thus, the transport formula by Bijker (1971) is selected. Accordingly, in this section, only the transport formula proposed by Bijker (1971) is described.

Bijker (1971) developed a formula to calculate the sediment transport as a function of given wave and current parameters. It generally predicts sediment transport of the right order of magnitude under the combined action of currents and waves (Deltares 2014b) The Bijker transport formula consists of two components, namely the bed load transport component S_b and suspended load transport component S_s:

$$S_b = bD_{50}\left(\frac{q}{C}\sqrt{g}\left(1-\phi_b\right)\right)\exp\left(A_r\right) \quad 4.43$$

$$S_s = 1.83S_b\left(I_1 Ln\left(\frac{33.0h}{k_s}\right)+I_2\right) \quad 4.44$$

Where, k_s is the roughness height, q the mean flow velocity magnitude; C is the Chezy coefficient, h the water depth, φ_b the porosity of the sand bed, and A_r a dimensionless parameter which includes the bed shear stress (Gu¨ner et al., 2011). The parameters I_1 and I_2 are also known as the Einstein integrals:

$$b = BD + \max\left(0, \min(1, \frac{hw/h - C_D}{C_S - C_D})\right)(BS - BD) \quad 4.45$$

$$C = 18Log\left(\frac{12h}{k_s}\right) \quad 4.46$$

$$I_1 = 0.216\frac{\left(\frac{k_s}{h}\right)^{z^*-1}}{\left(1-\frac{k_s}{h}\right)^{z^*}}\int_{r_c}^{1}\left(\frac{1-y}{y}\right)^{z^*}dy \quad 4.47$$

$$I_2 = 0.216\frac{\left(\frac{k_s}{h}\right)^{z^*-1}}{\left(1-\frac{k_s}{h}\right)^{z^*}}\int_{r_c}^{1}\ln y\left(\frac{1-y}{y}\right)^{z^*}dy \quad 4.48$$

$$z^* = \frac{w_s}{\kappa q\frac{\sqrt{g}}{c}\sqrt{\left(1+0.5\left(\psi\frac{u_b}{q}\right)^2\right)}} \quad 4.49$$

$$A_r = \max\left(-50, \min\left(100, A_{ra}\right)\right) \quad 4.50$$

$$A_{ra} = -0.27\frac{\rho_s-\rho_w}{\rho_w}\frac{D_{50}C^2}{\mu q^2\left(1+0.5\left(\psi\frac{u_b}{q}\right)^2\right)} \quad 4.51$$

$$\mu = \left(\frac{C_{d_{90}}}{C} \right)^{1.5} \qquad 4.52$$

Where
BS: Coefficient *b* for shallow water (default value 5)
BD: Coefficient *b* for deep water (default value 2)
Cs: Shallow water criterion (default value 0.05)
Cd: Deep water criterion (default value 0.4)
C: Chézy coefficient
C_{d90}: Chézy coefficient based on d_{90}
Z^***:** Modified Rouse Parameter

Bijker (1971) introduced the effect of waves through modification of the bottom shear stress using horizontal wave orbital velocity U_b and Bijker parameter ψ, where

T: wave period
k: wave number
w_s**:** sediment fall velocity [m/s]

$$U_b = \frac{\omega H_{rms}}{2\sinh(k_w h)} \qquad 4.53$$

$$\omega = \frac{2\pi}{T} \qquad 4.54$$

$$\psi = \begin{cases} C\sqrt{\frac{f_w}{2g}} & T > 0 \\ 0 & Otherwise \end{cases} \qquad 4.55$$

$$f_w = \exp\left(-5.977 + \frac{5.123}{a_0^{0.194}} \right) \qquad 4.56$$

$$a_0 = \max\left(2, \frac{U_b}{\omega k_s} \right) \qquad 4.57$$

(c) Turbulence closure models

There are four turbulence closure models available in DELFT3D-FLOW, namely Algebraic closure (ALG), Prandtl's Mixing Length (PML), k-L model, and k-ε. All these models are based on the so-called 'eddy viscosity' concept (Kolmogorov, 1942) which expresses the eddy viscosity ν_v as:

$$\nu_v = c_\mu L\sqrt{k} \qquad 4.59$$

Where c_μ is a constant parameter, L is the mixing length and k is the turbulent kinetic energy. These turbulence closure models differ in their description of the turbulent kinetic energy k and the mixing length L.

Algebraic closure model (ALG) is restricted to logarithmic flow assumption, which might not be valid for complex flow conditions. Zero equation models like Prandtl model are not also appropriate for complex flow conditions, where advective and diffusive transport might be important and it is not easy to determine the parameter L analytically (Rodi, 1993). For the same reason, k–L closure does not seem to be appropriate for the complex flow condition because in this closure L is still determined analytically. On the other hand, two-equation models such k-ε model are more applicable to complex flow conditions (Rodi,-1993). Most of all, the k-ε model is the most widely successfully applied turbulence model (Rodi, 1993). It should be noted that, in DELFT3D, k-ε model is further improved to account for the production of turbulent energy directly associated with wave breaking and energy dissipation due to bottom friction Based on the discussion above, in this study, k−ε turbulence closure model is used. In order to apply k-ε model, the values of k and ε in every grid cell are treated as water-borne constituents and calculated by the following transport equations:

$$\frac{\partial k}{\partial t}+U\frac{\partial k}{\partial x}+V\frac{\partial k}{\partial y}+\frac{\omega}{(h+\zeta)}\frac{\partial k}{\partial \sigma}= \\ +\frac{1}{(h+\zeta)^2}\frac{\partial}{\partial \sigma}\left(D_k\frac{\partial k}{\partial \sigma}\right)+P_k+P_{kw}+B_k-\varepsilon \tag{4.60}$$

$$\frac{\partial \varepsilon}{\partial t}+U\frac{\partial \varepsilon}{\partial x}+V\frac{\partial \varepsilon}{\partial y}+\frac{\omega}{(h+\zeta)}\frac{\partial \varepsilon}{\partial \sigma}= \\ +\frac{1}{(h+\zeta)^2}\frac{\partial}{\partial \sigma}\left(D_\varepsilon\frac{\partial \varepsilon}{\partial \sigma}\right)+P_\varepsilon+P_{\varepsilon w}+B_\varepsilon-c_{2\varepsilon}\frac{\varepsilon^2}{k} \tag{4.61}$$

$$P_\varepsilon=c_{1\varepsilon}\frac{\varepsilon}{k}P_k \tag{4.62}$$

$$B_\varepsilon=c_{1\varepsilon}\frac{\varepsilon}{k}(1-c_{3\varepsilon})B_k \tag{4.63}$$

Based on Rodi (1993) the constant parameters in Eqs 4.61, 4.62 and 4.63 are: $c_{1\varepsilon}$ = 1.44, $c_{2\varepsilon}$ = 1.92, and $c_{3\varepsilon}$ =(0.0 for unstable stratification and 1.0 for stable stratification).

Based on Walstra et al. (2001), the distribution of turbulent kinetic energy production and dissipation due to wave breaking and wave energy decay in the bottom boundary layer (see Fig. 4.5) are expressed as:

$$P_{kw}=\frac{4D_w}{\rho_w H_{rms}}\left[1-2\frac{z'}{H_{rms}}\right] \quad for \quad 0\le z'\le\frac{1}{2}H_{rms} \tag{4.64}$$

$$P_{kw}=\frac{2D_f}{\delta}\left[1-\frac{d+\bar{\zeta}-z'}{\delta}\right] \quad for \quad d+\bar{\zeta}-\delta\le z'\le d+\bar{\zeta} \tag{4.65}$$

$$P_{\varepsilon w} = c_{1\varepsilon}\frac{\varepsilon}{k}P_{kw}(z') \qquad 4.66$$

Where, z' is the vertical coordinate with its origin at the (wave averaged) water level and is positive downwards, D_w and D_f represent wave energy dissipation due to wave breaking and bottom friction respectively. After calculating k and ε, the mixing length L is determined as:

$$L = C_D\frac{k\sqrt{k}}{\varepsilon} \qquad 4.67$$

$$C_D \approx C_\mu^{3/4} = 0.1925 \qquad 4.68$$

where c_μ is another constant in k–ε model.

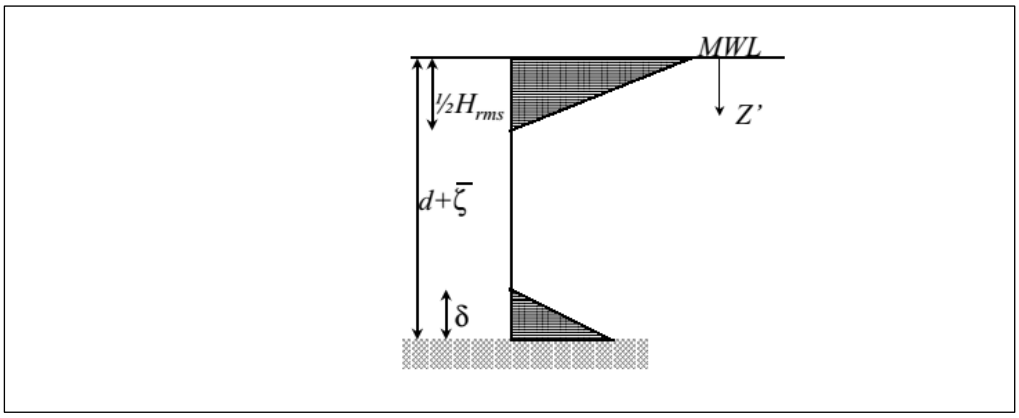

Fig 4.5: Vertical distribution of turbulent kinetic energy production and dissipation (Walstra et al. ,2001)

4.2 Implementation of Submerged Porous Breakwaters (SPB) in DELFT3D-WAVE

In this section, a new approach for implementing submerged porous breakwaters (SPB) in DELFT3D-WAVE is proposed and the model extended using this approach will be validated. DELFT3D-WAVE is not able to account for the dissipative effects of breakwater porosity on wave transmission (see section 2.3). On the other hand, the model has some limitations with respect to steep-slope submerged breakwaters (see section 4.2.1), though it can account for the effect of breakwater submergence. Introducing the proposed approach in DELFT3D-WAVE allows us to extend the model applicability to account for the combined effect of breakwater porosity and submergence on wave transmission at SPB, even for steep slope breakwaters, where the current DELFT3D cannot adequately predict the effect of submergence on wave transmission.

The approach proposed in this study for the SPB implementation in DELFT3D–WAVE consists of two consecutive steps:

(i) Implementation of the effect of breakwater submergence
(ii) Implementation of the effect of breakwater porosity

Steps (i) and (ii) are respectively described in Sections 4.2.1 and 4.2.2. The application of the proposed approach in DELFT3D-WAVE is described and validated against laboratory measurements in Section 4.2.3, which also includes a discussion on the applicability of the proposed SPB implementation approach.

4.2.1 Implementation of the Effect of Submergence in DELFT3D-WAVE

DELFT3D-WAVE can be applied to simulate the wave field leeward of submerged breakwaters (e.g. El Shinawy et al., 2012, Vlijm, 2011, Van der Hout, 2008). For this purpose, two approaches can be applied:

a. **Introducing the submerged breakwater as an obstacle**

In this approach, the bathymetry in the wave module is introduced without submerged breakwater. Indeed, the submerged breakwater in DELFT3D-WAVE is represented as a sub-grid obstacle (an obstacle with dimensions that are too small to be resolved by the computational grid) which is defined as a line. This linear obstacle reduces the height of the waves propagating from up-stream of the obstacle line, all along its length. The ratio of the transmitted wave height at the immediately down-wave side of the obstacle over the incident wave height at the immediately up-wave side of the obstacle is equal to the wave transmission coefficient K_t of the obstacle. Thus, in this approach, the effect of the submerged breakwater on the transmitted wave field can be simply taken into account using an appropriate wave transmission coefficient (see section 4.1.1). Fig. 4.6 schematically depicts the wave height reduction at the sub-grid linear obstacle:

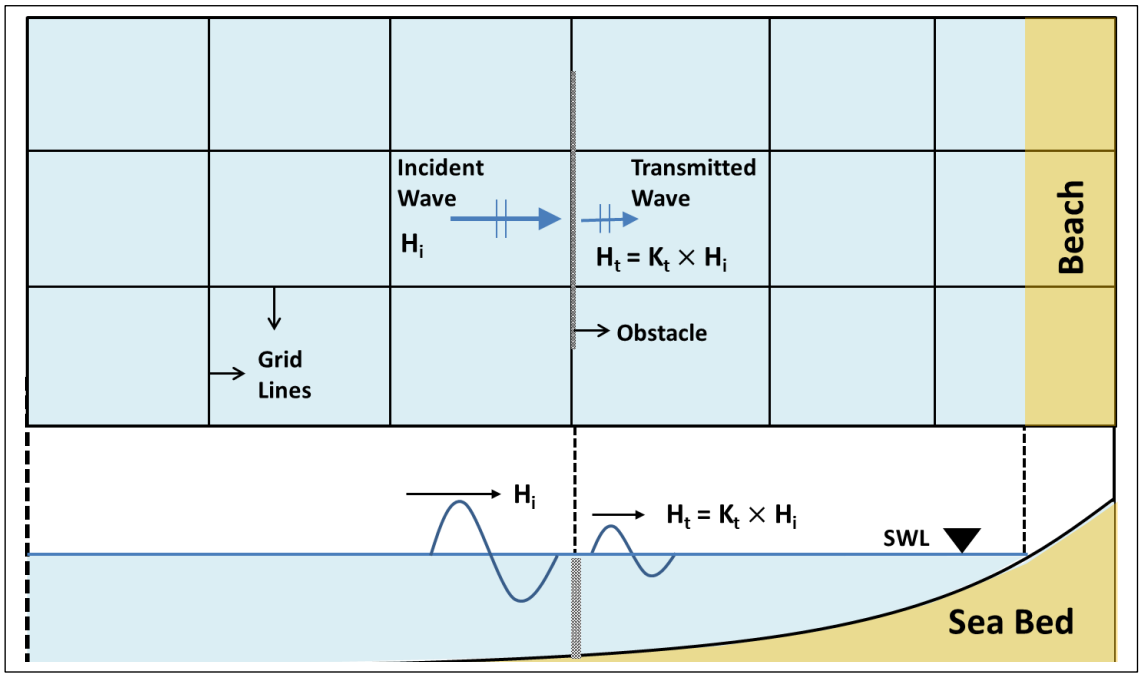

Fig 4.6: Wave height reduction at sub-grid obstacle

Although this first approach might be adequate for the prediction of the wave field leeward of the breakwater, the main limitation of this approach appears when the flow and sediment transport simulation are considered. In such a case, the bathymetry used in the DELFT3D-FLOW module, which also includes submerged breakwater, is passed to the DELFT3D-WAVE.

This causes an extra and unrealistic wave energy dissipation, because the wave module once calculates the energy dissipation due to wave breaking over the submerged breakwater and once again due to existence of the obstacle (represented by the introduced wave transmission coefficient).

On average, the calculation of this extra dissipation in the DELFT3D-WAVE might result in ca. 50% overestimation of the total wave energy dissipation at submerged breakwaters. This would result in an unrealistic prediction of the wave field which may adversely affects the predicted flow and sediment transport leeward of the submerged breakwater.

b. Introducing the submerged breakwater as bathymetric feature

In this approach, the bathymetry introduced in the wave module also includes the topography of the submerged breakwater. Thus, the dissipative effects of the submerged breakwater on the transmitted waves are calculated using the wave transformation and wave breaking parameterization available in DELFT3D-WAVE (see section 4.1.1). In this second approach, the main limitation appears particularly for submerged breakwaters with steep side slopes. Vlijm (2011) carried out a number of numerical tests using DELFT3D-WAVE and showed that, introducing submerged breakwaters with side slopes of 1:5 (V:H) as a bathymetric feature would result in calculated wave transmission coefficients very close to values calculated by the van der Meer formulae VDM2003 (see Section 2.2.1, Eq. 2.7). However, further investigations on the breakwater with steeper side slopes 1:2 (Johnson et al., 2006; El Shinawy and Zeidan, 2012) showed that the Battjes and Janssen (1978) wave breaking model (Hereafter BJ78) as applied in DELFT3D-WAVE would result in a large underestimation of transmitted waves in the lee of the breakwater. This large underestimation could be attributed to premature wave breaking over the steep slope breakwater, and thus to larger wave energy dissipation. To overcome this limitation, Zanuttigh et al. (2006) suggested that the default breaking parameterization in BJ78 should be adjusted, in order to make it applicable for steep slopes. Adjusting the default wave breaking parameters in BJ78 may result in an improved agreement between numerical results and measurements in the close proximity to the breakwater (Johnson at al., 2006; El Shinawy et al., 2012). This approach, although locally efficient over steep slopes of submerged breakwaters, might cause the incipient of wave breaking to occur closer to the shoreline. This limitation results in an unreliable prediction of surf zone hydrodynamics, which might eventually result in an unreliable prediction of sediment transport and coastal morphological changes. However, modifying the model at the coding level, might improve the model so that it uses appropriate breaking parameters on the basis of bottom slope.

Based on the above discussion, and since in this study flow and sediment transport are also considered, introducing the submerged breakwaters as an obstacle in DELFT3D-WAVE leads to the inevitable overestimation of predicted wave dissipation (ca. 50%) at the structure. Thus, the first approach described above, i.e. introducing the submerged breakwaters as an obstacle, is not applicable in this study

Accordingly, in this study, it is preferred to represent the effect of submergence through the introduction of submerged breakwaters as a bathymetric feature. However, it is necessary to overcome the difficulties associated with submerged breakwaters with side slopes steeper than 1:5 (which is often the case in practice) and to implement such steep breakwaters, so that the transmitted wave field and surf zone hydrodynamics are both predicted with sufficient accuracy.

Van der Hout (2008) showed that enlarging the grid size over the breakwater decreases the wave dissipation in DELFT3D-WAVE. This implies that it is possible to locally adjust the mesh size, in order to achieve a sufficiently accurate transmitted wave field leeward of the steep slope breakwaters.

To implement the latter approach in this study, it is proposed to define within the computational domain two distinct regions with different mesh sizes seaward ***(R1)*** and shoreward ***(R2)*** of the breakwater (Fig. 4.7).

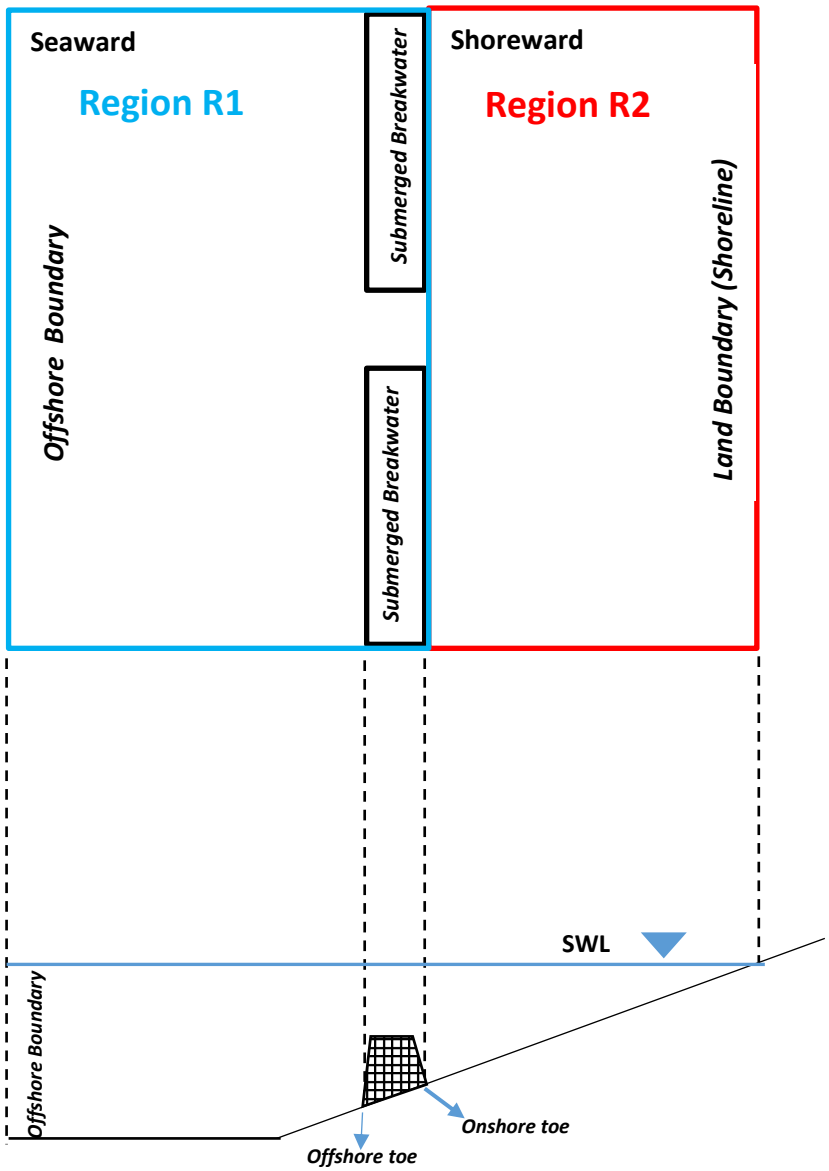

Fig 4.7: Dividing the computational domain into two distinct regions seaward and shoreward of the breakwater, namely R1 and R2

As shown in Fig.4.7, seaward region ***R1*** (borders in blue) is extended from the offshore boundary to the onshore toe of the breakwater, and shoreward region ***R2*** (borders in red) is extended from the onshore toe of the breakwater to the shoreline. Lateral borders of ***R1*** and ***R2*** coincides with the lateral boundaries of the computational domain. In order to generate an optimal and efficient mesh, a step by step procedure is proposed in this study. In each step of the proposed procedure, the effects of the mesh size on the simulation results in ***R1*** and ***R2*** are evaluated separately. Then, based on the results, the optimal mesh size for each region is selected. The stepwise procedure for the selection of the optimal mesh size is depicted by Fig. 4.8, where K_t and $K_{tVDM2003}$ respectively represent the wave transmission coefficient computed from the model and by applying the Van der Meer formula (VDM2003).

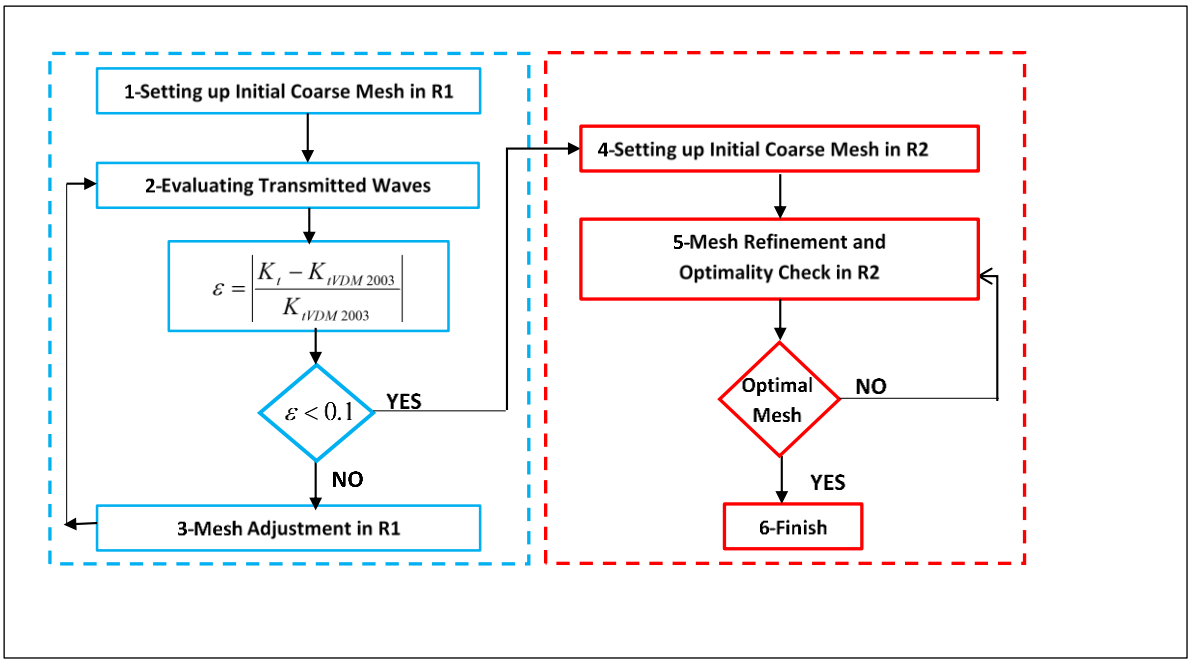

Fig 4.8: Proposed stepwise procedure for the selection of the optimal mesh size

The stepwise procedure proposed in Fig. 4.8 consists of the following 6 consecutive steps:

- *Step 1: Setting up the initial coarse mesh in seaward region R1*

This is the first step of generating an optimal mesh size in *R1*. In this step, a coarse mesh in *R1* is defined initially. The initial mesh size might be selected on the basis of judgement or experience.

- *Step 2: Performing numerical test with initial coarse mesh from Step 1*

The relative error ε (Fig 4.8) between predicted transmission coefficient K_t and transmission coefficient obtained from VDM2003, $K_{tVDM2003}$ (see Section 2.2.1, Eq. 2.7), is calculated for the evaluation of the simulation results. If the calculated relative error ε becomes smaller than 0.1 (10%) then mesh size selecting in R2 is started through Step 4, otherwise the computational mesh in R1 is adjusted through Step 3.

- *Step 3: Adjusting the mesh size in seaward region R1*

This step is performed only if the requirement $\varepsilon < 0.1$ is not met in Step 2. If $\varepsilon \geq 0.1$, the mesh size is adjusted in region ***R1*** to reduce the relative error ε. Then Step 2 is repeated to evaluate the results.

- *Step 4: Setting up the initial* coarse *mesh in shoreward region R2*

This first step for generating an optimal mesh in ***R2,*** is performed only if the requirement $\varepsilon<0.1$ is meet in Step2.

- Step 5*: Mesh refinement in shoreward region R2*

In this step numerical tests are performed to optimize the mesh in **R2**. For this purpose, computational mesh in **R2** is refined and the simulation results are evaluated. The optimum mesh size is reached if the maximum change of calculated wave height due to mesh refinement is limited to 5 %. In this case, the mesh generation is completed and the final Step 6 is initiated; otherwise Step 5 is repeated.

- *Step 6: Completion of the selection procedure*

As a result, the final optimal mesh size is obtained for both regions 1 and 2.

It should be noted that the mesh size in R2 not only depends on the incident wave height, but also on the wave period and relative submergence, all of which affect the wave breaking and thus the degree of mesh size adjustment needed in R2.

4.2.2 Implementing the Effect of Porosity

After the implementation of the effect of the breakwater submergence in DELFT3D-WAVE, the dissipative effects of the breakwater porosity needs to be implemented, in order to account for the porosity effect on wave transmission at submerged breakwaters.

As mentioned in section 2.3.1, DELFT3D is not able to account for the effect of breakwater porosity on wave transmission. Thus in this section, a novel approach is proposed to implement the dissipative effect of breakwater porosity on wave transmission at submerged breakwaters. This new proposed approach is based on the virtual transmissive sub-grid (thin) obstacle (see paragraph a, section 4.2.1) which is located at onshore toe of the breakwater with: i) the same length and orientation as the submerged breakwater. ii) the transmission coefficient determined by PEF formula which is developed and introduced in section 3.4.

It should be noted that the Virtual Transmissive Obstacles (VTO) concept was successfully applied by Tajziyechi and Cox (2007) for simulating wave induced currents in presence of submerged breakwaters. However, in the approach proposed in the present study, the VTO concept is only intended to represent the dissipative effect of breakwater porosity on wave transmission. Accordingly, the transmission coefficient of the obstacle needs to be determined using the porosity effect factor PEF which is introduced in chapter 3 (see section 3.4)

Fig. 4.9 shows virtual obstacles which are implemented in the computational domain immediately leeward of the breakwaters:

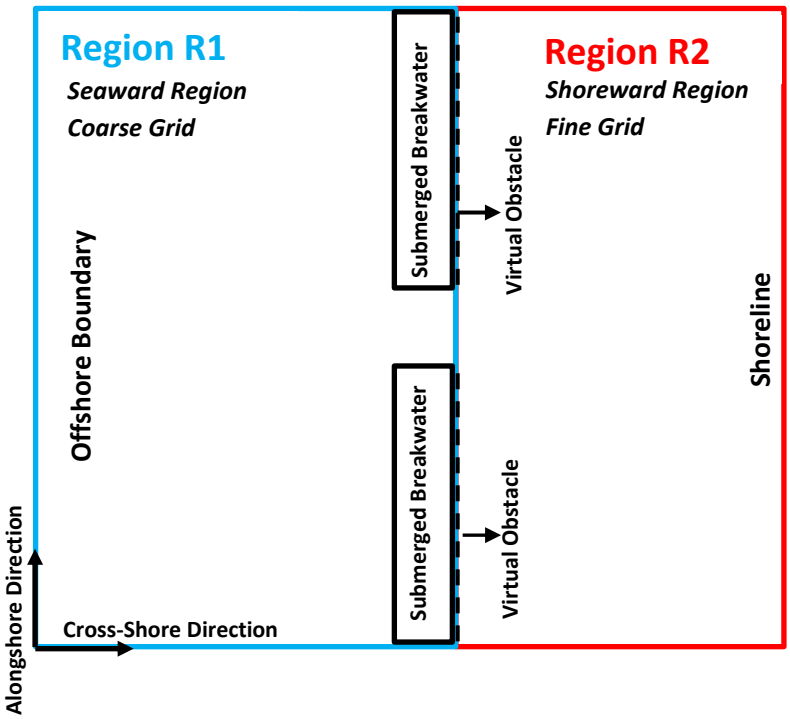

Fig 4.9: Virtual obstacles (represented by dashed lines) immediately leeward of the submerged breakwaters

The approach proposed for the implementation of both submergence and porosity effects on wave transmission at submerged porous breakwaters (SPB) according to the two-step procedure described in Sections 4.2.1 and 4.2.2 is called hereafter *"SPB Implementation Approach"*.

Based on step i and step ii of the SPB implementation approach, which are respectively discussed in sections 4.2.1 and 4.2.2, the submergence effect is first implemented through step i (see section 4.2.1), so that the calculated WTC lies within 10% of WTC calculated by $K_{tVDM2003}$ (see Fig. 4.8).

Then, through step ii, a virtual obstacle, with the transmission coefficient calculated by PEF, is implemented at onshore toe of the breakwater to apply dissipative effect of breakwater porosity on the WTC predicted by the model, which is very close to WTC calculated using VDM2003 (the relative difference is limited to 10%, See Fig. 4.8). This *SPB Implementation Approach* is schematically represented by Fig. 4.10:

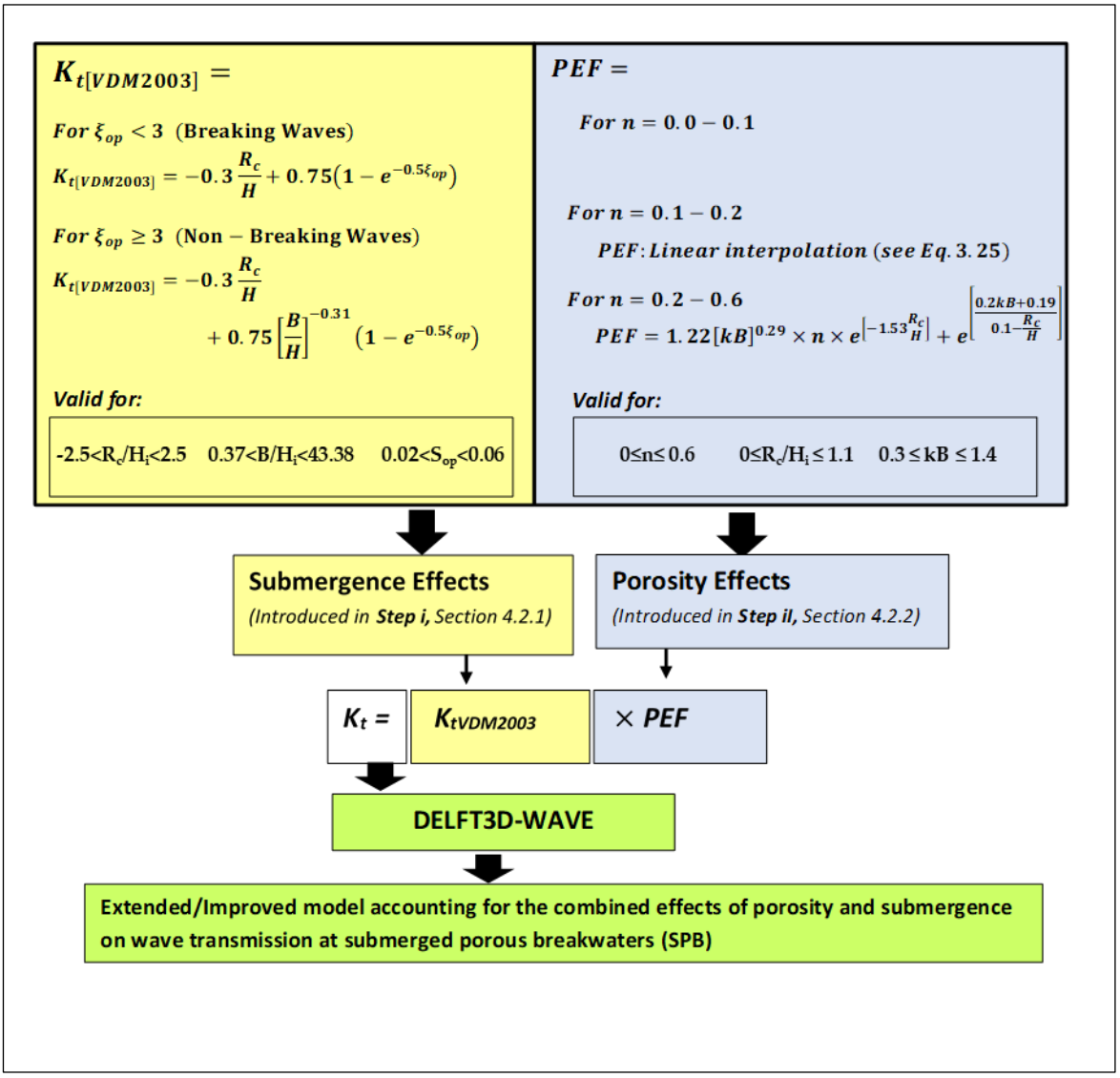

Fig 4.10: The "SPB Implementation Approach" proposed to the implement the effects of breakwater submergence and porosity on wave transmission in DEFLT3D-WAVE, on the basis of the new WTC formulae (see section 3.4)

As shown in Fig. 4.10, using the SPB implementation approach, the numerical model will calculate WTC according to the new WTC formulae developed in Chapter 3 (see section 3.4), i.e. $K_t=K_{tVDM2003}\times$ PEF (see section 3.3).

The virtual transmissive obstacle in the cross-section view and the way it affects incident wave transmission are schematically shown in Fig. 4.11 (also depicting that the virtual obstacles are thin):

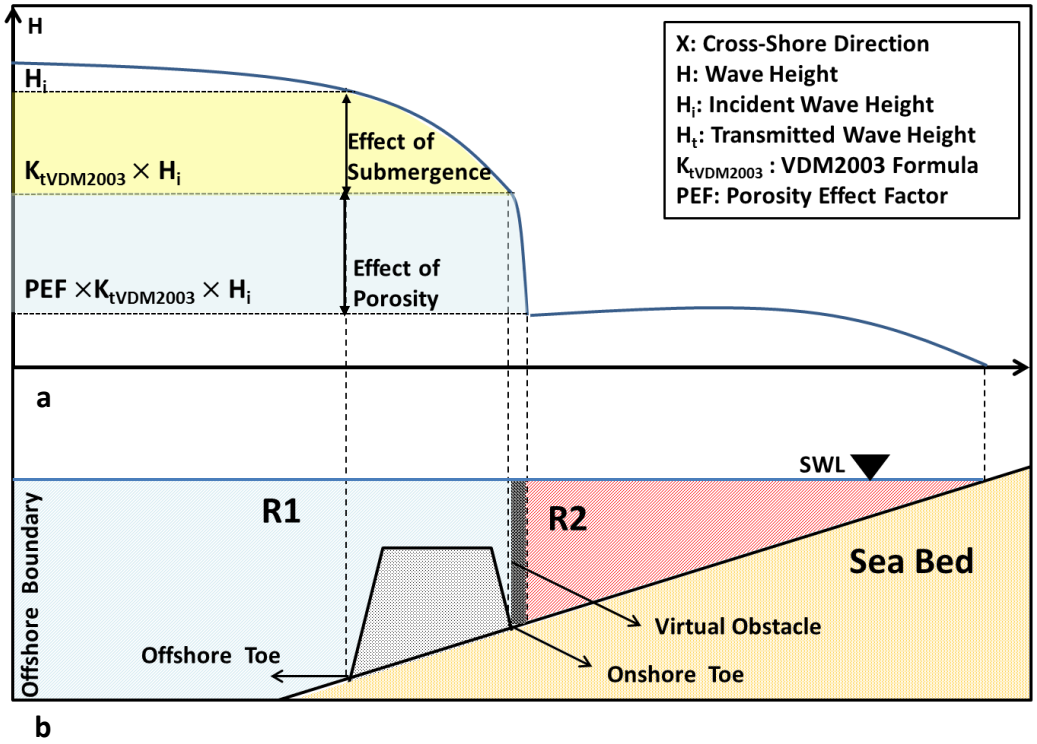

Fig 4.11: Illustration of Virtual Obstacle Concept: a) the effect of transmissive virtual obstacle on wave transmission. b) The virtual obstacle in cross-section view

It should be noted that the approach proposed in this section to implement the effect of breakwater porosity using the virtual obstacle can be potentially applied for any phase-averaged model in which linear obstacles can be defined (e.g. MIKE SW, see Section 2.4).

The implementation of this approach in DELFT3D-WAVE will be described and validated in the following section, and the model validation results will be critically discussed to confirm the applicability of the SPB implementation approach, before applying it in the simulation of coastal morphological changes in section 4.3, where DELFT3D-FLOW is also utilized.

4.2.3 Validation of the proposed SPB implementation approach

In this section, the applicability of the proposed SPB implementation approach is verified against the results of the laboratory tests of Kramer et al. (2005), which are briefly described below. The application of the SPB implementation approach in DELFT3D-WAVE, along with the numerical model set-up applied to reproduce the laboratory tests, are then described. Finally, the results of the model validation and a discussion on the applicability of the proposed SPB implementation approach are provided.

(a) Laboratory Tests

Kramer et al. (2005) carried out a series of laboratory experiments with a main focus on the wave and wave-induced flow field in the vicinity of low crested porous breakwaters made of rock material. The tests were performed in the directional wave basin of the Hydraulics and Costal Engineering Laboratory at Aalborg University, Denmark. The wave basin is 7.5m in cross-shore and 12.5 m in longshore direction. The water depth in all tests is equal to 0.43 m. A subset of these tests was aimed at investigating wave field and wave-induced flow patterns in the vicinity of submerged breakwaters. The tested submerged breakwaters consist of an armour layer of quarry rocks with porosity n=0.44 which is built on a core with slopes 1:2 and porosity n=0.43. The experimental configuration was designed in a model scale of 1:20.

One of the tested layouts was a symmetric arrangement of two detached breakwaters separated by a gap of 2.0m. This layout is shown in Fig. 4.12b, where the locations of 21 wave gauges are depicted by filled circles (number 1 to 21). The tested breakwaters have the submergence depth R_c=0.05m and two crest widths B=0.1m and B=0.25m, which respectively represent a narrow and a wide crested structure. Along the lateral boundaries, wave guides were placed from the wave maker to the breakwater (For further details, see Kramer et al., 2005). These laboratory tests include 3D random directional waves with a mean wave direction normal to the breakwater, JONSWAP spectral shape and directional spreading of 22.7°. A summary of the laboratory tests used in this study to evaluate the numerical results is given in Table 4.1, where H_{m0} is the significant wave height, T_p the peak period, L_p the wave length calculated on the basis of T_p, k_p the wave number calculated on the basis of L_p, θ the mean wave direction measured clockwise with respect to shore normal direction, and σ_θ the directional spreading of the waves.

Table 4.1: Selected laboratory tests for the evaluation of the numerical results in this study

Test	Average Measurements (Wave gauges 3-7)		Wave Properties		Crest Width B° (m)	Wave Type*	Directional spreading σ_θ °(degree)	Wave direction Θ (degree)°
	H_{m0}(m)	T_p(s)	H_{m0}/L_p	k_ph				
21	0.065	1.32	0.03	1.00	0.10 (Narrow)	Irregular-Jonswap	22.7	0
33	0.141	1.97	0.04	0.72	0.25 (Wide)	Irregular-Jonswap	22.7	0
35	0.065	1.32	0.03	1.00	0.25 (Wide)	Irregular-Jonswap	22.7	0

peak enhancement factor γ=3.3

cosine power spreading function with spreading parameter S_θ = 50

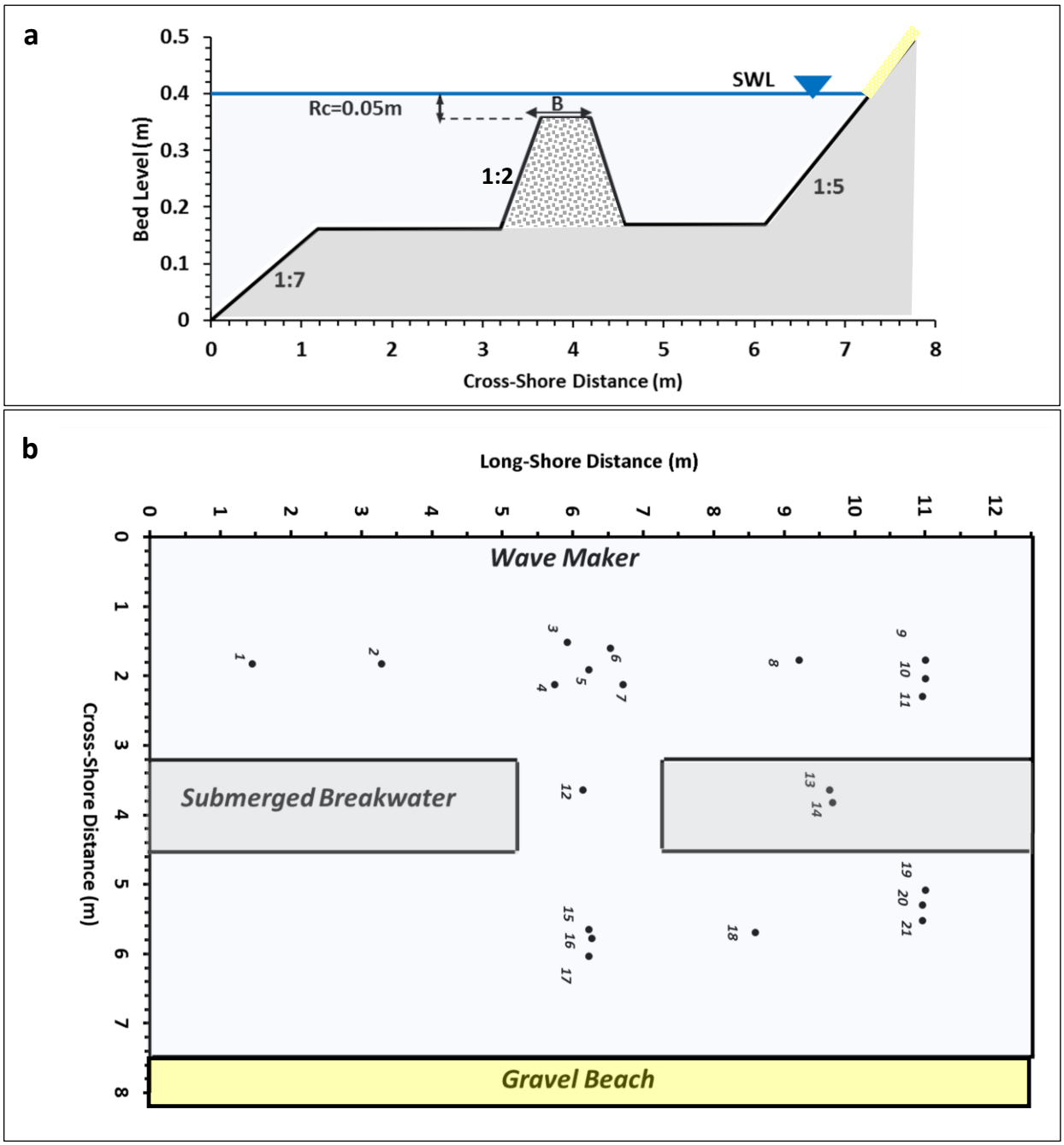

Fig 4.12: Model illustrating the symmetric arrangement of two detached submerged porous breakwaters in a basin: a) cross-section view with still water level at 0.43m. b) Plane view

(b) Numerical Model Set-up

The numerical model setup is aimed at reproducing the laboratory tests described in the previous section. The input parameters, computational grid and boundary conditions applied in DELFT3D-WAVE in order to set-up the numerical model are provided below.

Input Parameters

In order to solve the action balance equation and calculate the wave energy density E (σ,θ) over the computational domain, DELFT3D-WAVE(SWAN) distributes the wave energy in directional and frequency bins. In this study, default value of 72 directional bins is used to account for the effect of the directional spreading of waves.

The number of frequency bins is also set to the default value of 24, in which the wave frequencies range from 0.05 Hz to 1.0 Hz. Higher resolution in frequency and direction space has been observed not to influence the results. The depth induced breaking dissipation is represented in the model using the BJ78 parameterization (see Section 4.1.1). According to Holthuijsen (2007), the triad wave-wave interaction is of significant importance in shallow water regions. Thus, triad wave-wave interaction is activated in the model. Bottom friction is also turned on with defaults settings to account for wave friction.

Table 4.2: Overview of the model setting applied in DELFT3D-WAVE (SWAN)

Obstacle	PEF formulation
Wave Diffraction	On
Wave Braking	BJ78 parameterization
Triad Wave-Wave Interaction	On
White Capping	On (Kommen 1984)
Wave Friction	JONSWAP formulation
Directional Spreading	22.7°
T_p	1.97s
H_{m0}	0.14m

Grid and Bathymetry

Fig. 4.13 shows that the computational domain covers an area of 16.5m in longshore direction and 9m in cross-shore direction. In order to avoid boundary effects, the computational grid boundaries are selected conservatively far from the side walls of the basin. Thus, as shown in Fig. 4.13, the computational mesh is extended 2m beyond each side wall of the basin and the offshore boundary is located 1 m seaward of the wave maker:

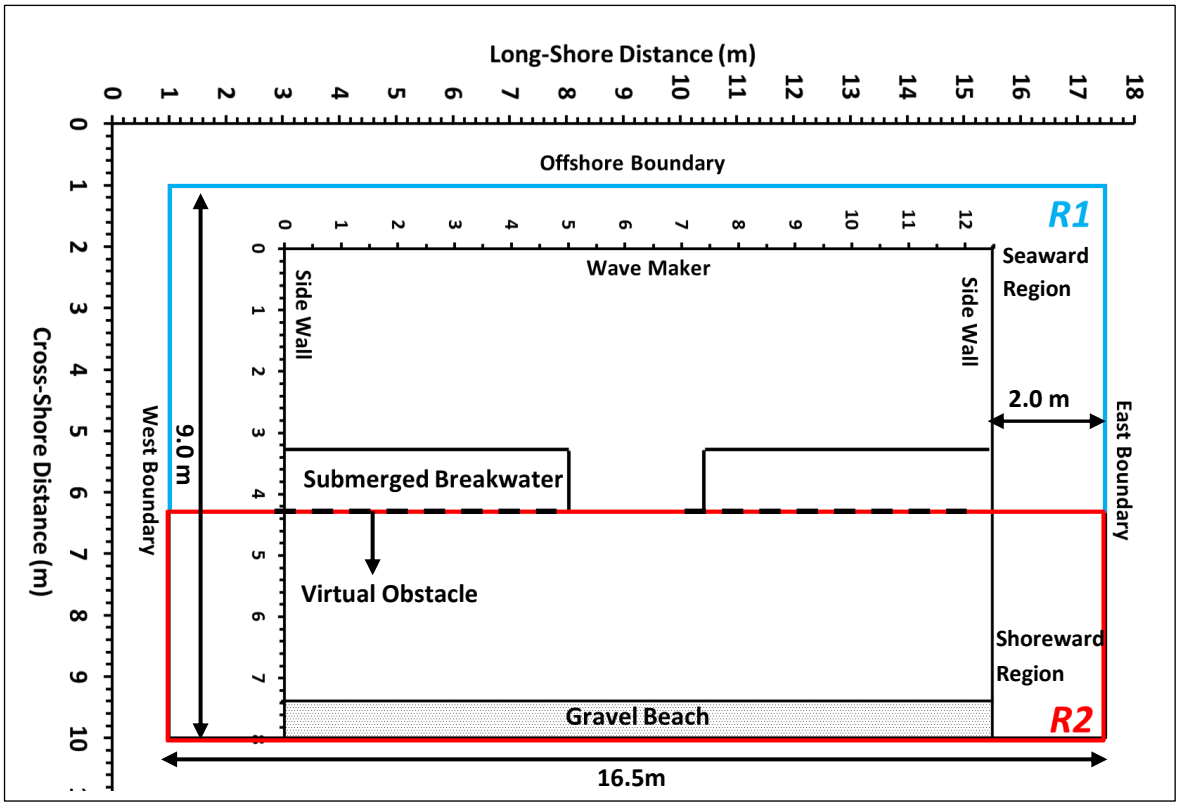

Fig 4.13: Computational domain subdivided in regions R1 and R2 respectively seaward and shoreward of the virtual obstacles located immediately behind the submerged breakwaters

Following the approach described in section 4.2.1 for implementing the SPB in DELFT3D-WAVE (SWAN), the computational domain is divided in two regions, namely ***R1*** and ***R2***. As shown in Fig. 4.13, the border lines of ***R1*** and ***R2*** are respectively coloured in blue and red. Preliminary tests are performed to examine the effects of the grid size on the numerical results. For this purpose, different uniform mesh resolutions have been initially examined over the computational domain. The properties of the examined meshes are given by Table 4.3, where M and N respectively stand for the number of computational cells in cross-shore and alongshore directions, and **Δx** and **Δy** are grid sizes in cross-shore and alongshore directions respectively.

Table 4.3: Computational mesh properties examined in the preliminary tests

Mesh	M	N	Δx (m)	Δy (m)
M1	15	21	0.66	0.8
M2	30	42	0.33	0.4
M3	60	84	0.17	0.2
M4	120	168	0.08	0.1

In order to evaluate the effect of the mesh size on the numerical results, five sections as shown in Fig. 4.15 are considered along the cross-shore bed profile.

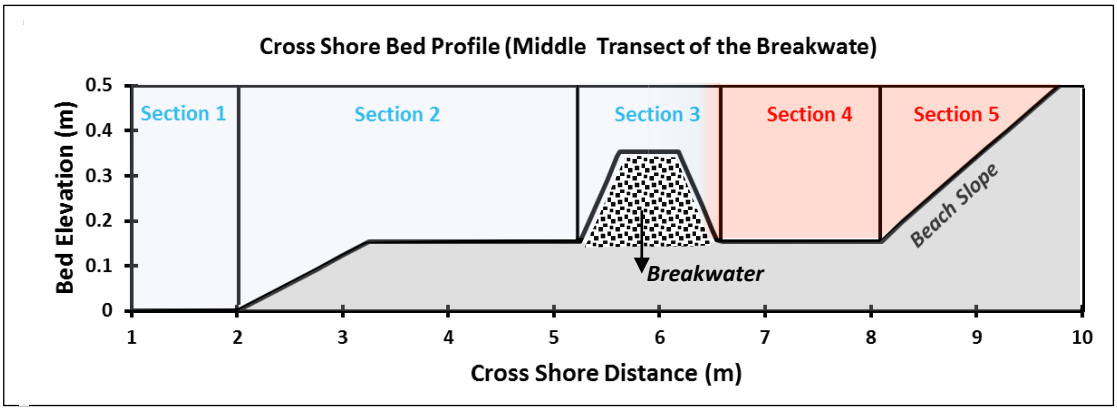

Fig 4.14: Cross-shore bed profile with five sections considered for the evaluation of numerical results

As depicted in Fig. 4.14, borders between different sections are indicated by black vertical lines, and the sections located within ***R1*** and ***R2*** are respectively coloured in blue and red. The results of the preliminary tests illustrating the effects of grid size on the calculated wave height in each section are depicted in Fig. 4.15.

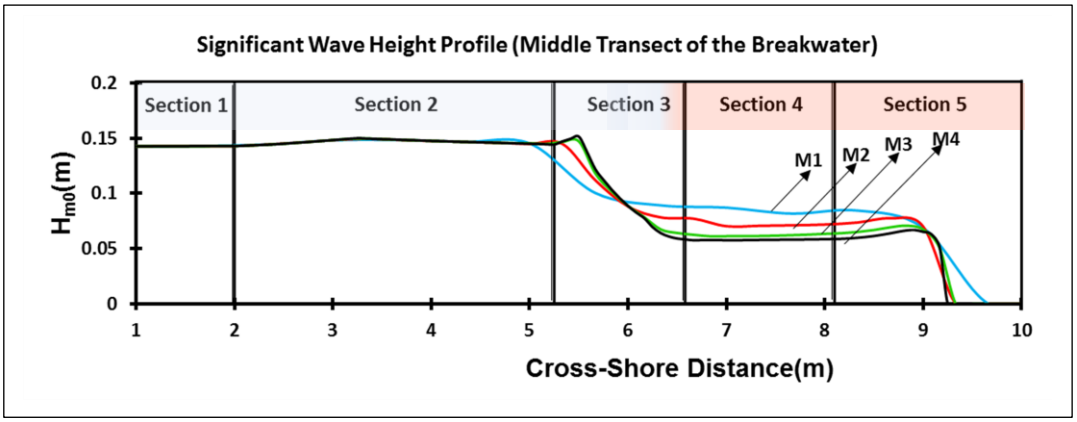

Fig 4.15: Results of preliminary tests with incident wave of H_{m0}=0.141m and T_p=1.97s in water depth h=0.43m for the different mesh sizes M1-M4 in Table 4.3

Fig. 4.15 shows that, in *section 1 and section 2*, located in seaward region ***R1***, the wave height slightly increases due to shoaling and the mesh size has almost no effects on the calculated wave height.

However, in section 3, which extends from the offshore toe to the onshore toe of the breakwater, the mesh size noticeably affects the height of the transmitted waves, and thus possibly the wave dissipation. Therefore, in Region ***R1*** the mesh size should be selected so that the transmitted wave height in *section 3* meets the accuracy criterion $\varepsilon < 0.1$ (see Fig. 4.8). Accordingly, Mesh M2 is selected for ***R1***.

Regarding the mesh size in the shoreward region ***R2***, the results of the preliminary tests in Fig. 4.15 reveal that, changing the computational mesh from Mesh M3 to Mesh M4 (see Table 4.3,) would result in 300% percent increase of mesh resolution, but only in a maximum difference of 4 % in the numerical results. This initially implies that the Mesh M3 could be used as the optimal mesh in Region ***R2***.

Using Mesh M2 in R1, it was found that changing the computational mesh from M3 to M4 (see Table 4.3,) would result only in 2 % difference in the numerical results. This confirms the initial implication given by the results shown in Fig. 4.15.

Based on the above discussion, the optimal grid is achieved by using M2 with $\Delta x = 0.33$m & $\Delta Y = 0.4$m in Region ***R1*** and M3 with $\Delta x = 0.17$m & $\Delta Y = 0.2$m in Region ***R2***. The relation between mesh size (i.e. Δx and Δy) in R2 and wave period can also be described as the dimensionless mesh size expressed by $\Delta x/L_p$ and $\Delta y/L_p$, where L_p is the wave length. The dimensionless grid size can give a measure of the number of grid points per unit wave length. Here, the dimensionless mesh size in R2 becomes $\Delta x/L_p \approx 0.05$ and $\Delta y/L_p \approx 0.06$, representing almost 20 grid point per wave unit length. However, as mentioned in Section 4.2.1, this parameter may depend on incident wave heights and breakwater submergence, as well as wave period. In order to investigate the relation between dimensionless mesh size in R2 and wave parameters, a wide range of breakwater submergence, incident wave height and wave period need to be examined. This analysis is however beyond the scope of the present PhD research and might be a subject of future studies.

Following the approach described in Section 4.2.2 to account for the porosity effects, virtual obstacles are defined in the computational grid, at the end of Region ***R1***. The location of the virtual obstacle with respect to the submerged breakwater in the plan view is represented by dashed lines in Fig. 4.13. Based on the reported values of the porosity of the core and armour layers of the breakwater (see section 4.2.3, paragraph a), the porosity n=0.44 is selected for the virtual obstacles.

- **Boundaries**

In this study, DELFT3D-WAVE uses one boundary condition from north (on the basis of SWAN convention in which the upper boundary is referred as north and other boundaries are named west, south and east with respect to the north boundary). The north boundary which is located 1m seaward of the wave maker in the laboratory basin is labelled as offshore boundary (See Fig. 4.13). The JONSWAP spectrum is used with a peak enhancement factor of 3.3 to reproduce the irregular shore-normal waves in the laboratory wave basin.

The uniform and stationary boundary condition is defined along the offshore boundary, with the boundary condition obtained from the wave conditions in Table 4.1

(c) Results and Discussion

In order to evaluate the applicability of the SPB implementation approach discussed in Sections 4.2.1 and 4.2.2, the calculated results are compared with laboratory measurements for tests 21, 33 and 35 (Table 4.1). The comparison between the laboratory measurements and the numerical prediction of the significant wave heights H_{m0} obtained at wave gauges G3-G21 (for locations see Fig. 4.12) using the DELFT3D-WAVE with (Improved D3D-Wave) and without (Original D3D-Wave) the proposed SPB implementation is shown in Fig. 4.16:

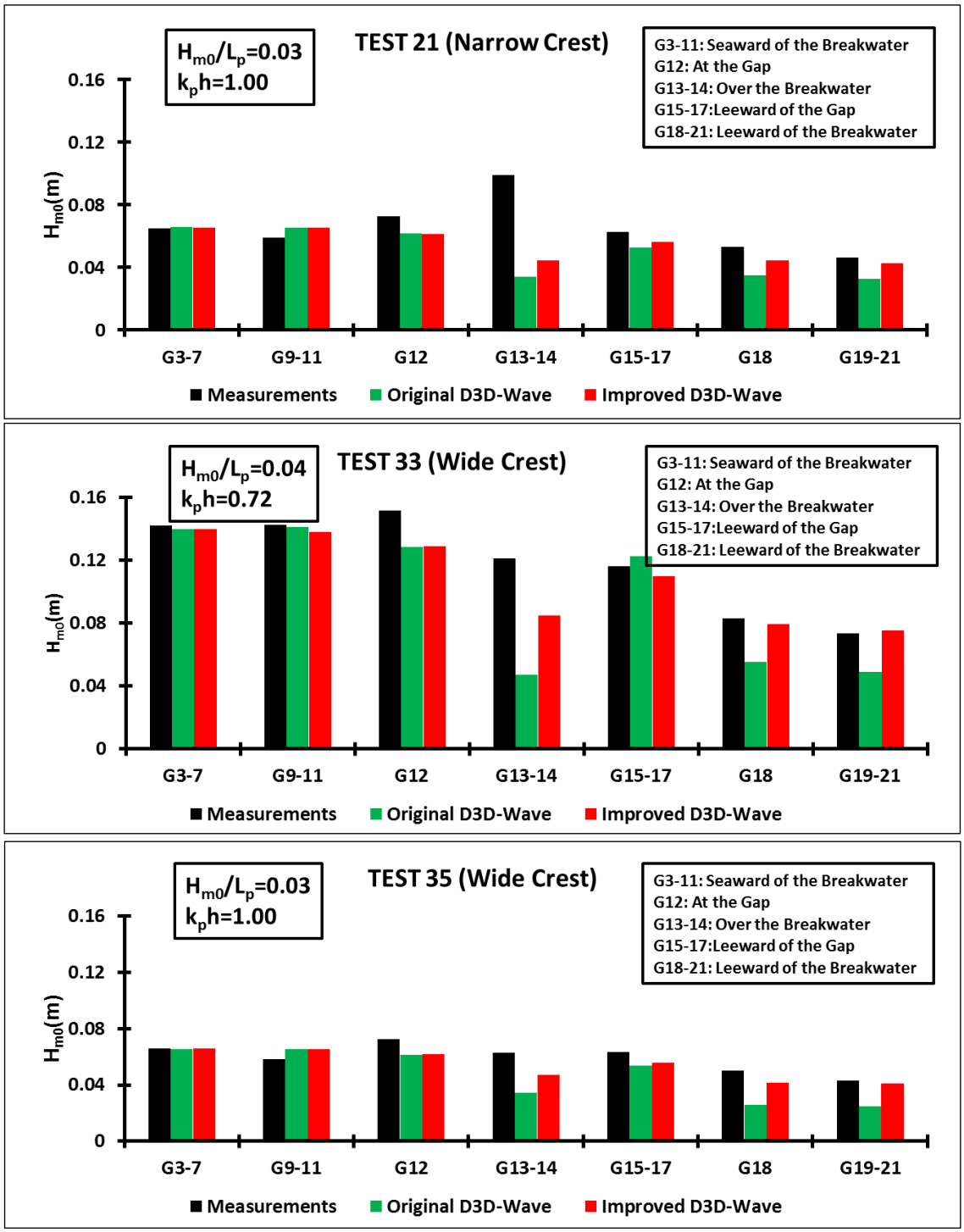

Fig 4.16: Comparison of wave heights H_{m0} obtained from laboratory tests 21, 33 and 35 (see Table 4.1) at wave gauges G3-G21 (for locations see Fig. 4.12) and from the DELFT3D-WAVE with (Improved D3D-Wave) and without (Original D3D-Wave) the proposed SPB implementation.

As shown in Fig. 4.16, applying DELTF3D-WAVE without the SPB implementation largely underestimates the transmitted wave height leeward of the submerged porous breakwater (SPB). The application of the proposed SPB implementation approach substantially reduces the wave height underestimation by the model leeward of the SPB (G18 and G19-21). In this study, the absolute relative difference E (in %) between the predicted and measured wave heights can be used to quantify the underestimation of wave height leeward of the SPB (G18-G21)

$$E = 100 \times \left| \frac{(H_{m0})_{Predicted} - (H_{m0})_{Measured}}{(H_{m0})_{Measured}} \right| \qquad 4.69$$

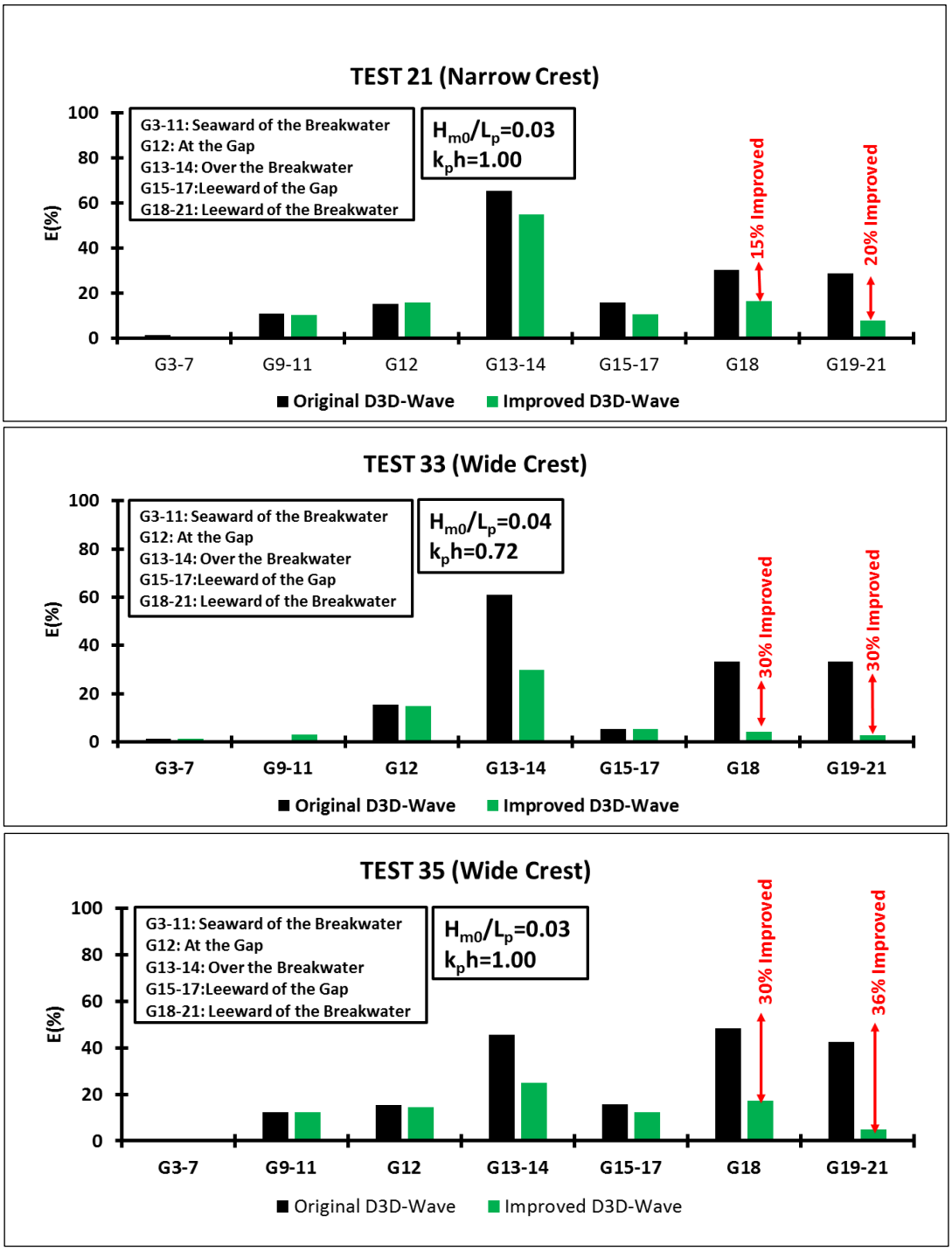

Fig 4.17: Absolute relative deviation E (see Eq. 4.69) of the predicted wave heights at wave gauges G3-G21 (for locations see Fig. 4.12) from the measured values for Tests 21, 33 and 35 (see Table 4.1), as obtained by using the improved DELFT3D-WAVE model (with SPB implementation approach) and by using the original DELFT3D-WAVE (with SPB implementation approach).

For Test 35 (wide berm as defined in Table 4.1), the numerical results obtained using the improved DELFT3D-WAVE model instead of the original model show that the value of error E (as defined by Eq 4.69) decreases from E= 48% to E= 18% at gauge G18 and from E= 42% to E= 6 % at gauges G19-G21, implying to 30% and 36% improvement of wave height prediction leeward of the SPB respectively at G18 and G19-21.

For Test 21 (narrow berm as defined in Table 4.1), however, this improvement in wave height prediction leeward of the SPB is only 15% at G18 and 21% at G19-G21.This implies that the efficacy of the SPB implementation approach is more noticeable for wide-crested SPBs, compared to narrow-crested SPBs. This important issue will be further discussed in section 4.2.3d.

The comparison of the values of the absolute relative deviation E (see Eq. 4.69) between the measured wave heights at gauges G3-G21 (for locations see Fig. 4.12) and the predicted values obtained by using the improved DELFT3D-WAVE model (with SPB implementation approach) and those obtained by using the original DELFT3D-WAVE (with SPB implementation approach) for Tests 21, 33 and 35 (see Table 4.1) is summarized in Fig. 4.17, also indicating the achieved improvements of the prediction of wave height leeward of the SPBs.

Fig. 4.17 also shows that, although not quantified, the underestimation of the wave height over the breakwater at gauges G13-14, is also noticeably improved except for Test 21 (narrow berm). As shown in Fig. 4.16, the measured wave height at G13-14 in Tests 21 and 35 are respectively 0.1m and 0.065m. Although the location of the wave gauges and the incident wave conditions are exactly similar in both tests, this rather large difference (50%) between the two measurements at the same location with the same incident wave conditions is possibly due to measurement error in Test 21, where the measured wave height at G13-14 is roughly twice larger than the measured wave height at G3-G7.

Although it was shown that the application of the proposed SPB implementation approach in DELFT3D-WAVE noticeably improves the prediction capability of the model, especially in the lee of the breakwater, the overall performance of the improved DEFLT3D-WAVE model still needs to be evaluated using statistical indicators. The scatter plots for measured and calculated transmitted wave heights H_{m0} leeward of the SPB, at G18 and G19-21 are shown in Fig. 4.18, where the results of DELFT3D-WAVE model without (Fig. 4.18a) and with (Fig. 4.18b) the implemented improvement are compared using Root Mean Square Error (RMSE) as a statistical indicator.

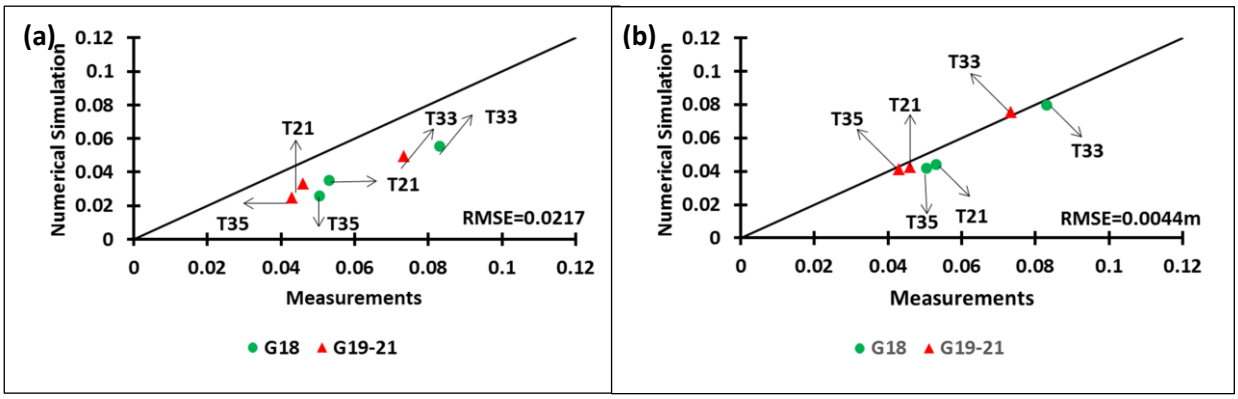

Fig 4.18: Scatter plots for measured and predicted transmitted wave height H_{m0} leeward of the SPB at gauges G18 and G19-21 (see Fig. 4.13 for locations) using the DELFT3D-WAVE model applied without (a) and with (b) the SPB implementation approach

Fig. 4.18 shows that the application of the improved DELFT3D-WAVE model noticeably reduces the scatter between the numerical results and the measurements leeward of the breakwater (reduction of RMSE by a factor of 5 at G18 and G19-21). However, the data points which are mostly located below

the perfect agreement line imply that the predicted wave height leeward of the SPB still remains slightly underestimated in most cases (see Also Fig. 4.16).

Although the proposed SPB implementation approach is able to significantly enhance the prediction performance of the DELFT3D-WAVE model in terms of transmitted wave heights H_{m0} leeward of the SPB, it is still not clear to which extent the predicted wave height evolution over the SPB is improved. In fact, applying the proposed SPB implementation approach in DELFT3D-WAVE noticeably enhances the accuracy of the transmitted wave height prediction leeward of the SPB through: i) calculating adequately breaking-induced dissipation even for SPBs with steep side slope, as described in section 4.2.1 ii) applying the dissipative effect of breakwater porosity as described in section 4.2.2. However, the improvement which has been achieved in agreement between measured and predicted wave heights over the breakwater, still needs some more clarification. In this study, the only available measurements carried out directly over the breakwater are at gauges G13 and G14 (see Fig. 4.12). Although the application of the proposed SPB implementation approach has been shown to improve the prediction of wave height at G13-G14 (see Figs. 4.16 and 4.17), the existing measurements are not sufficient to evaluate adequately the improvements in terms of the wave height evolution over the SPB. This might be a candidate topic for future researches, including more laboratory measurements directly over the SPB. Then, through the analysis of measured and calculated wave height over the entire SPB, the calculated wave height evolution over the SPB can be determined and compared with measurements.

(d) Applicability of the SPB Implementation Approach

A comparison between the improvement in the numerical results for Test 21 and Test 35 in Fig. 4.17 reveals that the improvement obtained by applying the proposed SPB implementation approach is about 15% lower in Test 21 (narrow SPB crest), compared to that calculated for Test 35 (wide SPB crest). In both Tests 35 and 21, the wave conditions at the offshore boundary (i.e. H_{mo}/L_p and k_ph) are the same and the only difference is the crest width, with B=0.25 m in Test 35 and B=0.10 m in Test 21. This clearly implies that, the improvement of the wave height prediction leeward of the breakwater due to the use of the SPB implementation approach proposed in this study might depend on the crest width B. The narrower crest in Test 21 would intuitively suggest weaker wave breaking-induced energy dissipation at the breakwater. Therefore, the effect of this dissipation on the predicted transmitted wave heights leeward of the breakwater is also weaker. Under such conditions, the effects on the predicted transmitted waves, which are responsible for the dissipation inaccuracies and caused by inappropriate wave breaking parameterization, decreases (see section 4.2.1). Thus, the improvement made by calculating the realistic breaking induced dissipation, which is achieved through reducing the overestimation of breaking induced dissipation (in case of steep slope breakwaters) by performing step i of the SPB implementation approach (Here after S1), becomes less prominent. Similarly, the increase of breakwater submergence makes the improvement achieved by performing S1 less significant.

The above discussion implies that design values of breakwater parameters, namely crest width B and submergence R_c, might exist for which reducing the overestimation of breaking-induced energy dissipation, which is made possible through performing S1 (see Section 4.2.1), has a negligible effect on improving the transmitted wave height prediction leeward of the breakwater. Under such conditions, the implementation of the submergence effects, which is the first step of the SPB implementation approach (see section 4.2.1) is not necessary and can be considered inapplicable. This important issue is further elaborated below in order to develop criteria for the applicability of step i of the SPB implementation approach (S1), which is proposed to overcome the large overestimation of breaking induced dissipation which is the case at steep slope submerged breakwaters

For this purpose, numerical simulations with different wave heights and periods are performed using the numerical settings of Test 33 described in Section 4.2b. Five incident wave heights (H_{m0}=0.02m, 0.05m, 0.08m, 0.11m and 0.14m) and six wave periods (T_p=1.3s, 1.5s, 1.7s, 2.0s, 3.0s and

4.0s) are considered in the numerical model, resulting in 30 numerical tests. For each numerical test, the relative difference between the WTC obtained from the model (K_t) and that obtained using van der Meer WTC formulae ($K_{tVDM2003}$) is calculated by the parameter ε

$$\varepsilon = \left| \frac{K_t - K_{tVDM2003}}{K_{tVDM2003}} \right| \times 100 \qquad 4.70$$

If the absolute value of relative difference between K_t and $K_{tVDM2003}$ exceeds 10%, i.e. ε > 10% (see also Fig. 4.8), then the application of S1 is required. The results of the numerical tests representing the relation between the applicability of S1 and design parameters B/L_p and R_c/H_{m0} are plotted in Fig. 4.19:

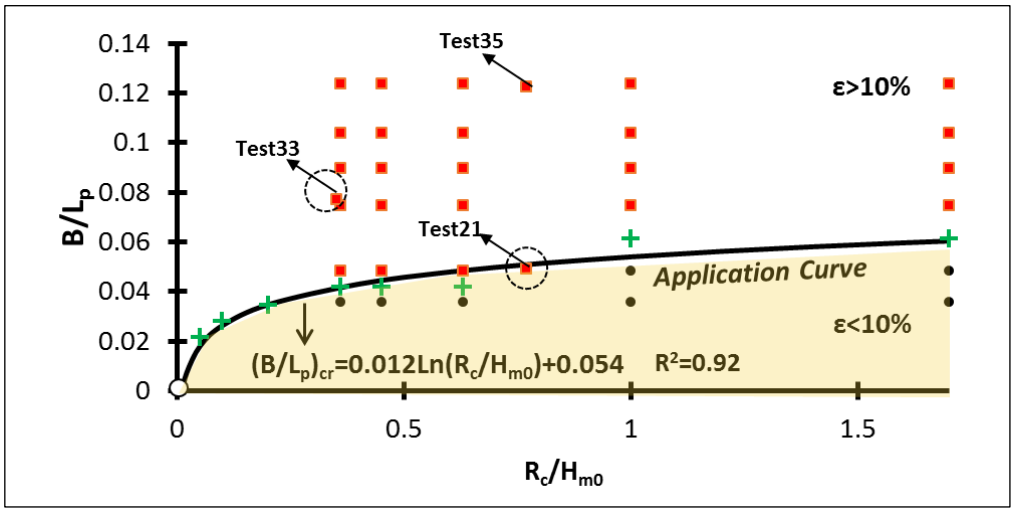

Fig 4.19: Applicability of the first step of the SPB implementation approach (S1) as a function of relative submergence R_c/H_{m0} and relative crest B/L_p. Shaded area represents the applicability condition where ε<10%

As indicated in Fig. 4.19, the black dots lie within the shaded area represent ε< 10% and the red squares represent ε > 10%. The *Threshold Curve,* which is the best fit curve to the border points denoted by green crosses in Fig. 4.19, represents a curve above which (B/L_P> $(B/L_P)_{cr}$) the proposed SPB implementation needs to be applied (i.e. ε > 10%). As shown by Fig. 4.19, for R_c/H_{m0}> 0.36 where data points exist, border points are selected in the middle of adjacent black dots and red squares with the same R_c/H_{m0}. However, for R_c/H_{m0} <0.36, where no data points exist in Fig. 4.19, the border points are arbitrarily selected so that the following physical condition is met

$$\frac{R_c}{H_{m0}} \to 0 \quad \Rightarrow \frac{B}{L_p} \to 0 \qquad 4.71$$

The physical condition expressed by Eq. 4.71 implies that when the relative submergence of the breakwater becomes very low, even for very narrow-crested breakwaters the application of the proposed submergence implementation approach becomes necessary. Based on the selected border points, the *Threshold Curve* shown in Fig. 4.19 expresses the critical crest width $(B/L_P)_{cr}$ as a function of relative submergence R_c/H_{m0}.

Fig. 4.19 shows that, in general, for a given relative submergence R_c/H_{m0}, if the relative crest width of structure B/L_P is higher than the critical relative crest width $(B/L_P)_{cr}$ calculated by the *Threshold Curve* equation (see Eq. 4.72), then ε > 10% and thus the application of S1 would be required to adequately account for the submergence effects.

As also shown in Fig. 4.19, four red square data points are located very close to the *Threshold Curve*, two of which are not above the curve. These two points mark critical points which clearly show that, if $(B/L_p)_{cr}$ is very close to B/L_p the criterion proposed to evaluate the applicability of the S1 should be used with caution. This implies that, a minimum absolute difference between $(B/L_p)_{cr}$ and B/L_p may exist for which the *Threshold Curve* can be utilized to determine the applicability of S1. For the critical points exist in the figure, it is found that $\left|\left(B/L_p\right)_{cr} - \left(B/L_p\right)\right| \leq 0.002$. This clearly suggests that, the value of 0.002 can be considered as the minimum absolute difference between $(B/L_p)_{cr}$ and B/L_p for which the *Threshold Curve* can be utilized to determine the applicability of S1. Therefore, in order to be on the safe side, in this study, the minimum absolute difference between $(B/L_p)_{cr}$ and B/L_p is suggested to be 0.005 which is almost two times larger than minimum absolute difference of 0.002 obtained from the critical points shown in Fig 4.19 Accordingly, $\left|\left(B/L_p\right)_{cr} - \left(B/L_p\right)\right| \geq 0.005$ is proposed as the validity condition for which the *Threshold Curve* can be utilized to determine applicability of S1. Based on the above discussion the applicability condition of S1 can be expressed as:

Step i of SPB implementation approach (i.e. S1) is applicable for the following relative crest width of SPB

$$\left(B/L_p\right)_{cr} < \left(B/L_p\right) \textbf{ and } \left|\left(B/L_p\right)_{cr} - \left(B/L_p\right)\right| \geq 0.005$$

With

$$\left(\frac{B}{L_p}\right)_{cr} = 0.012 Ln\left(\frac{R_c}{H_{m0}}\right) + 0.054 \qquad R^2 = 0.92 \qquad 4.72$$

Based on the above discussion, if the validity condition $\left|\left(B/L_p\right)_{cr} - \left(B/L_p\right)\right| \geq 0.005$ is not satisfied, the threshold curve expressed by Eq. 4.72 should be applied with caution and more numerical tests might be required to determine if S1 is necessary. Thus, for $\left|\left(B/L_p\right)_{cr} - \left(B/L_p\right)\right| \geq 0.005$ the applicability of step i of the SPB implementation approach (S1), which is proposed to adequately consider the effect of submergence on wave transmission, can be determined using Threshold Curve expressed by Eq 4.72. Nevertheless, Eq 4.72 has two major limitations which might be overcome by future research:

- The effect of the breakwater slope is not taken into account. This clearly implies that, for steep slope breakwater
- For $R_c/H<0.36$, the Threshold Curve is based on arbitrary points introduced to represents the physical conditions expressed by Eq 4.72

The aforementioned limitations imply that, for breakwaters with side slope steeper than 1:2 where the bed slope effect described before tends to be stronger, the threshold calculated by Eq. 4.72 might be overestimated. For breakwaters with relative submergence of $R_c/H<0.36$, the best would be to check the applicability of step I of the SPB implementation approach through a trial and error attempt.

Since the original DELFT3D model is not able to account for the dissipative effect of porosity in SPBs (see section 2.3.1), Step ii of the SPB implementation approach (Hereafter S2) needs to be always performed in DELFT3D .

4.3 Set-up, calibration and validation of the morphological model

In this section, the set-up, calibration and validation of the numerical model in DELFT3D to simulate the effect of submerged porous breakwater on costal morphology are described. The validated model will be used in chapter 5 for a systematic parameter study. The numerical model is set-up to reproduce the laboratory experiments of Claessen and Groenewoud (1995) (Hereafter CG95). A detailed description of these laboratory experiments is given in Section 4.3.1. The details of the numerical model set-up calibration and validation are described in Section 4.3.2. Finally, the results of the model calibration and validation are presented and discussed in Section 4.3.3.

4.3.1 Laboratory experiments with movable bed

The laboratory experiments of Claessen and Groenewoud (1995), Hereafter CG95,were carried out by with moveable bed leeward of the submerged brealwater in the wave flume of the Laboratory of Fluid Mechanics at Delft University of Technology. The wave flume is 32.0 m long, 0.8 m wide and 1.0 m deep. The experimental configuration was designed in a scale of 1:15 with respect to a prototype case (Fig. 4.20).

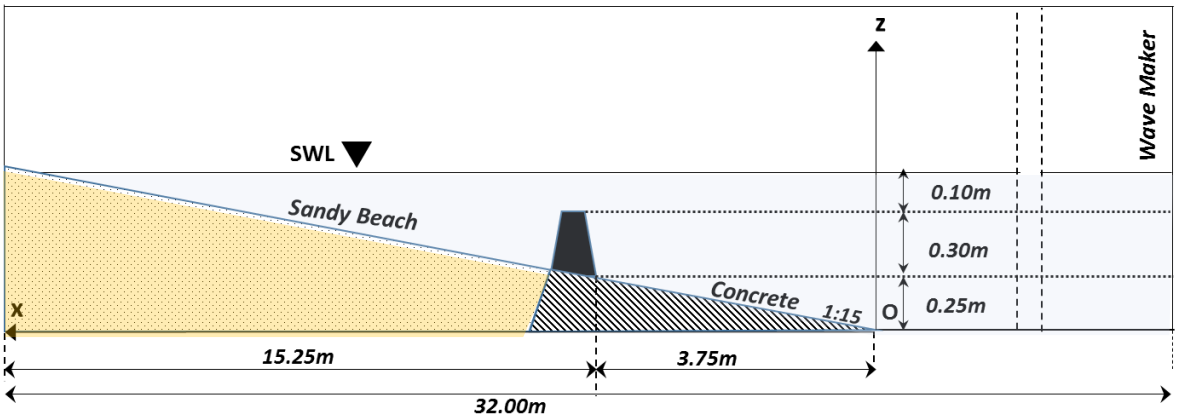

Fig 4.20: Experimental set-up of the submerged rubble mound breakwater in a wave flume by Claessen and Groenewoud (1995)

The breakwater is located on a 1:15 slope, which consists of a movable sandy beach leeward and aconcrete foreshore to avoid scour hole at the seaward toe of the breakwater. The sandy beach consists of sand with D_{50} = 95 μm. The breakwater consists of a porous armour layer that covers an impermeable core, which together make up a permeable breakwater as will be further explained in this section. The scaled model of the armour layer is made of quarry rock with D_{n50}=0.05m (Fig. 4.21).

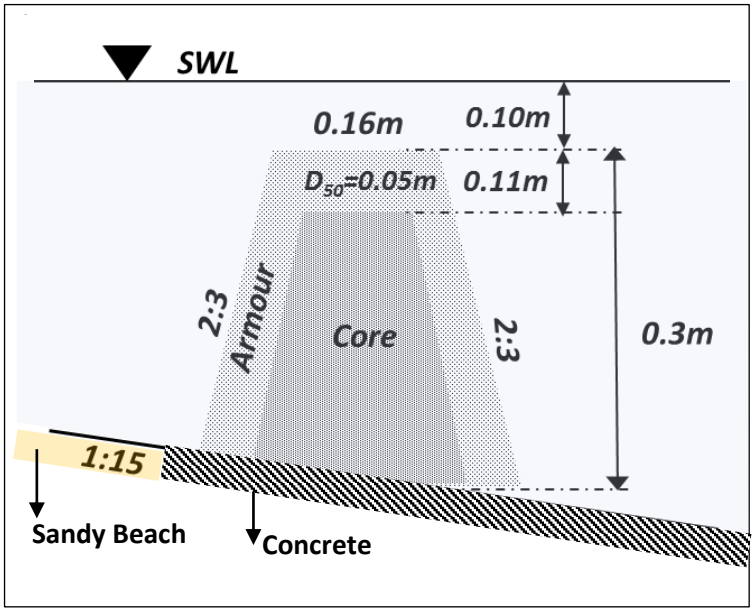

Fig 4.21: Cross-section of submerged rubble mound breakwater model with impermeable core in Fig 4.20.

Although, the core is impermeable, the flow still passes through the upper part of the permeable armour layer. Thus, the overall structure, which is made of a permeable amrour layer and an impermeable core layer, may be considered as a permeable breakwater with two layers of different porosities. As mentioned in chapter 3, in order to calculate WTC for submerged breakwaters with a core and armour layers of different porosities, the new WTC formula (see section 3.3) should be applied indirectly (see section 3.5). Accordingly, in this study, it is suggested that, for submerged breakwaters which are composed of an impermeable core and porous armour layer (see Fig 4.21), the porosity of the armour layer can be applied in the new WTC formula to estimate wave transmission coefficient.

In order to justify this approach, the effect of using an impermeable core on the wave transmission at SPBs needs to be discussed. Thus, considering the wave energy conservation concept (see Eq. 2.1), the effect of impermeable core on wave dissipation inside and the reflection from the structures is elaborated in the following paragraphs:

(i) The impermeable core is located in low parts of the water column, as compared to upper porous armour layer. Thus, the area which contains the impermeable core, involves the parts of the SPB where the magnitude of wave-induced flow is smaller than that in area that contains upper porous armour layer[roughly between 2 and 3 times lower, as shown by Lara et al., (2006)]. Thus, considering the fact that the energy dissipation inside the porous structures decreases with the decrease of the wave-induced flow velocity inside the porous medium (Solitt and Cross, 1972), the wave energy dissipation in the area that contains impermeable core is expected to be small compared to the dissipation in the area that contains upper armour porous layer. This implies that, the use of impermeable core in SPBs does not have a noticeable effect on the overall energy dissipation inside the structure, because the energy dissipation mainly occurs in the area which contains the upper armour where the wave induced flow magnitude is noticeably higher (almost 2-3 times higher).

(ii) The impermeable core layer stops the wave energy penetration through the breakwater and thus increases the overall wave reflection from the breakwater

Based on what discussed by paragraphs i and ii, considering the energy conservation concept described in section 2.2.1, due to the increase of wave reflection and a minor effect (see paragraph i) on

the overall energy dissipation inside the breakwater, the use of impermeable core in SPBs is expected to reduce the WTC. Thus, the assumption that, in SPBs with permeable armour and impermeable core, the porosity of armour layer can be used for estimating the transmission coefficient using the new WTC formula is a conservative assumption that may lead to the over estimation of WTC because the increase of the wave reflection and minor change of energy dissipation due to the presence of impermeable core are not considered. Thus, the implication of assuming a homogeneously porous breakwater, in which the porosity equals to the porosity of armour layer, is that the transmission coefficient and the associated morphological changes leeward of the breakwater might be overestimated. The amount of this overestimation may depend on various parameters such as wave conditions, porosity of the breakwater and geometry of the impermeable core layer

Moreover, since the wave-induced flow velocity is generally higher in the upper parts of the water column, upper porous armour layer is subjected to higher wave energies (roughly between 4 times to 9 times higher). Therefore, it is reasonable to assume that, as well as wave dissipation inside the breakwater, the wave transmission through the structure mainly occurs in the area which involves upper armour layers. Therefore, the porosity of the armour layer (as compared to the core porosity) will dominate the effect on the wave transmission. Thus, it is also physically meaningful to use the porosity of armour layer in the new WTC formula to estimate wave transmission in SPBs with impermeable core and porous armour layer

Based on the above discussion, the assumption that, in SPBs with impermeable core and porous armour layer, the porosity of armour layer can be used for estimating the transmission coefficient using the new WTC formula is a physically meaningful and conservative assumption. Therefore, the porosity of the armour layer is considered in the new WTC formulae (see Fig. 4.10) to calculate wave transmission leeward of the submerged breakwater. However, no measured porosity is reported for the armour layer in the scale model of the submerged breakwater. Based on the Table 4.4, which summarizes the porosities of different materials tested by Van Gent (1995), the porosity of the armour layer made of quarry rock with D_{n50}=0.05m is set to n=0.45.

Table 4.4: Porosities of materials tested by Van Gent (1995)

Materials	D_{n50} (m)	N
Irregular Rock	0.0610	0.442
Semi Round Rock	0.0487	0.454
Round Rock	0.0488	0.393
Irregular Rock	0.0202	0.449
Irregular Rock	0.0310	0.388
Spheres	0.0460	0.476

Five laboratory tests A-E with different wave conditions were carried out by Claessen and Groenewoud (1995), as summarized in Table 4.5 where H_s and H_{si} respectively stands for significant wave height at offshore and just in front of the breakwater, T_p for the peak period, k_p for the wave number related to the peak period, h for the water depth at the wave maker and R_c for the breakwater submergence:

Table 4.5: Measured wave conditions in the laboratory by Claessen and Groenewoud (1995)

Test	H_s (m)	T_p (s)	H_{si}/L_p (%)	R_c/H_{si}	k_ph
A	0.1	2.07	2.90	0.93	0.93
B	0.1	1.55	4.2	0.85	0.66
C	0.1	1.29	4.9	0.95	1.17
D	0.133	1.81	4.3	0.71	0.77
E	0.067	1.29	3.56	1.44	1.17

In each laboratory test, which lasted 7.5 hours, the wave height, flow velocity, suspended sediment concentration and bed profile were measured. The wave height, flow velocity and sediment concentration were measured at specific locations as shown in Fig. 4.22, where WG and V respectively represent the wave gauge location and the vertical lines along which flow velocity and sediment concentration were measured.

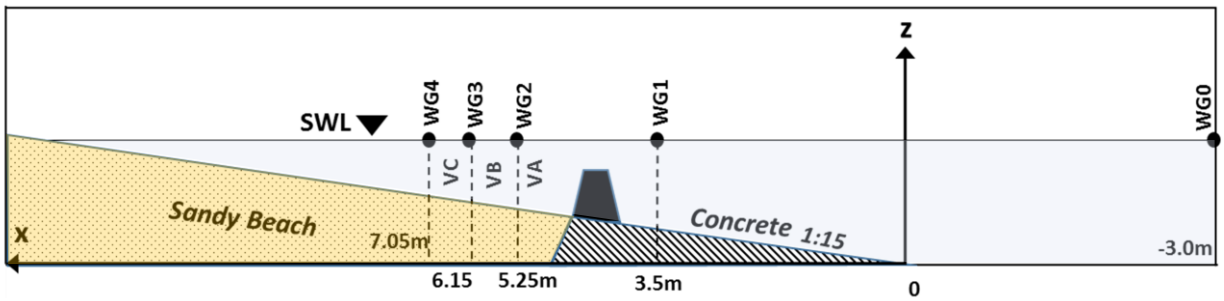

Fig 4.22: Cross-section of the wave flume with the model set-up and locations for the measurement of the wave height (WG0-WG4), flow velocity and sediment concentration (VA, VB & VC)

4.3.2 Numerical model set-up, calibration and validation

The numerical model is set-up in DELFT3D Version 6.00.01.5583. The enhancement of the wave-induced bed shear-stress is taken into account using the Fredsøe formulation (1984). The k-ε turbulence closure in DELFT3D-FLOW (see section 4.1.2, paragraph c) is applied for turbulence modelling. The Bijker (1971) formula (see Eqs 4.43 and 4.44.) is used to calculate the bed-load and suspended load sediment transport. The sandy beach in the experiment is represented by non-cohesive sediments with D_{50}=95μm and density equal to 2650 kg/m^3. The dry bulk density of the sand bed is set equal to 1600 kg/m^3.

In this study, the modules DELFT3D-WAVE and DELFT3D-FLOW are applied with online-coupling (two-way coupling) which is available for the DELFT3D model system. The reliability of the numerical model predictions largely depends on the input free parameters, which are simplified representations of real processes. If the free parameters do not represent physical attributes which are directly measureable, their appropriate values need to be determined through model calibration. The free parameters of the model and the calibration procedure applied in this study are discussed in Section 4.3.2.b. The model calibration performed in this study represents a systematic selection of free parameters to achieve the best possible agreement between numerical results and measurements. In this study, the model calibration is performed so that the numerical model yields the best possible agreement with measured wave heights, flow velocities and bed level changes. The measured suspended sediment concentration reported by Claessen and Groenewoud (1995) is possibly not reliable enough for model calibration, because, as also reported by Claessen and Groenewoud (1995), the suspended sediment transport rate obtained from direct measurements of sediment concentration was noticeably larger than the total sediment transport calculated from measured bed level changes using sediment continuity equation. This large deviation cannot be physically explained, implying that the measured sediment concertation might not be suitable for model calibration/validation.

The agreement between calculated flow velocities and wave heights with measurements is quantified using Willmot index **W** and Root Mean Square Error **RMSE**. Besides, for evaluating the bed level change calculations, the Root Mean Square Error **RMSE** and Brier Skill Score (**BSS**) are applied to quantify the agreement between the numerical simulation results and measurements:

$$BSS = 1 - \frac{\sum\left[\left|z_{bc-} z_{bm}\right| - \Delta z_{bm}\right]^2}{\sum\left[z_{b0-} z_{bm}\right]^2} \qquad 4.73$$

Where, z_{bc} is the calculated bed level, z_{bm} the measured bed level, Δz_{bm} =0.02m bed level measurement error under laboratory conditions (Van Rijn et al., 2002), and z_{bo} is the baseline (initial bed level). Brier Skill Score (BSS) is very suitable for the evaluation of bed level changes calculations (Van Rijn et al., 2002); it compares the mean square difference between the prediction and measurements with the mean square difference between the initial bathymetry and observation. Based on Van Rijn et al. (2002), the interpretation of the BSS index values is depicted in Fig 4.23:

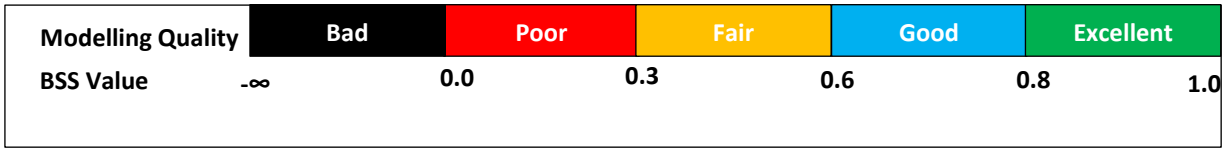

Fig 4.23: Model performance evaluation based on BSS values

In the following sections, the numerical model calibration against measurements carried out in Test B (see Table 4.5) is first described. Then, the applicability of the calibrated model to various wave conditions is assessed by applying the model to Tests A, C and D described in Table. 4.5. It should be noted that, Test E with R_c/H_{si} =1.44 is fully outside the applicability range ($0<R_c/H_i<1.1$) of the new WTC formulae (Eq 3.28) and is thus not considered for model validation.

(a) Numerical Model Set-up

As illustrated in Fig, 4.24, the numerical model set-up represents a cross-shore profile model of 14 meters extending from the elevation of -0.65m to +0.10m with respect to still water level (SWL). The initial bathymetry in the model set-up, which represents the bed profile described in section 4.3.1 (see Figs. 4.20 and 4.22), is shown in Fig. 4.24, where **WG** represents wave gauge location, and **VA-VC** the vertical lines along which flow velocities are measured.

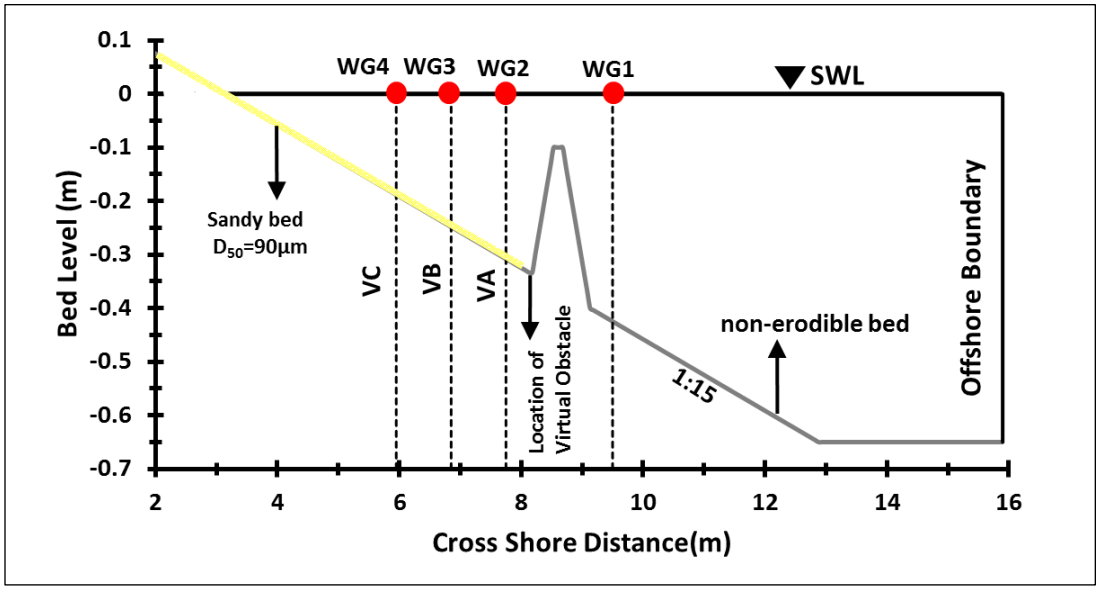

Fig 4.24: Initial bathymetry in the numerical model set-up

Applying the *Threshold Curve* equation expressed by Eq. 4.72 would result in $\left|(B/L_p)_{cr} - (B/L_p)\right| < 0.005$. Thus additional numerical tests need to be performed to decide whether DELFT3D-WAVE is able to adequately account for the effect submergence without applying Step i of the SPB implementation approach described in Section 4.2.1. In this case, the results showed that this is not necessary.

Accordingly, only Step ii of the SPB implementation approach is applied. For this purpose, a rectangular uniform mesh with 4 cells in longshore direction and 175 cells in cross-shore direction is used for both wave simulations (DELFT3D-WAVE) and flow simulations (DELFT3D-FLOW). Further

mesh refinement did not noticeably improve the numerical results. A plan view of the computational grid is shown in Fig.4.25, where M is the number of computational cells in cross-shore direction, N is the number of computational cell in long-shore direction, Δx grid size in cross-shore direction and Δy grid size in long-shore direction.

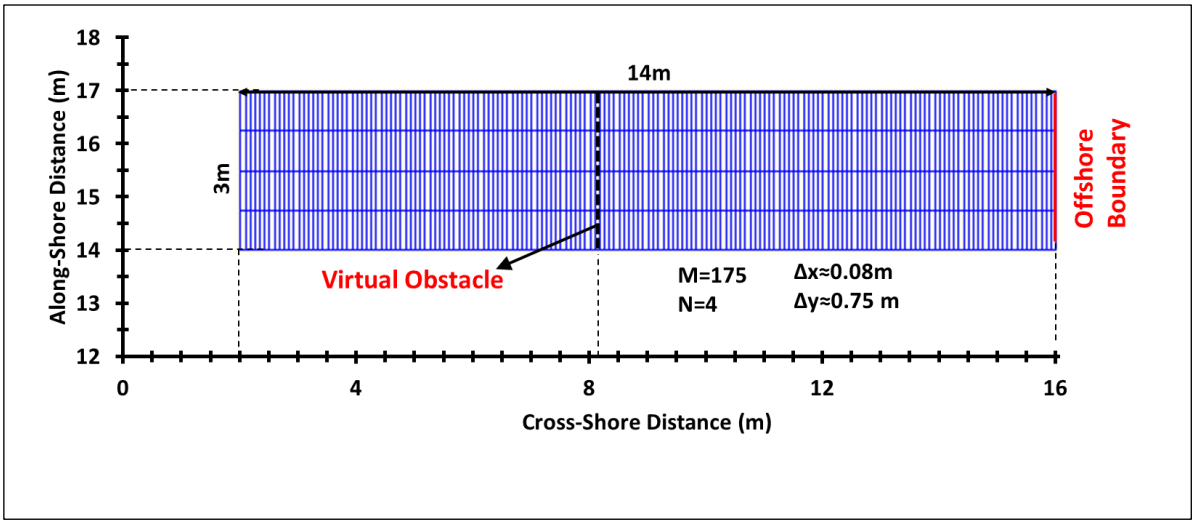

Fig 4.25: Plan View of the *Computational Grid* (M = number of computational cells in cross-shore direction, N = number of computational cell in long-shore direction, Δx =grid size in cross-shore direction and Δy =grid size in long-shore direction).

As indicated in Fig. 4.26, the water column in the numerical model set-up is divided in 15 layers over the entire water depth. Further mesh refinement in vertical direction did not induce any noticeable change in the results.

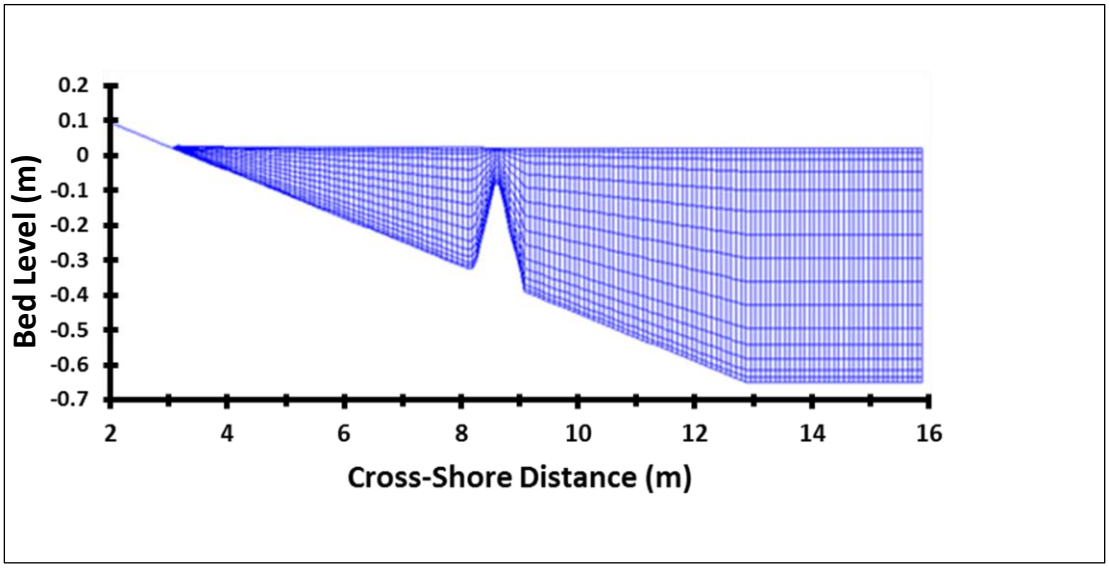

Fig 4.26: Cross-section of the computation grid

Based on the suggestions in the DELFT3D-FLOW manual (Deltares, 2014b), the following criteria are met to select the relative thickness of the layers over the entire water depth (The relative thickness of each layer is defined as the ratio of layer thickness to total water depth):

I. The bed layer thickness should be set about 2 % of the water depth.
II. The thickness of the vertical layers should vary smoothly over the water depth.
III. The layer thickness near the surface should not exceed 2 % of the water depth.

Based on the aforementioned criteria, the relative thickness of each layer over the entire water depth is selected as given by Table 4.6

Table 4.6: Relative thickness of layers over entire water depth (% of water depth)

Layer	***1***	***2***	***3***	***4***	***5***	***6***	***7***	***8***	***9***	***10***	***11***	***12***	***13***	***14***	***15***
Relative Thickness (% of Water Depth)	2	3	5	8	9	10	10	10	10	10	7	6	5	3	2

(b) Numerical Model Calibration and Validation

The model calibration is performed to determine the unknown free parameters, so that the calibrated model yields the best possible estimation of the reality. This section summarizes the selection of the appropriate values for the free model parameters in DELFT3D-FLOW, which are considered as the most important and relevant to this study. Test B (see Table 4.5) is used for model calibration because the measured relative submergence R_c/H_{si} and the incident wave steepness H_{si}/L_p in Test B represent the average of all tests (i.e. Tests A, B, C and D in Table 4.5) considered for model calibration and validation.

DELFT3D-FLOW can simulate the flow, sediment transport and subsequent morphological changes. The main free parameters which represent simplifications of real hydrodynamic and sediment transport/morphology processes in DELFT3D-FLOW are given in Table 4.7, where free parameters are categorized in hydrodynamic and sediment transport/morphology parameters, which are involved respectively in flow and sediment transport/morphology calculations.

Table 4.7: Free parameters in DELFT3D-FLOW

Free Parameter	Symbol	Unit	Description
Hydrodynamics	z_0	M	Roughness Length
	V_h	m^2/s	Background Horizontal Eddy Viscosity
	V_v	m^2/s	Background Vertical Eddy Viscosity
Sediment Transport / Morphology	f_{sus}	-	Suspended Sediment Transport Scaling Factor
	f_{bed}	-	Bed Load transport Scaling Factor
	α_{bs}	-	Stream-wise Bed Slope Effect Factor
	α_{bn}	-	Transverse Bed Slope Effect Factor
	f_{morfac}	-	Morphological Acceleration Factor
	D_v	m^2/s	Background Vertical Eddy Diffusivity
	D_h	m^2/s	Background Horizontal Eddy Diffusivity

The description of the free parameters in Table 4.7 and the selection of their appropriate values are provided below.

Roughness Parameter z_0

The roughness length z_0 directly affects the bottom friction values in the momentum equation solved by DELFT3D-FLOW (see Eqs 4.28 and 4.29). The parameter z_0 is directly related to the geometrical roughness of the bed, k_s which is represented by the RMS value of the sub-grid bottom fluctuations:

$$z_0 = \frac{k_s}{30} \qquad 4.74$$

The bottom roughness k_s used to determine z_0 typically ranges from 0.15 m for very rough riverbeds down to 0.01 m for very smooth beds (Deltares, 2014b). In this study, the bottom roughness k_s is set to the value of 0.02m as measured in the laboratory experiments.

Background Horizontal Eddy Viscosity V_h and Diffusivity D_h

According to the DELFT3D-FLOW manual (Deltares, 2014b), the values of the horizontal Eddy viscosity and diffusivity, which are respectively represented by V_h and D_h, depend on the hydrodynamics and the grid size used in the computational domain. For relatively detailed models with grid sizes in the order of tens of meters, typical values are in the range of 1 – 10m²/s whereas for larger grids of hundred meters or more, the values ranges between 10 – 100 m²/s (Deltares, 2014b). Default settings for V_h and D_h are respectively 1 and 10 m²/s in the model. On the basis of the experience and a sensitivity analysis, Throuw et al. (2012) suggested that these default values are too high and V_h and D_h should be reduced respectively from 1 and 10 m²/s to 0.1 and 0.1 m²/s.The small grid size used in this study ($\Delta x \approx 0.08$m) also suggests that default values of V_h and D_h must be reduced. However, there is still no agreement on the appropriate values for V_h and D_h, so that the value of these free parameters should be obtained through the model calibration. Accordingly, horizontal background viscosity V_h and diffusivity D_h are varied between 0.1 and 0.01 in numerical simulations performed for model calibration purposes.

Streamwise (α_{bs}) and Transverse Bed Slope Effect Factor (α_{bn})

Bed load is influenced by longitudinal (stream-wise) and transverse bed slope (see section 4.1.2.b). Walstra et al (2004) showed that the longitudinal bed slope effect factor α_{bs} has a very limited effect when applied within a realistic range (0 to 5). Initial numerical tests performed in this study also confirm that α_{bs} has a negligible effect on the calculated morphological changes. Thus, in this study the default value of 1.0 for α_{bs} is kept unchanged. Since no bed level gradient perpendicular to the flow direction exists, the transverse bed slope contribution to sediment transport becomes zero and does not affect the numerical simulation results (see Eqs 4.36 and 4.37). Thus, the transverse bed slope effect factor α_{bn} is also set equal to the default value α_{bn} =1

Background Vertical Eddy Viscosity (V_v) and Diffusivity (D_v)

In this study, k-ε turbulence model (see section 4.1.2.c) is applied to calculate the vertical eddy viscosity and diffusivity. Background vertical eddy viscosity, which is added to vertical eddy viscosity, might be necessary in special cases such as strongly stratified flow (for more details see Deltares, 2014b). The background eddy diffusivity is also normally not necessary. However, for compatibility with the horizontal eddy viscosity V_h and further specific purposes, the access to this parameter has been made available in the DELFT3D (Deltares, 2014b). Based on the above discussion, the vertical background eddy viscosity V_v and diffusivity D_v, are set to zero.

Suspended and Bed Load Transport Contribution (f_{sus} and f_{bed})

The sediment transport calculation in DELFT3D contains two contributions: Bed Load Transport and Suspended Load Transport. DELFT3D can be tuned through scaling the suspended load and bed load contributions. For this purpose, the source term in the advection-diffusion equation (see Eq. 4.31) is multiplied by f_{sus} and the bed load transport is directly multiplied with f_{bed} (see Eq. 4.39). Still, there is no general agreement on the proper values for the suspended load and bed load scaling factors f_{sus} and f_{bed}. Thus, both f_{sus} and f_{bed} should be determined by model calibration.

Morphological Acceleration Factor f_{MORFAC}

Morphological Acceleration Factor (f_{MORFAC}) is introduced in DELFT3D to make morphological calculations faster. At one simulation time step Δt, waves, currents, sediment transport rates and bed level changes are calculated in the model. Afterwards, the bed level changes are multiplied with f_{MORFAC}. This way, after one time step Δt, the morphological changes are actually computed over a period equal to f_{MORFAC} x Δt. The fundamental assumption of this approach is that, changes in morphology will occur over a much longer time scale than changes in hydrodynamics (Roelvink, 2006). In order to avoid further complication in model calibration, at the expense of longer computational time, the morphological acceleration factor is not applied in this study (i.e. $f_{MORFAC} = 1$); and thus waves, currents, sediment transport rates and bed level changes are calculated at each simulation time step Δt.

Implications and Stepwise Procedure for Model Calibration

Based on the discussions on the input parameters presented above, only the free parameters f_{bed}, f_{sus}, V_h and D_h. need to be obtained through model calibration. In the experimental study described in Section 4.3.1, the flow measurements are carried out on a movable bed, implying the interdependency between the measured flow and morphological changes. Because of this interdependency, it is not possible to separately evaluate the predicted flow and morphological changes. Therefore, in order to calibrate the model, the free parameters associated with Hydrodynamics and Sediment Transport (see Table 4.7) need to be examined together. Therefore, a relatively large number of simulations would be needed to calibrate the model in the parameter space. In order to reduce the number of simulations required for model calibration, a step-wise calibration approach is proposed and adopted in this study. The underlying idea of the step-wise calibration approach is to obtain appropriate values of calibration parameters on a step-by-step basis, instead of examining all parameters together. Therefore, the step-wise calibration approach may substantially reduce the number of unnecessary simulations by eliminating inappropriate parameter values at each calibration step.

In this study, a three-step calibration approach is adopted, in which Brier Skill Score **BSS** and Willmot index **W** are respectively used to evaluate the calculated bed level changes and flow velocity (Fig. 4.27):

- ***Step 1: Suspended and bed load transport contribution factors f_{bed} and f_{sus}***. The initial value of V_h and D_h is set equal to 0.1 as proposed by Throuw et al (2012). Then the suspended and bed load transport contribution factors are continuously adjusted to find $(f_{bed}, f_{sus})_{best}$, which yields a *Good* or *Excellent* agreement between the measured and calculated bed profile (i.e. BSS>0.6).

- ***Step 2: Horizontal Eddy Viscosity V_h***. The set of free parameters obtained in Step 1 $(f_{bed}, f_{sus})_{best}$ is kept constant, while the horizontal eddy viscosity V_h is varied to find the $(V_h)_{best}$, which yields a good agreement between calculated and measured flow velocities (i.e. W>0.8).

- ***Step 3: Horizontal Diffusivity D_h.*** The set of parameters $(f_{bed}, f_{sus})_{best}$ and $(V_h)_{best}$, which are obtained in Step 1 and Step 2, are kept constant. Then, the initial value of D_h= 0.1 m²/s is varied to find $(D_h)_{best}$, which yields a *Good* or *Excellent* agreement between the measured and calculated bed profile (i.e. BSS>0.6). At this point, the model calibration is completed.

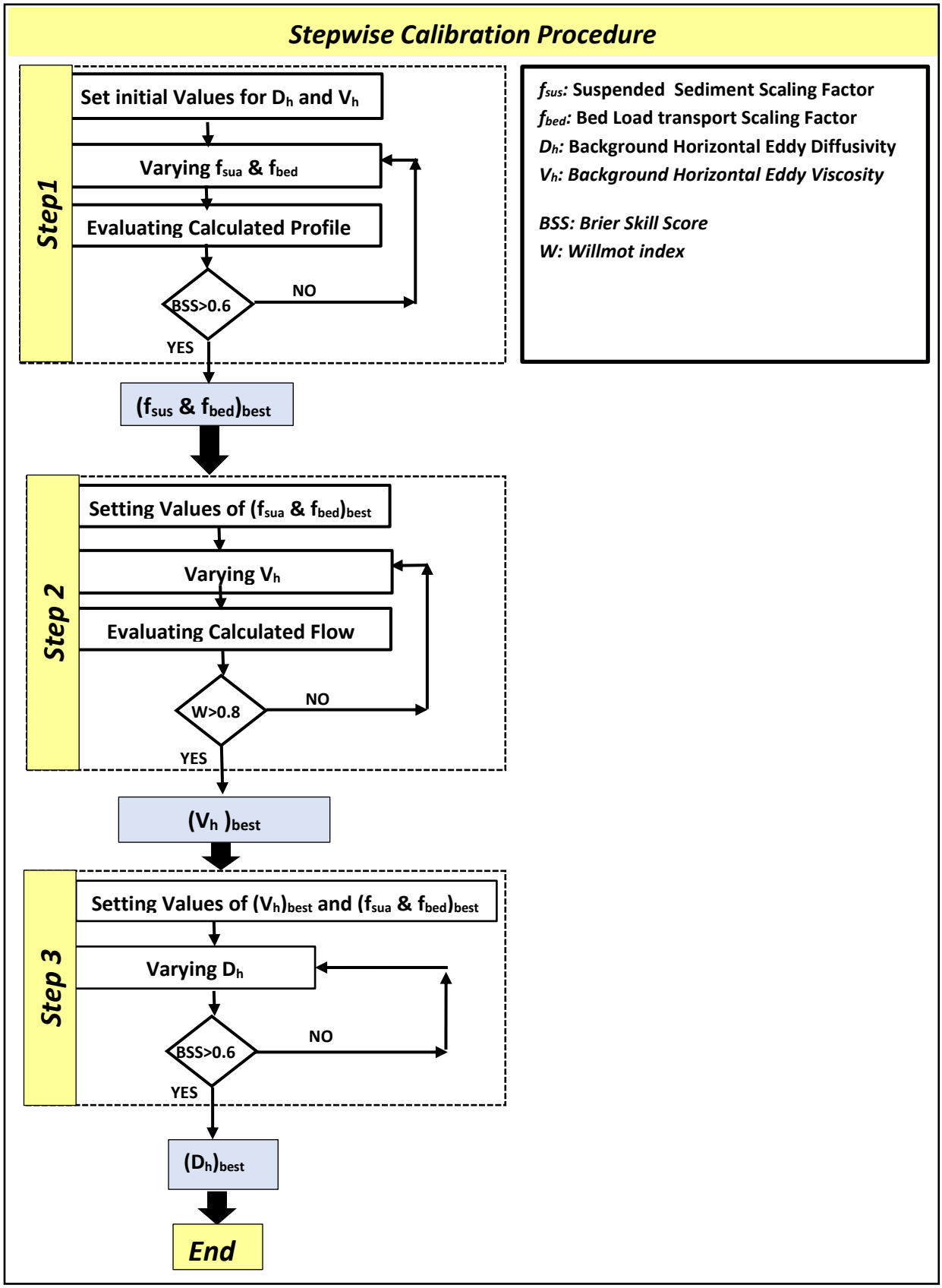

Fig 4.27: Stepwise model calibration procedure

(c) Results of Model Calibration and Validation

In the numerical simulations, the JONSWAP wave spectrum with peak enhancement factor γ=3.3 and no directional spreading is used to generate the irregular waves with H_s=0.120 m, T_p=1.55, as measured in Test B (see Table 4.5) at WG0 located far in front of the structure (see Fig. 4.22), along the offshore boundary (see Fig. 4.25). Since the numerical simulations reproduce the two-dimensional flume experiments, the wave refraction is deactivated. Besides, due to the two-dimensional (2D) nature of tests in the wave flume, the wave diffraction is also deactivated. The porosity of breakwater is set to n=0.45, as discussed in section 4.3.1. The other parameter settings in DELFT3D-WAVE (e.g. whitecapping and bed friction) are the same as those described in Table 4.2 (see Section 4.2.3.b). Claessen and Groenewoud (1995) performed a similar numerical modelling using UNIBEST-TC (Walstra, 2000) and observed that, the wave height leeward of the breakwater is overestimated by about 6%. Fig. 4.28 shows the comparison between the root mean square wave height H_{rms} calculated using the improved DELFT3D-WAVE with porosity effects, DELFT3D-WAVE without porosity effects, UNIBEST-TC and measurements 30 min after the beginning of the tests. In order to quantify the accuracy of the modelled wave height, the Wilmott index **W** and the Root Mean Square Error **RMSE** are utilized.

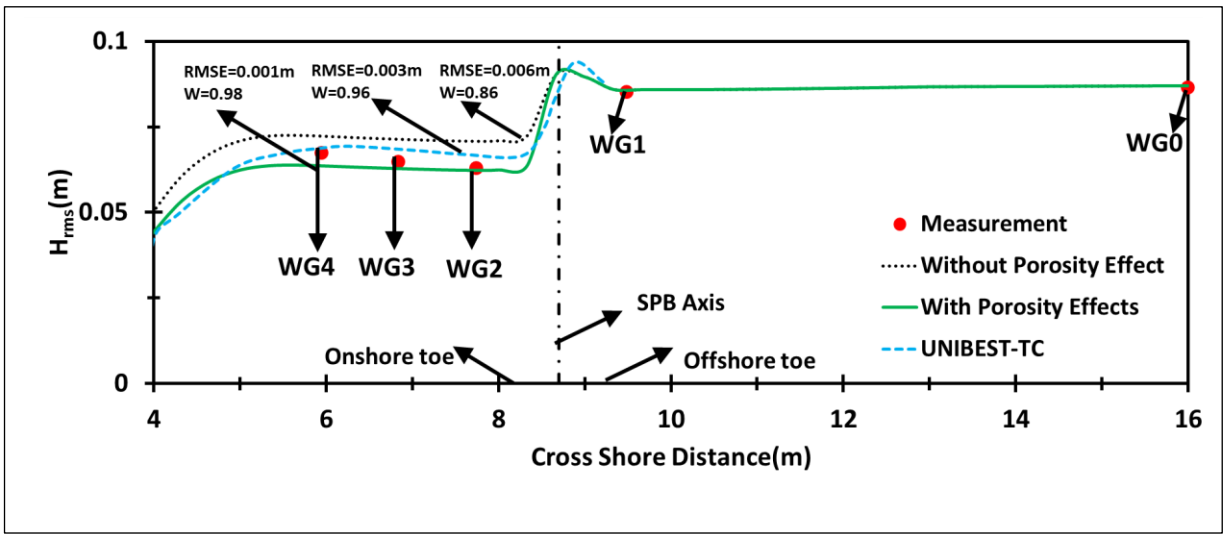

Fig 4.28: Measured (red dots) and calculated wave height H_{rms} with and without consideration of the porosity effect, 30 min after the beginning of the tests

In order to evaluate the effect of breakwater porosity on wave transmission, the results of DELFT3D-WAVE with and without porosity effects are shown and compared to other results presented in Fig. 4.28. As shown in the figure, without including the porosity effect, like UNIBEST-TC, the DELFT3D model overestimates the wave height transmitted leeward of the breakwater. This overestimation might be attributed to the missing dissipative effect of the porosity (see Chapter 2, section 2.2.1) in both models UNIBEST-TC and original (i.e. without porosity effect) DELFT3D-WAVE. Fig. 4.28shows that, the maximum overestimation (ca. 10%) pertains to DELFT3D simulation results without porosity effects. However, including the porosity effects in DELFT3D-WAVE noticeably enhances the numerical simulation results. The calculated Willmot **W** and root mean square **RMSE** index shown in Fig. 4.28 also confirms that including the porosity effect significantly enhances the overall agreement between predicted and measured wave height transmitted leeward of the breakwater.

After evaluating the performance of the model in terms of wave transmission, the performance in terms morphological changes is also evaluated through the proposed stepwise calibration procedure in Fig. 4.27.

Model Calibration, Step1 (Bed Load and* Suspended Sediment Scaling Factors f_{bed} *and* f_{sus}*)

For sediment transport calculations in DELFT3D, a minimum water depth h_{min} needs to be predefined, below which the water becomes so shallow that the applied formulations in the numerical model are not applicable anymore. Claessen and Groenewoud (1995) suggested that the minimum water depth h_{min} can be calculated as follows:

$$h_{\min} = g.\left[\frac{T_p}{21}\right]^2 \qquad 4.75$$

Where T_p is the peak wave period and g is gravity acceleration. Based on Eq 4.75, the minimum depth for sediment transport calculations in this study is set to h_{min}=0.05m. Fig. 4.29 represents the comparison between measured and calculated bed level obtained for defaults values of f_{sus}=1.0 and f_{bed}=1.0 (see Table 4.6) and for the initial value of $\mathbf{D_h}$=$\mathbf{V_h}$=0.1 m²/s (as proposed by Throuw et al., 2012).

In this study, the point of the bed profile where the water depth becomes equal to h_{min}=0.05m is called "*sediment transport calculation limit*" and is located at X=3.8m (Fig. 4.29). In order to get a realistic evaluation of the numerical results on the basis of the model limitations and capabilities, morphological calculations should be considered up to the sediment transport calculation limit, above which sediment transport calculations become unreliable. Thus, the part of the bed profile which falls beyond the sediment transport calculation limit (X<3.8m) is excluded from the evaluation of the performance of the numerical model

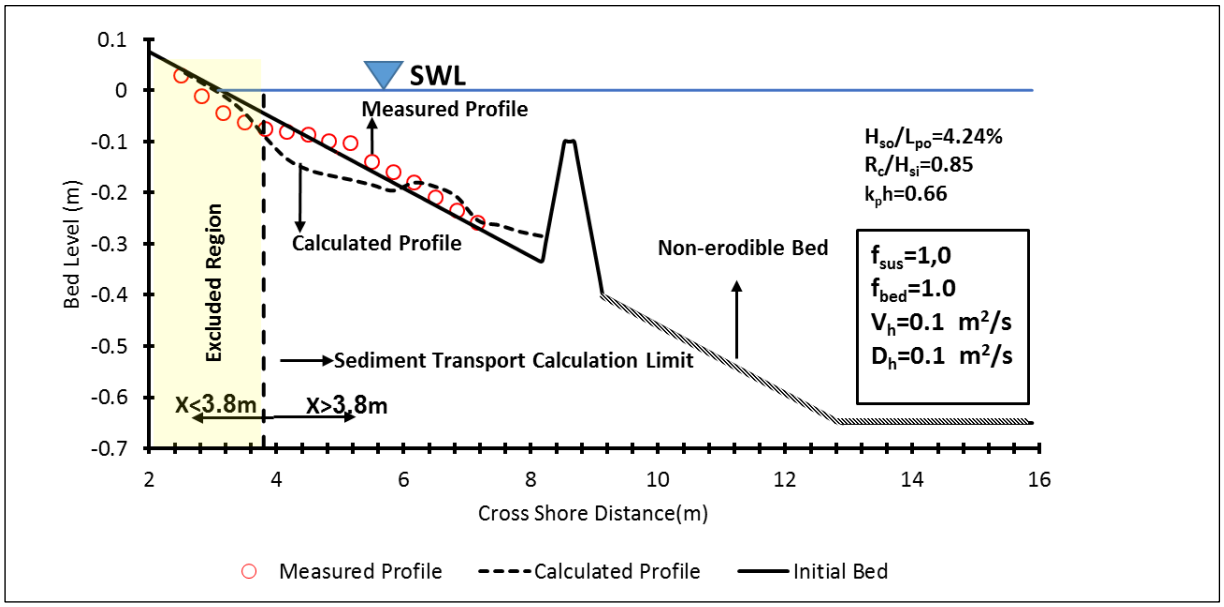

Fig 4.29: Preliminary numerical results with sediment transport calculation limit (h_{min}=0.05m) at X=3.8m for f_{sus}=f_{bed}=1.0 and D_h=V_h= 0.1m²/s. The shaded area represents the region excluded for sediment transport calculations in DELFT3D (X<3.8m)

As shown in Fig.4.29, in the region X>3.8m, where calculations of sediment transport using DELFT3D make sense, the comparison between calculated and measured bed profile is shown for f_{sus}=f_{bed}=**1.0** and $\mathbf{D_h}$=$\mathbf{V_h}$=**0.1m²/s.** This comparison results in a Brier Skill Score **BSS=-0.16,** suggesting a ***"Bad"*** model performance according to Fig. 4.23.

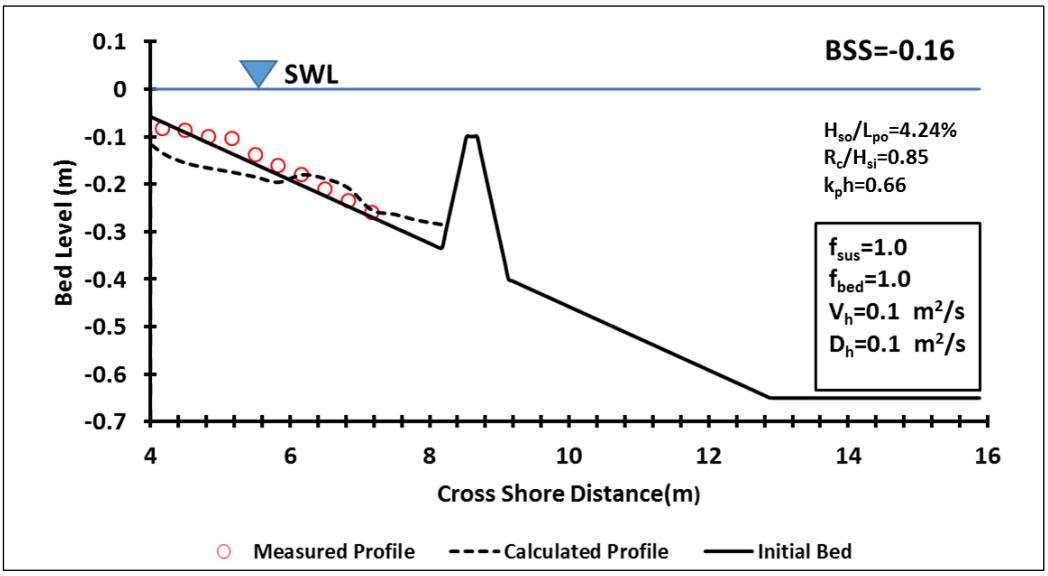

Fig 4.30: Comparison between measured and computed bed profile changes in the morphological calculation region X>3.8m for f_{sus}=f_{bed}=1.0 and D_h=V_h= 0.1m²/s.

As mentioned in Step 1 of Fig. 4.27, instead of the default settings of f_{sus}=1.0 and f_{bed}=1.0, f_{sus} and f_{bed} need to be adjusted in order to achieve BSS values larger than 0.6, implying a ***Good*** to ***Excellent*** morphological modelling accuracy according to Fig. 4.23. Thus, it is important to examine how f_{sus} and f_{bed} should be adjusted. Fig. 430 clearly shows that the erosion in the upper part of the bed profile is largely overestimated by the numerical model. This overestimation might be due to both suspended and bed load transport contributions.

In a first model calibration trial, the contribution of suspended sediment transport (f_{sus}) is reduced. Although reducing f_{sus} improves the calculated erosion close to the water line, it is found that reducing this parameter unrealistically vanishes sediment deposition in the lower parts of the bed profile, close to the shoreward toe of the breakwater. Therefore, after some iterations, the optimum value of f_{sus}, is determined to f_{sus}=0.4.

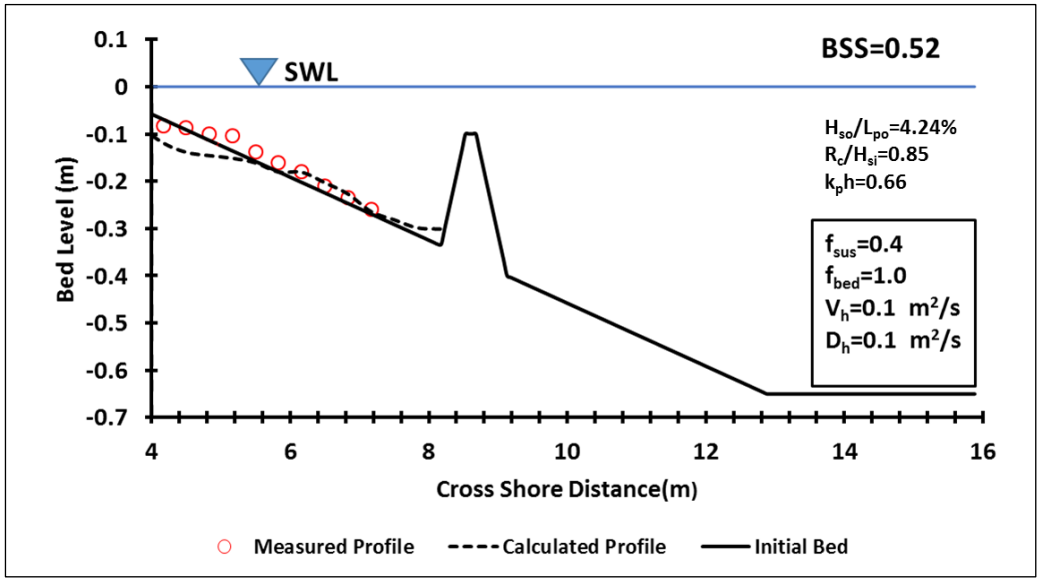

Fig 4.31: Comparison between measured and computed bed profile changes for f_{sus}=0.4 and f_{bed}=1.0, and D_h=V_h=0.1m²/s.

Fig.4.31 shows the comparison between the measurements and numerical model results for f_{sus}=0.4 and f_{bed}=1.0. The calculated BSS shows a significant improvement compared to the results in Fig. 4.30 for the default settings of f_{sus}=1.0 and f_{bed}=1.0, but the model performance is still not good enough (BSS>0.6), so that a further model calibration *trial* is required for the bed load.

In a second model calibration trial, f_{sus}= 0.4 is kept constant for the suspended load and bed load contribution factor f_{bed} is lowered. Similar to the suspended sediment contribution factor, f_{sus}, the reduction of f_{bed} can further improve the overall predicted erosion in the upper part of the bed profile. However, an excessive reduction of f_{bed} reduces the extent of the eroded region so that the calculated profile does not show the acceptable agreement with the measured profile. Therefore, after some iterative variations, the optimum f_{bed} value that results in the best fit with the measured bed profile and satisfies the condition BSS>0.6 is determined as f_{bed}= 0.5. As shown in Fig. 4.32, the overall agreement between calculated numerical results and measurements is significantly improved with **BSS=0.8**, which represents the upper limit of the ***Good*** performance and the lower limit of the ***Excellent*** performance (Fig. 4.23). Therefore, the calculated BSS satisfies the condition BSS>0.6 required to complete Step 1 of the calibration procedure in Fig. 4.27.

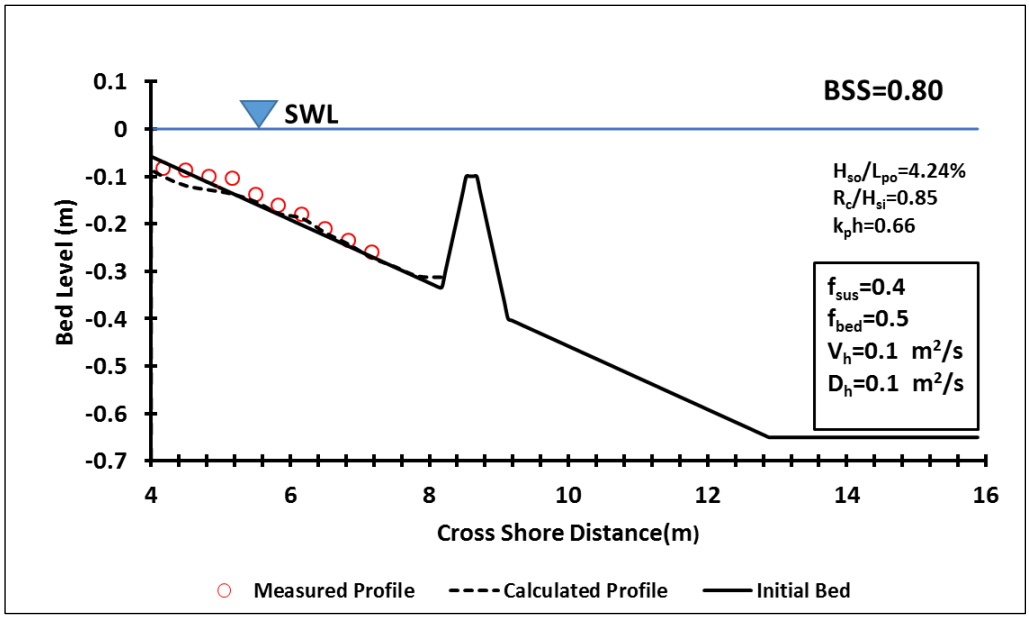

Fig 4.32: Comparison between measured and computed bed profile changes for f_{sus}=0.4 and $f_{bed.}$= 0.5, and D_h=V_h= 0.1m²/s.

Model Calibration, Step2 (Background Horizontal Eddy Viscosity V_h)

In Step 2, the values f_{sus}=0.4 and f_{bed}=0.5 obtained from Step 1 are kept unchanged, and the horizontal eddy viscosity value V_h, which satisfies the condition ***Willmott index*** W > 0.8, is determined, according to Fig. 4.27. Before examining different V_h values, the vertical distributions of calculated and measured flow velocity, averaged over the time interval between t=3.5 and t=7.5 hours after the start of the tests, are compared for V_h =0.1m²/s (Fig. 4.33).

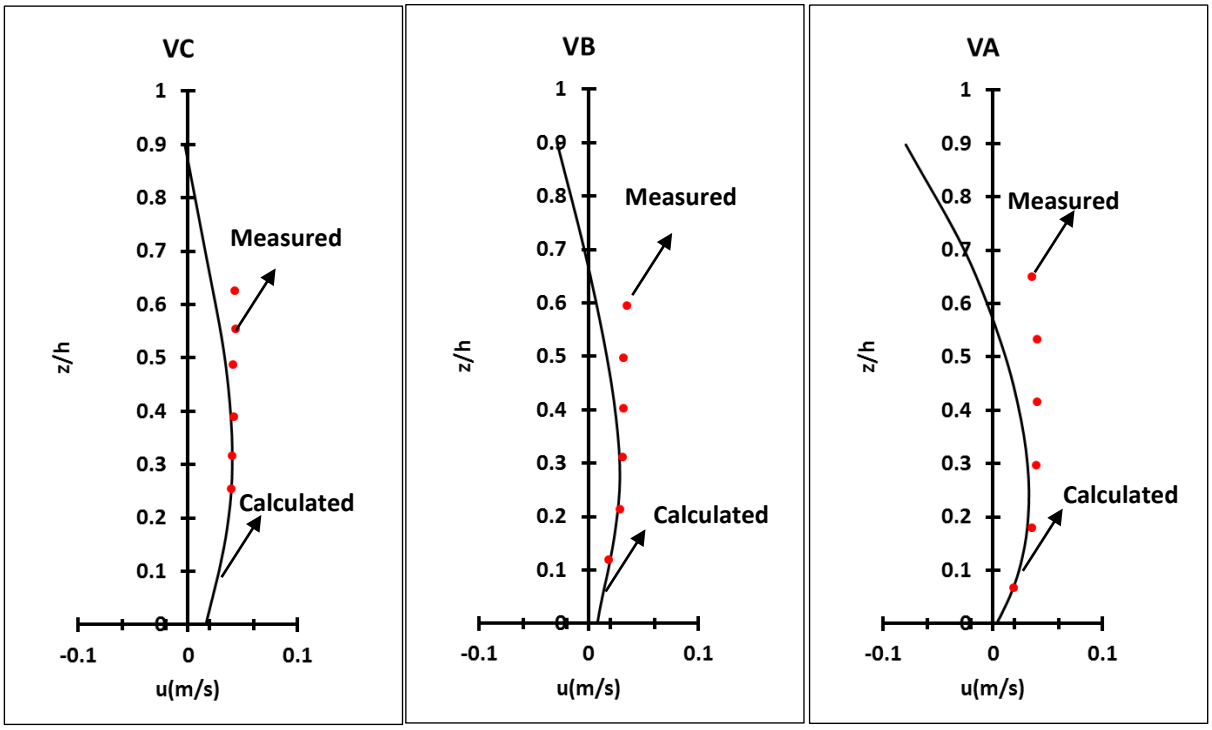

Fig 4.33: Measured and calculated vertical distributions of horizontal flow velocity u over entire water depth h at locations VA, VB and VC (as indicated in Fig 4.22) for horizontal eddy viscosity V_h =0.1m²/s.

As can be seen in Fig. 4.33, there is apparently a good agreement between numerical results and measurement at the lower part of the water column (0 <z/h <0.4), but significant differences are observed in the upper part (0.4 <z/h <1.0). The measured flow velocity profile shows a more uniform distribution than the calculated profile, in the upper part of the water column. This shows that the momentum transfer through the upper region of the water column is not adequately reproduced by the numerical model, implying that the calculated eddy viscosity by DELFT3D-FLOW is underestimated in this upper region. The locations VA, VB and VC are in the close proximity of shoreward toe of the breakwater, where the breaking waves generate a highly turbulent complex flow field. Thus, it is expected that the velocity profile in VA, VB and VC is affected by this wave-induced highly turbulent flow. Based on the discussion above, the observed differences between the vertical distributions of calculated and measured flow velocities might be attributed to the inadequate representation of wave action effects on the vertical eddy viscosity, which is calculated by means of the k-ε turbulence closure model in DELFT3D-FLOW. Improving this limitation in DELFT3D needs further research and a detailed validation of DELFT3D against measured distribution of wave-induced turbulence and horizontal flow velocity profiles, especially in the region of breaking and broken waves. Meanwhile, it is important to examine how and to which extent this limitation of DELFT3D would affect the results of this study. For this purpose, the advective suspended sediment transport rates in the upper part of the water column are compared to the total suspended sediment transport rates calculated over the entire water column as follows:

$$S_U = \frac{\int_{0.4h}^{h} \overline{c(\xi)}\,\overline{u(\xi)}\,dz}{h} \qquad 4.76a$$

$$S_L = \frac{\int_{0}^{0.4h} \overline{c(\xi)}\,\overline{u(\xi)}\,dz}{h} \qquad 4.76b$$

$$R_s = \frac{S_U}{S_U + S_L} \qquad 4.77$$

Where h is the water depth, S_U(m/s) is suspended sediment transport rate per unit depth in the upper part of the water column (z/h>0.4), S_L(m/s) is the suspended sediment transport rate per unit depth in the lower part of water column (z/h<0.4), R_s is the ratio between S_U and S_U+S_L which quantifies the ratio between suspended sediment transport rate in the upper part of the water column and suspended sediment transport rate over the entire depth, $\bar{c}$ is the time averaged suspended sediment concentration, $\bar{u}$ is the averaged flow velocity and $\xi = z/h$ is the relative elevation above the seabed. The suspended sediment transport rates S_U (z/h>0.4) and S_L (z/h<0.4) at locations VA, VB and VC are calculated for f_{sus}=0.4 and f_{bed}=0.5 and initial setting of V_h =0.1m²/s, with positive values indicating seaward transport (Fig. 4.34).

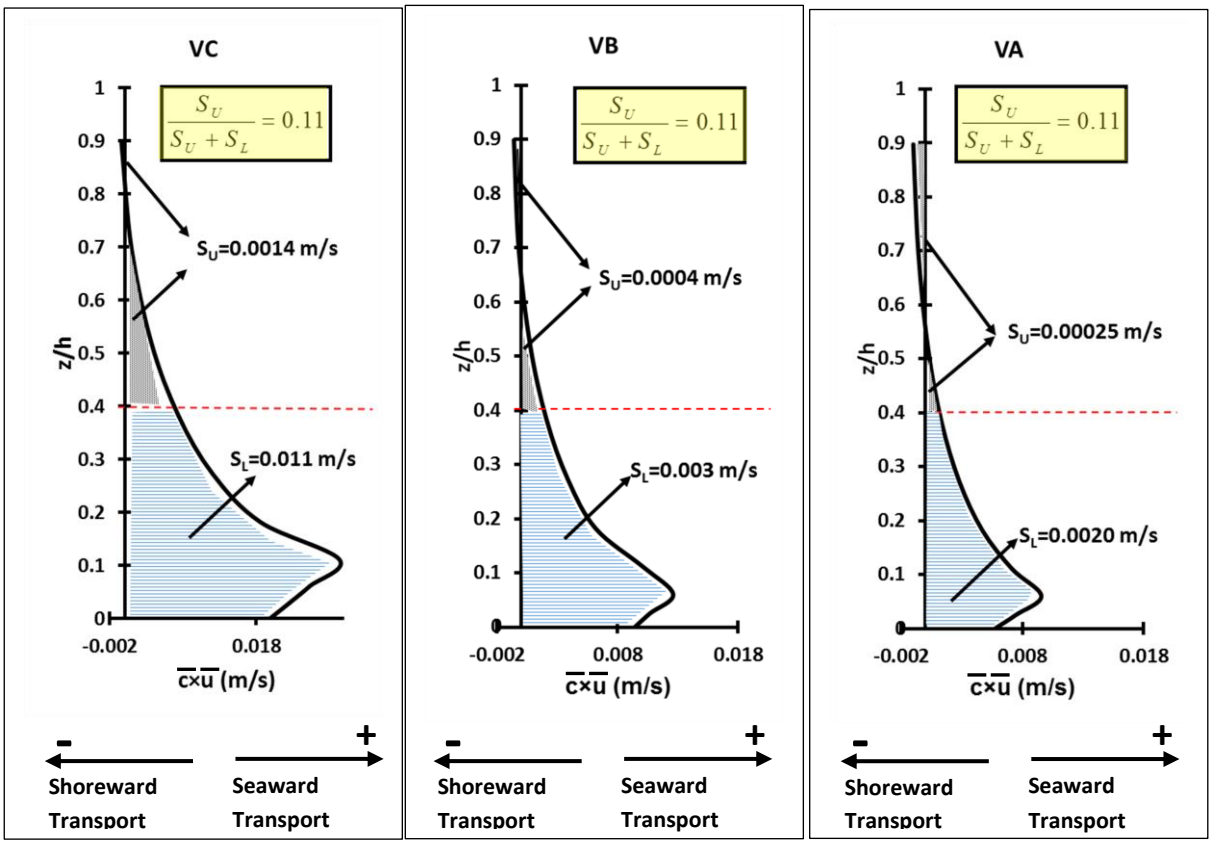

Fig 4.34: Calculated suspended sediment transport rate per unit depth (see Eqs 4.76a and 4.76b) in the upper part S_U and lower part S_L of the water column at the locations VA,VB and VC indicated in Fig. 4.22

The results shown in Fig. 4.34 clearly suggests that the suspended sediment transport rate in the upper part S_U, accounts for 11% of the total suspended sediment transport rate over the entire water column. Intuitively, it could be understood that the advective suspended sediment transport affects the suspended sediment concentration profile. Thus, the deviation between measured and calculated flow velocity profile in upper part of the water column, which affects the sediment transport in this part, is expected to affect the suspended sediment transport over the entire water depth and consequently suspended sediment concentration profile. However, because of the relatively low suspended sediment transport rate S_U at the upper part of the water column, neglecting this deviation might have a small effect on vertical suspended sediment concentration profile.

In order to examine the effect of horizontal eddy viscosity V_h on the calculated horizontal flow velocity u, a series of numerical tests are performed for V_h=0.01-0.1 m²/s. The outcomes show that the closest agreement between numerical results and measurement is obtained for V_h=0.05-0.1 m²/s. Thus,

in order to better illustrate the selection of the optimal V_h value, the numerical simulation results for V_h=0.01 m²/s, V_h=0.05 m²/s and V_h=0.1 m²/s are comparatively plotted in Fig. 4.35, where the upper part of the water column (i.e. 0.4<z/h<1.0) is excluded.

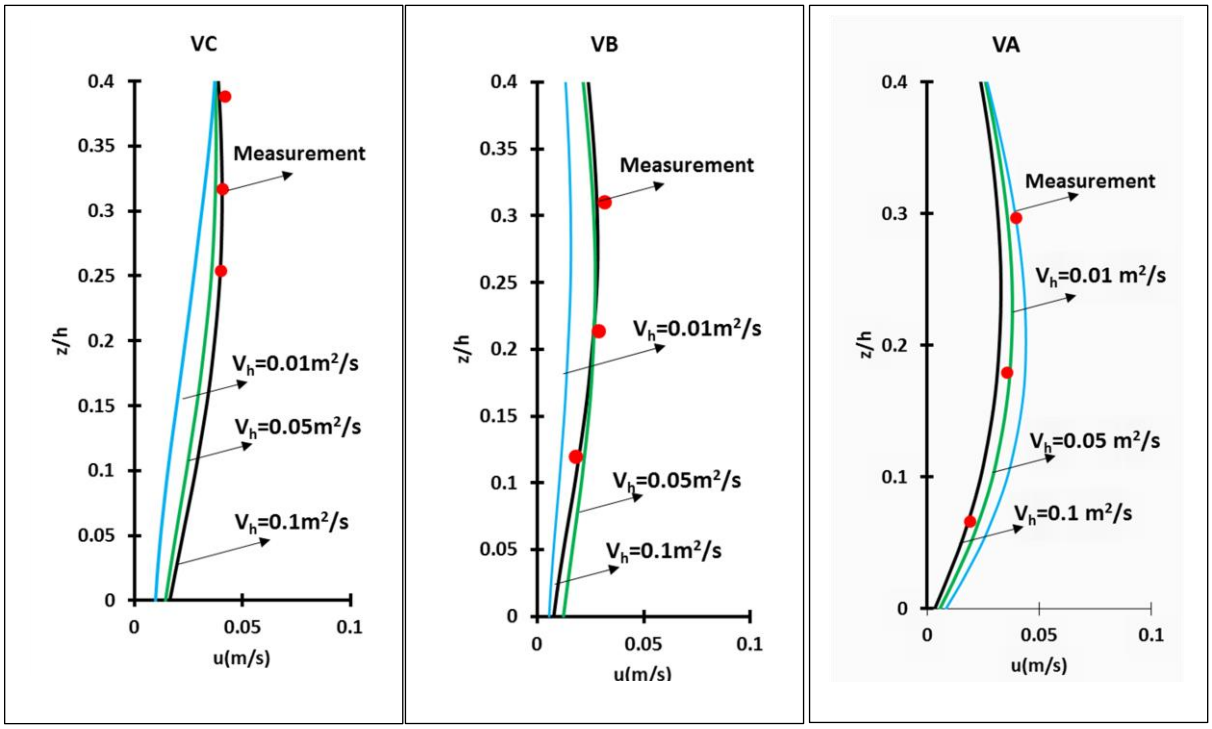

Fig 4.35: Measured and calculated vertical distributions of horizontal flow velocity over the lower part of the water column (z/h≤0.4) at locations VA, VB and VC (indicated in Fig. 4.22), for horizontal eddy viscosity V_h=0.1, 0.05 & 0.1 m²/s

Based on the results in Fig. 4.35, the Wilmot index **W** and Root Mean Square Error **RMSE** describing the degree of agreement between numerical results and measurement are given in Table. 4.8:

Table 4.8: Wilmott Index (W) and Root Mean Square Error (RMSE) calculated based on the results in Fig. 4.35

Locations	**VA**		**VB**		**VC**	
index	**W**	**RMSE**	**W**	**RMSE**	**W**	**RMSE**
V_h=0.10 m2/s	**0.78**	**6.2×10^{-3}**	**0.82**	**6.2×10^{-3}**	**0.95**	**2.7×10^{-3}**
V_h=0.05 m2/s	**0.83**	**5.4×10^{-3}**	**0.78**	**6.4×10^{-3}**	**0.93**	**3.7×10^{-3}**
V_h=0.01 m2/s	**0.56**	**9.1×10^{-3}**	**0.31**	**9.2×10^{-3}**	**0.60**	**7.6×10^{-3}**

The results in Table. 4.8 show that different values of V_h satisfy the condition W>0.8 at VA, VB and VC. In other word, the calculated Wilmott Index W values given in Table 4.8 show that**,** at the farthest location behind the breakwater, i.e. VC, the condition W>0.8 is satisfied for V_h=0.05 and V_h=0.1 m²/s. However, at VA and VB, the acceptable values of V_h are respectively V_h =0.05 and V_h =0.1 m²/s. Thus, in order to set a unique value for V_h at all locations VA, VB and VC, in addition to Willmot index W, the calculated RMSE is also considered. The calculated RMSE at locations VA and VB shows that using V_h=0.05 m²/s at VA would result in a 14% lower RMSE compared to the RMSE obtained for V_h=0.10 m²/s. However, at VB, the use of V_h=0.05 m²/s yields only 3% higher RMSE compared to the use of V_h=0.10 m²/s, implying no significant difference between the use of V_h=0.05 m²/s and V_h=0.10 m²/s. This is also visually observable in Fig. 4.35, where the differences between measurement and numerical results obtained for V_h=0.10 m²/s and V_h=0.05 m²/s are nearly the same at location VB. Finally, the horizontal eddy viscosity is set to V_h=0.05 m²/s and Step 2 of the calibration procedure in Fig. 4.27 is completed.

Model Calibration, Step3 (Background Horizontal Eddy Diffusivity D_h)

In Step 3, which is the last step of the model calibration procedure in Fig. 4.27, the horizontal eddy diffusivity D_h is selected. Accordingly, a series of numerical simulations are performed for D_h =0.01-0.10 m²/s, while f_{sus}=0.4 and f_{bed}=0.5 and V_h=0.05 m²/s, which have been determined so far, are kept constant. The numerical results obtained for D_h=0.01 m²/s, D_h=0.05 m²/s and D_h=0.10 m²/s are plotted in Fig. 4.36, showing that the horizontal eddy diffusivity D_h does not affect noticeably the numerical results for the considered range of D_h values, implying that the advective suspended sediment transport dominates over the diffusive suspended sediment transport

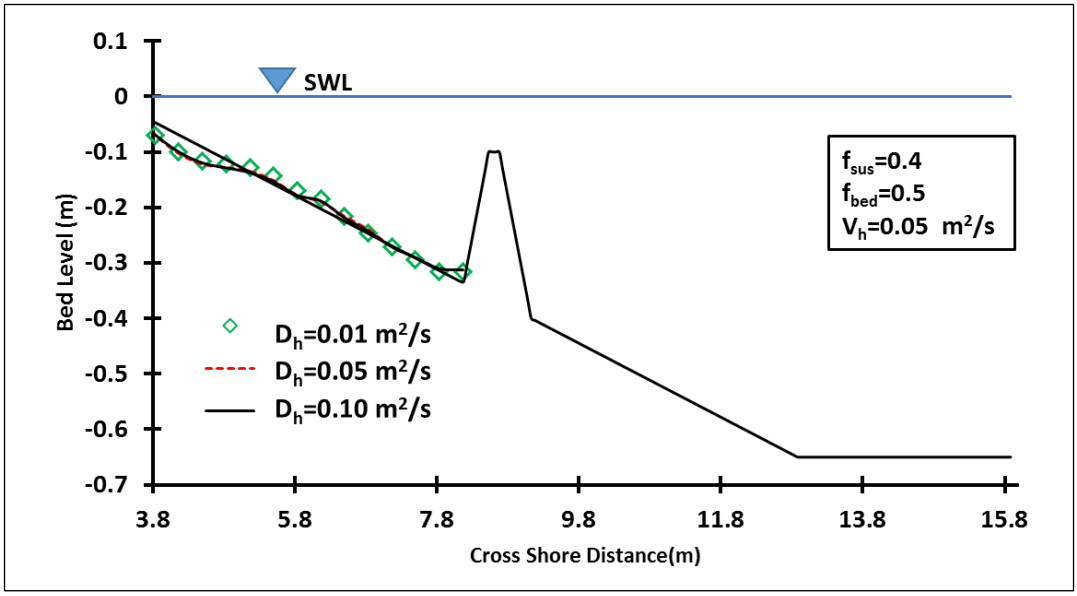

Fig 4.36: Effect of horizontal eddy diffusivity D_h on the calculated bed profile

For D_h =0.05-0.10 m²/s, almost no change in the numerical results is observed. However, for D_h=0.01 m²/s, slightly less erosion on the upper part of the profile is observed. Thus, D_h might be arbitrarily selected between 0.01 and 0.1m²/s. However, further numerical tests revealed that D_h =0.01 m²/s yield better results when the calibrated model is applied to the other tests (Tests A, C, and D in Table 4.5). Finally, for the horizontal eddy diffusivity D_h=0.01 m²/s, the numerical results and the measurements are compared in Fig. 4.37b, showing a relatively good agreement with BSS=0.83. Therefore, Step 3 of the calibration procedure in Fig. 4.27 is completed.

Model Validation

After the model calibration for the simulation of the morphological changes in the lee of submerged breakwaters, which resulted in the determination of the calibration parameters (i.e. Background Horizontal Eddy Viscosity V_h=0.05 m²/s, Background Horizontal Eddy Diffusivity D_h=0.01 m²/s, Suspended Sediment Transport Scaling Factor f_{sus}=0.5 and Bed Load Transport Scaling Factor d f_{bed}=0.4), the model validation is carried out. For this purpose, the calibrated numerical model is applied to reproduce the laboratory tests A, B, C and D, described in Table 4.5. The results of the model validation against tests A, B, C and D are respectively plotted in Figs. 4.37 a, b & c.

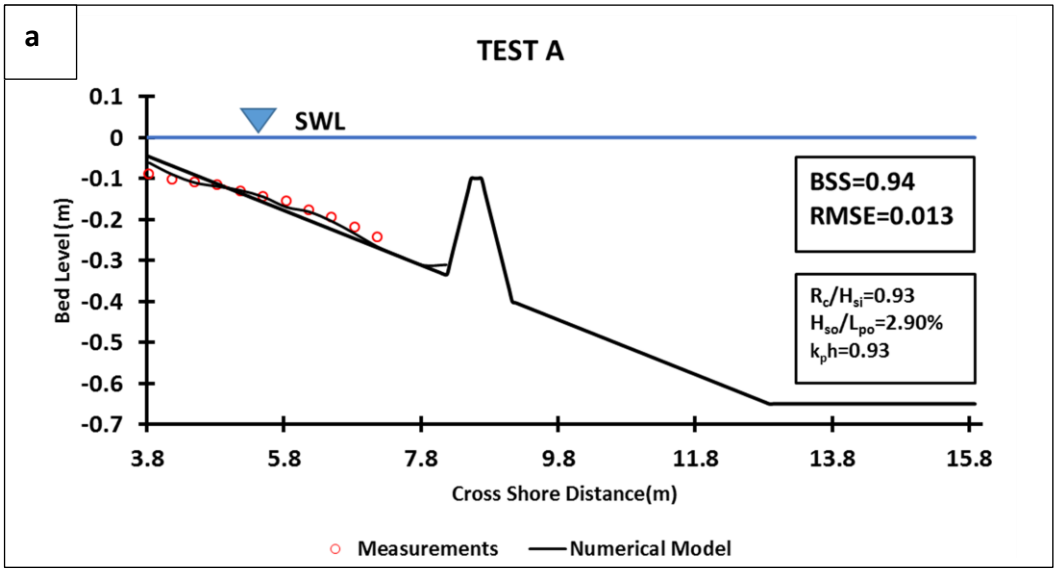
a
TEST A
SWL
BSS=0.94
RMSE=0.013
R_c/H_{si}=0.93
H_{so}/L_{po}=2.90%
k_ph=0.93
Bed Level (m)
Cross Shore Distance(m)
Measurements
Numerical Model

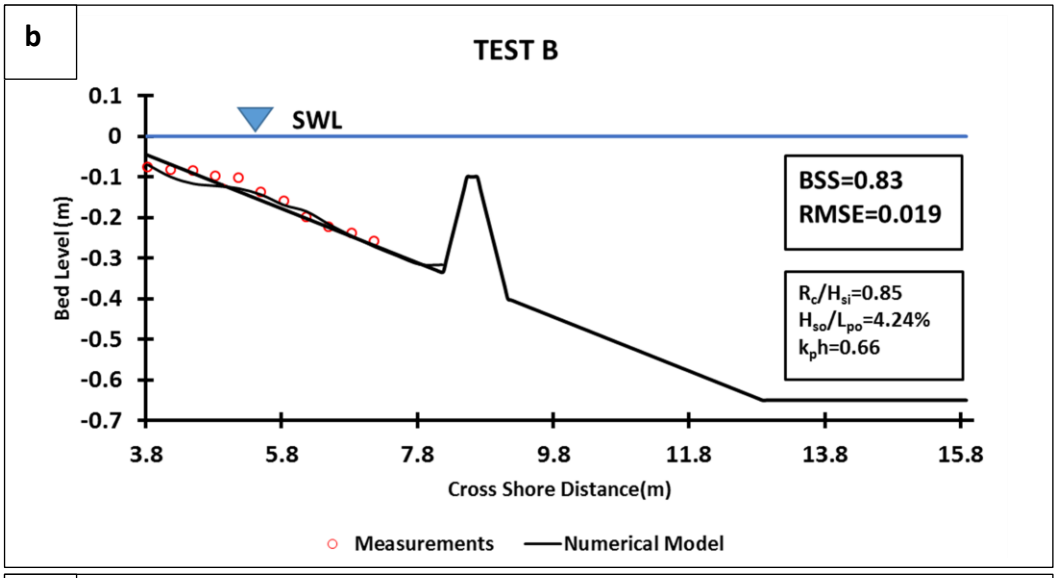
b
TEST B
SWL
BSS=0.83
RMSE=0.019
R_c/H_{si}=0.85
H_{so}/L_{po}=4.24%
k_ph=0.66
Bed Level (m)
Cross Shore Distance(m)
Measurements
Numerical Model

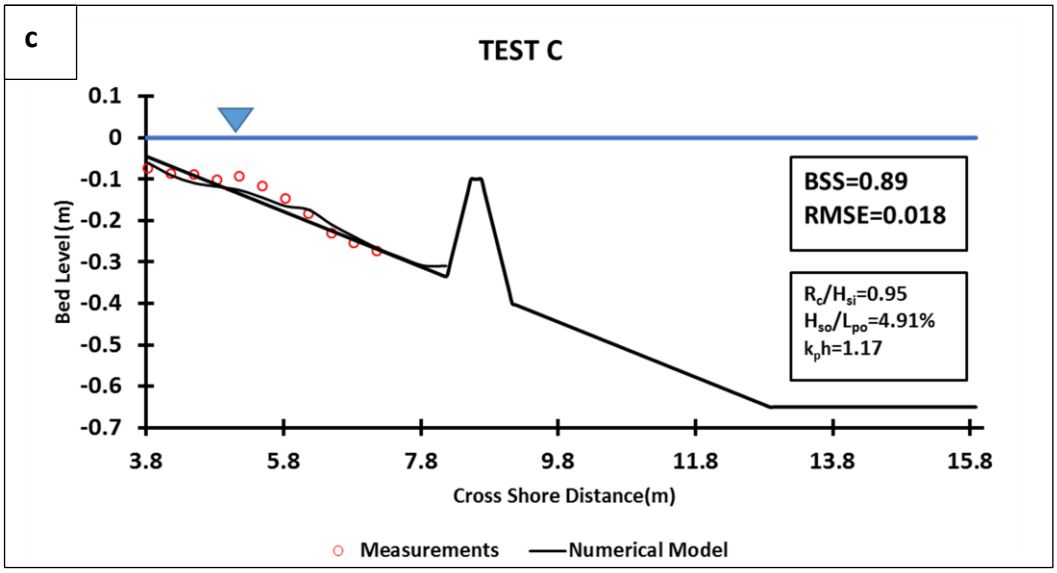
c
TEST C
BSS=0.89
RMSE=0.018
R_c/H_{si}=0.95
H_{so}/L_{po}=4.91%
k_ph=1.17
Bed Level (m)
Cross Shore Distance(m)
Measurements
Numerical Model

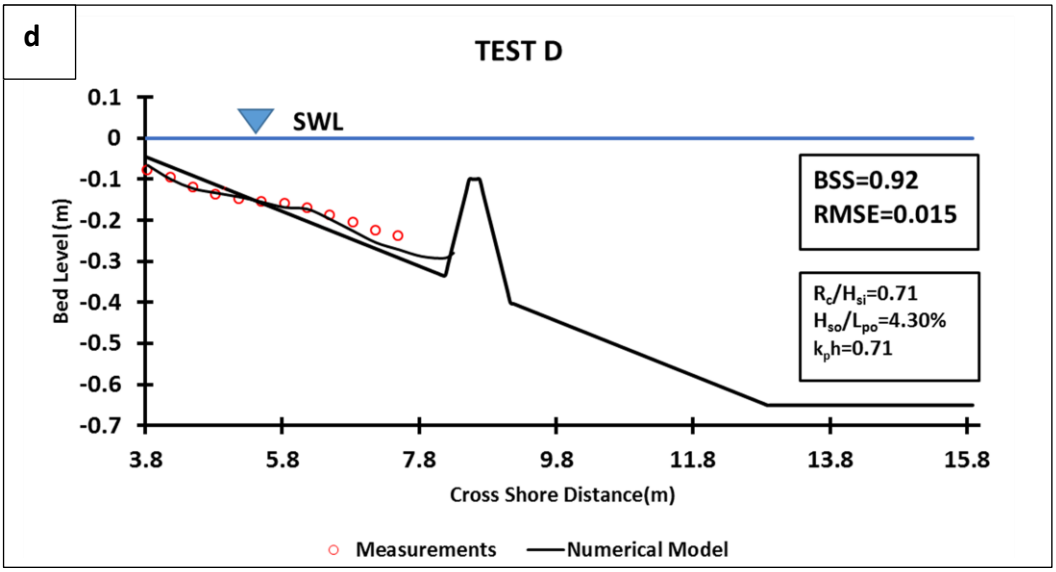

Fig 4.37: Results of model validation against laboratory tests A, B, C and D described in Table 4.5

For each test, the BSS parameter and RMSE is determined in Table 4.9 to quantify the agreement between numerical results and measurements.

Table 4.9: Statistical indicators BSS and RMSE for the numerical simulations of the laboratory tests A,B,C and D described in Table 4.5

	H_{si}/L_p (%)	H_{si}/R_c	k_ph	BSS	RMSE (m)
Test A	**2.90**	**1.08**	**0.93**	**0.94**	**0.013**
Test B	**4.2**	**1.18**	**0.66**	**0.83**	**0.019**
Test C	**4.9**	**1.05**	**1.17**	**0.89**	**0.018**
Test D	**4.3**	**1.41**	**0.77**	**0.92**	**0.015**

The values of the BSS parameter obtained in Table 4.9 for all numerical simulations (i.e. Tests A, B, C and D) imply a **Good** to **Excellent** agreement between measured and calculated bed profiles (according to the score in Fig 4. 23). Due to lack of experimental data for wider range of wave conditions, the validation described in this section should be considered as tentative.

The BSS values suggest that the agreement is highest for Tests A and D. This is also confirmed by the obtained RMSE values. Therefore, the calibrated model can be applied to simulate properly the morphological changes in the lee of submerged breakwater for the wave conditions (H_{si}/L_p and k_ph) specified in Table 4.9.

4.4 Summary and implications of model calibration/validation results

Considering the necessity and importance to extend/improve the applicability of DELFT3D for simulating morphological changes leeward of submerged porous breakwaters (SPB), in this chapter a new approach with two steps is proposed for implementing the effect of breakwater submergence (Step i) and porosity (Step ii) in DELFT3D, called "SPB implementation approach" (Fig. 4.11). The so improved DELFT3D model is calibrated and validated against laboratory experiments. The key results and their implications for this study are summarized below:

- For hydrodynamic, sediment transport and morphological simulations, submerged breakwaters are introduced in DELFT3D-WAVE as an integral part of the bathymetry-and not as obstacles (section 4.2.1).

- Introducing submerged breakwater as bathymetric features in the DELFT3D-WAVE model, with its original wave breaking parameterization from Battjes and Janssen (1978), might not be applicable to steep slope breakwaters as it cannot adequately reproduce the effect of breakwater submergence on wave transmission (see Section 4.2.1)

- The necessity of applying Step i of the proposed SPB implementation approach (see section 4.2.1), which is proposed for implementing steep slope breakwaters in DELFT3D-WAVE, essentially depends on relative submergence R_c/H_{m0} and relative crest width B/L_p. For this purpose, a decision criterion is developed, based on the results of numerical tests performed in this chapter (see Section 4.2.3d)

- Based on Step ii of the proposed SPB implementation approach (see section 4.2.2), the dissipative effect of porosity on transmitted waves is implemented using a virtual sub-grid obstacle (with a specified porosity and placed immediately behind the actual breakwater). For this purpose, the virtual obstacle with the transmission coefficient determined by the PEF formula (Eq. 3.26) is implemented at the onshore toe of the breakwater.

- The approach proposed to account for the porosity effect in Step ii, which is based on the virtual obstacle concept to overcome the inherent limitation of DELFT3D to account for the effect of breakwater porosity on wave transmission, can be potentially applied in any phase-averaged numerical model (e.g. MIKE SW) in which linear obstacles can be defined (see Section 2.4).

- The SPB implementation approach, which is proposed to implement the combined effect of submergence and porosity in the DELFT3D-WAVE model, is applied to reproduce the laboratory experiments by Kramer et al. (2005) on wave transmission. Based on the results, it was observed that the application of the proposed SPB implementation approach in DELFT3D extends the applicability of the model and noticeably enhances the agreement between predicted and transmitted wave heights (see section 4.2.3). Moreover, the laboratory tests by Claessen and Groenewoud (1995) on the effect of SPB on the changes of a beach profile under irregular waves have been reproduced much more accurately by the DELFT3D-WAVE model improved by SPB implementation approach compared to the original DELFT3D-WAVE model and to the UNIBEST-TC model (see Fig. 4.28) which both overestimate the transmitted wave heights significantly (see Fig. 4.28)

- In the numerical reproduction of the laboratory tests by Claessen and Groenewoud (1995), it was observed that the predicted horizontal flow velocity shows a large deviation from its measured counterpart in the upper part of the water column (see Fig. 4.33). It is also shown that this large deviation is not relevant for the purpose of this study, because the advective suspended sediment transport dominates over the diffusive suspended sediment transport and the advective sediment transport rate in the upper part of the water column is relatively small as compared to the total advective suspended sediment transport over the entire water column.

- The numerical set-up in DELFT3D to reproduce the laboratory tests by Claessen and Groenewoud (1995) (see Section 4.3.2a) has been successfully calibrated (see Section 4.3.2.b). The calibrated model is then applied to the wave conditions tested in the laboratory (see Section 4.3.2.c). The measured and calculated morphological changes show "Good to Excellent"

agreements (see Fig. 4.37) based on the BSS (Brier Skill Score) qualification scale as defined in Fig. 4.23.

The results of the model calibration and validation imply that the model can be applied within the range of wave conditions (see Fig. 4.37 and Table 4.9) considered in the validation process to perform in the next chapter a systematic parameter study on the effect of breakwater submergence and porosity on coastal morphology.

5 Parameter study on the effect of breakwater porosity and submergence on coastal morphology

This chapter is devoted to the numerical parameter study of the effect of the porosity and submergence of the breakwater on the coastal morphological changes and to the analysis of the results. The main aim of the parameter study is to assess the effects of submerged breakwater design parameters on the protective efficacy of the structure and thus on the morphology of sand beaches protected by submerged breakwaters. The estimation of the erosion of the protected beaches leeward of the submerged breakwaters is very important for a reliable design of the submerged structures in coastal protection systems. Therefore, a series of numerical tests of the parameter study and their analysis are performed with the main objective to advance the current knowledge on the effects of the porosity and submergence of breakwaters on their protective efficacy against beach erosion. However, the effects of other design parameters such as crest width and location depth of the breakwater are also considered for the sake of completeness. The results of the numerical tests are utilized to evaluate the effects of different breakwater configurations on the morphological changes of the protected beaches. Accordingly, design criteria and predictive formulae are proposed for the preliminary design of efficient porous submerged breakwaters in coastal protection systems.

The calibrated and validated numerical model set-up, as described in section 4.3, is used for the numerical parameter study. A total of 90 submerged porous breakwater configurations have been tested in the numerical set-up by varying the structure design parameters such as porosity, submergence, crest width and location depth.

The first section of this chapter is devoted to the methodology applied for the numerical parameter study. The analysis of the numerical test results is presented in section 5.2. In the latter, the effect of various examined breakwater design parameters on the protective efficacy of the submerged porous breakwaters and on the morphological changes of the protected beaches are discussed, followed by the development of predictive formulae and design criteria. Finally, a summary of the key outcomes of this chapter, their relevance, limitations and implications for future research are provided in the concluding section 5.3

5.1 Methodology for the parameter study

The low RMSE values and the good to excellent BSS values obtained in section 4.3 for each validation case confirm a very good agreement between calculated and measured bed level changes leeward of the breakwater. Consequently, the calibrated and validated numerical model set-up presented in section 4.3.2 is utilized for the numerical parameter study.

In this study, the volume of the beach erosion per unit width V_e (m^3/m), as depicted in Fig. 5.1, is selected to characterize the severity of beach erosion.

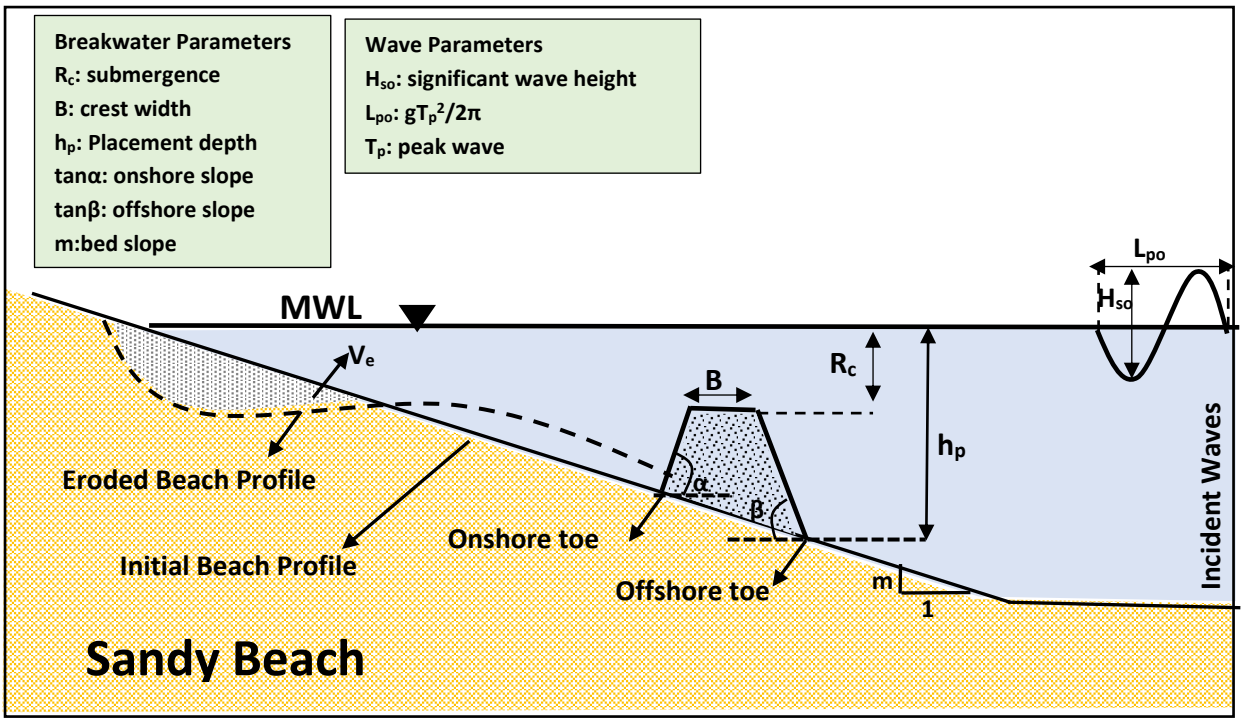

Fig 5.1: Definition of parameters in the numerical model set-up

Based on the experimental data, Özölcer (2008) evaluated the relative effect of different wave and beach parameters on erosion volume as follows: **wave height (67.80%), wave period (14.8%), sediment size (15.4%) and beach slope (2%).** On the other hand, for beach erosion leeward of the breakwater, the wave and beach parameter in the protected area leeward of the breakwater should be considered. Considering what discussed above, and the fact that for the final formulation of results the focus is on the most widely used dimensionless structure design parameters (i.e. R_c/H_{rmsi}, B/L_p and possibly H_{rmso}/h_p), in this study only the structure design parameters are changed on the basis of the following reasons:

- Varying wave height, which is the most effective **(67.80%)** parameter in the protected beach (leeward of the breakwater), is already generated by varying wave transmission through changing the structure design parameters (e.g. R_c, B,n), resulting in the transmitted wave height ranging from minimum root mean square transmitted wave height of H_{rmst}=0.026m to maximum transmitted wave height of H_{rmst}=0.080m

- The effect of wave period (14.7%) is perceived to be almost 4 times smaller than the effect of wave height (67.8%). Besides, varying B/L_p which is necessary for the formulation of the results in terms of the structure design parameters (i.e. R_c/H_{rmsi}, B/L_p and possibly H_{rmso}/h_p) can be generated only by varying the crest with (without varying wave period) resulting in $0.026 \leq H_{rmst} \leq 0.080$. and $0.05 \leq B/L_p \leq 0.17$ Based on the two reasons given above, in order to ***avoid unnecessarily large number of tests***, wave period is not changed

- The effect of sediment size (15.4%) is perceived to be roughly 4 times smaller than the effect of wave height (67.8%). Besides, the change of sediment size may violate the calibration of sediment transport module (described in section 4.3) which might be influenced by the size and settling velocity of sediments in the benchmark experimental test used for model calibration and validation

- Beach slope is not considered as its effect is perceived to be negligible (**2%**) compared to that of other parameters

Based on the reasons outlined above, as shown in Table 5.1, the breakwater parameters varied in the parameter study are breakwater porosity (five n values), submergence (three R_c values), crest width (three B values), and location depth (two h_p values). All these parameters are defined in the parameterized model configuration shown in Fig. 5.1.

Table 5.1: Range of parameters varied in the numerical study

Parameter	Symbol	Values
Breakwater Porosity	N	0, 0.3, 0.4, 0.5, 0.6
Submergence	Rc	0.03m, 0.07m , 0.10m
Crest Width	B	0.15m, 0.30m, 0.45m
Water depth at Breakwater Location	h_p	0.27m, 0.40m

Regarding the incident wave conditions, the offshore significant wave height and peak period of experiment D (H_{so}=0.133 m, T_{po}=1.81s) described in section 4.3.1 have been selected for the numerical tests because: i) There is a good visual and quantitative agreement between numerical simulation results and measured erosions for experiment D. ii) Experiment D features the highest wave height tested in the laboratory study used to validate the model, implying to the most favorable condition to study the beach erosion. Similar to the laboratory tests for which the numerical model set-up is calibrated and validated, each test of the parameter study lasts 7.5 hours.

In order to make the results applicable to practical design problems, the erosion volume per unit beach length V_e (m^3/m) obtained for each test is expressed in non-dimensional form.

Considering the dominant effect of the wave height on erosion volume, compared to the effect of wave period (67.8% influence of wave height versus 14.7% effect of wave period), the calculated erosion volume V_e (m^3/m) is made non-dimensional by the incident root mean square wave height H_{rmsi} (m) at the offshore toe of the breakwater. As a result, the dimensionless erosion parameter e_p (beach erosion for a unit incident wave height) and its inverse counterpart p_i =1/e_p are obtained:

$$e_p = \frac{\sqrt{V_e}}{H_{rmsi}} \qquad 5.1$$

and

$$p_i == \frac{H_{rmsi}}{\sqrt{V_e}} \qquad 5.2$$

Where parameter p_i can be considered as a measure of the efficacy of the breakwater to protect the beach against erosion and might be therefore called “protection index”.

There are many studies focused on the beach profile changes as a function of simple environmental parameters such as wave height (e.g. Larson and Kraus, 1989, Kraus et al., 1991, Günaydın and Kabdaşlı, 2003) and Özölcer, 2008). Among these, the most recent laboratory study which is perfomed using irregular waves is carried out by Günaydın and Kabdaşlı (2003).

Günaydın and Kabdaşlı (2003) performed a series of laboratory tests to evaluate the realtion between irrugalr wave parameters, beach characteristics (sediment grain size) and beach erosion. Based on the results, Günaydın and Kabdaşlı (2003) formulated the beach erosion volume as a function of beach characteristics and incident wave parameters and obtained the following predictive formula:

$$\tilde{V}_e = \frac{D_{50}^2}{1.5\times10^{-6}}\left[Ln\left(\frac{H_{so}\xi_{op}}{G_s D_{50}}\right) - 4.1396\right] \qquad 5.3$$

where H_{so} is the deep water wave height, G_s dimensionless specific gravity of sand, ξ_{op} tsurf similiraty parameter

In the present study, the erosion volume $V_e = (e_p \times H_{rmsi})^2$ obtained from the numerical parameter study is compared with the erosion volume $\tilde{V}_e$ calculated by Eq 5.3, in which the deep water wave height H_{so} is calculated on the basis of the transmitted wave height at the onshore toe of the breakwater (see Fig. 5.1). Fig. 5.2 shows that, in spite of the numerical model limitation to accurately simulate sediment transport in the swash zone, as mentioned in section 2.3, there is a strong functional relationship (R^2=0.96) between V_e and $\tilde{V}_e$ that suggests very close similarity of trends between variation of beach erosion volume V_e obtained from the parameter study, and that calculated using Eq 5.3 proposed by Günaydın and Kabdaşlı (2003). Indeed, Fig. 5.2 shows that the results of the parameter study and those obtained from Eq 5.3 represent closely similar variations of the beach erosion with the variation of the design parameters.

Therefore, with more confidence, the erosion volume V_e obtained from the numerical parameter study and the associated dimensionless erosion parameter e_p and p_i might be considered as relevant parameters for the analysis of the results.

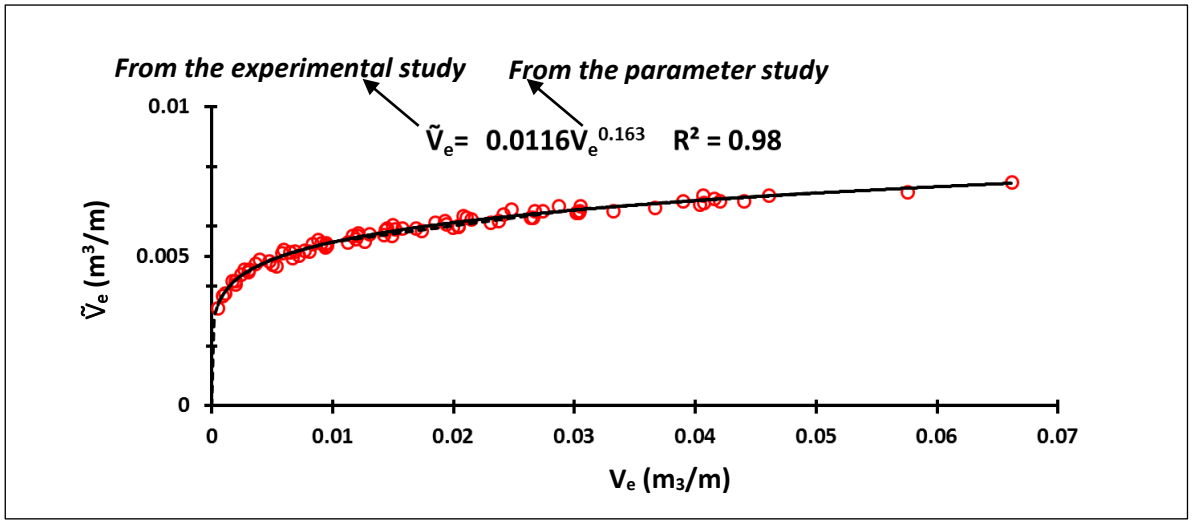

Fig 5.2: Variations of erosion volume V_e obtained from the present parameter study versus erosion volume $\tilde{V}_e$ calculated by Günaydın and Kabdaşlı (2003) empirical formula

As can be seen, the erosion volume predicted by formula ($\tilde{\mathbf{V}}_e$) is almost an order of magnitude smaller than the erosion volume obtained from numerical simulation results ($\mathbf{V}_e$). The physical explanation for this difference is that, in the experimental tests performed to develop Eq. 5.3, Günaydın and Kabdaşlı (2003) used bed sediments with d_{50}=0.35 mm, which is three times larger than the sediment size used for numerical simulations performed for the parameter study (based on the laboratory tests used for model calibration and validation as described in section 4.3). Therefore, it is obvious that this formula underestimates the beach erosion volume when applied to noticeably smaller grain size

Based on the above discussion and the definition expressed by Eq. 5.1, for the same incident wave energy and consequently the same incident wave height, the lower erosion parameter e_p implies a smaller volume of beach erosion in the protected area, and thus a higher protective efficacy of the structure which corresponds to the higher protection index p_i. Therefore, parameter e_p can be adopted as a proper measure for the erosion of the beach protected by the submerged breakwater, and its inverse counterpart p_i as a "protection index" to describe the protective efficacy of the structure against erosion.

Results of the numerical parameter study along with the examined parameters are summarized in Table 5.2, where $\Omega_t = \frac{H_{rmst}}{w_s \times T_p}$ is the Dean parameter, T_p peak period, L_p wave length related to the peak period and calculated at offshore toe of the breakwater, h_p the location depth (water depth at offshore toe the breakwater), w_s the sediment fall velocity, and H_{rmso} the root mea square deep water wave height. Although wave period T_p and sediment size D_{50} are not explicitly considered in this parameter study because of the reasons stated at the beginning of this section, the variation of Dean Parameter Ω_t within erosive state, i.e. Ω_t >1 (Kamphuis , 1991), has not been overlooked. In fact, although T_p and D_{50} are excluded from the parameter study, a wide range of Dean Parameter values (i.e. 1.57< Ω_t <4.33) in erosive state (Ω_t >1) has been tested through varying the transmitted wave height H_{rmst}.

Table 5.2: Summary of the results of the numerical parameter study (For Hso=0.133m and Tp=1.81s in all tests)

Test Number	n (-)	h_p (m)	B (m)	R_c (m)	H_{rmsi} (m)	H_{rmst} (m)	e_p (-)	p_i (-)	R_c/H_{rmsi} (-)	B/L_p (-)	B/L_{op} (-)	H_{rmst}/L_p (-)	Ω_t (-)
1	0	0.27	0.15	0.03	0.1	0.062	1.78	0.56	0.3	0.06	0.03	0.025	3.83
2	0.3	0.27	0.15	0.03	0.1	0.040	1.41	0.71	0.3	0.06	0.03	0.016	2.46
3	0.4	0.27	0.15	0.03	0.1	0.044	1.54	0.65	0.3	0.06	0.03	0.018	2.71
4	0.5	0.27	0.15	0.03	0.1	0.048	1.62	0.62	0.3	0.06	0.03	0.019	2.95
5	0.6	0.27	0.15	0.03	0.1	0.052	1.68	0.59	0.3	0.06	0.03	0.021	3.19
6	0	0.27	0.3	0.03	0.1	0.053	1.59	0.63	0.3	0.11	0.06	0.020	3.17
7	0.3	0.27	0.3	0.03	0.1	0.032	1.06	0.94	0.3	0.11	0.06	0.012	1.89
8	0.4	0.27	0.3	0.03	0.1	0.036	1.18	0.85	0.3	0.11	0.06	0.013	2.14
9	0.5	0.27	0.3	0.03	0.1	0.040	1.33	0.75	0.3	0.11	0.06	0.015	2.38
10	0.6	0.27	0.3	0.03	0.1	0.044	1.45	0.69	0.3	0.11	0.06	0.016	2.63
11	0	0.27	0.45	0.03	0.1	0.046	1.31	0.76	0.3	0.17	0.09	0.013	2.83
12	0.3	0.27	0.45	0.03	0.1	0.026	0.70	1.43	0.3	0.17	0.09	0.007	1.57
13	0.4	0.27	0.45	0.03	0.1	0.030	0.89	1.13	0.3	0.17	0.09	0.008	1.82
14	0.5	0.27	0.45	0.03	0.1	0.034	1.03	0.97	0.3	0.17	0.09	0.010	2.07
15	0.6	0.27	0.45	0.03	0.1	0.038	1.16	0.86	0.3	0.17	0.09	0.011	2.31
16	0	0.27	0.15	0.07	0.1	0.072	2.15	0.46	0.7	0.06	0.03	0.029	4.33
17	0.3	0.27	0.15	0.07	0.1	0.056	1.93	0.52	0.7	0.06	0.03	0.022	3.38
18	0.4	0.27	0.15	0.07	0.1	0.059	1.98	0.51	0.7	0.06	0.03	0.024	3.55
19	0.5	0.27	0.15	0.07	0.1	0.062	2.02	0.49	0.7	0.06	0.03	0.025	3.73
20	0.6	0.27	0.15	0.07	0.1	0.065	2.07	0.48	0.7	0.06	0.03	0.026	3.90
21	0	0.27	0.3	0.07	0.1	0.065	1.93	0.52	0.7	0.11	0.06	0.024	3.72

22	0.3	0.27	0.3	0.07	0.1	0.047	1.69	0.59	0.7	0.11	0.06	0.017	2.72
23	0.4	0.27	0.3	0.07	0.1	0.051	1.76	0.57	0.7	0.11	0.06	0.019	2.94
24	0.5	0.27	0.3	0.07	0.1	0.055	1.80	0.55	0.7	0.11	0.06	0.020	3.13
25	0.6	0.27	0.3	0.07	0.1	0.057	1.84	0.54	0.7	0.11	0.06	0.021	3.28
26	0	0.27	0.45	0.07	0.1	0.056	1.72	0.58	0.7	0.17	0.09	0.016	3.39
27	0.3	0.27	0.45	0.07	0.1	0.039	1.48	0.67	0.7	0.17	0.09	0.011	2.34
28	0.4	0.27	0.45	0.07	0.1	0.042	1.53	0.66	0.7	0.17	0.09	0.012	2.54
29	0.5	0.27	0.45	0.07	0.1	0.045	1.57	0.64	0.7	0.17	0.09	0.013	2.71
30	0.6	0.27	0.45	0.07	0.1	0.048	1.60	0.62	0.7	0.17	0.09	0.013	2.88
31	0	0.27	0.15	0.1	0.1	0.080	2.31	0.43	1	0.06	0.03	0.032	4.44
32	0.3	0.27	0.15	0.1	0.1	0.066	2.13	0.47	1	0.06	0.03	0.026	3.66
33	0.4	0.27	0.15	0.1	0.1	0.068	2.16	0.46	1	0.06	0.03	0.027	3.79
34	0.5	0.27	0.15	0.1	0.1	0.070	2.19	0.46	1	0.06	0.03	0.028	3.91
35	0.6	0.27	0.15	0.1	0.1	0.073	2.22	0.45	1	0.06	0.03	0.029	4.04
36	0	0.27	0.3	0.1	0.1	0.073	2.16	0.46	1	0.11	0.06	0.027	4.06
37	0.3	0.27	0.3	0.1	0.1	0.057	1.93	0.52	1	0.11	0.06	0.021	3.16
38	0.4	0.27	0.3	0.1	0.1	0.060	1.98	0.51	1	0.11	0.06	0.022	3.33
39	0.5	0.27	0.3	0.1	0.1	0.062	2.01	0.50	1	0.11	0.06	0.023	3.45
40	0.6	0.27	0.3	0.1	0.1	0.065	2.06	0.49	1	0.11	0.06	0.024	3.61
41	0	0.27	0.45	0.1	0.1	0.066	2.03	0.49	1	0.17	0.09	0.018	3.67
42	0.3	0.27	0.45	0.1	0.1	0.049	1.77	0.57	1	0.17	0.09	0.014	2.71
43	0.4	0.27	0.45	0.1	0.1	0.051	1.82	0.55	1	0.17	0.09	0.014	2.86
44	0.5	0.27	0.45	0.1	0.1	0.054	1.87	0.53	1	0.17	0.09	0.015	3.01
45	0.6	0.27	0.45	0.1	0.1	0.057	1.94	0.52	1	0.17	0.09	0.016	3.15
46	0	0.4	0.15	0.03	0.1	0.062	1.98	0.50	0.3	0.05	0.03	0.020	4.03
47	0.3	0.4	0.15	0.03	0.1	0.040	1.56	0.64	0.3	0.05	0.03	0.013	2.62
48	0.4	0.4	0.15	0.03	0.1	0.044	1.69	0.59	0.3	0.05	0.03	0.015	2.86
49	0.5	0.4	0.15	0.03	0.1	0.048	1.77	0.57	0.3	0.05	0.03	0.016	3.10
50	0.6	0.4	0.15	0.03	0.1	0.051	1.83	0.55	0.3	0.05	0.03	0.017	3.34
51	0	0.4	0.3	0.03	0.1	0.052	1.81	0.55	0.3	0.09	0.06	0.016	3.33

52	0.3	0.4	0.3	0.03	0.1	0.032	1.20	0.84	0.3	0.09	0.06	0.010	2.03
53	0.4	0.4	0.3	0.03	0.1	0.035	1.31	0.76	0.3	0.09	0.06	0.011	2.26
54	0.5	0.4	0.3	0.03	0.1	0.040	1.48	0.68	0.3	0.09	0.06	0.012	2.53
55	0.6	0.4	0.3	0.03	0.1	0.043	1.63	0.62	0.3	0.09	0.06	0.013	2.76
56	0	0.4	0.45	0.03	0.1	0.046	1.60	0.63	0.3	0.14	0.09	0.011	2.98
57	0.3	0.4	0.45	0.03	0.1	0.026	0.89	1.12	0.3	0.14	0.09	0.006	1.70
58	0.4	0.4	0.45	0.03	0.1	0.030	1.07	0.94	0.3	0.14	0.09	0.007	1.96
59	0.5	0.4	0.45	0.03	0.1	0.034	1.20	0.84	0.3	0.14	0.09	0.008	2.20
60	0.6	0.4	0.45	0.03	0.1	0.038	1.30	0.77	0.3	0.14	0.09	0.009	2.44
61	0	0.4	0.15	0.07	0.1	0.071	2.22	0.45	0.7	0.05	0.03	0.023	4.55
62	0.3	0.4	0.15	0.07	0.1	0.056	2.04	0.49	0.7	0.05	0.03	0.018	3.59
63	0.4	0.4	0.15	0.07	0.1	0.059	2.06	0.49	0.7	0.05	0.03	0.019	3.78
64	0.5	0.4	0.15	0.07	0.1	0.061	2.09	0.48	0.7	0.05	0.03	0.020	3.91
65	0.6	0.4	0.15	0.07	0.1	0.064	2.13	0.47	0.7	0.05	0.03	0.021	4.10
66	0	0.4	0.3	0.07	0.1	0.063	2.07	0.48	0.7	0.09	0.06	0.019	3.91
67	0.3	0.4	0.3	0.07	0.1	0.047	1.85	0.54	0.7	0.09	0.06	0.014	2.94
68	0.4	0.4	0.3	0.07	0.1	0.050	1.91	0.52	0.7	0.09	0.06	0.015	3.13
69	0.5	0.4	0.3	0.07	0.1	0.053	1.96	0.51	0.7	0.09	0.06	0.016	3.31
70	0.6	0.4	0.3	0.07	0.1	0.056	1.98	0.50	0.7	0.09	0.06	0.017	3.49
71	0	0.4	0.45	0.07	0.1	0.057	1.95	0.51	0.7	0.14	0.09	0.013	3.56
72	0.3	0.4	0.45	0.07	0.1	0.040	1.66	0.60	0.7	0.14	0.09	0.009	2.53
73	0.4	0.4	0.45	0.07	0.1	0.043	1.73	0.58	0.7	0.14	0.09	0.010	2.70
74	0.5	0.4	0.45	0.07	0.1	0.047	1.80	0.55	0.7	0.14	0.09	0.011	2.92
75	0.6	0.4	0.45	0.07	0.1	0.050	1.86	0.54	0.7	0.14	0.09	0.012	3.10
76	0	0.4	0.15	0.1	0.1	0.080	2.47	0.40	1	0.05	0.03	0.026	4.67
77	0.3	0.4	0.15	0.1	0.1	0.066	2.29	0.44	1	0.05	0.03	0.022	3.87
78	0.4	0.4	0.15	0.1	0.1	0.068	2.31	0.43	1	0.05	0.03	0.022	3.97
79	0.5	0.4	0.15	0.1	0.1	0.070	2.34	0.43	1	0.05	0.03	0.023	4.11
80	0.6	0.4	0.15	0.1	0.1	0.073	2.37	0.42	1	0.05	0.03	0.024	4.25
81	0	0.4	0.3	0.1	0.1	0.073	2.29	0.44	1	0.09	0.06	0.022	4.26

82	0.3	0.4	0.3	0.1	0.1	0.058	2.11	0.47	1	0.09	0.06	0.017	3.36
83	0.4	0.4	0.3	0.1	0.1	0.061	2.15	0.47	1	0.09	0.06	0.018	3.53
84	0.5	0.4	0.3	0.1	0.1	0.063	2.17	0.46	1	0.09	0.06	0.019	3.66
85	0.6	0.4	0.3	0.1	0.1	0.065	2.19	0.46	1	0.09	0.06	0.020	3.79
86	0	0.4	0.45	0.1	0.1	0.066	2.08	0.48	1	0.14	0.09	0.015	3.85
87	0.3	0.4	0.45	0.1	0.1	0.050	1.87	0.54	1	0.14	0.09	0.012	2.93
88	0.4	0.4	0.45	0.1	0.1	0.052	1.91	0.52	1	0.14	0.09	0.012	3.04
89	0.5	0.4	0.45	0.1	0.1	0.055	1.96	0.51	1	0.14	0.09	0.013	3.23
90	0.6	0.4	0.45	0.1	0.1	0.057	1.99	0.50	1	0.14	0.09	0.013	3.35

The results of the parameter study presented in Table 5.2 provide the data set with the widest range of parameters of submerged porous breakwaters yet available and their effects on the efficacy of the structure to protect sand beaches against erosion. Yet, it might be worth to mention that, to the author's knowledge, the effect of breakwater porosity has not yet been considered in any of the previous studies on beach erosion in the lee of submerged breakwater (e.g. Claessen and Groenewoud, 1995; Lorenzoni et al., 2012; Lorenzoni et al., 2016; Postacchini et al., 2016). In this study, considering the effect of breakwater porosity represents a novel contribution for the design and protective efficacy of submerged breakwaters against wave-induced coastal erosion.

5.2 Analysis of the results of the parameter study

In this section, the dataset obtained from the numerical parameter study (see Table 5.2) are analyzed to develop formulae and criteria relating the submerged breakwater parameters to the beach erosion and protective performance of the breakwater, which are represented by erosion parameter e_P and "protection index" p_i in Eqs 5.1 & 5.2, respectively. For this purpose, the erosion parameter e_P and its inverse counterpart p_i are expressed as a function of dimensionless breakwater parameters:

$$e_p = \frac{\sqrt{V_e}}{H_{rmsi}} = \psi\left[n, \frac{R_c}{H_{rmsi}}, \frac{B}{L_p}, \frac{H_{rmso}}{h_p}\right] \qquad 5.4$$

$$p_i = \frac{1}{e_p} \qquad 5.5$$

Where ψ.is a function that relates the erosion parameter e_P to the dimensionless breakwater parameters (i.e. porosity n, relative submergence R_c/H_{rmsi}, relative crest width B/L_p and relative location depth h_p/H_{rmso}) and H_{rmso} is the root mean square deep water wave height. In order to develop the function ψ, various combinations of the independent variables (i.e. n, R_c/H_{rmsi}, B/L_p and H_{rmso}/h_p) in Eq 5.4 can be applied. Postacchini et al. (2016) introduced the non-dimensional parameter χ_0 to relate the breakwater parameters such as relative crest width B/L_p and the relative depth h/H_{si} to the erosion/accretion around submerged impermeable breakwaters (see also Fig. 2.33):

$$\chi_0 = \left[\frac{H_{si}}{h}\right]^2 \left[\frac{B}{L_p}\right]^{0.5} \qquad 5.6$$

Where h, H_{si} and L_p are respectively the total water depth, incident significant wave height and wave length (related to peak period) at the breakwater location Postacchini et al. (2016) stated that the parameter χ_0 given by Eq 5.6 can usefully describe the relation between erosion/accretion and wave energy dissipation over the impermeable submerged breakwater. However, the parameter χ_0 has two main limitations in terms of the effect of breakwater porosity and submergence:

I. The parameter χ_0 does not account for the relative submergence R_c/H_{rmsi} which strongly affects breaking induced dissipation in the presence of submerged breakwaters, and thus their hydraulic performance.
II. The parameter χ_0 does not account for the breakwater porosity.

Based on limitations stated by I and II, and because the effect of breakwater porosity and submergence are the main focus of this study, the parameter χ_0 needs to be modified/extended for porous submerged breakwaters. For this purpose, the non-dimensional parameter χ is defined as follows:

$$\chi = \begin{cases} \left(\frac{R_c}{H_{rmsi}}\right)^{\alpha 1}\left(\frac{B}{L_p}\right)^{\alpha 2}\left(\frac{H_{rmso}}{h_p}\right)^{\alpha 3} & For \quad n=0 \qquad 5.7a \\ \left(\frac{R_c}{H_{rmsi}}\right)^{\alpha 1}\left(\frac{B}{L_p}\right)^{\alpha 2}\left(\frac{H_{rmso}}{h_p}\right)^{\alpha 3} F(n) & For \quad n\neq 0 \qquad 5.7b \end{cases}$$

Where $\alpha 1$, $\alpha 2$ and $\alpha 3$ are constant coefficients which respectively depend on the relative importance of dimensionless submergence (R_c/H_{rmsi}), relative crest width (B/L_p) and relative location depth h_p/H_{rmso} for the beach erosion and protective efficacy of the submerged breakwater. The function also F(n) accounts for the effects of the breakwater porosity.

The parameters $\alpha 1$ and $\alpha 2$ are selected in analogy with the parameter χ_0 (see the similarity between χ_0 and χ) which is suggested by Postacchini et al. (2016) and is expressed by Eq. 5.6. Accordingly:

- The absolute value of $\alpha 1$ is selected to be 2 and its sign is selected to be positive (see the similarity between the first terms in χ_0 and χ)

- The absolute value of $\alpha 2$ is selected to be 0.5 (see the similarity between the second terms in χ_0 and χ) and the sign is selected to be negative in order to show that the effect of B/L_p is opposite to the effect of R_c/H_{rmsi} and make the parameter χ more physically meaningful

  Finally, the value of the only remaining parameter, i.e. $\alpha 3$ is obtained by trial and error, resulting in $\alpha 1=2$, $\alpha 2=-0.5$ and $\alpha 3=1.5$, for impermeable structures (n=0). The variation of the erosion parameter e_p versus the non-dimensional design parameter χ can be well described by a smooth indicative curve for each value of the relative crest width B/L_p (see Fig. 5.3)

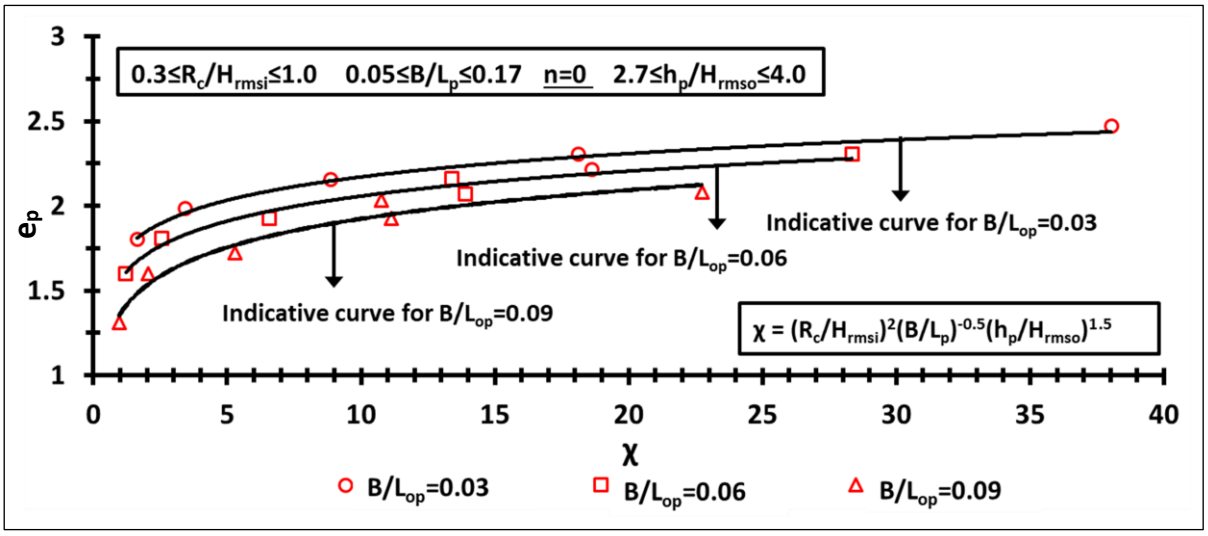

Fig 5.3: Variation of erosion parameter e_P from numerical tests for an impermeable structure (n=0) in Table 5.2 versus non-dimensional parameter χ from Eq 5.7 for $\alpha 1$=2, $\alpha 2$=-0.5 and $\alpha 3$=1.5

As suggested by Eq. 5.6, two classes of non-dimensional design parameter χ exist, one for porous (n≠0) and the other one for impermeable breakwaters (n=0). It is clear that, the trend of variations of erosion parameter e_P has to be the same for both classes of design parameter χ defined for n=0 and n≠0, otherwise it would not be possible to expresses the function ψ (see Eq. 5.5) using a unique functional relationship. As shown by Fig. 5.3, for impermeable breakwaters (n=0), the increase of the design parameter χ leads to the increase of the erosion parameter e_P. Thus the function F(n) must be defined so that, for porous breakwater (0.3≤n≤0.6), the increase of design parameter χ leads to higher values of erosion parameter e_P. Accordingly, the following relationship is proposed for the function F(n):

$$F(n) = e^n - 1 \quad for \quad 0.3 \le n \le 0.6 \qquad 5.8$$

The properties of F(n) outlined below justify the use of the function expressed by Eq. 5.8 to account for the effect of porosity:

- For a given breakwater configuration defined by R_c, B and h_P within the range of examined porosities (n=0 and 0.3≤n≤0.6), an impermeable structure (n=0) results in higher values of design parameter χ, which are expected to result in higher values of erosion parameter e_P (see Fig. 5.3). This agrees with the expected dissipative effect of porosity which results in lower transmitted wave energy behind the porous breakwater (e.g. Losada et al., 1997), compared to the impermeable breakwater with the same other design parameters subjected to the same wave conditions '

- For porous breakwaters (0.3≤n≤0.6), the increase of porosity leads to the increase of the design parameter χ, which is expected to induce an increase of erosion parameter e_P (see Fig. 5.4). This behaviour also agrees with the increase of transmitted wave energy with higher breakwater porosity, resulting in higher erosion.

Based on these properties of function F(n), the variation of erosion parameter e_P against design parameter χ reflects the effect of porosity variation on the transmitted wave energy and thus on the erosion of the protected beach.

Inserting the function F(n) from Eq 5.8 in Eq 5.7 yields Eq. 5.9 for the non-dimensional design parameter χ which can be used to analyse the relation between erosion parameter e_P and the parameters n, R_c, B and h_P of the porous submerged breakwater:

$$\chi = \begin{cases} \left(\frac{R_c}{H_{rmsi}}\right)^2 \left(\frac{B}{L_p}\right)^{-0.5} \left(\frac{H_{rmso}}{h_p}\right)^{1.5} & For \quad n = 0 \qquad 5.9a \\ \left(\frac{R_c}{H_{rmsi}}\right)^2 \left(\frac{B}{L_p}\right)^{-0.5} \left(\frac{H_{rmso}}{h_p}\right)^{1.5} \left[e^n - 1\right] & For \quad 0.3 \le n \le 0.6 \qquad 5.9b \end{cases}$$

The variations of erosion parameter $\mathbf{e_P}$ against the design parameter χ are presented in Fig. 5.4:

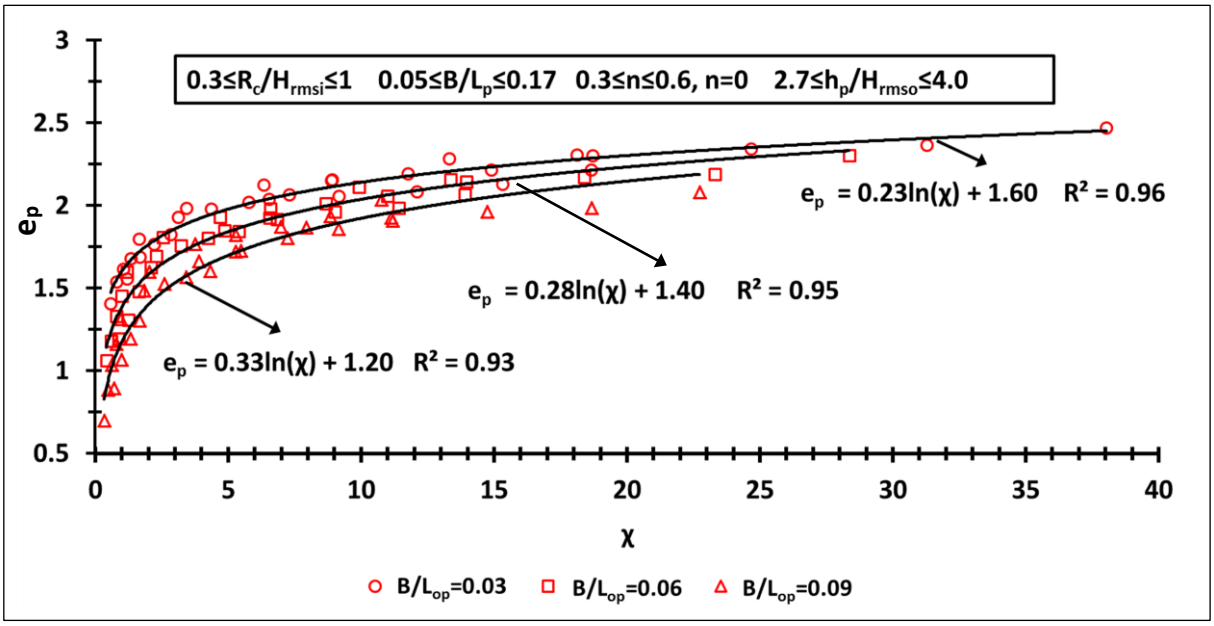

Fig 5.4: Erosion parameter e_P from numerical tests (Table 5.2) versus design parameter χ from Eq. 5.9

As shown by Fig 5.4, for each value of the relative crest width (B/L_{op}=0.03, B/L_{op}=0.06 and B/L_{op}=0.09 with L_{op} = deep water wave length) a curve, best-fitted by the following logarithmic function, is obtained:

$$e_p = Y \times Ln(\chi) + Z \qquad 5.10$$

where coefficients Y and Z depend on the relative crest width B/L_{op}. The values of Y and Z providing the best fit for each for the three B/L_{op} values as well as the associated coefficient of determination (R^2) are summarized in Table 5.3.

Table 5.3: Coefficients Y and Z of the logarithmic best fit function in Eq 5.10

Relative crest width	Y	Z	R^2
B/L_{op}=0.03	0.23	1.60	0.96
B/L_{op}=0.06	0.28	1.40	0.95
B/L_{op}=0.09	0.33	1.20	0.93

Based on the B/L_{op} values in Table 5.3, a linear relationship between coefficients Y and Z, and parameter B/L_{op} is proposed which is valid for $0.03 \le B/L_{op} \le 0.09$:

$$Y = 1.67\frac{B}{L_{op}} + 0.18 \qquad 5.11a \qquad 0.03 \le \frac{B}{L_{op}} \le 0.09$$

$$Z = -6.50\frac{B}{L_{op}} + 1.84 \qquad 5.11b$$

Introducing the Eqs 5.11a and 5.11b into Eq 5.10 yields

Impermeable Breakwaters 5.12a

$$e_p = \left[1.67\frac{B}{L_{op}} + 0.18\right] \times Ln\left[\frac{\left(\frac{R_c}{H_{rmsi}}\right)^2 \left(\frac{H_{rmso}}{h_p}\right)^{1.5}}{\left(\frac{B}{L_p}\right)^{0.5}}\right] + \left[-6.50\frac{B}{L_{op}} + 1.84\right] \quad For \quad n = 0$$

Porous Breakwaters 5.12b

$$e_p = \left[1.67\frac{B}{L_{op}} + 0.18\right] \times Ln\left[\frac{\left(\frac{R_c}{H_{rmsi}}\right)^2 \left(\frac{H_{rmso}}{h_p}\right)^{1.5} \left[e^n - 1\right]}{\left(\frac{B}{L_p}\right)^{0.5}}\right] + \left[-6.50\frac{B}{L_{op}} + 1.84\right] \quad For \quad 0.3 \le n \le 0.6$$

Based on Eqs. 5.10 and 5.12, the parameter Y and Z could be interpreted as:

- Parameter Y may be interpreted as the parameter that quantitatively describes the importance of the effect of design parameter χ on the erosion parameter e_p. Thus, from a physical point of view, Y is expected to constantly increase with the increase of B/L_{op}, because changing the structure design parameter in breakwaters with wider crests (and consequently larger size of breakwater body) is expected to have more pronounced effect on wave transmission and thus on beach erosion. Therefore:

  $Y \rightarrow \infty$ For $B/L_{op} \rightarrow \infty$ (see Eq 5.12a) is physically meaningful

- Parameter Z may be interpreted as the value of erosion parameter e_p for χ=1. With a constant value of χ=1, the increase of crest width would require the increase of R_c/H_{rmsi} and/or the increase of porosity n (For 0.3<n<0.6). From the physical point of view, the former reduces erosion while the latter increases erosion and the resultant effect is not clear. Thus:

Z→-∞ For $B/L_{op}\rightarrow\infty$, (see Eqs 5.10b) is not physically meaningful,

It should be noted that, for $\boldsymbol{B/L_{op}\rightarrow 0}$, although bounded, Y and Z does not also show physically meaningful tendency. Therefore, the validity range for Eqs 5.1 which expresses Y and Z in terms of B/L_{op} is expressed as $0.03<B/L_{op}<0.09$. Eq 5.12a can be utilized to evaluate the effect of the most relevant structure parameters on the efficacy of an impermeable submerged breakwater to protect beach against erosion while Eq. 5.12b accounts in addition for the effect of the breakwater porosity on this efficacy. Fig. 5.5 shows the scatter plot of the protection index $p_i = 1/e_p$ predicted by Eqs. 5.12a & 5.12b, and p_i obtained from the numerical tests.

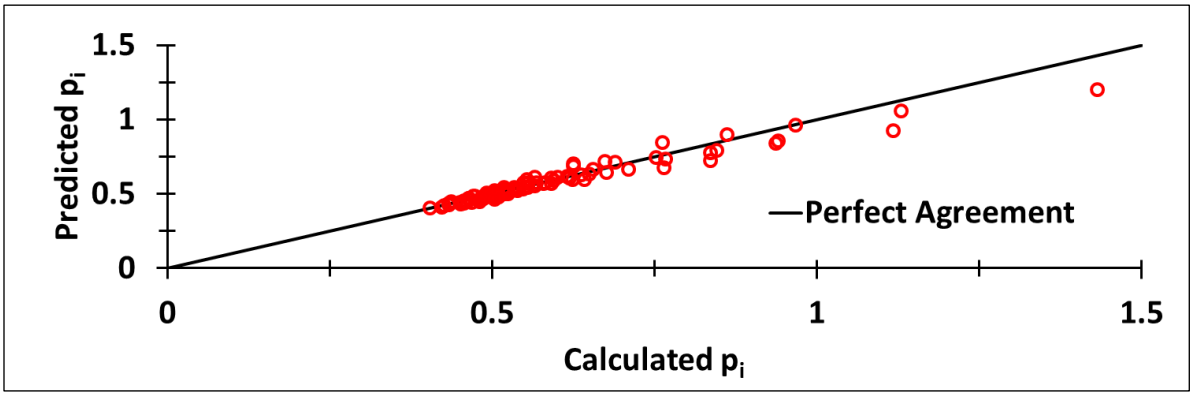

Fig 5.5: Scatter plot of predicted protection index p_i by Eqs. 5.12a & 5.12b against obtained p_i from the numerical tests

The calculated coefficient of determination (R^2=0.96) suggests a close agreement between the results of the numerical parameter study and those obtained from Eqs. 5.12a & 5.12b

Based on the results of parameter study, the variation of the protection index $p_i=(e_p)^{-1}$ is plotted against the design parameter χ in Figs. 5.6a, 5.6b and 5.6c respectively for a relative crest width B/L_{op}=0.03, B/L_{op}=0.06 and B/L_{op}=0.09. The corresponding logarithmic best fit function with the associated determination coefficient R^2 are also provided.

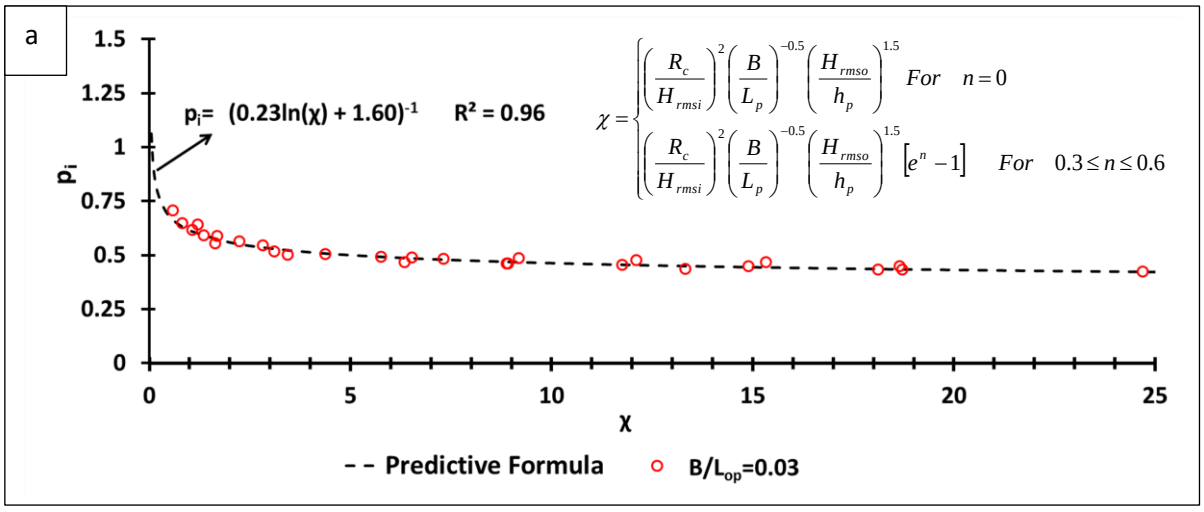

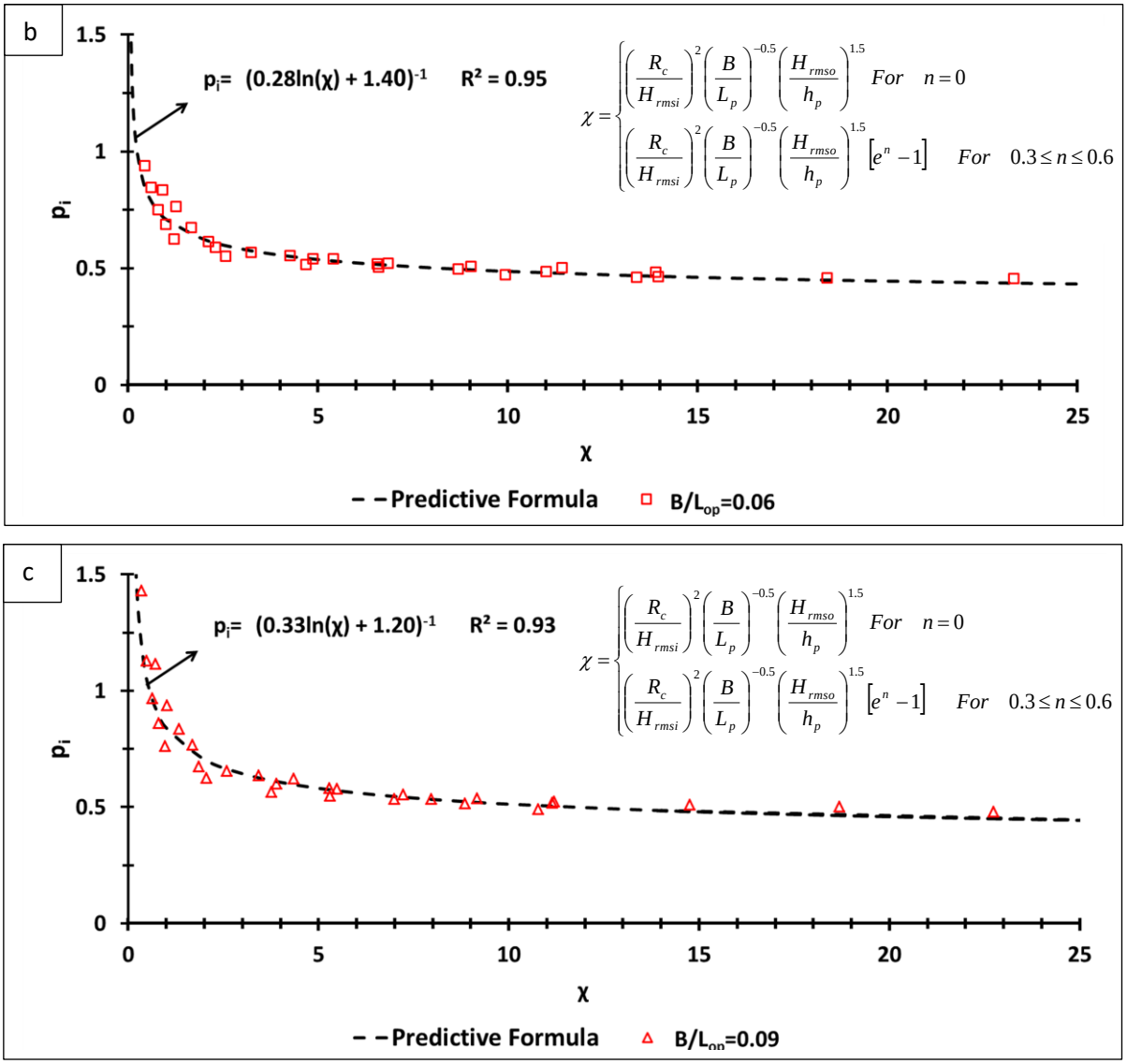

Fig 5.6: Protection index p_i against design parameter χ (see Eqs 5.7a and 5,7b for impermeable and porous breakwaters respectively) for relative crest width a) B/L_{op} =0.03, b) B/L_{op} =0.06 and c) B/L_{op} =0.09

Figs. 5.6 also show that, in general, with the increase of the design parameter χ, the protective efficacy of the breakwater tends to zero:

$$\chi \to \infty \Rightarrow p_i \to 0 \qquad 5.14$$

Based on the mathematical expression of design parameter χ given by Eq 5.9 and the condition sated by Eq 5.15, for infinitely submerged and infinitely narrow crested submerged breakwater p_i tends to zero:

$$\left[\frac{R_c}{H_{rmsi}}\right] \to \infty \Rightarrow \chi \to \infty \Rightarrow p_i \to 0 \qquad 5.15a$$

$$\left[\frac{B}{L_p}\right] \to 0 \Rightarrow \chi \to \infty \Rightarrow p_i \to 0 \qquad 5.15b$$

Eqs 5.15a and 5.15b express that no protective efficacy exists for infinitely submerged and infinitely narrow crested submerged breakwaters. In spite of physically meaningful tendency of parameter $p_i=(e_p)^{-1}$ for $B/L_p\rightarrow 0$ and $R_c/H_{rmsi}\rightarrow\infty$ (see Eqs. 5.15), p_i does not not have a physically meaningful behaviour for $B/L_p\rightarrow\infty$ and $R_c/H_{rmsi}\rightarrow 0$. However, Eqs 5.12a ane 5.12b are very well bounded within the validity range of the examined parameters (see Fig. 5.4).

Now, with a relatively good functional relationship in hand, the effect of various breakwater design parameters (i.e. porosity n, submergence R_c, crest width B and location depth h_p) on the erosion of the protected beach expressed by e_p and on the protective efficacy of submerged breakwater expressed by p_i ($p_i= 1/e_p$) can be analysed. For the rest of this study, however, only the protection index p_i will be considered as it simply represents more engineering relevance to the design of submerged breakwaters in coastal protection systems.

5.2.1 Effect of breakwater porosity

In order to analyse the effect of breakwater porosity on the erosion of the protected beach and on the protective efficacy of submerged breakwaters, for each breakwater configuration with a given R_c, B and h_p, five values of the breakwater porosity are examined: n=0 (impermeable), n=0.3, n=0.4, n=0.5.and n=0.6. The porosity range of 0<n<0.3 is not considered in this study because:

- In practical coastal engineering problems, the values of structure porosity varies between n=0.3 and n=0.6 (Karim et al., 2009).
- As elaborated in section 3.3.3, the applicability of the new developed WTC (Eq. 3.28) to porosity 0<n<0.3 is questionable. Accordingly, all results obtained by applying the new wave transmission formula to submerged breakwaters with 0<n<0.3 become questionable

The variations of protection index p_i against breakwater porosity n for all examined values of B/L_{op}= {0.03, 0.06, 0.09} are shown by Figs. 5.7a-c and Figs. 5.8a-c respectively for h_p/H_{rmso}=2.7 and h_p/H_{rmso}=4.0.

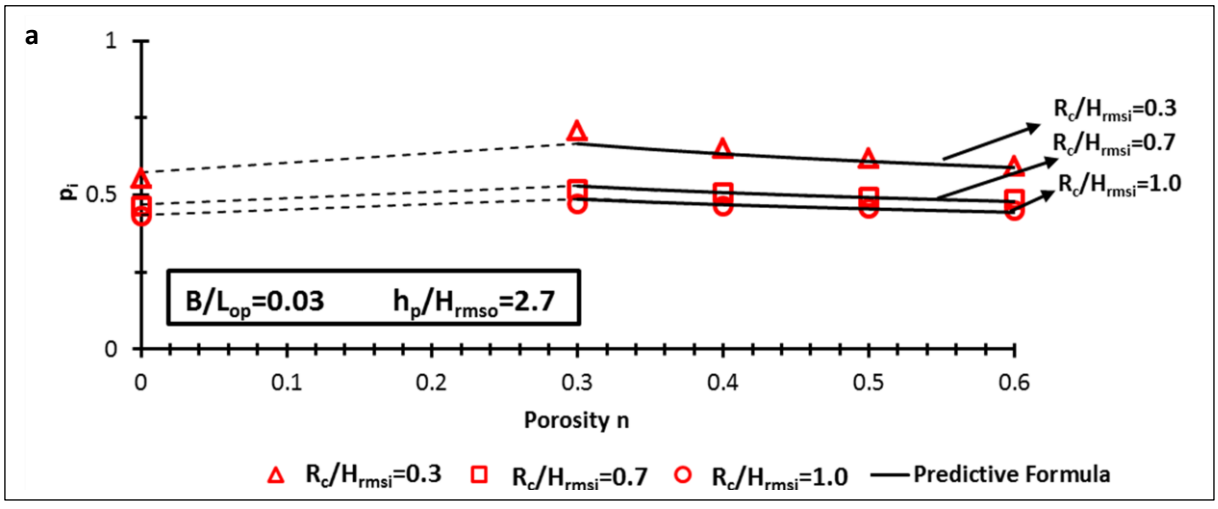

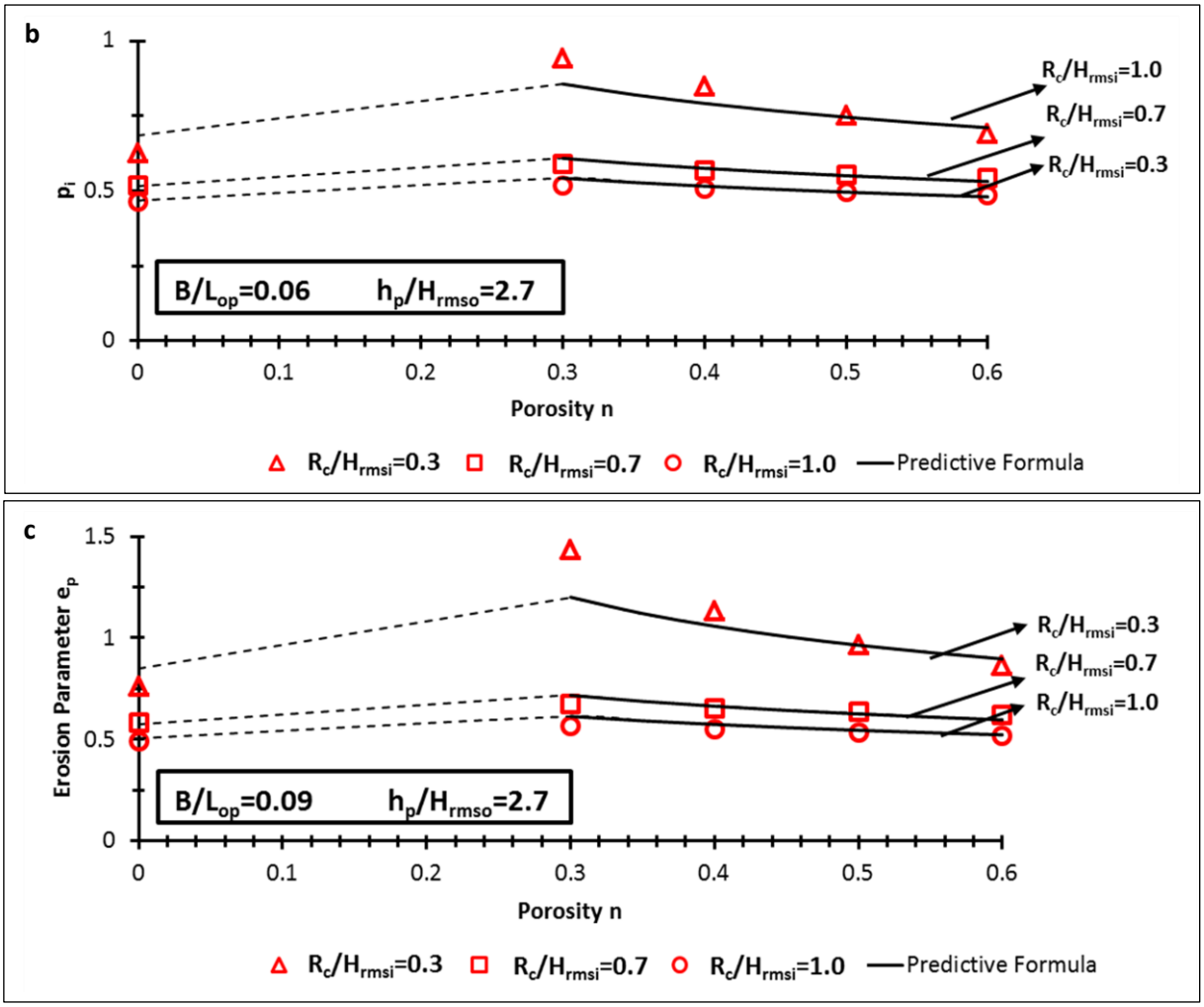

Fig 5.7: Variations of protection index p_i versus breakwater porosity n for h_p/H_{rmso}=2.7 with a) B/L_{op}=0.03, b) B/L_{op} =0.06 and c) B/L_{op} =0.09 Red dots and black lines respectively represent the numerical results and predictive equation Eqs. 5.12

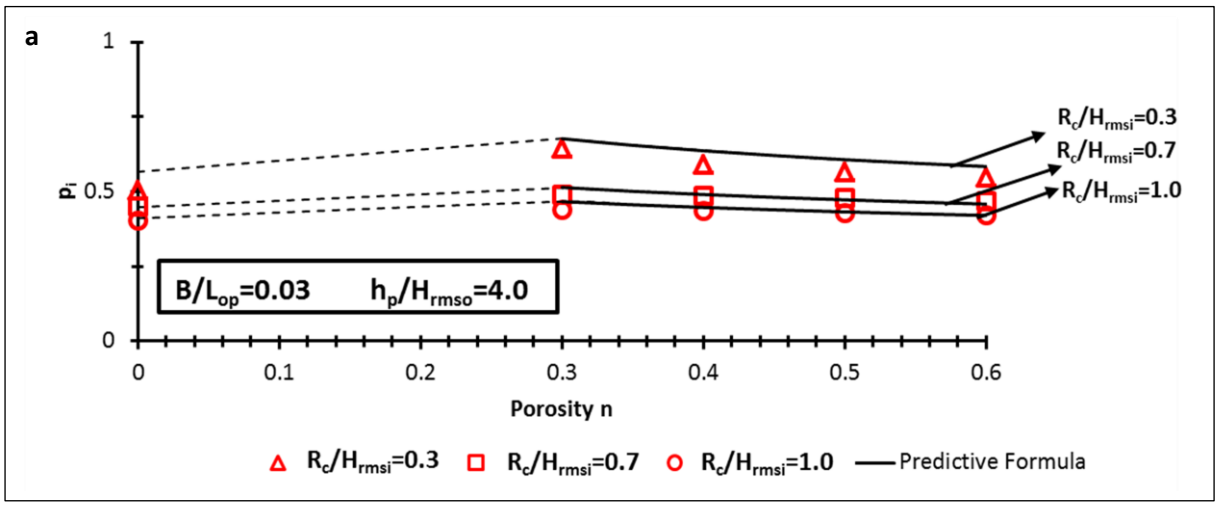

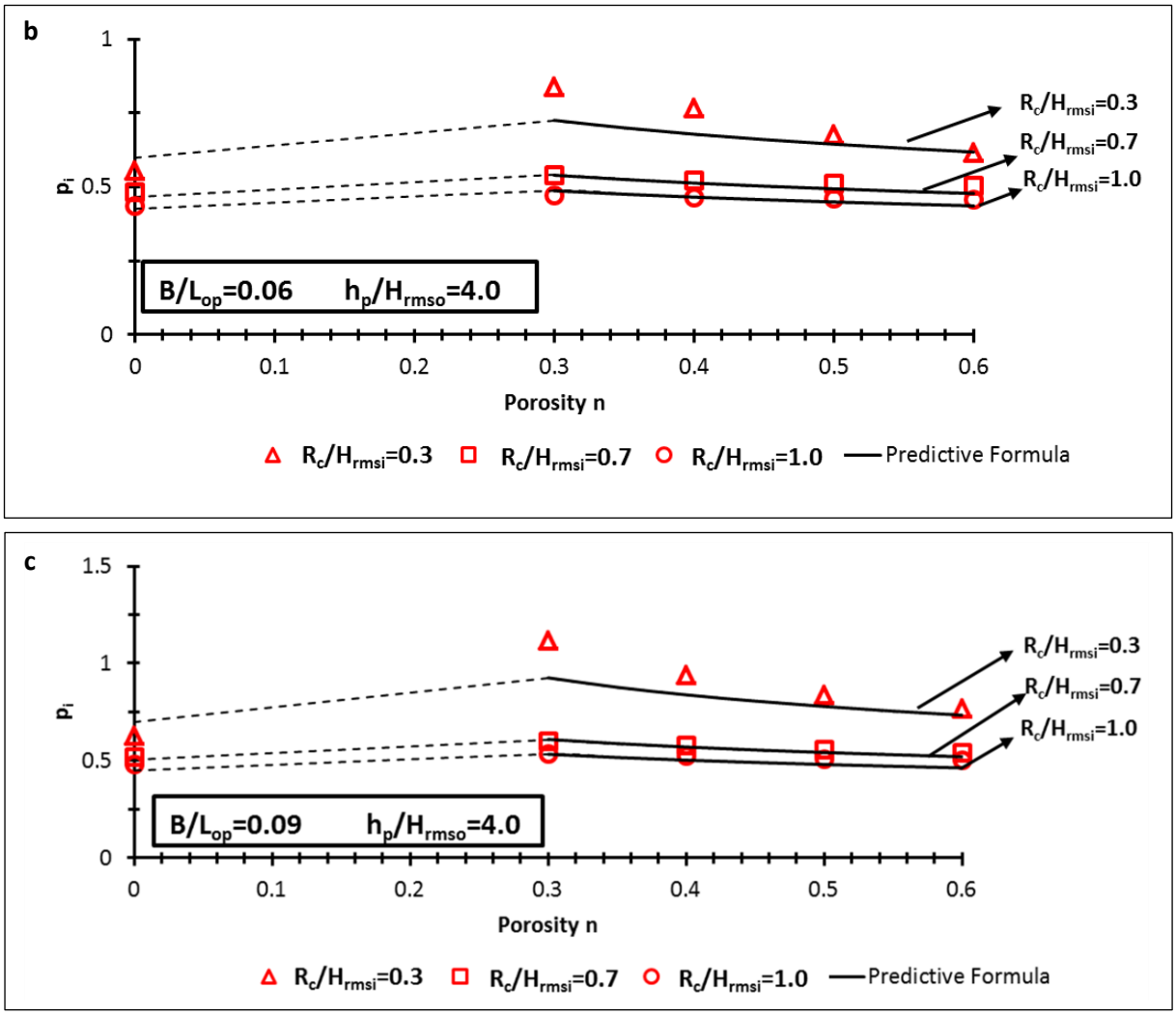

Fig 5.8: Variations of protection index p_i versus breakwater porosity n for h_p/H_{rmso}=4.0 with a) B/L_{op}=0.03, b) B/L_{op} =0.06 and c) B/L_{op} =0.09 Red dots and black lines respective represent the numerical results and predictive equation Eqs. 5.12

As shown in Figs. 5.7a-5.7c and Figs. 5.8a-5.8c, for each given relative crest width B/L_{op} and relative location depth h_p/H_{rmso}, the existing data are divided into three categories, each corresponds to one of the three relative submergences R_c/H_{rmsi} examined in this study. Solid black lines, which are shown in in Figs. 5.7a-5.7c and Figs. 5.8a-5.8c, represent the predictive formula expressed by Eq. 5.12b for $0.3 \le n \le 0.6$, while the dashed lines connect the values calculated by the predictive formula Eq. 5.12a for n=0 (impermeable breakwater) and by Eq. 5.12b for n=0.3. The close agreement between the results of the predictive formulae (Eqs. 5.12a & 5.12b) and the results of the parameter study in Figs. 5.7 and 5.8, is expected as suggested by the high determination coefficient (R^2=0.96, see Fig. 5.5).

Data points plotted in Figs. 5.7 and 5.8 show that, although the increase of breakwater porosity from n=0.3 to n=0.6 decreases protection index p_i for a given breakwater configuration (i.e. R_c, B, h_p), n=0 (impermeable breakwater) yields the minimum p_i. This implies that, for a given breakwater configuration (i.e. R_c, B, h_p), the use of a porous structure with n=0.3-0.6 instead of an impermeable structure (n=0) would result in the increase of the protective efficacy of the submerged breakwater, and thus in the decrease of the protected beach erosion. The mitigation of the erosion of the protected beach by using a porous structure might be attributed to the mitigation of the transmitted wave energy due

to the dissipative effects of the porous material, as it is represented by the new WTC formula (Eq. 3.28) developed and applied in this study and reported by the previous laboratory studies (e.g. Losada et al., 1997 and Ting et al., 2004) described in section 2.2.1.

The other possibility that ***might*** result in the mitigation of the beach erosion is the possible reduction of the wave set-up due to offshore directed filtration flow through the porous breakwater (see section2.1.1). However, this process ***is not*** considered in this study (see also Fig. 2.5)

Moreover, the decrease of protection index p_i for a porosity increase from n=0.3 to n=0.6, also agrees with the increase of transmitted wave energy in the protected beach due to the increase of porosity from n=0.3 to n=0.6.

Based on the above discussion, for a given submerged breakwater configuration, using a porous structure with n=0.3-0.6 instead of impermeable structure (n=0) enhances the protective efficacy of the breakwater and thus mitigates the erosion of the protected beach. In order to quantitatively evaluate the enhancement of protective efficacy of a given submerged breakwater configuration (i.e. R_c, B, h_p) induced by porosity n, the Enhancement Factor EF is defined:

$$EF(n)=\left[1-\frac{p_i(n=0)}{p_i(n)}\right]\times 100 \qquad 5.16$$

where $p_i = (e_p)^{-1}$ is the protection index of the breakwater, and EF(n) expresses the relative difference between $p_i(n)$ and $p_i(n=0)$ in %. The parameters $p_i(n)$ and $p_i(n=0)$ respectively represent the protection index of a given breakwater configuration with porosity n≠0 and porosity n=0 (impermeable). In fact, the enhancement factor EF(n) provides a quantitative measure of the improvement of the protective efficacy by adding porosity n in a given submerged breakwater configuration.

Based on the existing data presented in Figs. 5.7 and 5.8, for a given breakwater configuration, the Protection Index p_i becomes respectively maximum and minimum for porosity values of n=0.3 and n=0 (impermeable). This implies that, for a given configuration, n=0 results in minimum p_i while n=0.3 results in maximum p_i. Thus, the enhancement factor EF(n) for n=0.3, i.e. EF(n=0.3), is termed as the maximum achievable enhancement factor associated with a given breakwater configuration, because EF(n=0.3) is the maximum enhancement factor that could be obtained through using porous materials with n=0.3-0.6 (i.e. practical range in coastal engineering) in a given breakwater configuration (see Eq 5.16). It should be noted that, as mentioned before, the range 0<n<0.3 is not possible to be considered because due to adequate data the wave transmission results are hard to interpret for 0<n<0.3.

From the physical point of view, in impermeable submerged breakwaters (n=0) no dissipation inside and no transmission through the breakwater occurs. When the structure becomes porous, both dissipation inside and transmission through the breakwater exist. However, as can be observed in the results of parameter study on wave transmission in section 3.3.3, for porous structures with n=0.3-0.6, wave energy dissipation dominates and consequently wave transmission is lower compared to that obtained for impermeable condition (n=0). Due to the increase of porosity from n=0.3 to n=0.6, more wave energy transmitted through the breakwater and less energy is dissipated inside the breakwater, resulting in the increase of wave transmission with the increase of porosity. (This is also observed the parameter study on wave transmission presented in section 3.3.3)

In other word, on the basis of the existing data, enhancement factor EF(n) provides a quantitative measure to evaluate the maximum enhancement of the efficiency of a given submerged breakwater configuration for n=0.3, which could be made through the use of porous structures instead of impermeable structures.

The results of the parameter study presented in Figs. 5.7 and 5.8 can be further analysed to obtain a predictive formula which expresses the enhancement factor EF(n=0.3) as a function of breakwater configuration parameters (i.e. R_c,B,h_p). As discussed before, the enhancement of the breakwater protective efficacy by making the structure porous is the result of dissipative effects induced by the porosity, which itself depends on the relative submergence R_c/H_{rmsi} and relative crest width B/L_p. Therefore, it is reasonable to assume that the maximum enhancement factor, i.e. EF(n=0.3), can be expressed as a function of relative submergence R_c/H_{rmsi} and relative crest width B/L_p. In order to define a dimensionless parameter through which the maximum enhancement factor EF(n=0.3) could be related to the breakwater configuration, the dimensionless design parameter λ is defined:

$$\lambda = \frac{\left(R_c / H_{rmsi}\right)^2}{B / L_p} \qquad 5.17$$

The variation of the maximum enhancement factor EF(n=0.3), which is calculated in percent as expressed by Eq. 5.18, against the parameter λ is shown by the Fig. 5.9 where the relative submergence and relative crest width associated with the highest values of EF(n=30) are given inside the text box labelled by Max:

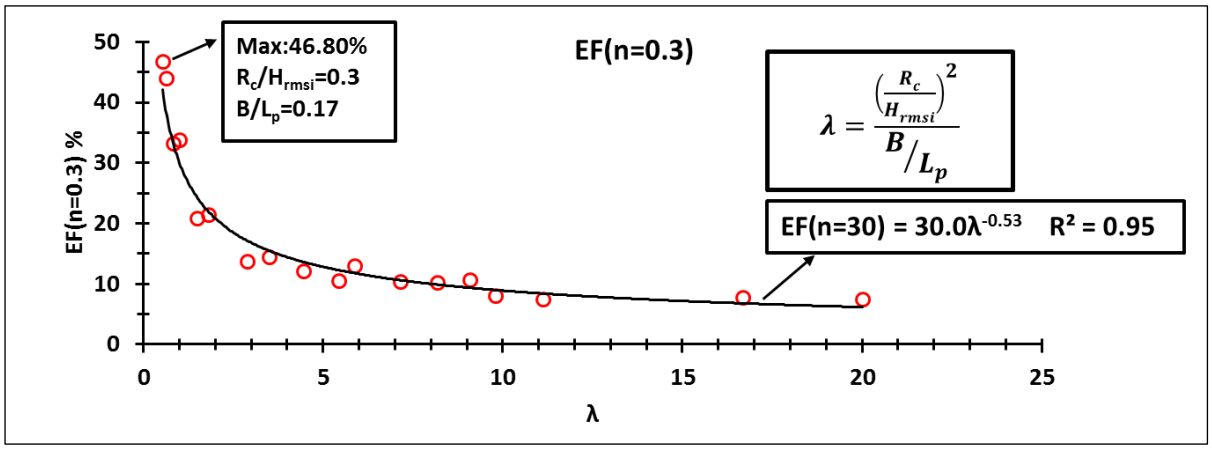

Fig 5.9: Maximum enhancement factor EF induced by breakwater porosity n=0.3 versus parameter λ

The best fitting curve to the data points, which is obtained through regression analysis as shown in Fig. 5.9, is expressed by Eq 5.18:

$$EF(n=0.3) = 30 \times \left[\frac{\left(R_c / H_{rmsi}\right)^2}{B / L_p}\right]^{-0.53} \qquad R^2 = 0.95 \qquad 5.18$$

$$For \quad 0.08 \le \frac{B}{L_p} \le 0.28 \qquad 0.3 \le \frac{R_c}{H_{rmsi}} \le 1.0$$

Data points presented in Fig. 5.9 shows that the maximum value of EF(n=0.3) is 46.8% for which relative submergences are respectively R_c/H_{rmsi} =0.3. The predictive formula given by Eq. 5.18 suggests that, for extremely high submergence ($R_c/H_{rmsi} \rightarrow \infty$) or narrow crest width ($B/L_p \rightarrow 0$), EF(n=0.3) tends to zero. This is a physically meaningful behaviour of Eq. 5.18 when $\lambda \rightarrow \infty$, implying that in highly submerged or extremely narrow crested configurations, structure porosity does not enhance the protective efficacy of submerged breakwaters. The variation trend of the data points in Fig. 5.8 suggests that, with the increase of parameter $\lambda=(R_c/H_{rmsi})^2(B/L_p)^{-1.0}$, the rate of change of EF(n=0.3) becomes lower. This point could be expressed as:

$$EF(n=0.3)=30\times\lambda^{-0.53}\Rightarrow\frac{dEF(n=0.3)}{d\lambda}=-15.9\lambda^{-1.53} \qquad 5.19$$

$$\Rightarrow\frac{dEF(n=0.3)}{d\lambda}\to 0 \quad for\ \lambda\to\infty$$

Where dEF(n=0.3) and dλ stand for variations of EF(n=0.3) and $\lambda=(R_c/H_{rmsi})^2(B/L)^{-1.0}$ respectively. Eq. 5.19 implies that, with the constant increase of parameter λ, reducing the relative submergence R_c/H_{rmsi} and/or increasing the crest width B/L_p might have a negligible influence on the variation of EF(n=0.3). In this study, the condition in which the variation of EF(n=0.3) becomes less than 2% of the variation of the parameter λ, is arbitrarily selected as a reasonably defined condition in which the variation of breakwater submergence and crest width has a negligible effect on EF(n=0.3):

$$\left|\frac{dEF(n=0.3)}{d\lambda}\right|\le 2\% \qquad 5.20$$

Based on Eq. 5.19 which is obtained on the basis of the data points in Fig. 5.9, the minimum value of λ which satisfies the condition expressed by Eq. 5.20, can be calculated as follows (see Eq 5.19):

$$\left|\frac{dEF(n=0.3)}{d\lambda}\right|\le 2\%\Rightarrow 15.9\lambda^{-1.53}\le 2\%\Rightarrow\lambda\ge 3.89 \qquad 5.21$$

The solution expressed by Eq. 5.21 can be approximated as λ≥4 because the resultant criteria will be more straightforward to express mathematically (see Eq. 5.22) Thus, λ≥4 is assumed to define conditions in which the decrease of the parameter λ (equivalent to the decrease of submergence R_c/H_{rmsi} and/or increase of crest width B/L_p) has a negligible enhancing effect on the maximum enhancement of protective efficacy of submerged breakwaters, and thus on the reduction of the erosion of the protected beach due to porosity in a given breakwater configuration.

Based on the above discussion, the conditions in which the decrease of the relative submergence and/or the increase of relative crest width do not enhance noticeably the maximum reduction of the erosion of the protected beach that can be achieved by introducing porosity in a given breakwater configuration, can be obtained as follows:

$$\lambda>4\to\frac{\left[\frac{R_c}{H_{rmsi}}\right]^2}{B/L_p}>4\Rightarrow\frac{R_c}{H_{rmsi}}>2\times\sqrt{B/L_p} \qquad 5.22$$

Based on the data points plotted in Fig. 5.9 and the corresponding best fit curve given by Eq. 5.18, a critical condition, in which porosity can't efficiently enhance the protective efficacy of the breakwater, can be defined. In this study, on an arbitrary basis, the condition in which EF(n=0.3) becomes less than 10%, is selected as a condition which reasonably defines breakwater configurations in which porosity does not efficiently enhance the protective efficacy. This criterion is expressed as:

$$\lambda=\frac{\left(R_c/H_{rmsi}\right)^2}{B/L_p}>9\Leftrightarrow EF(n=0.3)<10\% \qquad 5.23$$

Eq 5.23 states that, for a given breakwater configuration, the dissipative effects of porosity can't efficiently enhance the breakwater protective efficacy for $R_c/H_{rmsi} > 3.0\ (B/L_p)^{0.5}$. Eq 5.23 is graphically shown by Fig. 5.10 where Max.EF stands for EF(n=0.3):

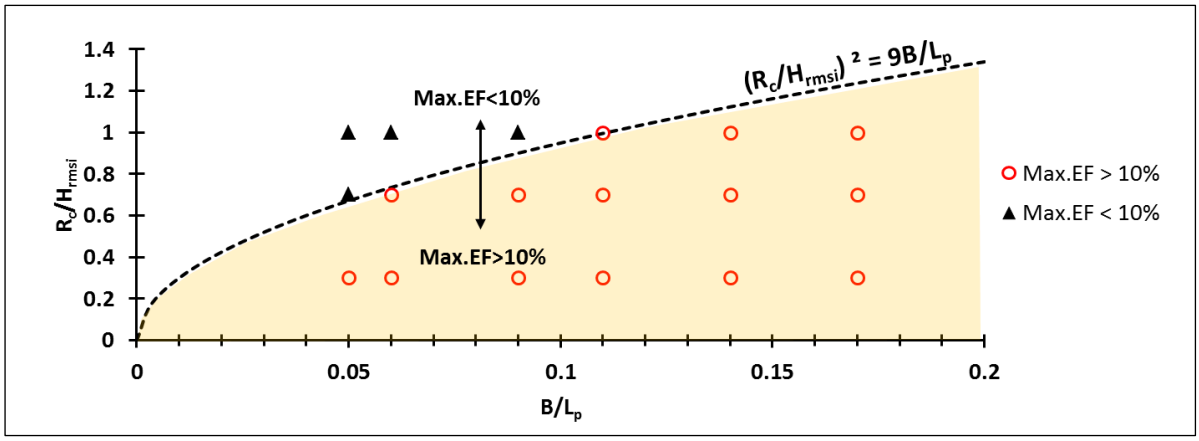

Fig 5.10: Range of structure parameters (R_c/H_{rmsi}) and B/L_p (shaded area) above which the effect of submerged breakwater porosity on the reduction of the erosion of the protected beach is negligible (Max.EF<10%)

The curve $(R_c/H_{rmsi})^2=9(B/L_p)$ plotted in the Fig. 5.10 specifies the boundary of the shaded area in the B/L_p- R_c/H_{rmsi} plane, above which the maximum enhancement of the breakwater protective efficacy due porosity, as defined by Eq. 5.18, becomes smaller than 10%. Thus, breakwater configurations with the relative submergence and relative crest width in this area, i.e. where $(R_c/H_{rmsi})^2>9(B/L_p)$, represent configurations which do not allow to make an efficient use of the dissipative effect of porosity for reducing beach erosion. For SPBs with an impermeable core similar to that used for model validation (see section 4.3), this conclusion might be conservative because this type of SPBs is expected to have a lower WTC than that in homogeneous SPBs. In other word, in porous SPBs with an impermeable core, even for $(R_c/H_{rmsi})^2>9(B/L_p)$, it might be possible to make an efficient use of the porosity to enhance the protective efficiency of submerged breakwaters.

5.2.2 Effect of Relative Breakwater Submergence

Intuitively, it could be understood that the increase of the relative breakwater submergence reduces the beach erosion leeward of the breakwater. The results of the parameter study presented in Figs. 5.7 and 5.8 also show that, for a given breakwater porosity n, relative crest width B/L_p and relative location depth h_p/H_{rmso}, the decrease of relative breakwater submergence induces an enhancement in the breakwater protective efficacy, and thus a decrease of the erosion in the protected beach leeward of the breakwater. This effect of submergence might be attributed to the decrease of transmitted wave energy, also due to the higher wave energy dissipation induced by wave breaking and porous flow inside the breakwater. Further analysis of the results reveals that:

I. In porous breakwaters, the same amount of relative submergence (R_c/H_{rmsi}) reduction causes a higher increase of protection index p_i than that in impermeable breakwaters. Therefore, in porous breakwaters, the breakwater submergence might have a stronger effect on the mitigation of the erosion of the protected beach than in impermeable breakwaters.

II. For $0.3\leq n\leq 0.6$, the increase of porosity reduces the favourable effect that submergence reduction might have on the enhancement of protection index p_i. Therefore, with the increase of porosity from n=0.3 to n=0.6, the effect of submergence on the protected beach erosion becomes weaker.

Based on results expressed in paragraphs I and II, the importance effect of the relative breakwater submergence on the mitigation of the erosion of the protected beach depends on the breakwater porosity. This may be attributed to the dissipative effect of breakwater porosity which, in addition to the wave breaking induced dissipation, results in lower transmitted wave energy, and thus in lower erosion of the protected beach. In order to consider what stated by I and II in the analysis of the submergence effects on beach erosion, the effective submergence parameter R_{ce} is introduced by rearranging the design parameter χ defined in Eq 5.9 as follows:

$$\chi = \left(\frac{R_{ce}}{H_{rmsi}}\right)^{2}\left(\frac{B}{L_p}\right)^{-0.5}\left(\frac{h_p}{H_{rmso}}\right)^{1.5} \qquad 5.24$$

$$R_{ce} = \begin{cases} R_c & For \quad n=0 \ (impermeable) \\ R_c \times \sqrt{e^n - 1} & For \quad 0.3 \le n \le 0.6 \end{cases} \qquad 5.25$$

Eq 5.24 and Eq 5.25, suggest that: i) The use of a porous structure for a given breakwater configuration (i.e. R_c, B and h_p) increases the effect of submergence on the protective efficacy of breakwaters (See also paragraph I above). ii) For a given breakwater configuration (i.e. R_c, B and h_p), the increase of porosity from n=0.3 to n=0.6 leads to higher effective submergence R_{ce}, implying to a weaker effect of submergence on protective efficacy according to paragraph II above.

Based on the discussion above, the effective submergence R_{ce}, which is introduced in Eqs 5.24 and 5.25, adequately represents the influence of breakwater porosity on the effects that breakwater submergence has on the protective efficacy of the structure, as elaborated at the beginning of this chapter (see statements I and II).

Fig 5.11 shows the protection index p_i plotted against the relative effective submergence parameter R_{ce}/H_{rmsi}. The variation of p_i against R_{ce}/H_{rmsi}, which may be quantified by the slope of the best fit line, represents the influence of the R_{ce}/H_{rms} on the performance of the breakwater in protecting the beach against erosion.

As shown in Fig. 5.11 for a given crest width B, two distinctive regions with noticeably different variations of p_i versus relative effective submergence R_{ce}/H_{rmsi} can be identified: Region with R_{ce}/H_{rmsi} <0.3 and Region with R_{ce}/H_{rmsi} >0.4. The difference between the two aforementioned regions becomes more pronounced with the increase of crest width. This effect of the crest width can be attributed to the widening of the region where energy dissipation induced by both breaking and porosity occurs.

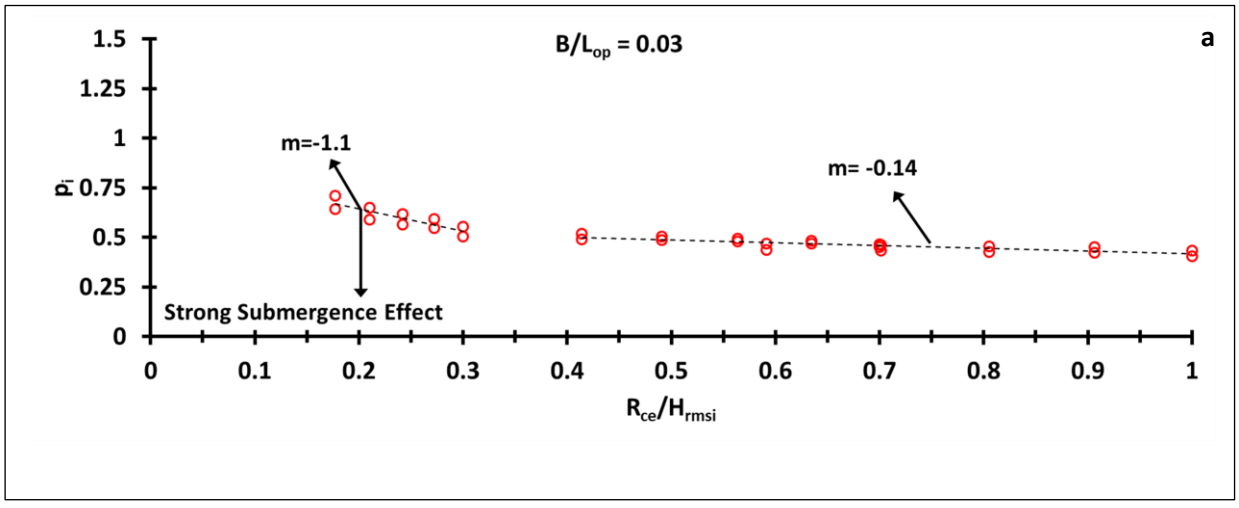

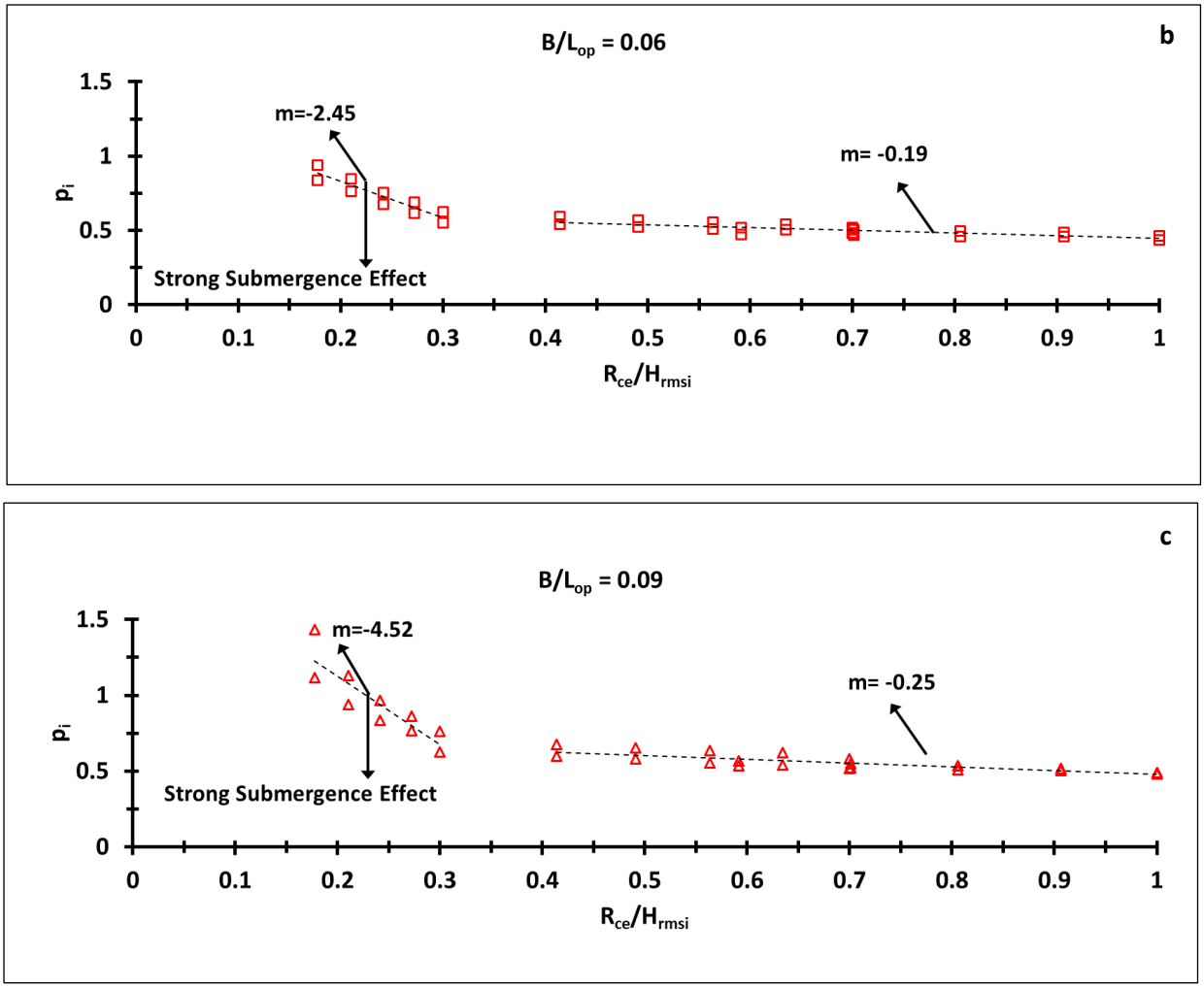

Fig 5.11: Protection index p_i against relative effective submergence R_{ce}/H_{rmsi} for relative crest width a) B/L_{op}=0.03, b) B/L_{op}=0.06 & c) B/L_{op}=0.09, where m is the slope of best fit line

The region with R_{ce}/H_{rmsi} <0.3 is characterised by a noticeably stronger influence of the effective relative submergence R_{ce}/H_{rmsi} on protective efficacy of submerged breakwaters.

This stronger effect might be due to the fact that the influence of both breaking and porosity induced dissipations becomes stronger for smaller values of relative submergence R_c/H_{rmsi}. Accordingly, the conditions for which beach erosion leeward of submerged breakwaters can effectively be reduced by the reduction of the breakwater submergence can be expressed by:

$$R_{ce} < 0.3 \times H_{rmsi} \Rightarrow \qquad 5.26$$

$$\begin{cases} \dfrac{R_c}{H_{rmsi}} < 0.3 & For \quad n = 0 \ (impermeable) \\ \dfrac{R_c}{H_{rmsi}} \times \sqrt{e^n - 1} < 0.3 & For \quad 0.3 \le n \le 0.6 \end{cases}$$

The criterion expressed by Eq 5.26 suggests that, in comparison with impermeable breakwaters, porous breakwaters might have higher relative submergence R_c/H_{rmsi}, while maintaining a strong effect of submergence on their protective efficacy and thus on the beach erosion leeward of the structure,

5.2.3 Effect of relative breakwater crest width

Intuitively, the breakwater configurations with wider crests would dissipate more wave energy and result in lower beach erosion leeward of the structure.The results of the parameter study in Figs. 5.12 also reveal that, for a given breakwater porosity n and relative submergence, the increase of the relative breakwater crest width mitigates beach erosion, as suggested by the increase of protection index p_i with increasing B/L_{op} (see Fig 5.12a to 5,12c).

This effect may be attributed to the increase of energy dissipation due to wave breaking and porous flow inside the porous breakwater with the increase of crest width. Figs. 5.12 show the variations of protection index p_i against the porosity n for different values of relative crest width B/L_p. Two indicative curves represented by dotted lines in Fig. 5.12 tentatively indicate the variation trends of p_i versus n for the considered maximum and minimum values of the relative crest width B/L_p=0.17 and B/L_p=0.05, which respectively correspond to maximum p_i and minimum p_i for a given value of the relative submergence R_c/H_{rmsi}. These two indicative curves are typical as they also describe a similar trend as those corresponding to the other intermediate B/L_p values, for which the indicative curves are not plotted to avoid unnecessary complexity of the figures.

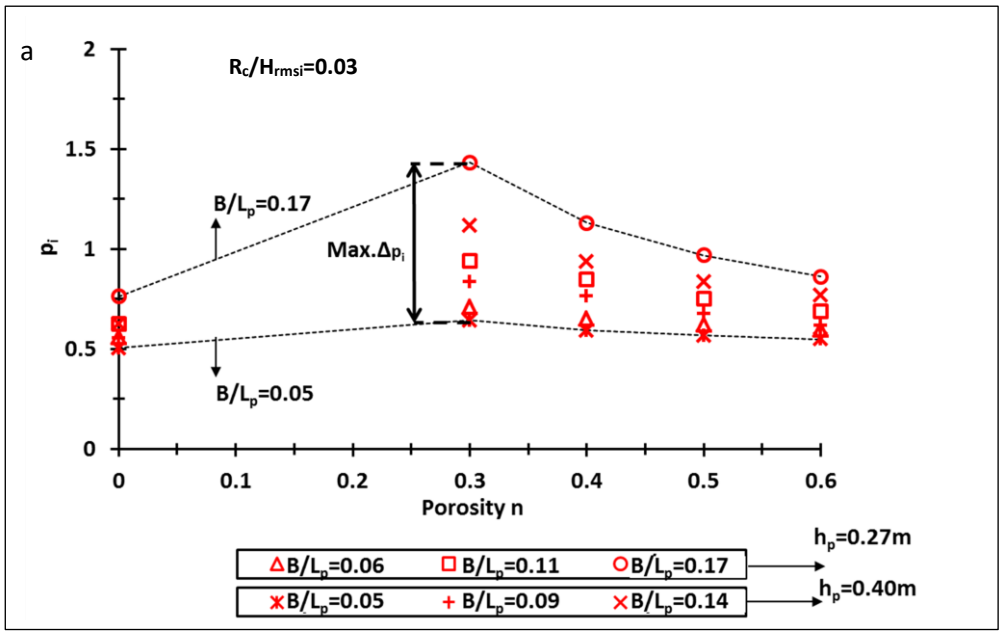

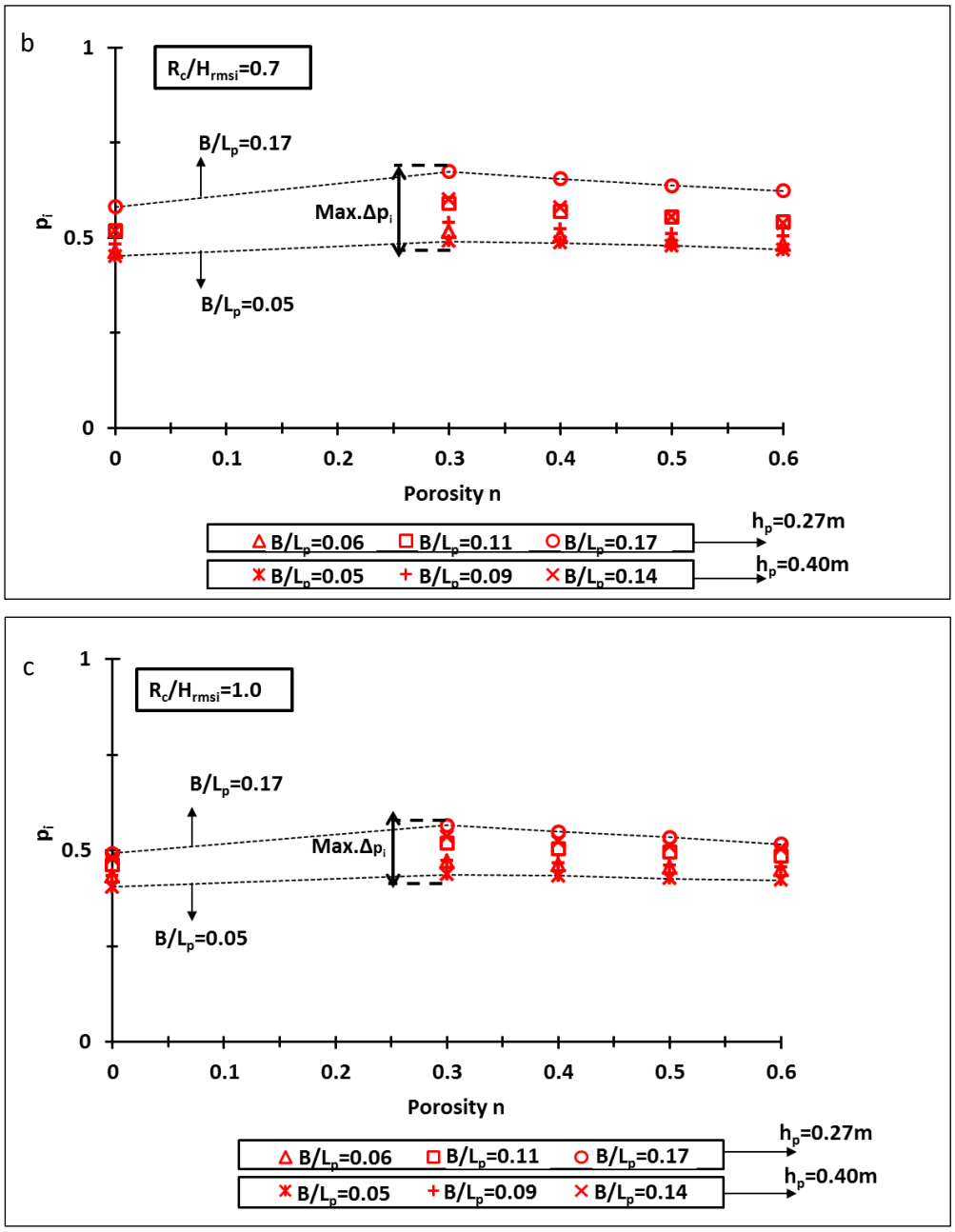

Fig 5.12: Effect of crest width on protection index p_i versus porosity n

The maximum difference between p_i for B/L_p=0.05 and B/L_p=0.17, which is represented in Figs. 5.12 by Max.Δp_i, is a measure to evaluate the maximum effect of the relative crest width on the efficacy of the breakwater to protect the beach against erosion. The following implications might be drawn from Figs. 5.12:

I. For a given breakwater submergence R_c, the effect of the relative crest width on the protective efficacy is slightly more pronounced in porous breakwaters (n=0.3-0.6), compared to that in impermeable breakwaters (n=0).

II. In porous submerged breakwaters, the effect of crest width B on the protective efficacy becomes slightly weaker with the increase of porosity n. In fact, the favourable effect of breakwater crest

width on beach erosion becomes maximum for n=0.3 (i.e. the lowest porosity value considered). This might be attributed to the fact that, the effect of porous flow dissipation on wave transmission becomes weaker with the increase of breakwater porosity (see also chapter 3).

III. The maximum effect of crest width, which is represented by Max.Δp_i, show that the effect of crest width on the protective efficacy becomes weaker with increasing relative submergence from R_c/H_{rmsi} =0.3 in Fig 5.12a to R_c/H_{rmsi} =1.0 in Fig 5.12c.

Based on the aforementioned implications, the effect of the relative crest width on the protective efficacy of the submerged breakwater, which is mainly due the energy dissipation over and inside the structure, depends also on the breakwater porosity. In order to relate the effect of the relative crest width to the breakwater porosity, the effective crest width parameter B_e is introduced by rearranging parameter χ defined in Eq 5.9:

$$\chi = \left(\frac{R_c}{H_{rmsi}}\right)^2 \left(\frac{B_e}{L_p}\right)^{-0.5} \left(\frac{h_p}{H_{rmso}}\right)^{1.5} \qquad 5.27$$

$$B_e = \begin{cases} B & For \quad n = 0 (impermeable) \\ \dfrac{B}{\left(e^n - 1\right)^2} & For \quad 0.3 \le n \le 0.6 \end{cases} \qquad 5.28$$

Eq 5.27 and Eq 5.28, suggest that, for a given breakwater submergence R_c and location water depth h_p, the breakwater porosity increases the effective crest width B_e. This might explain why the effect of crest width is more pronounced in porous breakwaters compared to that in impermeable breakwaters, as discussed before in implication I above. Moreover, based on Eq 5.28, the increase of porosity from n=0.3 to n=0.6 decreases the effective crest width B_e, implying a weaker effect of the crest width. Therefore, the effective crest width B_e, as described by Eq 5.27and 5.28, is able to reflect the effect of breakwater porosity on the effect of crest width B. The protection index $p_i = (e_p)^{-1}$ is plotted against the relative effective crest width B_e/L_p for relative submergence R_c/H_{rmsi} =0.03, R_c/H_{rmsi} =0.07 and R_c/H_{rmsi} =1.0 in Fig. 5.13a,b&c, respectively.

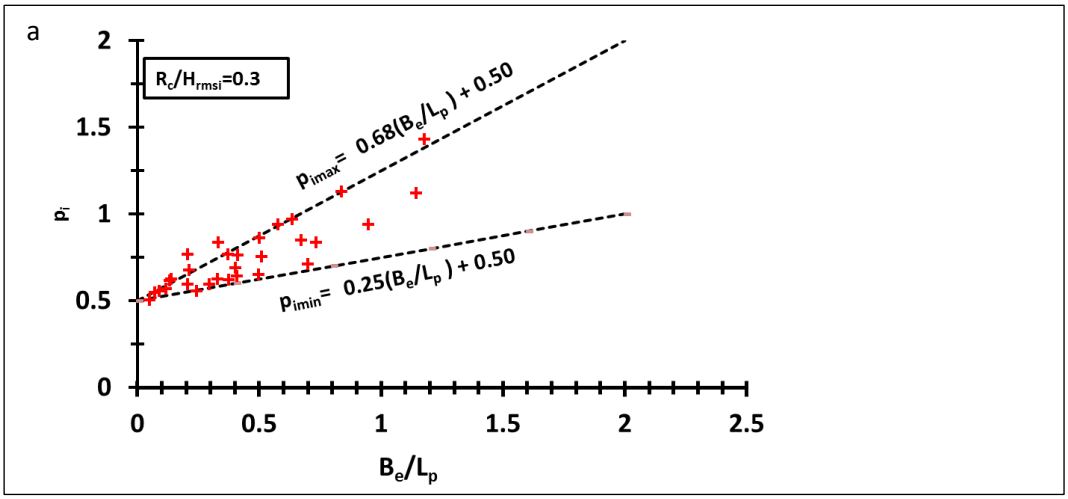

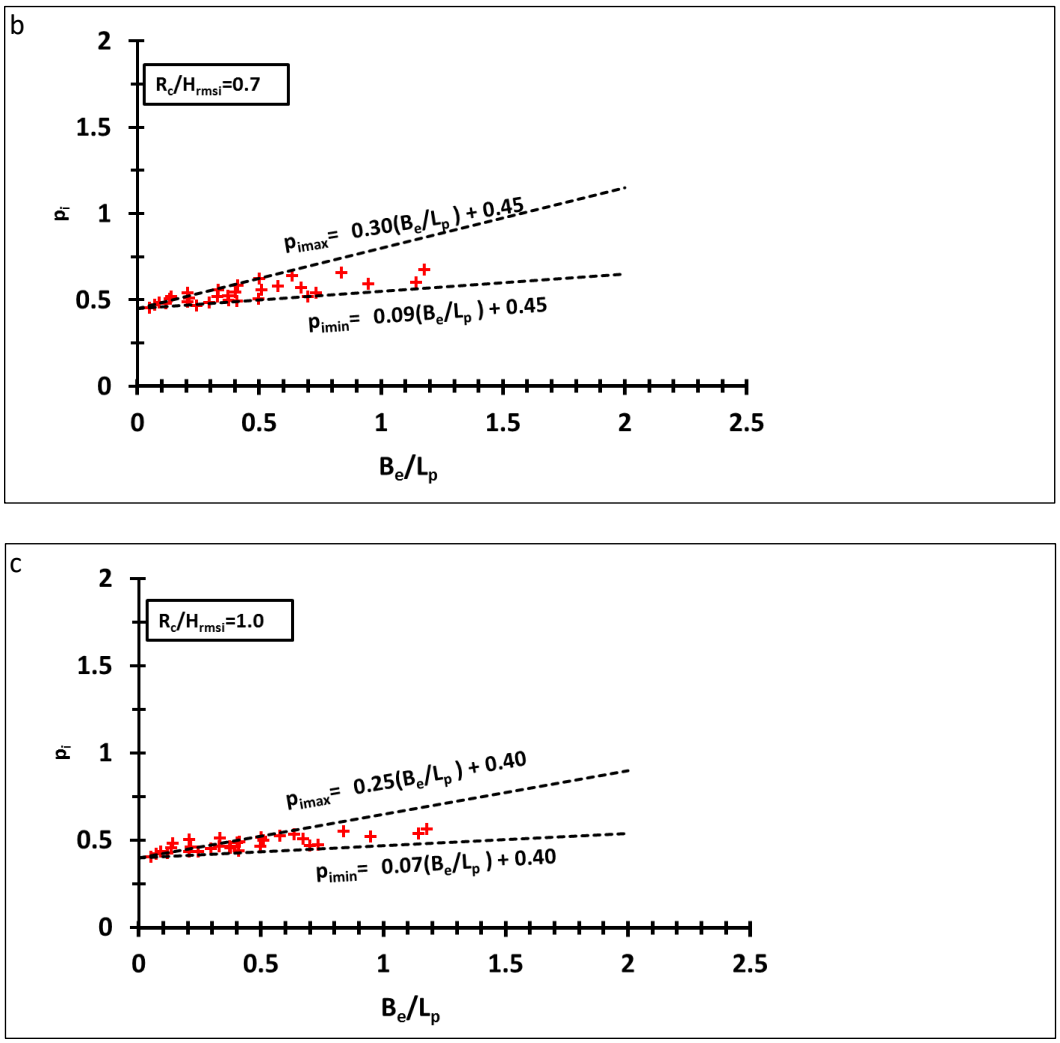

Fig 5.13: Protection index p_i against relative effective crest width B_e/L for relative breakwater submergence (a) R_c/H_{rmsi} =0.03, (b) R_c/H_{rmsi} =0.07 and (c) R_c/H_{rmsi} =1.0

As seen in Fig. 5.13, for a given relative breakwater submergence R_c/H_{rmsi}, the plotted data points are scattered inside a triangle shaped area. The upper and lower boundaries of the triangle shaped area can be approximated through fitting a straight line to the data points representing the maximum and minimum values of p_i that prevail for a given relative effective crest width B_e/L_p. The equations of the straight line approximating the maximum and minimum p_i, which are respectively represented by p_{imax} and p_{imin}, are given in Fig 5.13. The slope steepness of the regression lines (p_{imin} & p_{imax}) may represent an indicative measure for the influence of the relative effective crest width B_e/L_p on the protective efficacy of submerged breakwaters:

Table 5.4: Slope steepness of the regression lines (p_{imax} & p_{imin}) given in Fig. 5.13 for different values of relative breakwater submergence R_c/H_{rmsi}

R_c/H_{rmsi}	Steepness for Lower Boundary	Steepness for Upper Boundary
0.3	0.25	0.68
0.7	0.09	0.30
1.0	0.07	0.25

Figs. 5.13a-c and Table 5.4 show that, as mentioned before in implication III, the influence of effective crest width becomes more noticeable with decreasing values of relative submergence R_c/H_{rmsi}. Based on the ***Slope steepness*** presented by Table 5.4, the decrease of the relative submergence from $R_c/H_{rmsi}=1.0$ to $R_c/H_{rmsi}=0.7$ causes the slope of upper and lower boundaries to increase respectively by 25% and 30 %. However, with the further decrease of relative submergence from $R_c/H_{rmsi}=0.7$ to $R_c/H_{rmsi}=0.3$, the increase of the slope steepness becomes noticeably higher, i.e. 130% and 180%, respectively for upper and lower boundaries defined by p_{imax} and p_{imin} (This is almost 6 times higher than what was obtained for $0.7<R_c/H_{rmsi}<1.0$)

This trend clearly shows that, for $R_c/H_{rmsi}<0.7$, the influence of the effective crest width B_e on the protective efficacy of breakwaters noticeably increases with the decrease of relative submergence. However, for $0.7<R_c/H_{rmsi}<1.0$, reducing relative submergence does not noticeably affect the influence of effective crest width compared to what already discussed for $R_c/H_{rmsi}<0.7$. Based on the aforementioned considerations, the following criteria can be suggested to assess the importance of the relative effective crest width B_e/L_p for the efficacy of porous submerged breakwaters

$$0 < \frac{R_c}{H_{rmsi}} < 0.7 \Rightarrow \qquad 5.29a$$

Significant influence of relative submergence R_c/H_{rmsi} on the effect of relative effective crest width B_e/L_p

$$\frac{R_c}{H_{rmsi}} \geq 0.7 \Rightarrow \qquad 5.29b$$

Weak influence of relative submergence R_c/H_{rmsi} on the effect of relative effective crest width B_e/L_p

5.2.4 Effect of relative location depth

As shown by Figs. 5.12, all data points corresponding to the location depth $h_p=0.40$m represent slightly lower protection index p_i compared to those corresponding to $h_p=0.27$m. This observation complies with flume experiments reported by Lorenzoni et al (2012), where the submerged breakwaters located closer to the beach caused less erosion compared to those located farther from the beach. This effect of the location depth may be explained by larger wave length in larger water depths, resulting in a lower relative crest width B/L_p, which leads to higher transmitted wave energy in the protected area. The comparison between the data points corresponding to $h_p=0.27$m and those corresponding to $h_p=0.40$m, reveals that, although the breakwater configurations located at smaller water depth have a higher protective efficacy, for $R_c/H_{rmsi}>0.3$, the location depth h_p has a negligible effect on the protection index p_i so that data points pertain to a same breakwater geometry (i.e. R_c and B) with different breakwater location h_p are hardly distinguishable. Based on what discussed above, the conditions in which the effect of the breakwater location becomes negligible *tentatively* expressed as:

$$\frac{R_c}{H_{rmsi}} > 0.3 \qquad 5.30$$

5.2.5 Relation between Dean parameter and protective efficacy

Under certain wave and beach conditions, sand tends to move offshore, causing beach erosion (e.g. Kamphuis, 1991). The dean parameter $\Omega = \frac{H_o}{w_s \times T_p}$ is the most widely used parameter applied to predict the mode of cross-shore beach profile response to the wave condition in the open coasts. Based on the Dean parameter, many criteria have been proposed to predict the cross-shore beach response to the incident waves in the open coasts. A detailed review on these criteria is given in **C**oastal **E**ngineering **M**anual (CEM, 2006a). However, the relation between the Dean parameter and erosion of the protected beach has rarely been investigated. Lorenzoni et al (2012) showed that the Dean parameter related to transmitted waves at the onshore toe of the submerged breakwaters (see Fig. 5.1), can be used to predict the mode of beach profile response in the area protected by the submerged breakwater.

However, a functional relationship between the Dean parameter at the onshore toe of the submerged breakwater and the protective efficacy of submerged breakwaters has never been studied. Based on the results of this numerical parameter study, it is attempted to develop a predictive formula which relates the protective efficacy of the submerged breakwaters to the Dean parameter. For this purpose, the variation of protection index, $p_i = (e_p)^{-1}$, against the Dean parameter related to the transmitted waves at the onshore toe of the breakwater (see Fig. 5.1) is plotted in Fig. 5.14.

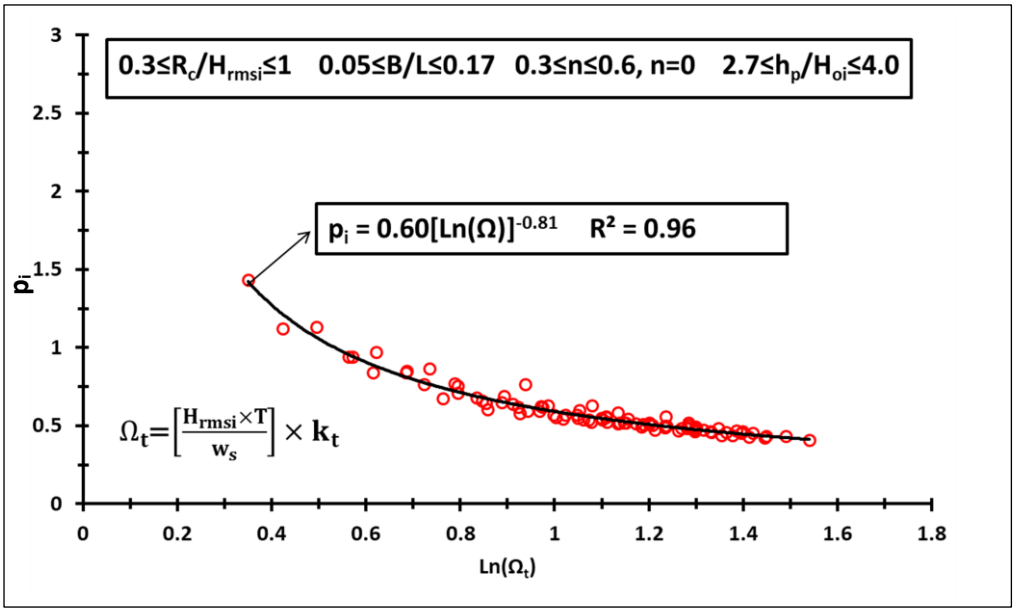

Fig 5.14: Protection index $p_i=(e_p)^{-1}$ against Dean Parameter Ω_t for transmitted waves at the onshore toe of submerged breakwaters

Based on the regression analysis, the best fit curves to the data points plotted in Fig. 5.14 could be given by Eq 5.30, for which the validity range is given in Fig 5.14:

$$p_i = 0.6 \times \left[Ln(\Omega_t)\right]^{-0.81} \qquad R^2 = 0.96 \qquad 5.30$$

$$\Omega_t = \left[\frac{H_{rmsi}}{w_s \times T_p}\right] \times k_t \qquad K_t = \frac{H_{rmst}}{H_{rmsi}}$$

Here, H_{si} and H_{st} respectively stand for the significant incident and transmitted wave height. In order to calculate the Dean Parameter Ω_t, as clearly shown in previous studies (e.g. Garcia et al., 2014), the peak period Tp is assumed to remain unhanged due to wave transmission at SPBs.

The calculated determination coefficient suggests a good agreement between Eq 5.30 and the results of the parameter study. In spite of the good agreement between the predictive formula given by Eq 5.30 and the results of the parameter study, Eq 5.30 should be applied cautiously, because in this parameter study, among all parameters influencing the Dean parameter Ω_t (i.e., sediment fall velocity w_s, incident wave height H_{rmsi}, and wave period T_p), only the transmitted wave heights are varied.

5.3 Implications for the present study

In this chapter, a systematic numerical parameter study is performed to investigate the effect of porous submerged breakwater on morphological changes of sandy beaches. The main aim of this study is to improve/extend the current knowledge of the effect of the parameters of porous submerged breakwater on its efficacy in terms of protection of sand beaches against wave-induced erosion. Although the main focus of this chapter is on breakwater porosity and relative breakwater submergence, for the sake of completeness, the effect of relative crest width and relative location depth have been also analyzed.

The calibrated and validated numerical model, which is described in section 4.3, is applied to perform a systematic parameter study. In the latter, possible combinations of five values of breakwater porosity n={0, 0.3, 0.4, 0.5 & .06}, three values of breakwater submergence R_c={0.03m, 0.07m, 0.10m}, three values of crest width B={0.15m, 0.30m, 0.45m} and two values of location depth h_p={0.27m, 0.40m} have been examined (see parameter definition in Fig. 5.1), resulting in a total of 90 breakwater configuration tested.

Given the importance of evaluating the erosion of the protected beach for an efficient design of porous submerged breakwaters, the results of the numerical parameter study are analyzed on the basis of beach profile erosion volume V_e (m^3/m) as depicted in Fig. 5.1. Accordingly, the dimensionless erosion parameter e_p, which is the ratio between the squared root of erosion volume V_e (m^3/m) and incident root mean square wave height H_{rmsi} (m) measured at the offshore toe of the breakwater (see Eq. 5.1), is introduced to make the applicability of the results more generic. The comparison between volume of erosion V_e obtained from the numerical tests and the volume of erosion $\tilde{V}_e$ calculated by Eq 5.2 (derived from laboratory tests by Günaydın and Kabdaşlı (2003), revealed a very close similarity of variation trends between V_e and $\tilde{V}_e$ (see Fig. 5.2). Therefore, the dimensionless erosion parameter e_p defined by Eq. 5.1 is considered as the relevant parameter, the variation of which can describe the variation in the erosion of protected beach (see Fig. 5.2). Accordingly, the erosion parameter e_p and its inverse counterpart $p_i=(e_p)^{-1}$, called "protection index", which are obtained from the numerical tests, are analyzed and novel predictive formulae and design criteria are developed to assess the effect of breakwater parameters (i.e. porosity n, submergence R_c, crest width, B and location depth h_p) on the erosion of the protected beach and on the protective efficacy of submerged breakwaters.

The main contributions of this study to expand the current knowledge on the protective efficacy of submerged breakwaters in terms of mitigation of beach erosion are summarized below:

- The effect of structure porosity on the protected beach erosion leeward of submerged breakwaters and the protective efficacy of the structure is investigated in details for the first time. In spite of its crucial importance for the erosion of the protected beach, it is rather surprising that this effect was not considered in previous studies.

- The dimensionless parameter χ_0 (see Eq 5.6), which is proposed by Postacchini et al. (2016) to relate erosion and accretion in the vicinity of submerged impermeable breakwaters to the structure design, is modified to account for both breakwater submergence and porosity (see Eq 5.9).

- Based on the analysis of the dataset generated in the numerical tests, a formula (Eqs. 5.12a and 5.12b) is developed to predict the effect of structure parameters (i.e. porosity n, submergence

R_c, crest width B and location depth h_p) on the erosion of the protected beach and the protective efficacy of the porous submerged breakwaters. This predictive formula represent an important innovation as the available formulae (see section 2.2) do not account for the effect of breakwater porosity.

- A new formula (Eq. 5.18) is developed to assess the maximum enhancement of breakwater protective efficacy, which can be made through introducing structure porosity, as a function of breakwater submergence and crest width.

- A new formula (Eq. 5.30) is developed to predict the protective efficacy of the structure as a function of the Dean parameter at the onshore toe of the submerged breakwater. This is not only the first formula of this type, but also the first study that evaluate the protective efficacy of submerged breakwaters as a function of the Dean parameter immediately shoreward of the structure.

- The dataset generated in the numerical parameter study is, to the author's knowledge, the largest dataset to study the effect of structure parameters (including porosity) on the erosion of a protected beach and the protective efficacy of submerged breakwaters.

Based on the predictive formulae developed in this study, new criteria which might contribute to improve design of submerged breakwaters for coastal protection are proposed as outlined below:

For $\frac{R_c}{H_{rmsi}} > 2 \times \sqrt{B/L_p}$, decreasing relative breakwater submergence R_c/H_{rmsi} and/or increasing relative crest width B/L_p do not enhance noticeably the reduction of the erosion of the protected beach that can be achieved by introducing porosity in a given breakwater configuration (see Eq. 5.19)

- For $\left(R_c/H_{rmsi}\right)^2 > 9B/L_p$, the enhancement of the protective efficacy of the structure by using porosity in given breakwater configuration does not exceed 10% (see Eq. 5.23 and Fig, 5.9)

- For $R_{ce} < 0.3 \times H_{rmsi}$, the reduction of the effective submergence R_{ce} has a strong effect on improving the protective efficacy of submerged breakwaters (see Eq 5.24 and Fig. 5.11)

- For $0 < \frac{R_c}{H_{rmsi}} < 0.7$ the decrease of relative submergence has a strong influence on the effect of relative crest width B_e/L_p.(see Eq 5.28)

- For $\frac{R_c}{H_{rmsi}} > 0.3$, the effect of the location depth on the protective efficacy of submerged breakwaters is negligibly small.

In both research and engineering practice, the outcomes of this study may be applied for:

I. Improving specific designs for submerged breakwaters to reduce possible erosion in sandy beaches leeward of the submerged breakwaters;

II. Comparing various design alternatives of submerged breakwaters, in order to identify the most efficient alternative in terms of the efficacy of the structure to protect sandy beaches against erosion;

III. Explicitly considering the effect of various porosities on the protective efficacy of submerged breakwaters;

IV. Combining the large dataset generated in this study with prospective datasets from future research studies, in order to build a data base with wider ranges of application.

In spite of the relevance of the outcomes of this study for both research and engineering, the following limitations are worth to be mentioned:

- In this study, the flow through the porous breakwater (see section 2.1.1), which might affect the erosion of the protected beach and the protective efficacy of submerged breakwaters, is not considered.

- The numerical parameter study reproduces flume experiments related to sandy beach erosion leeward of submerged breakwaters (see section 4.2). Therefore, the results are primarily associated with the morphological changes of protected beaches induced by cross-shore sediment transport as a response to the short-term events such as storm waves (see Section 2.1).

- The lack of detailed experimental and field studies for the verification of the results represents a critical limitation.

Based on the aforementioned limitations, the following recommendations for future research might be considered:

- The effect of the flow through the porous breakwater should be considered, as it might affect the hydrodynamic processes and consequently also sediment transport and morphological changes in the beach protected by submerged porous breakwaters.

- The two dimensional approach applied in this study might be extended to account for the effect of the longshore transport and the long-term morphological changes in the protected beach.

- Experimental and field studies on the relation between breakwater design and protective efficacy of the submerged porous breakwaters should be performed to provide benchmark data which could be used to evaluate the results of this study.

6 Concluding remarks and outlook

Coastal regions are extremely important for population residence, economy and ecosystems. The socio-economic value of coastal areas becomes increasingly prominent due to rapid population growth in these areas Therefore, for a sustainable use and management of coastal zones, potentially threatened coastal stretches should be effectively protected against erosion. Submerged porous breakwaters (SPBs) might protect the beach with minimum adverse effects on the surrounding environment such as degrading water quality or obstructing the view of the sea. However, a wider application of SPBs, as a "softer" solution than their emerged counterparts, is hampered by the lack of knowledge about the efficacy of SPBs. Accordingly, the main objective of this PhD is set to identify and properly address the most critical knowledge gaps.

This chapter is mainly devoted to highlight the key achievements of this PhD study and outline the main limitations and applicability of the results. Accordingly, this chapter is organized as follows. First, a summary of the novel contributions of this study to expand the current knowledge on the performance of submerged breakwaters is provided. Second, the key results are briefly outlined. Third, the applicability and limitations of the results are discussed. Finally, based on the limitations of the results, recommendations are proposed to address the gaps which are not considered in this PhD study.

Novel contributions of this study

The major gaps of knowledge on the protective efficacy of submerged porous breakwaters (SPBs), which have been identified and addressed in this study, are outlined below:

- Lack of WTC (wave transmission coefficient) formulae for SPBs which explicitly include the effect of breakwater porosity. This represents a major limitation, because SPBs are porous (mostly made of rock material) are porous and porosity might have a prominent effect on the hydraulic performance of the structure and, subsequently, on the coastal morphology.

- Lack of adequately detailed studies on the effect of breakwater porosity in combination with breakwater submergence on morphological changes in sandy beaches protected by SPBs.

- Lack of design criteria and predictive formulae for evaluating morphological changes within sandy beaches leeward of the SPBs, in response to short-time events such as storm surges

- Relatively limited size of the existing datasets obtained from previous studies on the effect of SPBs on coastal morphology. Therefore, the available data are quantitatively and qualitatively inadequate for the development of any robust predictive formulae and design criteria to assess the protective efficacy of SPBs.

Based on the aforementioned gaps of knowledge, the major achievements of this study might be summarized as follows:

- A novel WTC formula is developed, which explicitly includes the effect of breakwater porosity, in addition to the effect of breakwater submergence and crest width.

- The numerical model DELFT3D is extended/improved to enable the model to account for the combined effect of breakwater porosity and submergence on wave transmission.

- The extended model is calibrated and validated, thus providing a systematically validated numerical model required to study the effect of breakwater porosity and submergence on coastal morphology.

- Using the well-validated model, a large data set is generated through a detailed numerical parameter study on the effect of SPB design parameters on the morphological changes in the protected beach induced by short-term events (e.g. a single storm).

- Design criteria and novel formulae to assess the protective efficacy of SPBs are developed, which can be used for preliminary design purposes.

Summary of key results

This study attempts to extend the current knowledge on the design and performance of submerged breakwater through providing an improved understanding of the effect of breakwater porosity and submergence on the hydraulic performance and protective efficacy of submerged porous breakwaters (SPBs). The key results associated with the aforementioned contributions of this study may be summarized as follows:

WTC Formula explicitly including breakwater porosity

In response to the lack of a WTC formula for submerged breakwaters which explicitly includes the structure porosity, a numerical parameter study is carried out using OpenFOAM (Hereafter parameter study P1 to avoid any confusion with another parameter study performed using DELFT3D on the effect of SPB design on coastal morphology) to systematically investigate the effect of breakwater porosity and submergence on wave transmission at SPBs. The key results of the parameter study P1, which has particularly contributed to achieve an improved understanding of the effect of porosity on wave transmission at submerged breakwaters, are outlined below:

I. The use of a SPBs with n=0.1-0.6 as compared to an impermeable SPB (n=0) results in a reduction of the WTC and thus enhances the hydraulic performance of the structure. This observation is in agreement with the results of available laboratory studies.

II. The WTC of submerged breakwaters steadily increases with the increase of structure porosity from n=0.3 to n=0.6. This is also in agreement with observations of previous studies.

III. The effect of breakwater porosity on WTC becomes stronger with decreasing submergence and/or increasing crest width.

IV. For improving the design of SPBs with low submergence, the use of porous structures may be the only practical way to achieve a desired level of enhancement in hydraulic performance while keeping the structure submerged.

V. Based on the WTC values obtained from parameter study P1, a new predictive WTC formula is developed (see Eq. 3.28). This is the first and only WTC formula yet available which explicitly includes the breakwater porosity. The developed WTC formula shows a good agreement with the numerical results of P1 (R^2=0.95, see Fig. 3.16)

VI. The comparison between the limited available laboratory measurements of WTC at SPBs and WTC values predicted by the new formula suggests a fairly good agreement between WTC values predicted by the new formula and available laboratory measurements (see Fig. 3.18, R^2=0.86)

Extending the applicability of DELFT3D

The numerical model DELFT3D is yet not able to consider the dissipative effect of porosity on wave transmission. In addition, for steep slope SPBs, the model may overestimate the energy dissipation induced by wave breaking. Thus, the model is also not able to adequately account for the effect of breakwater submergence on wave transmission. In order to overcome these limitations, a novel SPB implementation approach is proposed and validated in this study to improve/extend DELFT3D by enabling the model to account for the combined effect of breakwater porosity and submergence. The proposed *SPB implementation approach* consists of two steps: (i) *Submergence implementation* which enables the model to adequately account for the effect of the breakwater submergence on wave transmission, even for SPBs with steep slopes and (ii) *Porosity implementation* which enables the model to account for the dissipative effect of the breakwater porosity on wave transmission. The key results associated with the development of the *SPB implementation approach* are summarized below:

I. *Submergence implementation* (step i of SPB implementation approach). It is based on the local adjustment of the mesh size over the submerged breakwater. This approach can significantly enhance the numerical simulation results so that the relative error between WTC obtained from the model and WTC calculated by VDM2003 empirical formula becomes less than 10%. The necessity of applying the submergence implementation essentially depends on relative submergence R_c/H_{m0} and relative crest width B/L_p. For this purpose, a decision criterion is developed, based on the results of some additional numerical tests performed in this study (see section 4.3.2.d).

II. *Porosity implementation* (Step ii of SPB implementation approach). It is a novel approach proposed in this study to overcome the essential limitation of DELFT3D to account for the effect of porosity on the wave transmission. The porosity implementation is based on the virtual sub-grid obstacle defined at the onshore toe of the SPB with: (a) The same length and orientation as the structure and (b) The transmission coefficient which is determined by the formula for the Porosity Effect Factor (PEF) in Eq. 3.26. The porosity implementation can be potentially applied in any phase-averaged model which is able to consider sub-grid linear obstacles (e.g. MIKE SW), in order to overcome the model limitation to account for the dissipative effect of porosity on wave transmission at SPBs.

III. *SPB implementation approach*. It is applied in the DELFT3D-WAVE model to reproduce the laboratory experiments by Kramer et al., (2005) on wave transmission at SPBs. The outcome shows that the application of the SPB implementation noticeably enhances the numerical simulation results in terms of predicted transmitted wave height leeward of the SPB, thus extending the applicability of DELFT3D (see Figs. 4.16 and 4.17).

Calibrating/validating the extended DELFT3D model

A limited number of studies have been performed on developing predictive formulae for evaluating long-term morphodynamic effects of submerged breakwaters. However, no predictive formula is yet available to evaluate the short-term morphodynamic effect of submerged breakwaters, and this topic has rarely been studied. In order to provide a well-calibrated/validated numerical model which is required to study short-term morphological changes of a beach under irregular waves, DELFT3D is calibrated and validated against laboratory tests by Claessen and Groenewoud (1995). The key results are summarized below:

I. Using the SPB implementation approach yields a more accurate prediction of the transmitted wave height, as compared to the original DELFT3D-WAVE model and to the UNIBEST-TC model which both overestimate transmitted wave heights by ca. 10% and 6%, respectively.

II. In the numerical reproduction of the laboratory tests by Claessen and Groenewoud (1995) using, a large deviation between predicted horizontal flow velocity and its measured counterpart in the upper part of the water column (z/h>0.4) is observed (see Fig. 4.34). This deviation can be attributed to the inadequate representation of wave action effects on turbulence very close to the wave breaking region. However, it is shown that this large deviation is not relevant for the purpose of this study.

III. Based on the Brier Skill Score (BSS), the beach profiles calculated by the well-validated extended DELFT3D model show "Good and Excellent" agreements with measured profiles (see Fig. 4.37). This implies that, the model can be utilized within the range of wave conditions considered in the calibration/validation process (see section 4.3.2) to study the effect of SPBs on coastal morphology in response to short term events such as sea-storms.

Parameter Study on the Effect of Breakwater Porosity and Submergence on Coastal Morphology

The available studies on the morphodynamic effects of submerged breakwaters do not consider the effect of breakwater porosity. Moreover, they mostly provide limited datasets which are not adequate to develop robust predictive formulae and design criteria for engineering practice. In order to overcome these limitations, the (well-calibrated/validated) extended numerical DELFT3D model is deployed for performing a detailed parameter study (Hereafter parameter study P2) to provide a relatively large data set that describes the effect of SPB design parameters on morphological changes in the protected beach in short-term events (e.g single sea-storm). The breakwater porosity and submergence represent the main breakwater characteristics considered in the parameter study. However, for the sake of completeness, the effects of crest width and location water depth have also been considered. Parameter study P2 consists of 90 tested breakwater configurations including all possible combinations of 5 breakwater porosities n={0.0, 0.3, 0.4, 0.5, .06}, 3 submergences R_c={0.03m, 0.07m, 0.1m}, 3 crest widths B={0.15m, 0.30m, 0.45m} and 2 water depth h_p={0.27m, 0.40m}. The key results of the parameter study P2 are summarized below:

I. Considering the importance of beach erosion in coastal areas protected by submerged breakwaters, the results of the numerical parameter study are presented in terms of beach profile erosion volume V_e (m^3/m) (see also Fig. 5.1)

II. The variation trend of erosion volume V_e obtained from the parameter study P2 shows a very close similarity to that of erosion volume $\tilde{V}_e$ calculated by the empirical formula of Gunaydin and Kabdasli (2003). This very close similarity implies that the results of the parameter study can be applied with more confidence for the analysis of protective efficacy of SPBs and beach erosion of protected beaches leeward of SPBs.

III. To the author's knowledge, the dataset generated in the parameter study P2 is the largest among the datasets currently utilized to study the relation between the protective efficacy of SPBs and the structure design parameter, namely porosity, submergence, crest width and location depth. More importantly, it represents the only dataset yet available, which explicitly considers the effect of porosity.

New predictive formulae and design criteria

No predictive formulae or design criteria are yet available for the preliminary design of submerged breakwaters to assess the protective efficacy of the structure for short-term events such as single storms. In order to close this gap, the dataset from parameter study P2 is further analysed to develop novel predictive formulae and design criteria for the protective efficacy of SPBs as a function of design parameters of the structure.

Accordingly, a new dimensionless parameter, called *protection index* p_i, is introduced to quantify the protective efficacy of the structure. The parameter $p_i = \frac{H_{rmsi}}{\sqrt{V_e}}$ represents the ratio of the incident wave height H_{rmsi} to the square root of erosion volume V_e (m^3/m) describing the damage of the protected beach. The relevant predictive formulae and design criteria are then developed to express the protection index p_i in terms of SPB design parameters, namely porosity n, relative submergence R_c/H_{rmsi}, relative crest width B/L_p, and relative location depth h_p/H_{rmso}. The key results are summarized below:

I. The dimensionless parameter χ_0 (see Eq 5.6), which was developed earlier by Postachini et al., (2016) to relate the design parameters of impermeable breakwaters, namely B/L_p and H_{si}/h, to erosion/accretion in the vicinity of the structure, is extended to also account for both relative breakwater submergence R_c/H_{rmsi} and porosity n. As a result, the new parameter χ is obtained (see Eq 5.9), which relates the SPB parameters n, R_c/H_{rmsi}, B/L_p, and H_{rmsoi}/h_p to the erosion in the protected beach leeward of the structure.

II. Based on the results of the parameter study P2, there is a strong similarity between the variation of parameter χ and the variation of protection index p_i, implying a strong functional relationship between p_i and SPB parameters n, R_c/H_{rmsi}, B/L and H_{rmsoi}/h_p.

III. A predictive formula describing the functional relationship between protection index p_i and SPB parameters n, R_c/H_{rmsi}, B/L_p and H_{rmsoi}/h_p is developed (Eqs. 5.12a and 5.12b), which fits well (R^2=0.96) with the results of the parameter study P2 (see Fig 5.5).

IV. In this study, a new predictive formula (Eq. 5.18) is also developed to estimate the maximum enhancement of the protective efficacy of common rubble mound breakwaters (i.e. with porosity n=0.3-0.6) as a function of relative submergence R_c/H_{rmsi}, and relative crest width B/L_p.

V. An other novel predictive formula (Eq. 5.30) is obtained from further analysis of the results which describes the relation between the Dean parameter $\Omega_t = \frac{H_{rmst}}{w_s \times T_p}$ for the transmitted waves at the onshore toe of the submerged breakwater (Fig. 5.1 and Fig. 5.14) and protection index p_i. This is the first and only predictive equation for the protective efficacy of submerged breakwaters as a function of the Dean parameter immediately shoreward of the structure.

Based on the predictive formulae developed in this study, new design criteria are proposed, which might contribute to an improved design of submerged breakwaters for coastal protection by evaluating the importance of different design parameters for specific design conditions. These design conditions and their implications for the importance of design parameters are summarized below:

Implication for the importance of design parameters	Design condition
Decreasing relative breakwater submergence R_c/H_{rmsi} and/or increasing relative crest width B/L_p has a negligibly small effect (less than 2%, see Eq 5.18 and 5.19) on the maximum enhancement of protective efficacy of given submerged breakwater configuration that can be achieved by using common rubble mound structures (n=0.3-0.6)	**FOR** $\frac{R_c}{H_{rmsi}} > 2\sqrt{\frac{B}{L_p}}$
The maximum enhancement of the protective efficacy of given submerged breakwater configuration due to use of porous structures with n=0.3-0.6 does not exceed 10%	**FOR** $\left[\frac{R_c}{H_{rmsi}}\right]^2 > 9\frac{B}{L_p}$
The reduction of the effective submergence R_{ce} (see Fig. 5.11 and Eq. 5.24) has a noticeable effect on improving the protective efficacy of submerged breakwaters	**FOR** $\frac{R_{ce}}{H_{rmsi}} < 0.3$
The decrease of relative submergence noticeably increases the effect of relative effective crest width B_e/L_p (see Eqs. 5.27 and Fig. 5.12) on protective efficacy	**FOR** $0 < \frac{R_c}{H_{rmsi}} < 0.7$
The effect of the relative location depth h_p/H_{rmso} on the protective efficacy of submerged breakwaters becomes negligible.	**FOR** $\frac{R_c}{H_{rmsi}} > 0.3$

Applicability and limitations of the results

Among the potential applications of the results of this study in both research and practical engineering practice, the following examples might be worth to mention:

I. The relatively large data sets obtained from parameter studies P1 and P2 can be further combined with datasets that will be obtained in further research, in order to generate more reliable datasets with wider ranges of application.

II. This study provides a well-documented and validated approach which can be potentially applied in any phase-averaged wave model to overcome the basic limitation of this type of wave models which do not account for the dissipative effect of breakwater porosity.

III. The predictive formula and design criteria developed on the basis of the parameter study P2 can be utilized for improving the design of submerged breakwaters.

IV. In order to select the most appropriate SPB configuration for coastal protection, the predictive formulae developed in this study can be utilized for the comparative evaluation of various design alternatives for porous submerged breakwaters.

In spite of the relevance of the outcomes of this study and their potential applications, they still have some limitations as outlined below:

I. There is a crucial lack of detailed experimental and field studies for further verification of the results of this study.

II. Although the SPB implementation approach proposed in this study noticeably improves the numerical simulation results in terms of predicted transmitted wave height, it is still not fully clear to which extent this approach is able to improve the wave height evolution over the SPB.

III. The new WTC formula developed on the basis of the parameter study P1 is not readily applicable to breakwaters which consist of layers with different porosities (e.g. core, filter layer and armour layer). For this purpose, an equivalent overall porosity might be determined (Details are given in section 4.3.1 for two layer breakwaters which consist of impermeable core and permeable armour layer).

IV. The applicability of the new WTC formula (see section 3.4) to SPBs with porosity n betwen 0 and 0.3 might be questionable (see section 3.3).

V. The filtration flow through the porous breakwater, which might affect the wave set-up leeward of the structure, and thus possibly also the erosion in the protected beach, is not explicitly considered in this study.

VI. Although this study might represent a significant advancement toward evaluating the protective efficacy of submerged breakwaters in response to short-term events (e.g. storms), the results of this study are not applicable for longer time scales, where the longshore sediment transport becomes also important.

Recommendations for further research

Based on the limitations outlined above, the following recommendations might be considered for further research:

- The effect of the flow through the porous breakwater (filtration flow) should be considered, as filtration flow might affect the hydrodynamics and the associated sediment transport and morphological changes in sandy coasts protected by SPBs. For this purpose, the shallow water equations in DELFT3D-FLOW should be extended/modified to represent the flow in porous media.

- Experimental and field studies are needed to provide benchmark datasets required for further evaluation of the predictive formulae and design criteria which are developed in this study to evaluate the protective efficacy of the SPBs as function of structure design parameters.

- New experimental or field tests are needed to further evaluate the applicability of the new WTC formula especially for $0<n<0.3$, where no experimental data yet exist.

- The two dimensional approach applied in this study should be extended to 3D approach in order to also account for longshore shore transport which is crucial for the effect of breakwater design on long-term morphological changes in sandy coasts protected by SPBs.

References

Abanades, J., Greaves, D., & Iglesias, G. (2014). Wave farm impact on the beach profile: A case study. Coastal Engineering, 86, 36-44.

Ahrens, J. P. (2001). Wave transmission over and through rubble-mound breakwaters. Draft Contract Report submitted to the US Army Engineer Research and Development Center., Coastal and Hydraulics Laboratory, Vicksburg, MS.

Alsina, J. M. (2005). Development of a morphodynamic numerical model. Application to LCS impact assessment. Barcelona, Spain: Universitat Politècnica de Catalunya(Doctoral dissertation, Ph. D. thesis, 233p).

Amini Afshar, M. (2010). Numerical wave generation in Open FOAM®, M.sc Thesis, Chalmers University, Sweden.

Bagnold, R. A. (1966). *An approach to the sediment transport problem from general physics*. US government printing office, U.S. Geological Survey Professional Paper 422-I, 1-37

Bakhtyar, R., Barry, D. A., & Kees, C. E. (2012). Numerical experiments on breaking waves on contrasting beaches using a two-phase flow approach. Advances in water resources, 48, 68-78.

Battjes, J. A., & Janssen, J. P. F. M. (1978). Energy loss and set-up due to breaking of random waves. In *Coastal Engineering 1978* (pp. 569-587).

Battjes, J. A., & Stive, M. J. F. (1985). Calibration and verification of a dissipation model for random breaking waves. *Journal of Geophysical Research: Oceans*, Vol. 90(C5), 9159-9167.

Bayram, A., Larson, M., Miller, H. C., & Kraus, N. C. (2001). Cross-shore distribution of longshore sediment transport: comparison between predictive formulas and field measurements. Coastal Engineering, 44(2), 79-99.

Benoit, M., Marcos, F., & Becq, F. (1997). Development of a third generation shallow-water wave model with unstructured spatial meshing. Proceedings of the 27th International Conference on Coastal Engineering 1996 (pp. 465-478).

Berberović, E., van Hinsberg, N. P., Jakirlić, S., Roisman, I. V., & Tropea, C. (2009). Drop impact onto a liquid layer of finite thickness: Dynamics of the cavity evolution. *Physical Review E*, *79*(3), 036306.

Black, K. P., & Andrews, C. J. (2001). Sandy shoreline response to offshore obstacles Part 1: Salient and tombolo geometry and shape. Journal of coastal research, 82-93.

Booij, N., Ris, R. C., & Holthuijsen, L. H. (1999). A third-generation wave model for coastal regions: 1. Model description and validation. *Journal of geophysical research: Oceans*, *104* (C4), 7649-7666

Briere, C., Abadie, S., Bretel, P., & Lang, P. (2007). Assessment of TELEMAC system performances, a hydrodynamic case study of Anglet, France. Coastal engineering, 54(4), 345-356.

Browder, A. E., Dean, R. G., & Chen, R. (1996). Performance of a submerged breakwater for shore protection. Proceedings of the 27th International Conference on Coastal Engineering, Sydney, Australia, pp. 2312 – 2323

Buccino, M., & Calabrese, M. (2007). Conceptual approach for prediction of wave transmission at low-crested breakwaters. Journal of waterway, port, coastal, and ocean engineering, 133(3), 213-224.

Burcharth, H. F., & Andersen, O. K. (1995). On the one-dimensional steady and unsteady porous flow equations. *Coastal engineering*, *24*(3), 233-257.

Burcharth, H; Hawkins, S; Zanuttigh, B., & Lamberti, A. (2007). Environmental design guidelines for low crested coastal structures. Elsevier Science.

Cáceres, I. (2004). Q-3D Near-shore circulation, development and utilities (Doctoral dissertation), Universitat Politècnica de Catalunya. Barcelona, Spain.

Cáceres, I., Sánchez-Arcilla, A., Alsina, J. M., González-Marco, D., & Sierra, J. P. (2005). Coastal dynamics around a submerged barrier. 5th international conference on coastal dynamics, Barcelona, Spain, pp. 158-162.

Calabrese, M., Buccino, M., & Pasanisi, F. (2008). Wave breaking macrofeatures on a submerged rubble mound breakwater. *Journal of Hydro-environment Research*, *1*(3-4), 216-225.

Cappietti, L., Clementi, E., Aminti, P., & Lamberti, A. (2006). Piling-up and filtration at low crested breakwaters of different permeability. Proc., 30th Int. Conf. on Coastal Engineering, San Dieho, Vol. 5, World Scientific, Singapore, 4957–4969.

Cappietti, L. (2011). Converting emergent breakwaters into submerged breakwaters. Journal of Coastal Research, (64), 479.

Carevic, D., Loncar, G., & Prsic, M. (2013). Wave parameters after smooth submerged breakwater. Coastal engineering, 79(1), 32-41.

CEM. Coastal Engineering Manual. (2006a). Coastal Engineering Research Center, Department of Army Corps of Engineers, US, Chapter 3, Part III.

CEM. Coastal Engineering Manual. (2006b). Coastal Engineering Research Center, Department of Army Corps of Engineers, US, Chapter 2, Part III.

Claessen, E.W.M. and Groenewoud, M.D., 1995. Effect of submerged breakwater on profile development. Delft University of Technology, Faculty. of Civil Engineering.

Collins, J. I. (1972). Prediction of shallow-water spectra. *Journal of Geophysical Research*, *77* (15), 2693-2707.

Dally, W. R., & Pope, J. (1986). Detached breakwaters for shore protection (No. CERC-TR-86-1). Coastal Engineering Research Center Vicksburg Ms.

d'Angremond, K., van der Meer, J., de Jong, R., (1996). "Wave transmission at low- crested structures". In: *ASCE,* Proceedings 25th International Conference on Coastal Engineering, pp. 3305–3318.

Davies, A. G., Van Rijn, L. C., Damgaard, J. S., Van de Graaff, J., & Ribberink, J. S. (2002). Intercomparison of research and practical sand transport models. *Coastal Engineering*, *46* (1), 1-23.

Dean, R. G. (1991). Equilibrium beach profiles: characteristics and applications. Journal of coastal research, 53-84.

Dean, R. G., Browder, A. E., Goodrich, M. S., & Donaldson, D. G. (1994). Model tests of the proposed PEP Reef installation at Vero Beach, Florida. University of Florida, Department of Coastal and Oceanographic Engineering, Report No. UFL/COEL-94/012, Gainesville, FL.

Dean, R. G., Chen, R., & Browder, A. E. (1997). Full scale monitoring study of a submerged breakwater, Palm Beach, Florida, USA. Coastal Engineering, 29(3-4), 291-315.

Dean, R. G., & Dalrymple, R. A. (2004). Coastal processes with engineering applications. Cambridge University Press.

de France, E. (2007). 3D hydrodynamics Telemac-3D code–release 5.8. Operating Manual, EDF R&D.

Deigaard, R. (1992). Mechanics of coastal sediment transport (Vol. 3). World scientific publishing company.

Deltares, D. F. (2013). Simulation of multi-dimensional hydrodynamic flows and transport phenomena, including sediments. Deltares, Rotterdamseweg, The Netherlands, 1-706.

Deltares, D. F. (2014a). DELFT3D-WAVE User Manual Version. Delft, The Netherlands: Delft Hydraulics.

Deltares, D. F. (2014b). DELFT3D-FLOW User Manual Version. Delft, The Netherlands: Delft Hydraulics.

del Jesus, M., Lara, J. L., & Losada, I. J. (2012). Three-dimensional interaction of waves and porous coastal structures: part I: numerical model formulation. *Coastal Engineering*, *64*, 57-72.

DHI, MIKE. (2017a). Spectral Wave Module, Scientific documentation. DHI Water & Environment, Denmark

DHI, MIKE. (2017b). Parabolic mild slope wave module, Scientific documentation,. DHI Water & Environment, Denmark,

DHI, MIKE. (2017c). Boussinesq wave module. Scientific documenttaion,. DHI Water & Environment, Denmark,

DHI, MIKE. (2017d). MIKE 21 & MIKE 3 Flow Model FM, Hydrodynamic and Transport Module, Scientific Documentation,. DHI Water & Environment

DHI, MIKE. (2017e). MIKE 21 & MIKE 3 Flow Model FM, Sand Transport Module, Scientific Documentation,. DHI Water & Environment

DHI, MIKE. (2017f). MIKE 21 & MIKE 3 Flow Model FM, Mud Transport Module, Scientific Documentation,. DHI Water & Environment

Dingemans, M. W., Radder, A. C., & De Vriend, H. J. (1987). Computation of the driving forces of wave-induced currents.Coastal Engineering, 11(5-6), 539-563.

Du, Y., Pan, S., & Chen, Y. (2010). Modelling the effect of wave overtopping on nearshore hydrodynamics and morphodynamics around shore-parallel breakwaters. Coastal Engineering, 57(9), 812-826.

Ebersole, B. A., Cialone, M. A., & Prater, M. D. (1986). Regional coastal processes numerical modeling system. Department of the Army, US Army Corps of Engineers.

Edwards, B. (2006). Investigation of the effects of detached breakwaters at Holly Beach and Grand Isle, Louisiana, Msc Thesis, Louisiana State University

Eldeberky, Y., & Battjes, J. A. (1995). Parameterization of triad interactions in wave energy models. Proc. Proc. Coastal Dynamics Conf. '95, Gdansk, Poland, pp140-148

Eldeberky, Y., & Battjes, J. A. (1996). Spectral modeling of wave breaking: application to Boussinesq equations. *Journal of Geophysical Research: Oceans*, *101* (C1), 1253-1264.

Elsayed, S. M. (2017). Breaching of Coastal Barriers under Extreme Storm Surges and Implications for Groundwater Contamination (Doctoral dissertation, PhD dissertation, Leichtweiß-Institute for Hydraulic Engineering and Water Resources, Technische Universität Braunschweig, Braunschweig, Germany).

El-Shinnawy, A. I., Ahmed, A. S., & Zeydan, B. A. (2012). Validation of Numerical Model to Predict Wave Transmission at Submerged Breakwaters. International Conference of ASCE, Cairo, Egypt.

Garcia, N., Lara, J. L., & Losada, I. J. (2004). 2-D numerical analysis of near-field flow at low-crested permeable breakwaters. Coastal Engineering, 51(10), 991-1020.

Groeneweg, J., & Klopman, G. (1998). Changes of the mean velocity profiles in the combined wave–current motion described in a GLM formulation. Journal of Fluid Mechanics, 370, 271-296.

Gu̇ner, H. A. A., Yu̇ksel, Y., & Çevik, E. O. (2011). Determination of longshore sediment transport and modelling of shoreline change. In *Sediment Transport*. InTech.

Günaydın, K. and Kabdaşlı, M.S., 2003. Characteristics of coastal erosion geometry under regular and irregular waves. Ocean Engineering, 30(13), pp.1579-1593.

Hanson, H., & Kraus, N. C. (1989). GENESIS: Generalized Model for Simulating Shoreline Change. Report 1. Technical Reference (No. CERC-TR-89-19-1). Coastal Engineering Research Center Vicksburg Ms.

Hanson, H., Kraus, N. C., & Nakashima, L. D. (1990). Shoreline change behind transmissive detached breakwaters. Proc. Coastal Zone '89. ASCE, 568-582.

Hanson, H., & Kraus, N. C. (1990). Shoreline response to a single transmissive detached breakwater." Coastal engineering (1990), B. L. Edge, ed., ASCE, New York, 2034–2046.

Hanson, H., & Kraus, N. C. (2011). Long-term evolution of a long-term evolution model. Journal of Coastal Research, 118-129.

Harley, M., Armaroli, C., & Ciavola, P. (2011). Evaluation of XBeach predictions for a real-time warning system in Emilia-Romagna, Northern Italy. Journal of Coastal Research, (64), 1861.

Harris, L. E. (1996). Wave attenuation by rigid and flexible-membrane submerged breakwaters (Doctoral dissertation, Florida Atlantic University).

Harris, L. E. (2003). Status Report for the Submerged Reef Ball™ Artificial Reef Submerged Breakwater Beach Stabilization Project for The Grand Cayman Marriott Hotel.

Hasselmann, S., & Hasselmann, K. (1981). *A Symmetrical Method of Computing the Nonlinear Transfer in a Gravity Wave Spectrum, Max Planck Inst*. Tech. Report, Hamburg.

Hasselmann, K., Barnett, T. P., Bouws, E., Carlson, H., Cartwright, D. E., Enke, K., ... & Meerburg, A. (1973). *Measurements of wind-wave growth and swell decay during the Joint North Sea Wave Project (JONSWAP)*. Deutches Hydrographisches Institut

Hasselmann, K. (1974). On the spectral dissipation of ocean waves due to white capping. *Boundary-Layer Meteorology*, *6* (1-2), 107-127.

Hieu, P. D., & Tanimoto, K. (2006). Verification of a VOF-based two-phase flow model for wave breaking and wave–structure interactions. *Ocean engineering*, *33*(11), 1565-1588.

Hieu, P. D., & Vinh, P. N. (2012). Numerical study of wave overtopping of a seawall supported by porous structures. *Applied Mathematical Modelling*, *36*(6), 2803-2813.

Higuera, P., Lara, J. L., & Losada, I. J. (2014). Three-dimensional interaction of waves and porous coastal structures using OpenFOAM®. Part I: Formulation and validation. *Coastal Engineering*, *83*, 243-258.

Higuera, P., Lara, J. L., & Losada, I. J. (2013). Simulating coastal engineering processes with OpenFOAM®. *Coastal Engineering*, *71*, 119-134.

Holthuijsen, L. H., Booij, N., & Ris, R. C. (1993). A spectral wave model for the coastal zone. Proc. 2nd Intern. Symposium on Ocean Wave Measurement and Analysis in New Orleans, Louisiana, pp. 630-641

Holthuijsen, L. H., Herman, A., & Booij, N. (2003). Phase-decoupled refraction–diffraction for spectral wave models. *Coastal Engineering*, *49* (4), 291-305.

Holthuijsen, L. H. (2007). *Waves in oceanic and coastal waters*. Cambridge University Press.

Hur, D. S., Lee, K. H., & Choi, D. S. (2011). Effect of the slope gradient of submerged breakwaters on wave energy dissipation. Engineering Applications of Computational Fluid Mechanics, 5(1), 83-98.

Ikeda, S. (1982). Incipient motion of sand particles on side slopes. *Journal of the Hydraulics Division*, *108* (1), 95-114.

Jacobsen, N. G., Fuhrman, D. R., & Fredsøe, J. (2012). A wave generation toolbox for the open-source CFD library: OpenFoam®. *International Journal for Numerical Methods in Fluids*, *70*(9), 1073-1088.

Jackson, N. L., Nordstrom, K. F., & Farrell, E. J. (2017). Longshore sediment transport and foreshore change in the swash zone of an estuarine beach. Marine Geology, 386, 88-97.

Jiang, A. W., Hughes, M., Cowell, P., Gordon, A., Savioli, J. C., & Ranasinghe, R. (2011). A hybrid model of swash-zone longshore sediment transport on reflective beaches. Proceedings of International Conference on Coastal 710 engineering, Shanghai, China.

Jensen, B., Jacobsen, N. G., & Christensen, E. D. (2014). Investigations on the porous media equations and resistance coefficients for coastal structures. *Coastal Engineering*, *84*, 56-72.

Johnson, H., Brøker, I., & Zyserman, J. A. (1995). Identification of some relevant processes in coastal morphological modelling. Proc. 24th Intern. Conf. Coastal Engineering, Kobe, Japan, pp. 2871-2885.

Johnson, H. K., Karambas, T. V., Avgeris, I., Zanuttigh, B., Gonzalez-Marco, D., & Caceres, I. (2005). Modelling of waves and currents around submerged breakwaters. *Coastal Engineering*, *52* (10), 949-969.

Johnson, H. K. (2006). Wave modelling in the vicinity of submerged breakwaters. *Coastal Engineering*, *53* (1), 39-48.

Kamphuis, J. W. (1991). Introduction to coastal engineering and management. World Scientific.

Karim, M. F., Tanimoto, K., & Hieu, P. D. (2009). Modelling and simulation of wave transformation in porous structures using VOF based two-phase flow model. *Applied Mathematical Modelling*, *33*(1), 343-360.

Kraus, N.C., Larson, M. and Kriebel, D.L.(1991). Evaluation of beach erosion and accretion predictors. In Coastal Sediments (pp. 572-587). ASCE.

Kramer, M., Zanuttigh, B., Van der Meer, J. W., Vidal, C., & Gironella, F. X. (2005). Laboratory experiments on low-crested breakwaters. *Coastal Engineering*, *52* (10), 867-885.

Kristensen, S. E. (2013). Marine and Coastal Morphology: medium term and long-term area modelling (Doctoral dissertation, Technical University of Denmark (DTU)).

Kristensen, S. E., Drønen, N., Deigaard, R., & Fredsoe, J. (2013). Hybrid morphological modelling of shoreline response to a detached breakwater. Coastal Engineering, 71, pp.13-27.

Kolmogorov, A. N. (1941). Equations of turbulent motion in an incompressible fluid. In *Dokl. Akad. Nauk SSSR* Vol. 30, pp. 299-303).

Komen, G. J., Hasselmann, K., & Hasselmann, K. (1984). On the existence of a fully developed wind-sea spectrum. *Journal of physical oceanography*, *14* (8), 1271-1285.

Kubowicz-Grajewska, A. (2015). Morpholithodynamical changes of the beach and the nearshore zone under the impact of submerged breakwaters–a case study (Orłowo Cliff, the Southern Baltic). Oceanologia, 57(2), 144-158.

Lang, P. (2010). TELEMAC modelling system, 2D hydrodynamics, TELEMAC-2D software, version 6.0, user manual.

Lara, J. L., Losada, I. J., Maza, M., & Guanche, R. (2011). Breaking solitary wave evolution over a porous underwater step. *Coastal Engineering*, *58*(9), 837-850.

Lara, J. L., Garcia, N., &Losada, I. J. (2006). RANS modelling applied to random wave interaction with submerged permeable structures. *Coastal Engineering*, *53*(5), 395-417.

Larson, M. and Kraus, N.C., 1989. SBEACH: numerical model for simulating storm-induced beach change. Report 1. Empirical foundation and model development (No. CERC-TR-89-9). Coastal Engineering Research Center Vicksburg Ms.

Lesser, G. R., Roelvink, J. V., Van Kester, J. A. T. M., & Stelling, G. S. (2004). Development and validation of a three-dimensional morphological model. Coastal engineering, 51(8-9), 883-915.

Lesser, G. R. (2009). *An approach to medium-term coastal morphological modelling, PhD Thesis,*. UNESCO-IHE, Institute for Water Education.

Li, F., Dyt, C., & Griffiths, C. (1970). A coastal morphodynamic model for cross-shore sediment transport.WIT Transactions on The Built Environment, 70.

Liu, P. L. F., Lin, P., Chang, K. A., & Sakakiyama, T. (1999). Numerical modeling of wave interaction with porous structures. *Journal of waterway, port, coastal, and ocean engineering*, *125*(6), 322-330.

Lorenzoni, C., Mancinelli, A., Postacchini, M., Mattioli, M., Soldini, L., & Corvaro, S. (2009). Experimental tests on sandy beach model protected by low-crested structures. In Proceedings of the 4th International Short Conference on Applied Coastal Research, Barcelona, Spain (pp. 310-322).

Lorenzoni, C., Postacchini, M., Mancinelli, A., & Brocchini, M. (2013). The morphological response of beaches protected by different breakwater configurations. Proceedings of 33rd Conference on Coastal Engineering, Santander, SPAIN

Lorenzoni et al (2016). Experimental study of the short-term efficiency of different breakwater configurations on beach protection- .J. Ocean Eng. Mar. Energy (2016) 2, 195–210

Losada, I. J., Patterson, M. D., & Losada, M. A. (1997). Harmonic generation past a submerged porous step. Coastal Engineering, 31(1-4), 281-304.

Losada, I. J., Lara, J. L., Guanche, R., & Gonzalez-Ondina, J. M. (2008). Numerical analysis of wave overtopping of rubble mound breakwaters. *Coastal engineering*, *55*(1), 47-62.

Loveless, J., & MacLeod, B. (1999). The influence of set-up currents on sediment movement behind detached breakwaters. Coastal Sediments '99, Long Island, USA, pp. 2026 – 2041.

Manual, S. P. (1984). Coastal Engineering Research Center Department of The Army Waterways Experiment Station.Corps of Engineers.

Madsen, O. S., Poon, Y. K., & Graber, H. C. (1989). Spectral wave attenuation by bottom friction: theory. In *Coastal Engineering 1988* (pp. 492-504).

Mansard, E. P., & Funke, E. R. (1980). The measurement of incident and reflected spectra using a least squares method. *Coastal Engineering Proceedings*, *1*(17).

Martinelli, L., Zanuttigh, B. and Lamberti, A., 2006. Hydrodynamic and morphodynamic response of isolated and multiple low crested structures: Experiments and simulations. Coastal Engineering,53(4), pp.363-379.

Ming, D., & Chiew, Y. M. (2000). Shoreline changes behind detached breakwater. Journal of Waterway, Port, Coastal, and Ocean Engineering, 126(2), 63-70.

Mojabi, M. & Oumeraci.H (2016). Modelling of waves around porous submerged breakwaters using DELFT3D,1 2th International Conference on Coasts, Ports and Marine Structures, Vol.12, pp:279-280

Mori, E., Cappietti, L., & Aminti, P. L. (2007). Laboratory experiments for the rehabilitation of detached breakwaters at Marina di Massa (ITALY). Proc 5th Intern. Conf. Coastal Structures, Vol. 2, pp. 1421-1428, World Scientific.

Özölçer, İ.H., 2008. An experimental study on geometric characteristics of beach erosion profiles. Ocean Engineering, 35(1), pp.17-27.

Pérez Boloix, G. (2011). Shoreline response to detached breakwaters: overview of design guidelines and application to field cases. Ph. D. thesis Universitat Politècnica de Catalunya Barcelona, Spain,304p

Phillips, N. A. (1957). A coordinate system having some special advantages for numerical forecasting. *Journal of Meteorology*, *14*(2), 184-185.

Pilarczyk, K. W. (2003a). Design of low-crested (submerged) structures: An overview. In 6th COPEDEC (Int. Conf. on Coastal and Port Engng. in Develop. Countries), Colombo, Sri-Lanka, 1–16

Pilarczyk, K. W. (2003b, November). Alternative Systems for Coastal Protection-An Overview. In International Conference on Estuaries and Coasts, Zhejiang University Press, Hangzhou, China, 409–419. (pp. 409-419).

Postacchini, M., Russo, A., Carniel, S. and Brocchini, M. (2016). Assessing the hydro-morphodynamic response of a beach protected by detached, impermeable, submerged breakwaters: a numerical approach. Journal of Coastal Research, 32, No. 3, pp.590-602.

Pranzini, E., Rossi, L., Lami, G., Jackson, N. L., & Nordstrom, K. F. (2018). Reshaping beach morphology by modifying offshore breakwaters. Ocean & Coastal Management, 154, 168-177.

Rahman, M. A., & Akter, A. (2014). The effect of porosity of submerged and emerged breakwater on wave transmission. International Journal of Environmental Science and Development, 5 (5), 473.

Ranasinghe, R., & Turner, I. L. (2006). Shoreline response to submerged structures: a review. Coastal Engineering, 53 (1), 65-79.

Ranasinghe, R., Turner, I. L., & Symonds, G. (2006). Shoreline response to multi-functional artificial surfing reefs: A numerical and physical modelling study. Coastal Engineering,53 (7), 589-611.

Ranasinghe, R., Larson, M., & Savioli, J. (2010). Shoreline response to a single shore-parallel submerged breakwater. Coastal Engineering, 57 (11-12), 1006-1017.

Rambabu, A. C., & Mani, J. S. (2005). Numerical prediction of performance of submerged breakwaters. Ocean Engineering,32 (10), 1235-1246.

Rodi, W. (1993). *Turbulence models and their application in hydraulics*. CRC Press.

Roelvink, D. (2006). *A guide to modeling coastal morphology* (Vol. 12). World Scientific

Roelvink, D., Reniers, A., Van Dongeren, A. P., de Vries, J. V. T., McCall, R., & Lescinski, J. (2009). Modelling storm impacts on beaches, dunes and barrier islands. Coastal engineering, 56(11-12), 1133-1152.

Rojanakamthorn, S., Isobe, M., & Watanabe, A. (1989). A mathematical model of wave transformation over a submerged breakwater. *Coastal Engineering in Japan*, *32*(2), 209-234.

Rojanakamthorn, S., Isobe, M., & Watanabe, A. (1990). Modeling of wave transformation on submerged breakwater. *Coastal Engineering Proceedings*,*1*(22).

Rosati, J. D. (1990). Functional design of breakwaters for shore protection: Empirical methods (No. CERC-TR-90-15). Coastal Engineering Research Center Vicksburg Ms.

Ruggiero, P., Gelfenbaum, G., Sherwood, C. R., Lacy, J., & Buijsman, M. C. (2003). Linking nearshore processes and morphology measurements to understand large scale coastal change. Proceedings of Coastal Sediments '03, East Meets West Productions, CD-ROM, 13 pp

Ruggiero, P., Buijsman, M., Kaminsky, G. M., & Gelfenbaum, G. (2010). Modeling the effects of wave climate and sediment supply variability on large-scale shoreline change. Marine Geology, 273(1-4), 127-140.

Seabrook, S. R., & Hall, K. R. (1999). Wave transmission at submerged rubblemound breakwaters. Proc. 26th Int. Conf. on Coastal Engineering, ASCE, pp. 2000 – 2013..

Sharifahmadian, A., & Simons, R. R. (2014). A 3D numerical model of nearshore wave field behind submerged breakwaters. Coastal engineering, 83, 190-204.

Silvester, R., & Hsu, J. R. (1997). Coastal stabilization (Vol. 14). World Scientific.

Sollitt, C. K., & Cross, R. H. (1972). Wave transmission through permeable breakwaters. *Coastal Engineering Proceedings*, *1*(13).

Sorensen, R. M. (2006). *Basic coastal engineering* (Vol. 10). Springer Science & Business Media.

Stive, M. J. F. (1987). A model for cross-shore sediment transport. In Coastal Engineering 1986 (pp. 1550-1564).

Svendsen, I. A. (1984). Mass flux and undertow in a surf zone. Coastal Engineering, 8(4), 347-365.

Svendsen, I. A. (2006). Introduction to nearshore hydrodynamics (Vol. 24). World Scientific.

Tajziehchi, M., & Cox, R. (2007). Wave transmission and wave-induced current in presence of submerged breakwaters. Proc. 30th Intern. Conf. Coastal Engineering, San Diego ,2006, Vol. 5, pp. 4970-4982.

Tassi, P., & Villaret, C. (2014). Sisyphe v6. 3 user's manual. R&D, Electricite de France.

Ting, C. L., Lin, M. C., & Cheng, C. Y. (2004). Porosity effects on non-breaking surface waves over permeable submerged breakwaters. *Coastal engineering*, *50*(4), 213-224.

Trouw, K. J. M., Zimmermann, N., Mathys, M., Delgado, R., & Roelvink, D. (2012). Numerical modelling of hydrodynamics and sediment transport in the surf zone: a sensitivity study with different types of numerical models. *Coastal Engineering Proceedings*, *1*(33), 23.

Turner, I. L., Leyden, V. M., Cox, R. J., Jackson, L. A., & McGrath, J. E. (2001). Physical model study of the Gold Coast artificial reef. Journal of Coastal research, 131-146.

United Nations Conference on Environment and Development (UNCED), (1992). Agenda 21, ch.17, pp.44

Uittenbogaard, R. E., & van Kester JAThM, S. G. (1992) Implementation of three turbulence models in 3D-TRIUSULA for rectangular grids, Rep. *Z81 Z*, *162*.

US Army Corps. (1993). Engineering design guidance for detached breakwaters as shoreline stabilization structures. WES, Technical Report CERC–93-19, December.

Van De Graaff, J., Sistermans, P. G., & Jenniskens, M. J. (2003). Comparison of Bijker and van Rijn Formulae. In*Coastal Engineering 2002: Solving Coastal Conundrums* (pp. 2578-2590).

Van der Baan, A. L. (2013). Developing a design criterion for the shoreline response to multiple submerged breakwaters, Master of Science Thesis in Coastal Engineering. Delft University of Technology, The Netherlands.

Van der Biezen, S. C., Roelvink, J. A., Van de Graaff, J., Schaap, J., & Torrini, L. (1999). 2DH morphologyical modelling of submerged breakwaters. Proc 26th Intern. Conf. Coastal Engineering, Copenhagen, Denmark, Vol. 2, pp. 2028-2041.

Van der Hout, C. M. (2008). Morphological impact of a deep water reef., Master of Science Thesis in Coastal Engineering. Delft University of Technology, The Netherlands.

Van der Meer, J. W., & Daemen, I. F. (1994). Stability and wave transmission at low-crested rubble-mound structures. *Journal of waterway, port, coastal, and ocean engineering*, *120*(1), 1-19.

Van der Meer, J. W., Regeling, E., & De Waal, J. P. (2001). Wave transmission: spectral changes and its effects on run-up and overtopping. Proc 27th Int. Conf on Coastal Engineering, Vol. 3, pp. 2156-2168

Van der Meer, J. W., Wang, B., Wolters, A., Zanuttigh, B., & Kramer, M. (2003). Oblique wave transmission over low-crested structures. In Coastal Structures 2003 (pp. 567-579).

Van der Meer, J. W., Briganti, R., Zanuttigh, B., & Wang, B. (2005). Wave transmission and reflection at low-crested structures: Design formulae, oblique wave attack and spectral change. Coastal Engineering, 52(10-11), 915-929.

Van der Zanden, J. (2016). Sand transport processes in the surf and swash zones, PhD thesis, University of Twente, The Netherlands.

Van Gent, M. R. (1995a). Wave interaction with berm breakwaters. *ASCE, Journal of waterway, port, coastal, and ocean engineering*, *121*(5), 229-238.

Van Gent, M. R. A. (1995b). Porous flow through rubble-mound material. *ASCE,Journal of waterway, port, coastal, and ocean engineering*, *121*(3), 176-181.

Van Rijn, L. C. (1993). *Principles of sediment transport in rivers. Estuaries and coastal seas* (Vol. 1006). Amsterdam: Aqua publications.

Van Rijn, L. C. (2003). Sand transport by currents and waves; general approximation formulae. In Proceedings of Coastal Sediments, Clearwater Beach, Florida, USA, Vol. 3. pp 1-14

Van Rijn, L. C., Tonnon, P. K., & Walstra, D. J. R. (2011). Numerical modelling of erosion and accretion of plane sloping beaches at different scales. Coastal Engineering, 58(7), 637-655.

Van Rijn, L. (2013). Design of hard coastal structures against erosion. Accessed online: http://www. leovanrijn-sediment. com/papers/Coastalstructures2013. pdf (22/12/17).

Van Vossen, B. (2000). Horizontal large eddy simulations; evaluation of computations with DELFT3D-FLOW. Report MEAH-197. *Delft University of Technology*.

Villani, M., Bosboom, J., Zijlema, M., & Stive, M. J. (2012). Circulation patterns and shoreline response induced by submerged breakwaters. Proc 33nd International Conference on Coastal Engineering (ICCE) Vol. 1, pp 25-36

Vlijm, R. J. (2011). Process-based modelling of morphological response to submerged breakwaters, Master of Science Thesis in Coastal Engineering. Delft University of Technology, The Netherlands.

Walstra, D. J. R. (2000). *Userguide for Unibest-TC*. Deltares (WL).

Walstra, D. J. R., Roelvink, J. A., & Groeneweg, J. (2000). Calculation of wave-driven currents in a 3D mean flow model. 27th International Conference on Coastal Engineering (ICCE) July 16-21, 2000, Sydney, pp.1050-1063).

Walstra, D. J. R., & Steetzel, H. J. (2003). Description of improvements in the UNIBEST-TC model: Upgrade of UNIBEST-TC version 2.04 to 2.10. Z3412.

Walstra, D. J. R., Ormondt, M. V., & Roelvink, J. A. (2004). *Shoreface nourishment scenarios: detailed morphodynamic simulations with Delft3D for various shoreface nourishment designs*. Deltares (WL).

WAMDI Group. (1988). The WAM model—A third generation ocean wave prediction model. *Journal of Physical Oceanography*, *18* (12), 1775-1810.

Wamsley, T. V., Kraus, N. C., & Hanson, H. (2003). Shoreline response to breakwaters with time-dependent wave transmission. Proceedings Coastal Sediments '03, ASCE, Florida, U.S.A, pp.593-605.

Wamsley, T. V., & Hanson, H. (2003). Evaluation of Proposed Submerged Jetty Spur on Shoreline Evolution, Grays Harbor, Washington. Proc 28th Inter, Conf Coastal Engineering 2002: Solving Coastal Conundrums Cardiff, Wales, pp. 2625-2637.

Wellens, P. R., Borsboom, M. J. A., & Van Gent, M. R. A. (2010). 3D simulation of wave interaction with permeable structures. Proc., 32nd Int. Conf. on Coastal Engineering, ASCE, Shanghai, China.

Zanuttigh, B., & Lamberti, A. (2006). Experimental analysis and numerical simulations of waves and current flows around low-crested rubble-mound structures. ASCE; *Journal of waterway, port, coastal, and ocean engineering*, *132* (1), 10-27.

Zanuttigh, B., Martinelli, L., & Lamberti, A. (2008). Wave overtopping and piling-up at permeable low crested structures.Coastal Engineering, 55(6), 484-498.

Zhu, F., & Dodd, N. (2015). The morphodynamics of a swash event on an erodible beach. Journal of Fluid Mechanics, 762, 110-140.

Zyserman, J. A., & Johnson, H. K. (2002). Modelling morphological processes in the vicinity of shore-parallel breakwaters. Coastal Engineering, 45 (3-4), 261-284.

Zyserman, J. A., Johnson, H. K., Zanuttigh, B., & Martinelli, L. (2005). Analysis of far-field erosion induced by low-crested rubble mound sructures. Coastal Engineering, 52 (10-11), 977-994